Structural and electronic features of tungsten(0) and platinum(II) complexes with Fischer carbene ligands

by

Nora-ann Weststrate

Submitted in partial fulfilment for the degree of

Philosophiae Doctor (Chemistry)

in the

Faculty of Natural and Agricultural Sciences

UNIVERSITY OF PRETORIA

Pretoria

April 2017

Supervisor: Prof. Simon Lotz

Declaration

I, Nora-ann Weststrate, declare that the thesis, which I hereby submit for the degree PhD Chemistry at the University of Pretoria, is my own work and has not previously been submitted by me for a degree at this or any other institution.

The cyclovoltammetry, UV/Vis and IR spectroelectrochemistry, and emission spectroscopy was measured, in part, by Dr. Obadah S. Abdel Rahman, and completed by myself, at Universität Konstanz, Germany, under the supervision of Prof. Rainer Winter.

DFT calculations was obtained by Dr. Obadah S. Abdel Rahman and Dr. Michael Linseis, Universität Konstanz, Germany.

The femtosecond transient absorption spectroscopy was measured in assistance of Alexander Paradzah and supervised by Dr. Tjaart Kruger, from the Physics Department at the University of Pretoria.

Crystal structures were solved by Mr. Dave Liles from the Chemistry Department at the University of Pretoria and Dr. Helmar Görls, Universität Jena, Germany.

The financial assistance from the National Research Foundation (NRF) towards this research is hereby recognized and appreciated. Opinions expressed and conclusions arrived at, are those of the author and are not necessarily to be attributed to the NRF.

Signature: 

Date: 05/07/2017

Acknowledgements

First, and foremost, I would like to thank God for giving me the ability and determination to complete this degree.

This research would not have been possible without the constant support, whether it was close or from afar, from my supervisor, Prof. Simon Lotz. You have shown me that it is possible to have knowledge and authority without losing humility or grace. You are not only the best supervisor I could ask for, but a close friend. I am proud to have completed this degree under your supervision.

Prof. Rainer Winter, who accommodated me for two research visits at the Universität Konstanz, Germany. I am immensely grateful for the opportunity you have given me as well as your input in my work. And of course, the Winter research group. I want to thank every single one of you (listing twenty names will take too much space). There is not a single person who did not help me during my visits, whether experimental or emotional. I immensely enjoyed your German efficiency and humour.

Dr. Shankara Radhakrishnan and Dr. Tjaart Kruger who contributed valuable scientific insight and ideas towards the project and were always willing to help.

My lab mates at the University of Pretoria, especially Zandria Lamprect, who were always willing to help when I was not close to a lab.

My family, for their emotional support and prayers during the project.

My husband, Dr. Marnus Weststrate, who encouraged me through the tears and frustration. You have shown me that everything can be done with excellence and passion.

Summary

Fischer carbene complexes of tungsten pentacarbonyl were synthesised on N,N-dimethylaniline and anisole coordinated in a η^6-fashion to a $Cr(CO)_3$ fragment. Single carbene complexes were isolated on all (*o*-, *m*-, and *p*-) positions of the π-coordinated N,N-dimethylaniline while only mono- (*o*-isomer) and biscarbene (*o*, *o*-isomer) complexes were isolated for the π-coordinated anisole. The *o*-isomers of N,N-dimethylaniline and anisole form five-membered chelate complexes. Cyclovoltammetry and IR spectroelectrochemistry revealed the site dependence of the ring substituents of the N,N-dimethylaniline complexes. For the tungsten pentacarbonyl carbene complexes of N,N-dimethylaniline, electron density from the heteroatom was donated into the ring. The delocalisation effect was greatest *p*-isomer. No delocalisation of electron density present on the oxygen towards the stabilisation of the carbene complexes present in the compound, was observed. The structural study of the complexes revealed ring distortion because of η^6-coordination which also determined the orientation of the tricarbonylchromium tripod with respect to the arene carbons.

Further, a series of ethoxy- and aminocarbene tungsten pentacarbonyl complexes were synthesised at the *p*-position on several aromatic tertiary amines. The aminolysis of the ethoxycarbene complexes was achieved through an economic and novel method developed for the generation of dimethylamine. The remote stabilisation of the Fischer carbene complexes were investigated using NMR spectroscopy, cyclovoltammetry, IR spectroelectrochemistry and X-Ray crystallography. The ethoxycarbene complexes were influenced more by the substituents of the remote nitrogen while the aminocarbene complexes remained unaffected.

A series of multi-carbene complexes of Pt(II) was synthesised through a carbene transfer reaction from the previously synthesised tungsten carbene complexes with $Pt(COD)Cl_2$. Neutral

bisethoxycarbene complexes and positively charged Pt(II) trisaminocarbene complexes were isolated. The complexes were characterised through NMR spectroscopy, elemental analysis and mass spectrometry. Further, the photophysical properties of the mononuclear complexes were investigated using UV/Vis and emission spectroscopy. The compounds displayed blue fluorescence of low quantum yields, indicating that the photoexcited complexes return to the ground state through a dominant, non-emissive pathway.

Multicarbene complexes of binuclear Pt(II) bithienylene bridged compounds were synthesised using the same transmetallation approach. The multicarbene complexes isolated, all of which contained at least five carbene ligands, were singly or doubly charged. The complexes displayed the same blue fluorescence as the mononuclear complexes upon excitation at 380 nm, although at similar or lower quantum yields. Using femtosecond transient absorption spectroscopy, a long-lived charge separated state was observed for all the binuclear Pt(II) carbene complexes.

Finally, a comparison between analogous mono- and binuclear Pt(II) carbene complexes revealed that the blue fluorescence observed upon photoexcitation at 380 nm for both types of complexes is carbene ligand-based. Further, it was postulated that the charge separated state formed with the positive polaron found on the bithienylene bridge while the negative polaron is found on one of the carbene carbons at positively charged Pt(II) fragment.

The study represents the first comprehensive investigation of the electronic features of the photoactivation of selected Pt(II) Fischer carbene complexes.

Table of contents

List of Complexes

Series A

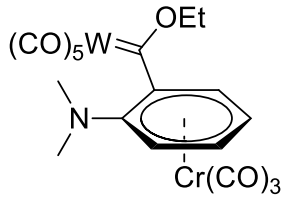

A1a

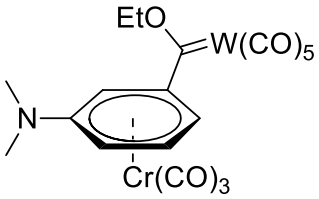

A1b

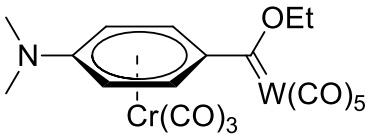

A1c

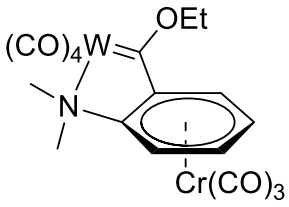

A1d

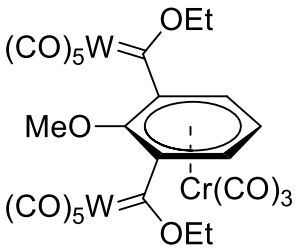

A2a

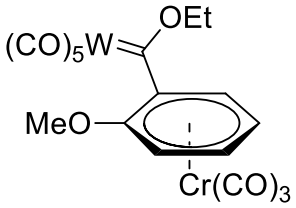

A2b

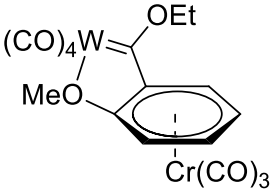

A2c

Series B

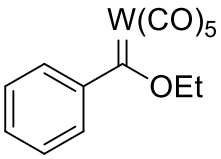

B1a

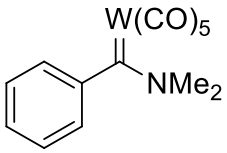

B1b

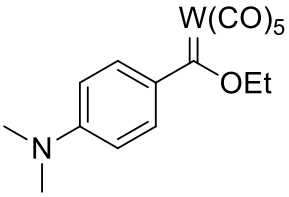

B2a

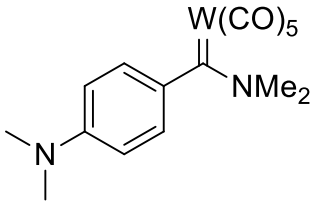

B2b

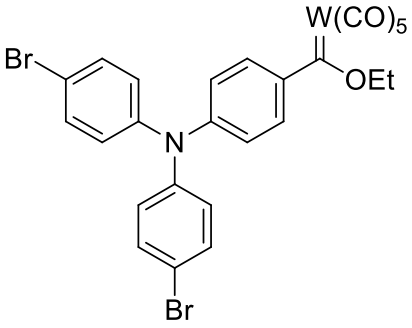

B3a

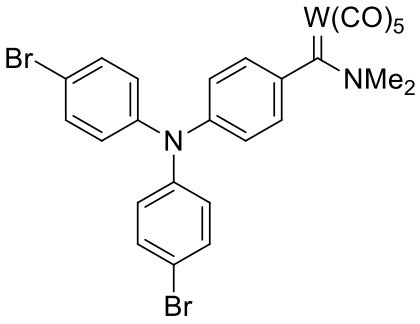

B3b

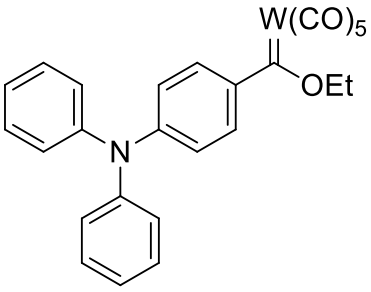

B4a

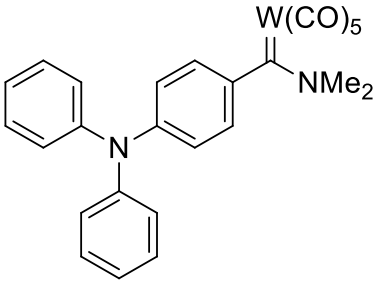

B4b

Series C

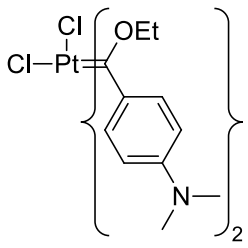

C1a

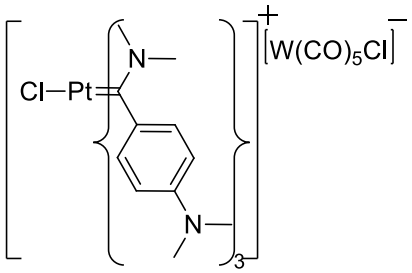

C1b(I)

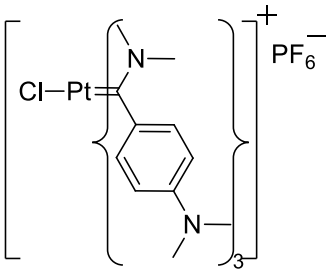

C1b(II)

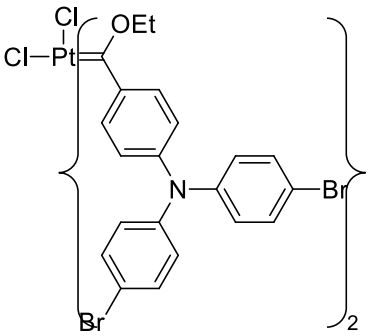

C2a

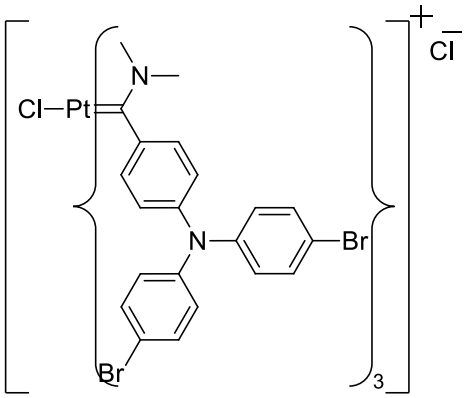

C2b

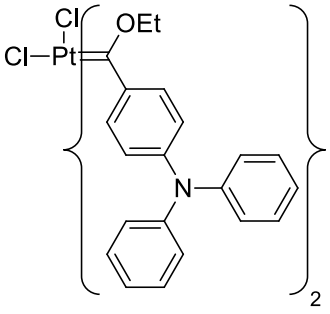

C3a

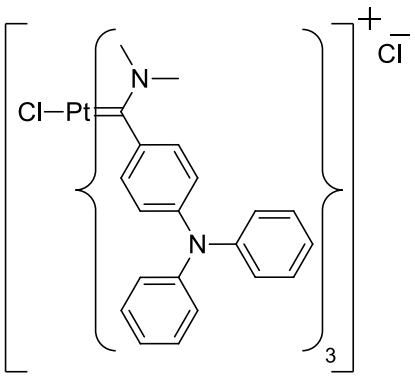

C3b

Series D

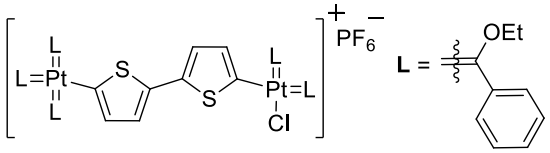

D1a

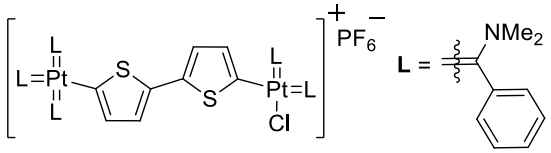

D1b

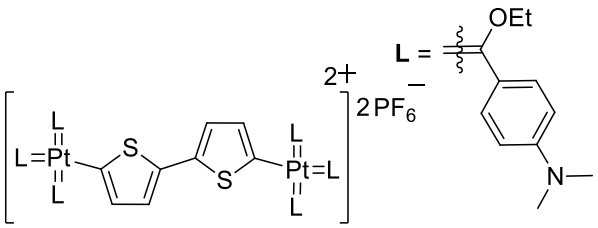

D2a

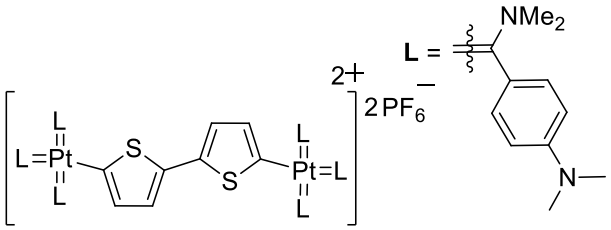

D2b

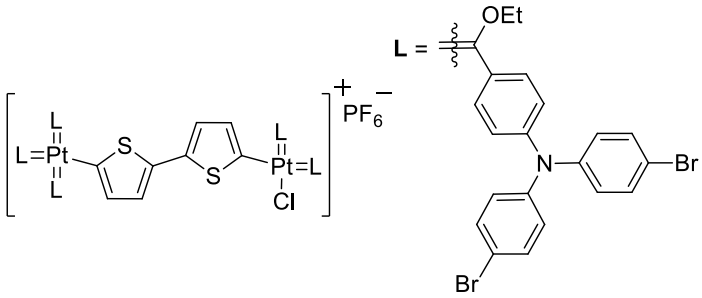

D3a

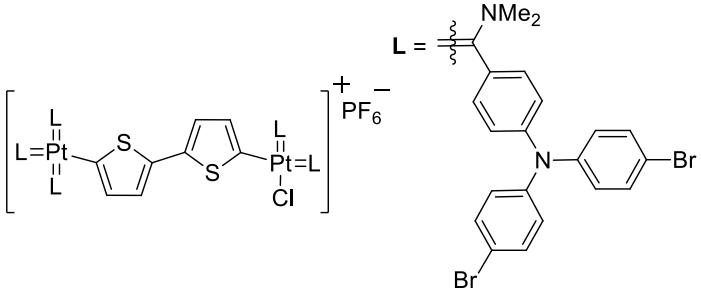

D3b

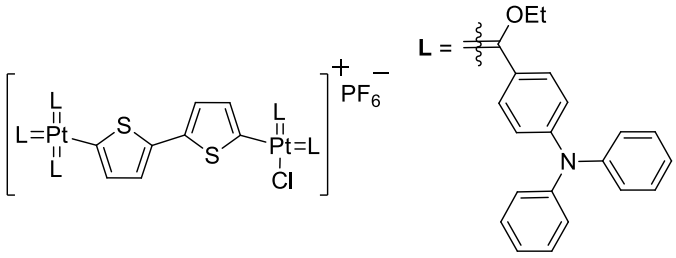

D4a

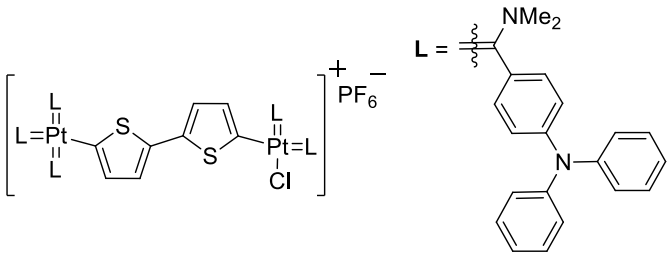

D4b

List of Abbreviations

ΔA	Change in absorbance
2D	two dimensional
Abs	Absorbance
br	broad
COD	Cyclooctadiene
CR	Charge recombination
CS	Charge separated
CT	Charge transfer
CV	Cyclovoltammetry
DCM	Dichloromethane
dd	doublet of doublet
ddd	doublet of doublet of doublet
DFT	Density Functional Theory
DmFc	Decamethylferrocene
E	eclipsed
EA	Elemental analysis
EADS	evolution associated difference spectra
E_{pa}	anodic potential
E_{pc}	cathodic potential
ESA	Excited-state absorption
FT-IR	Fourier Transform - Infrared spectroscopy
GSB	ground state bleach
HOMO	Highest occupied molecular orbital
HRMS	High resolution mass spectrometry
i	current
IR	Infrared
ISC	Intersystem crossing
LF	Ligand field
LLCT	Ligand to ligand charge transfer
LL'MCCT	Ligand to ligand charge transfer with metal character
LUMO	Lowest unoccupied molecular orbital
M	Metal / Molecular ion
m-	*meta*
MeCN	Acetonitrile
MeOH	Methanol
MeTHF	2-methyltetrahydrofuran
MIC	Mesoionic carbene

MLCT	Metal to ligand charge transfer
MS	Mass spectrometry
n.o.	not observed
*n*BuLi	*n*-butyl lithium
NHC	N-heterocyclic carbene
NMR	Nuclear Magnetic Resonance
NR	Non-radiative
o-	*ortho*
OEt	Ethoxy
OLED	Organic light emitting diodes
OMe	Methoxy
Ox	Oxidation
p-	*para*
PA	Product absorption
Ph	phenyl
ppm	parts per million
q	quartet
Red	Reduction
RT	Room temperature
s	strong (IR) / singlet (NMR)
S	staggered
SE	Stimulated emission
SEC	Spectroelectrochemistry
t	triplet
TA	triplet absorption
TAS	Transient absorption spectroscopy
TD-DFT	Time dependent Density Functional Theory
THF	Tetrahydrofuran
UV	Ultraviolet
Vis	Visible
vs	very strong
vw	very weak
w	weak

CHAPTER 1

INTRODUCTION

1.1 Carbene complexes: Introduction and applications

The unique properties of carbene carbons make them some of the most versatile ligands that exist today. A carbene carbon is a divalent, neutral carbon with six valence electrons.[1] There are mainly two classes of carbenes that exist: singlet and triplet carbenes which, when coordinated to transition metals are also known as Fischer and Shrock-type carbene ligands respectively (Figure 1.1). Triplet carbene complexes are best known for their significant contribution in olefin metathesis reactions while singlet carbene complexes are mainly known for their applications in organic synthesis.[2–4]

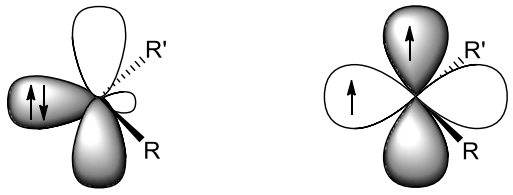

Figure 1.1. Schematic representations of Singlet (left) and Triplet (right) carbene carbons and their coordinating orbitals[1]

Fischer carbenes as ligands in complexes, are best described as being electrophilic in nature and are usually stabilised by a transition metal in a low oxidation state and at least one heteroatom substituent.[5,6] From the features of Fischer carbene complexes, another sub-class of singlet carbene ligand has developed over the last three decades to steel the carbene limelight: N-Heterocyclic carbenes (NHCs). These NHCs can be isolated as stable carbenes and, when compared to phosphine ligands, have matching electron donating abilities and can by design have superior steric features.[7–9] These ligands are described as heterocyclic compounds that contain

a normal or abnormal carbene carbon and at least one nitrogen atom within the structure of the ring.[8,10] The diversity and use of these ligands are remarkable, making them some of the most studied compounds in this era of research in catalysis as well as materials.[11,12] For this reason, little attention has been given to "traditional" Fischer carbene complexes in studies beyond that of organic transformations.[2]

A Fischer carbene complex can readily be synthesised from organolithium agents and metal carbonyl complexes. Its electrophilicity can be controlled by changing the heteroatom substituent which also significantly contributes to the stabilisation of the carbene carbon. Alkylation of the metal acylate is possible with several alkylating agents and their subsequent modification.[1,13] In this study both ethoxy as well as amino substituents are used. A second aromatic carbene substituent – benzene and its derivatives – are investigated for its role in the stabilisation of the carbene carbon. Even though benzene is seldom seen as an electron excessive molecule, it can act as such when in conjugation with an electron donating substituent on the ring. It acts as a spacer between a donating substituent and an electron withdrawing carbene carbon in a "push-pull" assembly (Figure 1.2).

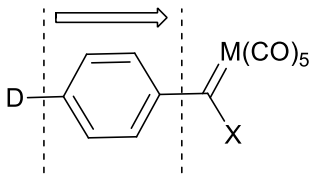

D = Donating substituent
X = OEt / NR_2

Figure 1.2. Aryl substituents as conjugated linkers between a donor substituent and a carbene carbon

1.2 Multimetal Fischer carbene complexes

The synthesis, characterization and properties of multimetal carbene complexes have been a topic of interest in our laboratories for many years. Fischer carbene complexes with one or two carbene substituents containing transition metal moieties have been investigated (Figure 1.3). The objective is to study metal-metal communication in such systems and compare the features and electronic properties to the more conventional Fischer carbene complexes with alkyl or aryl substituents.

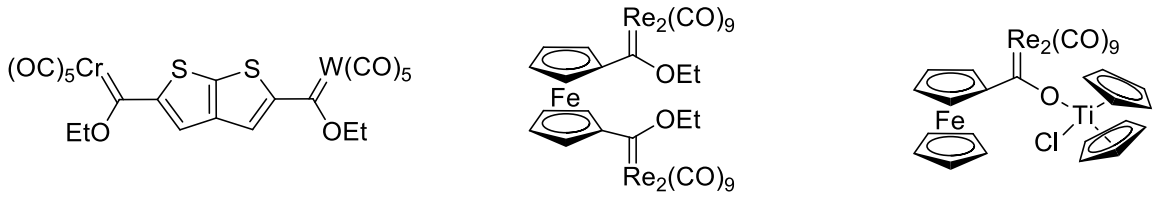

Figure 1.3. Examples of multimetal carbene complexes[13–15]

One of the goals of our research group is to incorporate Fischer carbene complexes in macromolecules and materials where the unique properties of carbene ligands contribute to the material's properties. Carbene ligands create unique abilities to allow a conjugated fragment to form over a part or whole ligand while being coordinated to a metal. This property has already been exploited to a limited extent in the study of NHC ligands in different materials where large aromatic groups can directly be coordinated to several metals through the carbene carbon.[16,17]

There are only a few examples of networks containing Fischer carbene complexes and in each case the unique properties of the carbene carbons themselves cannot be used beyond that of post-synthetic organic transformations.[18,19] It is, therefore, the goal of this project to incorporate Fischer carbene complexes into the coordination sphere of metals and investigate the role of the electron withdrawing carbene carbon in charge transfer processes.

1.3 Carbene transfer reactions

There are not many examples of carbene transfer reactions from one metal to another[1,20] as pre-synthesised carbenes rely on the metal centres to which they are coordinated for stabilisation. There are, however, several industrially important reactions where the transfer of carbene ligands play an important role in the generation of organic compounds. Examples of such processes include catalytic processes like olefin metathesis, Fischer-Tropsch reactions, as well as the cyclopropenation of alkenes.[21]

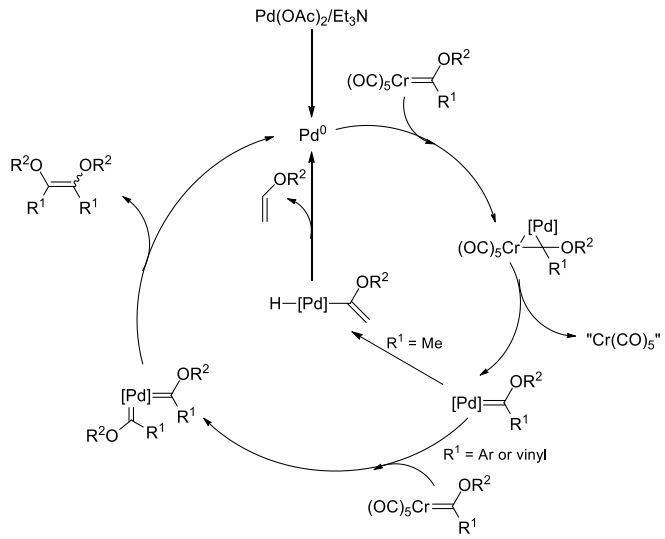

Scheme 1.1. The catalytic cycle for the dimerization of Cr(0) carbene complexes by Pd(0)[22]

More specifically, the carbene-carbene coupling reactions of Group 6 Fischer carbene complexes were first reported by Fischer himself,[23] after which the concept (cross-coupling reactions) was further used in the synthesis of organic compounds through a Pd-carbene intermediate.[24–26] In 2001 the research group of Sierra published a proposed mechanism of the carbene dimerization process in the presence of Pd(0).[22,27,28] The C(carbene)-C(carbene) coupling reaction pathway is illustrated in Scheme 1.1.

As Group 10 metals are well-known for their ability to cause dimerisation of carbene ligands, few examples of stable, classical Fischer carbene complexes exist. These are obtained through indirect or complex synthetic methods,[29] chelating complexes[30] or fall under the class of extremely electron rich NHC complexes.[31,32]

1.4 Carbene complexes in materials

Very few investigations have been conducted into the scope and usefulness of Fischer carbene units as components of modern day smart materials. Many potential areas of applications exist and include non-linear optical materials, molecular wires, liquid crystals, dendrimers, metal organic frameworks, polymers, etc. An attractive property of Fischer carbenes is their potential to act as polarizing units in macromolecular assemblies. Because Fischer carbene ligands have strong electron withdrawing properties, they can form part of a polarized molecule or cause a localized area of polarization in macromolecular compounds. This can lead to charge separation or charge transfer processes which is an important feature of many materials.

Square planar Pt(II) complexes, specifically, are extensively studied for their interesting photophysical properties,[31,33] their metal-metal interactions, and their distinctive supramolecular architectures.[34–36] Even though there are examples where carbene ligands have been used in many of the Pt(II) materials synthesised in more recent years, the carbene ligands used are limited to NHCs due to their significant stability.

1.5 Challenges, Aims and Objectives

1.5.1 Challenges

As described above, the incorporation of Fischer carbene complexes into the coordination sphere of transition metals – in this case Pt(II) and larger complexes or networks – is expected to be problematic due to the assumption that Fischer carbene complexes could represent the most active site in a molecule. Fischer carbene ligands can readily dimerise, react with water or oxygen, or be modified in subsequent reactions.[37,38] It is true, neutral Group 10 metals catalyse carbon–carbon coupling and in their presence the dimerisation of carbene ligands often take place. Due to the reactivity of the neutral metals, however, very few examples of Fischer alkoxy- or aminocarbene complexes coordinated to Group 10 metals in different oxidation states exist, and those that do, limit the compounds to single metal centres and small complexes.

Recently our group successfully synthesised Group VI Fischer carbene complexes on tri(2-furyl)phosphine and tris(4-bromophenyl)amine with the aim to incorporate multiple carbene ligands into macro-molecules and materials through a "piggyback" approach. The coordination properties of the phosphine were not significantly influenced by the strong electron-withdrawing character of the carbene carbon as the carbene's

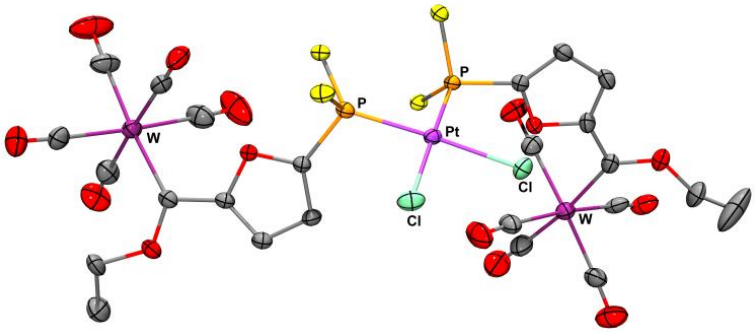

Figure 1.4. Solid-state structure of phosphine ligands carrying W(0) carbene complexes coordinated to Pt(II). Ancillary furyl rings (yellow) were omitted for clarity[39]

stabilisation was localised to one furyl ring. The resulting phosphine was used to escort Fischer carbene complexes into the coordination sphere of Pt(II) and several other transition metals (Figure 1.4). Unlike of the trifurylphosphine complex, the electron density present on the amine was completely delocalised over the phenylene ring towards the electron withdrawing carbene carbon, increasing the stability of the carbene moiety while deactivating the amine (Figure 1.5).[39]

Although the "piggyback" concept can be applied to many soluble complexes containing displaceable ligands. The carbene complex, however, is a spectator and is not influenced by the properties of the other metal. A different approach is required to directly incorporate Fischer carbene ligands into macromolecules or larger networks.

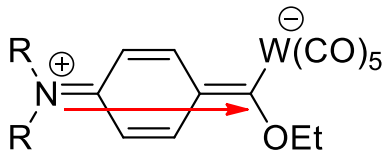

Figure 1.5. Delocalisation of electron density from amine towards carbene carbon of a phenylene linker

It is generally known that the electron density present on an amine is readily displaced towards its substituents, especially if it is an electron-withdrawing group. This stabilising property of amines has been exploited in NHC ligands, increasing their stability and allowing them to be easily transferred from one metal to another. It is also for this reason that several stable Pt(II) NHC complexes exist.[16,40,41] It would seem the key in synthesising Fischer Pt(II) carbene containing complexes through a transfer reaction, is the stabilisation of the carbene carbon by its non-metal substituents. By increasing the amount of electron density of the carbene carbon's aromatic substituent, it may be possible to mimic the electron rich character of an NHC ligand while still retaining the electron withdrawing properties of a "traditional" Fischer carbene carbon. Subsequently, allowing acyclic singlet carbene ligands to be incorporated into the coordination sphere of Pt(II) through a carbene transfer reaction from W(0).

1.5.2 Aims and Objectives

There is an obvious lack of macromolecular Fischer carbene complexes and materials due to their difficult synthesis and their reactivity once formed. The lack of such complexes also leaves the

field of Fischer carbene complexes in photoactive materials unexplored. These aspects are fundamentally addressed in this study by investigating a synthetic method which makes use of, while still accommodating, the reactivity of the Fischer carbene complexes. This is approached by first investigating the effect of a carbene substituent at different positions of a phenyl ring relative to a π electron donating and withdrawing substituent of an easily isolable Fischer carbene complex. Once concluding what the overall effect of the carbene carbon as substituent is, attempts will be made as to how to incorporate such complexes on to Pt(II) nodes and larger complexes. Should stable products be isolated, several photophysical techniques will be used to investigate how carbene ligands can function in photoactive materials.

This project is built around an aromatic tertiary amine as a substituent of the carbene carbon in which the electron density of the amine is not used to coordinate to a metal centre, but rather to provide stabilisation through electron delocalisation over the aromatic ring to the carbene carbon.[39] For this reason, a systematic study of Fischer carbene complexes with aminophenyl carbene substituents is relevant and is pursued.

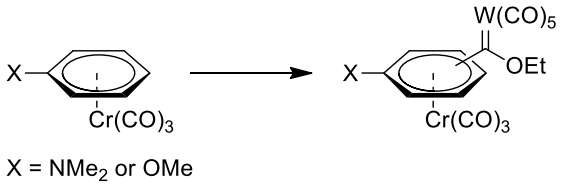

Scheme 1.2. Synthesis of W(0) ethoxycarbene complexes with π-coordinated $Cr(CO)_3$ and arene ligands with heteroatom substituents

In the first part of the study the electron delocalisation over a phenyl group containing electron donating and electron withdrawing substituents is investigated. Thus, the effect of the electron flow or delocalization in the spacer will be monitored by π-coordinating the benzene in a η^6-fashion to a $Cr(CO)_3$ fragment (Scheme 1.2). The aim is two-fold: i) How will changing the benzene substituents from an amino- to a methoxy-group affect the electronic properties in the benzene ring? ii) Do the relative positions of the carbene carbon and substituent influence the amount of electron density present on the aromatic ring.

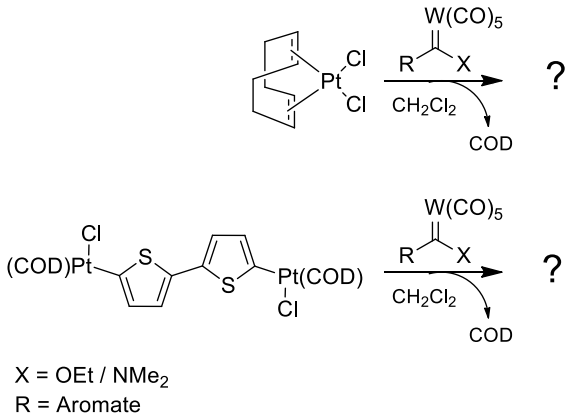

Scheme 1.3. Proposed synthesis of mono- and dinuclear Pt(II) Fischer carbene complexes via a transmetallation approach

In the second part of the study, a series of simple ethoxy- and amino- W(0) Fischer carbene complexes will be synthesised with the focus on being representative of varied electronic environments around the carbene carbon by changing electronic and steric properties of the substituents. The third section of the study will involve the transmetallation of the synthesised carbene complexes to Pt(II) precursors. Should the study prove successful, electronic and photophysical properties for which Pt(II) complexes are well-known, will be investigated.

To characterise all the synthesised complexes, nuclear magnetic resonance (NMR), infrared (IR) spectroscopy, elemental analysis (EA) and high resolution mass spectroscopy (HR-MS) will be used. The electronic properties of the tungsten carbene complexes will further be analysed using cyclovoltammetry (CV) as well as IR-spectroelectrochemistry (SEC). The photophysical and electrochemical properties of the platinum carbene complexes will be investigated using UV/VIS spectroscopy, emission spectroscopy, femto-second transient absorption spectroscopy, CV and UV/VIS-SEC.

1.6 References

[1] P. de Frémont, N. Marion, S. P. Nolan, *Coord. Chem. Rev.* **2009**, *253*, 862–892.

[2] J. Barluenga, M. A. Fernández-Rodríguez, E. Aguilar, *J. Organomet. Chem.* **2005**, *690*, 539–587.

[3] W. A. L. van Otterlo, C. B. de Koning, *Chem. Rev.* **2009**, *109*, 3743–82.

[4] K. H. Dötz, J. Stendel Jr., *Chem. Rev.* **2009**, *109*, 3227–74.

[5] S. Díez-González, S. P. Nolan, *Coord. Chem. Rev.* **2007**, *251*, 874–883.

[6] E. O. Fischer, *Angew. Chem.* **1974**, *86*, 651–663.

[7] S. Díez-González, N. Marion, S. P. Nolan, *Chem. Rev.* **2009**, *109*, 3612–3676.

[8] M. N. Hopkinson, C. Richter, M. Schedler, F. Glorius, *Nature* **2014**, *510*, 485–496.

[9] I. Anthony J. Arduengo, *Acc. Chem. Res.* **1999**, *32*, 913–921.

[10] D. Bourissou, O. Guerret, F. P. Gabbaï, G. Bertrand, *Chem. Rev.* **1999**, *100*, 39–92.

[11] R. H. Crabtree, *Coord. Chem. Rev.* **2013**, *257*, 755–766.

[12] S. Y.-L. Leung, E. S.-H. Lam, W. H. Lam, K. M.-C. Wong, W.-T. Wong, V. W.-W. Yam, *Chem. Eur. J.* **2013**, *19*, 10360–9.

[13] D. I. Bezuidenhout, S. Lotz, M. Landman, D. C. Liles, *Inorg. Chem.* **2011**, *50*, 1521–1533.

[14] Z. Lamprecht, N. A. van Jaarsveld, D. I. Bezuidenhout, D. C. Liles, S. Lotz, *Dalton Trans.* **2015**, *44*, 19218–19231.

[15] D. I. Bezuidenhout, E. Van der Watt, D. C. Liles, M. Landman, S. Lotz, *Organometallics* **2008**, *27*, 2447–2456.

[16] R. Visbal, M. C. Gimeno, *Chem. Soc. Rev.* **2014**, *43*, 3551–74.

[17] A. V. Zhukhovitskiy, M. J. MacLeod, J. A. Johnson, *Chem. Rev.* **2015**, *115*, 11503–11532.

[18] I. Fernández, M. J. Mancheño, M. Gómez-Gallego, M. A. Sierra, *Org. Lett.* **2003**, *5*, 1237–40.

[19] M. P. López-Alberca, M. J. Mancheño, I. Fernández, M. Gómez-Gallego, M. A. Sierra, C. Hemmert, H. Gornitzka, *Eur. J. Inorg. Chem.* **2011**, 842–849.

[20] H. G. Raubenheimer, *Dalton Trans.* **2014**, *43*, 16959–16973.

[21] E. W. Abel, F. G. A. Stone, G. Wilkonson, *Comprehensive Organometallic Chemistry II, Vol 12*, Elsevier, Oxford, UK, **1995**.

[22] M. A. Sierra, J. C. del Amo, M. J. Mancheño, M. Gómez-Gallego, *J. Am. Chem. Soc.* **2001**, *123*, 851–861.

[23] E. O. Fischer, K. Heinz Dötz, *Chem. Ber.* **1970**, *103*, 1273–1278.

[24] M. F. Semmelhack, R. D. Stauffer, *Tetrahedron Lett.* **1973**, *14*, 2667–2670.

[25] X. Zhao, J. Jing, K. Lu, Y. Zhang, J. Wang, *Chem. Commun.* **2010**, *46*, 1724.

[26] S. P. Stanforth, *Tetrahedron* **1998**, *54*, 263–303.

[27] I. Fernández, M. J. Mancheño, R. Vicente, L. A. López, M. A. Sierra, *Chem. Eur. J.* **2008**, *14*, 11222–30.

[28] I. Fernández, M. A. Sierra, F. P. Cossío, *J. Org. Chem.* **2006**, *71*, 6178–84.

[29] M. Werner, T. Lis, C. Bruhn, R. Lindner, D. Steinborn, *Organometallics* **2006**, *25*, 5946–5954.

[30] M. P. López-Alberca, M. J. Mancheño, I. Fernández, M. Gómez-Gallego, M. A. Sierra, R. Torres, *Chem. Eur. J.* **2009**, *15*, 3595–3603.

[31] V. W.-W. Yam, V. K.-M. Au, S. Y.-L. Leung, *Chem. Rev.* **2015**, *115*, 7589–7728.

[32] S.-T. Liu, K. Rajender Reddy, *Chem. Soc. Rev.* **1999**, *28*, 315–322.

[33] K. M.-C. Wong, V. W.-W. Yam, *Coord. Chem. Rev.* **2007**, *251*, 2477–2488.

[34] H.-L. Au-Yeung, A. Y.-Y. Tam, S. Y.-L. Leung, V. W.-W. Yam, *Chem. Sci.* **2017**, *8*, 2267–2276.

[35] A. Aliprandi, M. Mauro, L. De Cola, *Nat. Chem.* **2015**, *8*, 10–15.

[36] M. E. Robinson, D. J. Lunn, A. Nazemi, G. R. Whittell, L. De Cola, I. Manners, G. R. Whittell, M. A. Winnik, I. Manners, *Chem. Commun.* **2015**, *51*, 15921–15924.

[37] E. O. Fischer, U. Schubert, *J. Organomet. Chem.* **1979**, *170*, C13–C14.

[38] R. B. Silverman, R. A. Olofson, *Chem. Commun.* **1968**, 1313.

[39] N. Weststrate, I. Fernández, D. C. Liles, N. van Jaarsveld, S. Lotz, *Organometallics* **2015**, *34*, 696–710.

[40] M. Bachmann, D. Suter, O. Blacque, K. Venkatesan, *Inorg. Chem.* **2016**, *55*, 4733–4745.

[41] J. A. G. Williams, A. Beeby, E. S. Davies, J. A. Weinstein, C. Wilson, *Inorg. Chem.* **2003**, *42*, 8609–11.

CHAPTER 2

TUNGSTEN CARBONYL FISCHER CARBENE COMPLEXES OF N,N-DIMETHYLANILINE AND ANISOLE π-COORDINATED TO CHROMIUM TRICARBONYL

2.1 Introduction

The η^6-coordination of benzene rings to $Cr(CO)_3$ has been well known and thoroughly explored since the first π-coordinated chromium arene was recognised after synthesis by Hein in 1919.[1–5] The η^6-coordinated tricarbonylchromium complexes have been known to achieve enhanced benzene ring activation and to display unusual ring conformations which exhibit novel features and atypical characteristics.[6,7] Site specific activation of aryl rings has been a synthetic challenge to the fields of medicinal and organic chemistry. Relying on directing substituents has partially solved this problem, but still complete regioselective activation of aryl rings remains difficult.[8,9] Even though there has been recent advances in the field of selective site activation in chromium tricarbonyl π-coordinated arenes, the reasons as to how and why they function in a particular way have not yet been fully understood.[7] In the present study, the aim is to illustrate how charge delocalisation patterns of a π-coordinated electron rich and poor aryl rings can be probed by synthesizing Fischer carbene complexes of $W(CO)_5$ on phenyl rings. By monitoring present

vibrations in the carbonyl region of their IR spectra as well and the corresponding IR peak shifts during oxidation or reduction of the compounds, the effect of the π-coordinating $Cr(CO)_3$ group on the aryl ring can be further investigated.

In the study, an electron rich N,N-dimethylaniline and more electron poor anisole ring is π-coordinated to $Cr(CO)_3$. Preliminary results have been obtained in a previous study by the author in which N,N-dimethylaniline was coordinated to $Cr(CO)_3$.[10] These results will be summarised and used in a comparative study with analogous anisole complexes. The site activation properties of the two heteroatom substituents are investigated by synthesis of tungsten Fischer carbene complexes on the activated positions. Fischer carbene complexes have been specifically chosen for their electron withdrawing carbene carbons and that they also contain CO markers which can be monitored with IR spectroscopy as the compound is oxidised or reduced. Recently the redox properties of Fischer carbene complexes in multinuclear complexes have been receiving more attention as to investigate metal-metal communication.[11–14] It is expected that the redox properties of the complexes in this study, will reveal the effect that benzene π-coordination to $Cr(CO)_3$ has on the ring and its substituents.

2.2 Results and Discussion

2.2.1 Synthesis

The π-coordination of an arene ring to $Cr(CO)_3$ can be achieved through the substitution of carbonyl ligands of $Cr(CO)_6$ in high boiling solvents under inert reaction conditions. The sublimation of $Cr(CO)_6$ during such a procedure has been found to reduce significantly using a solvent mixture of dibutylether and THF.[15] In this study N,N-dimethylaniline and anisole are the two arene rings that are to be coordinated to $Cr(CO)_3$ and will also serve as the starting materials on which carbene complexes are synthesised.

During the coordination of the two arene rings to $Cr(CO)_3$ it becomes evident that N,N-dimethylaniline requires half the time that the anisole requires for a high yield of product to form.

This is ascribed to more electron density available on the aromatic ring of N,N-dimethylaniline provided by the amino substituent. Throughout this chapter the $Cr(CO)_3$ π-coordinated N,N-dimethylaniline and anisole which are the precursor complexes, will be referred to as **A1** and **A2** respectively. The products are isolated using silica column chromatography with hexane and dichloromethane as solvents. For both aniline and anisole π-complexes, the isolated compounds are light yellow of colour and can be stored for long periods of time under inert conditions.

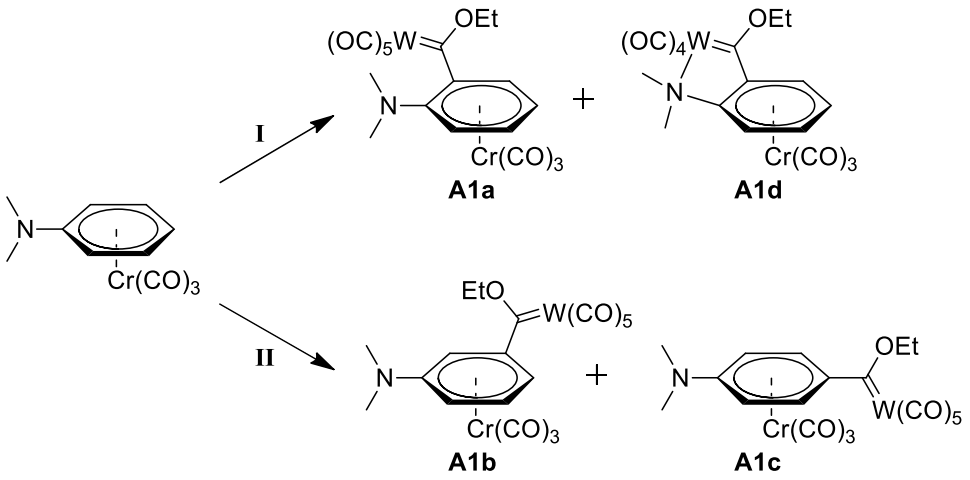

I (Thermodynamic reaction)
i. *n*BuLi, -40°C, THF, stir 30 min.
ii. 30°C, stir 60 min.
iii. $W(CO)_6$, -40°C, THF, stir 30 min.
iv. 30°C, stir 60 min.
v. Et_3OBF_4, -40°C, CH_2Cl_2

II (Kinetic reaction)
i. nBuLi, -40°C, THF, stir 15 min.
ii. $W(CO)_6$, -40°C, THF, stir 40 min.
iii. Et_3OBF_4, -40°C, CH_2Cl_2

Scheme 2.1. Synthesis of A1a – A1d

Synthesis of the tungsten Fischer carbene complexes with the two π-coordinated starting materials are conducted under an inert atmosphere using standard Schlenk techniques. Both **A1** and **A2** are lithiated in the same way: with *n*BuLi in cold THF, followed by addition of $W(CO)_6$ to the stirring solution, forming a metal acylate with a Li^+ counter ion. The final neutral ethoxycarbene complexes are formed by alkylation with Et_3OBF_4. It is clear from literature that the products obtained are largely controlled by the aromatic ring substituent which differ from that obtained for N,N-dimethylanaline and anisole.[16] It therefore comes as a surprise that during

the synthesis of the carbene complexes with **A1**, the products obtained can be regulated by controlling the reaction conditions.

By allowing long reaction times and a high reaction temperature (thermodynamically controlled reaction), mainly two products are obtained: an ethoxycarbene complex in the *o*-position where the dimethylamine remains uncoordinated (**A1a**), and a chelated complex where the amine has coordinated, by carbonyl substitution, to the W(0) carbene complex (**A1d**). By doing the same reaction at temperatures between –30 and –40 °C (kinetically controlled reaction), two different isomers of **A1a** are isolated: carbene complexes in the *m*- (**A1b**) and *p*- (**A1c**) positions relative to the dimethylamino substituent while the ring remains π-coordinated to the $Cr(CO)_3$ group (Scheme 2.1). During the thermodynamic reaction conditions, there is no indication that **A1b** or **A1c** forms. However, during the kinetic synthesis there are trace amounts of **A1a** and **A1d** that are observed.

These aspects were not investigated during the preliminary study mentioned above although **A1a** – **A1c** was isolated and characterised using IR, NMR and single crystal X-ray diffraction. **A1d** was not isolated or characterised using the general reaction conditions by which the other isomers were obtained in the previous study.

In Scheme 2.1, method **I** represents the thermodynamic reaction while **II** represents the kinetic method of synthesis. For **I,** the ratio between the **A1a** and **A1d** lies between 50:50 and 30:70 for the two compounds respectively. For **II**, the presence of a small amount of **A1a** leads to the formation of **A1d**. These two products are present in such small quantities that they are negligible to the amount of **A1b** and **A1c** which forms in a ratio of 10:1. This observation is in direct contradiction to what Card and Trahanovsky reported where the *o*-isomer is the major product in the synthesis of N,N-dimethyltoluidines via a lithiation route of (N,N-dimethylaniline)-tricarbonylchormium by using lower temperatures as in method **II**.[17] Their report indicates that the lithiation forms small amounts of the *m*- and *p*-products. Although the major contribution to

o-lithiation is the directing properties of the dimethylamino substituent, this would not seem to be the only reaction pathway followed as was concluded by Lepley and co-workers in their metalation reactions of N,N-dimethylaniline.[18] It is well known that by π-coordination of any arene ring that the acidity of all protons on the ring are markedly increased.[19] Without the significant delocalisation of electron density of any electron donating substituent (**D**) into the ring on which it is attached, the *m*-positions of the N,N-dimethylamino is activated due to the π-resonance effects as shown in Scheme 2.2 (increased stabilisation is observed at the *o*- and *p*-positions).

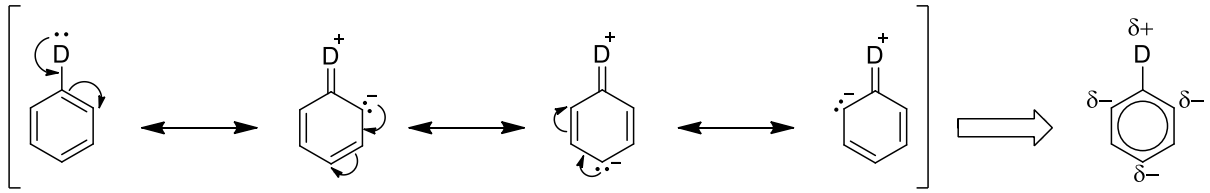

Scheme 2.2. π-Resonance activation of an aromatic ring by an electron donating substituent (D)

By contrast, for an electron withdrawing substituent such as the methoxy substituent of anisole, charge distributions in the arene ring and site activation is affected mainly by σ-inductive effects with a much smaller contribution of π-resonance effects (Scheme 2.3). As is the case for anisole, the greatest activation is by far at the positions closer to the electron withdrawing methoxy substituent (A).

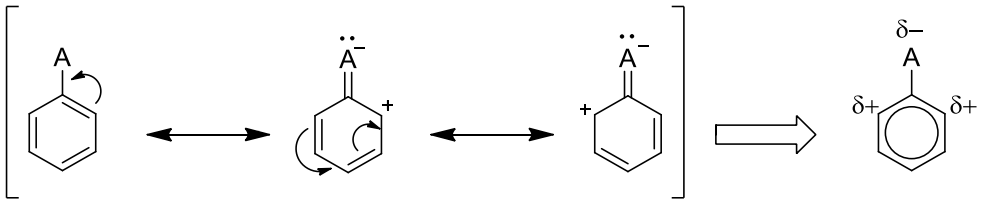

Scheme 2.3. π-Resonance and σ-inductive activation of an aromatic ring by an electron withdrawing substituent (A)

In the kinetic synthesis, the slightly activated *m*-position and the sterically available *p*-position are metallated during the lithiation step and react with tungsten hexacarbonyl. Since a different set of products are obtained by simply allowing the reaction mixture to reach room temperature during

the lithiation step, the dimethylamino substituent plays a role as a directing group as the *o*-position on the ring is not necessarily the most accessible position for steric reasons. This observation is further supported by Oishi, who showed that amine substituents present on the π-coordinated arene ring directly influence the amount of *m*- and *p*-products that form during reactions with *n*BuLi by effectively blocking the *o*-reaction position on the ring.[20]

Since the *o*-product is not the only product isolated for the carbene synthesis of **A1**, another pathway which does not make use of the directing properties of the arene ring substituent in **A1**, is followed. This alternative reaction pathway seems to be enhanced by the coordination of $Cr(CO)_3$ to the arene ring which activates all positions. It is also possible that the directing properties of the dimethylamino substituent is diminished in the presence of the carbene ligand and the bulky $W(CO)_5$ group. This would explain why Card and Trahanovsky observed a major *o*-product during their synthesis of N,N-dimethyltoluidines as the methyl substituent is small compared to the size of the much larger carbene ligand and $W(CO)_5$ group.[17] It can thus be stated that the presence of large amounts of *m*- and *p*-substituted products observed during the kinetic synthesis of the carbene complexes is largely due to the steric properties of the bulky carbene complex.[19]

Although there are several examples where tungsten compounds can act as π-acids in the activation of aryl rings, the carbene moiety itself does not seem to influence the position on the ring where the carbene is formed. This is because $W(CO)_6$ itself is not a good π-acid – only after formation of the metal acylate does it become good π-acid.[21–24] It is necessary to emphasise that (arene)chromium tricarbonyl complexes have been reported to exhibit kinetic and thermodynamic site preferences depending on the reaction conditions.[25]

In contrast to the observations made for π-coordinated N,N-dimethylaniline, π-coordinated anisole solely reacts at the *o*-positions of **A2**. Three products form on addition of a slight excess *n*BuLi, and equivalent amounts of $W(CO)_6$ and Et_3OBF_4 (Scheme 2.4). Firstly, a biscarbene

complex, where two tungsten Fischer carbene complexes form on both the *o*-positions relative to the OMe group (**A2a**), is isolated. The expected *o*-tungsten carbene complex (**A2b**) follows. Finally, a chelated complex where the oxygen atom of the methoxy group (**A2b**) substitutes one of the CO ligands on the $W(CO)_5$ group is isolated, **A2c**.

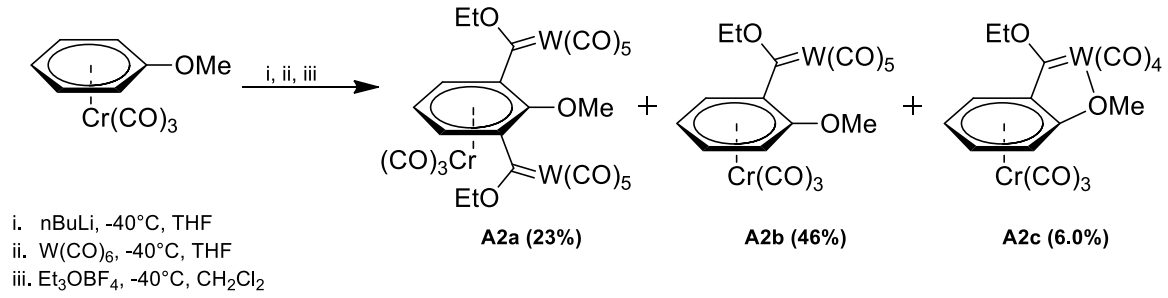

Scheme 2.4. Synthesis of A2a – A2c

The three products are red, brown-red and purple of colour respectively, and can be crystallised from hexane and DCM (CH_2Cl_2) mixtures. Although the amount **A2c** that forms during a controlled reaction is relatively small, the product can easily be formed quantitatively by UV irradiation of **A2b** in a hexane:THF mixture of 10:1.

A recent publication by the research group of Ricci shows that the π-coordination of the anisole leads to the selective *o*-arylation, products not obtainable without π-coordinated $Cr(CO)_3$.[7] In an earlier theoretical study by the same group it has also been shown that the *o*-position of the ring is specifically activated by the π-coordination of anisole to $Cr(CO)_3$. The $Cr(CO)_3$ coordinated to the ring facilitates the bending of the protons during the transition state of the reaction, thus selectively activating the protons in the *o*-positions.[6] It is clear from the products of **A2**, that the most acidic protons are those in the *o*-positions.

For both π-coordinated starting materials, **A1** and **A2**, chelated complexes are formed during the respective reactions. The proximity of the electron-rich substituent-groups to the tungstencarbonyl group allows for one of the CO ligands on the tungsten metal to be replaced, thus forming a complex with a bidentate ligand. Examples of such chelates have been published.[26]

This process can be enhanced by UV irradiation, forcing the substitution of a CO ligand, thereby opening a vacant site for coordination in the coordination sphere of the metal-carbonyl complex.[27] Loss of a carbonyl ligand from the $Cr(CO)_3$ group is possible during UV radiation,[28] but in this case seems to be minimal as a large yield of the desired tungsten chelated complex is obtained from the reaction. There are examples of chelated Fischer carbene complexes where the chelate ring is formed by two carbene ligands sharing the same metal centre on a single compound.[29–32]

2.2.2 *NMR Spectroscopy*

All NMR spectra are recorded in $CDCl_3$ at room temperature. For ease of discussion the carbene complexes formed from **A1** and **A2** will be discussed separately after which a general discussion will follow. The NMR spectra of the **A1a** – **A1c** are also reported as the previously recorded spectra were of poor quality.[10]

In summary, the previous study of **A1a** – **A1c** revealed that the π-coordination of the arene ring to $Cr(CO)_3$ moved the ring protons out of the aromatic region (a significant upfield shift of the ring protons – greater than 1 ppm – was observed), which displayed some localized coordinated olefinic properties. It was also observed that a fair amount of electron density was delocalised from the dimethylamino substituent over the ring to help quench the highly electrophilic nature and reactivity of the carbene carbon in the complexes. This allowed that the carbene complexes present at the *o*- and *p*-positions of the ring benefited more than the *m*-position as shown in Scheme 2.5. The extent of electron delocalisation from the nitrogen lone pair via the arene ring to the carbene carbon was reflected in, amongst other properties, the deshielding of the methyl protons of the NMe_2 group. The methyl chemical shift values were

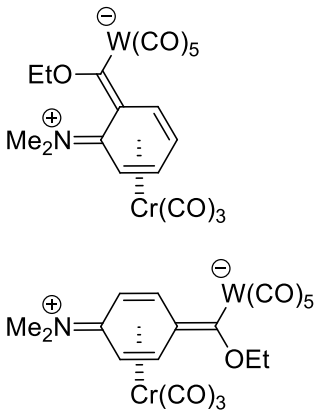

Scheme 2.5. π-Resonance effects *o*- and *p*-isomers of A1a and A1c

position-related and became more deshielded as the carbene substituent moved further away going from *o*- to *m*- to *p*-position in the aniline ring.

Table 2.1. ^{1}H NMR (*J*/Hz) assignments of compounds A1a – A1d recorded in $CDCl_3$ at 298 K

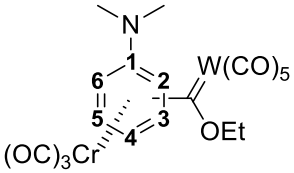

	A1a	**A1b**	**A1c**	**A1d**
NMe_2	2.71	2.97	3.01	3.66, 3.45
H_2	–*	5.53	4.87 (d, *J*=7.7)	–*
H_3	5.31 (d, *J*=6.9)	–*	6.34 (d, *J*=7.7)	5.85 (d, *J*=6.7, 0.9)
H_4	4.89 (dd, *J*=7.0, 6.2)	5.48 (d, *J*=6.6)	–*	5.34 (dd, *J*=7.1, 6.5)
H_5	5.54 (ddd, *J*=7.1, 6.1 1.4)	5.57 (dd, *J*=6.8, 7.3)	6.34 (d, *J*=7.7)	5.54 (ddd, *J*=7.2, 6.6, 0.9)
H_6	4.96 (dd, *J*=6.4, 1.4)	5.05 (d, *J*=7.0)	4.87 (d, *J*=7.7)	5.72 (d, *J*=6.8)
CH_2 (OEt)	5.04 (q, *J*=7.1)	5.08 (q, q *J*=7.0)	4.93 (q, *J*=7.1)	5.04, 4.96 (q, q, J = 7.1)
CH_3 (OEt)	1.78 (t, *J*=7.1)	1.70 (t, *J*=7.1)	1.65 (t, *J*=7.0)	1.70 (t, *J*=7.1)

* C_{ipso} to carbene substituent

The ^{1}H and ^{13}C NMR data of complexes **A1a** – **A1d** recorded in $CDCl_3$ are reported in Table 2.1 and Table 2.2 respectively. The focus of the discussion will remain on the chelate, **A1d**, and how it compares with the unchelated complex of **A1a**. A superimposition of the two ^{1}H NMR spectra recorded at 298 K in $CDCl_3$ are shown in Figure 2.1.

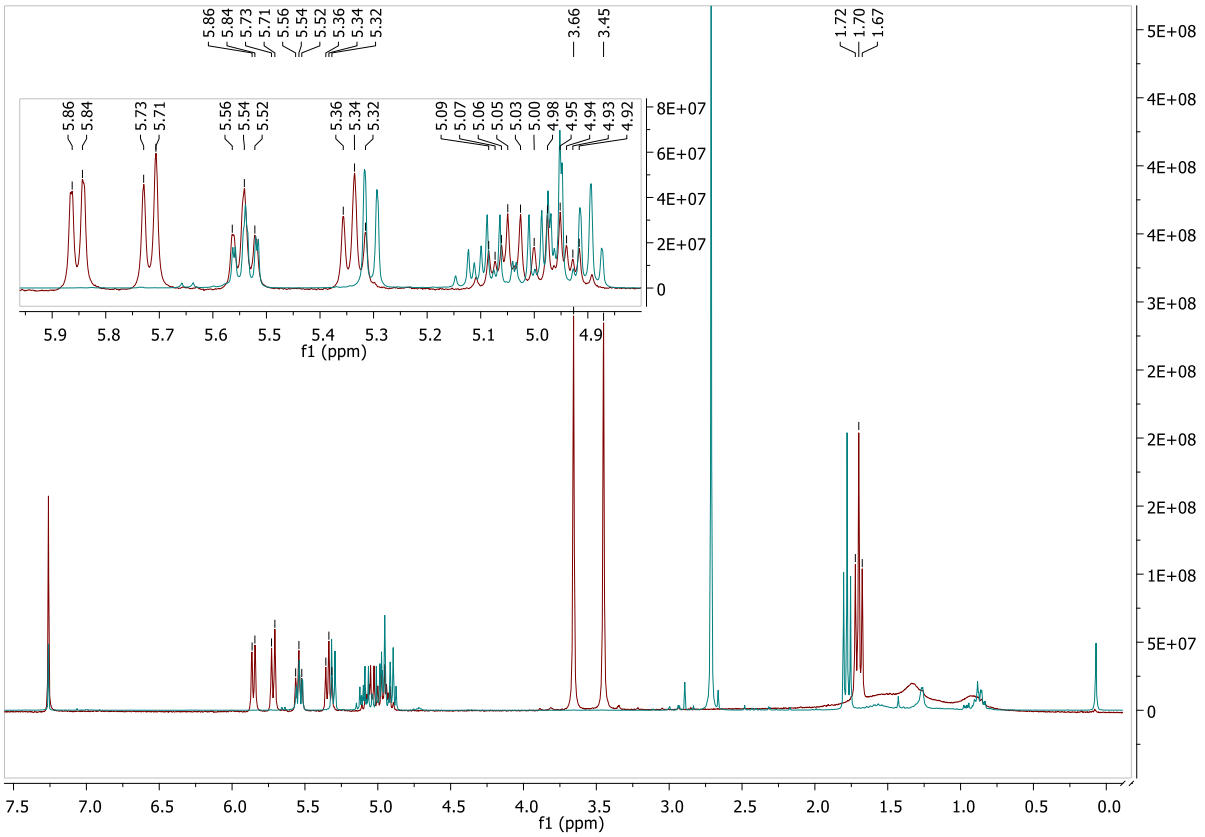

Figure 2.1. ^{1}H NMR spectra of A1a (blue) and A1d (red) in $CDCl_3$ at 298 K

In **A1a** (as well as **A1b** and **A1c**), the carbene carbon relies on electron density provided by the ring and the ethoxy substituent of the carbene carbon for its stabilisation. The resulting effect is that the electron lone pair present on the nitrogen atom is drawn into the ring and used for stabilisation of the carbene carbon. The effect is absent for **A1d** where the electron density is used for coordination to the tungsten tetracarbonyl group. This is evident in Figure 2.1 with a clear deshielding of the aromatic protons when the nitrogen is coordinated to the $W(CO)_4$ group (**A1d**). Further, the methyl ^{1}H NMR chemical shift value of the ethoxy group is found slightly upfield for **A1d** compared to **A1a** (1.70 and 1.78 ppm respectively). This is indicative that the carbene carbon of **A1d** requires less electron density from its ethoxy substituent upon coordination of the dimethylamino substituent to the tungsten carbonyl group.

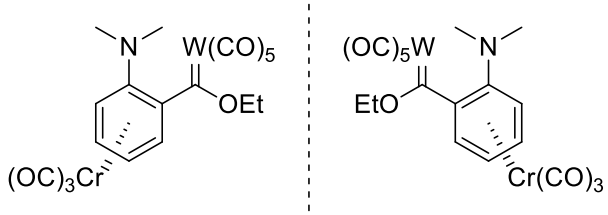

Figure 2.2. Graphical representation of the planar chirality observed for A1a

Another significant difference between **A1a** and **A1d**, is the large downfield shift of the NMe_2 methylene signals for **A1d** where two signals are observed rather than one (as for all unchelated complexes): one methyl will point towards the side with the $Cr(CO)_3$ moiety while the other methyl will point to the open side of the arene ring, thus giving two different chemical shift values. There is a clear deshielding effect upon coordination of the nitrogen to the tungsten carbonyl group. Further, the CH_2 groups display multiplicity beyond the quartet which is expected. This is ascribed to planar chirality, caused by the coordination of the $Cr(CO)_3$ group to the aromatic ring, in both complexes as displayed for **A1a** in Figure 2.2.

Table 2.2. ^{13}C NMR assignments of compounds A1a – A1d

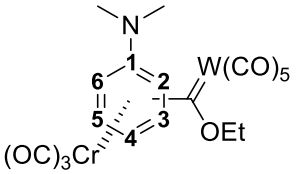

	A1a	A1b	A1c	A1d
C (carbene)	320.4	311.0	302.9	305.1
NMe_2	43.9	40.0	40.0	64.2, 57.3
C_1	114.9	115.1	105.6	110.2
C_2	125.8*	78.9	73.1	137.3*
C_3	83.1	133.1*	99.5	90.3
C_4	82.2	86.3	136.8*	83.2
C_5	94.6	94.3	99.5	91.2
C_6	91.6	75.5	73.1	84.3
CH_2 (OEt)	81.2	80.2	79.2	79.3
CH_3 (OEt)	14.5	14.9	15.1	15.1
$Cr(CO)_3$	234.0	234.4	231.9	230.5
$W(CO)_5$	203.5 (*trans*)	202.4(*trans*)	202.1 (*trans*)	–
	196.6 (*cis*)	197.1(*cis*)	197.3 (*cis*)	
$W(CO)_4$	–	–	–	222.0
				213.0
				205.6
				203.5

* C_{ipso} to carbene substituent

In **A1d** the carbene carbon has a chemical shift value of 305.1 ppm compared to that of **A1a** with a value of 320.5 ppm, clearly showing an increased stabilisation of the carbene complex because of the chelate ring. The two methyl ^{13}C NMR chemical shift values of the dimethylaniline substituent in **A1d** are found significantly downfield (64.2 and 57.3 ppm) compared to **A1a** (43.9 ppm). These shifts are a direct result of the nitrogen lone pair being coordinated to the W centre. Indirectly this means that the nitrogen donor atom will increase the electron density on W which will lead to greater backbonding to the carbene carbon affording better stabilization. The electronic contribution of the arene ring towards the stabilisation of the carbene substituent upon chelation is found in a common shared double bond of the arene and chelate ring. This leads to a small upfield shift in the chemical shifts of $Cr(CO)_3$ group: 230 ppm (**A1d, A2c**) vs 232-234 ppm (**A1a-A1c, A2a** and **A2b**) in their ^{13}C NMR spectra. This suggests that electron localisation in the chelate ring is a contributing factor in the stabilisation of the *o*-carbene complex. It is likely that crowding has a greater effect in **A1a**, resulting in poor overlapping of orbitals and subsequent distortion of the arene ring. However, upon coordination of the amine to the tungsten carbonyl, the structure becomes more rigid and the orbitals become better aligned so that the carbene complex can be stabilised with more electron density from the aromatic ring.

An electrochemical study by the research group of Landman was conducted on several tungsten carbonyl Fischer carbene complexes where a carbonyl group was substituted with a phosphine ligand. In each case the metal is oxidised at lower positive potentials when the phosphine ligand is coordinated to the metal centre while the carbene carbon is reduced at more negative potentials compared to their unsubstituted analogues.[33] This shows that upon substitution of a carbonyl ligand with a stronger electron donating ligand, more electron density is provided to the metal and subsequently the carbene carbon. Hence, the metal is more easily oxidised while the carbene carbon becomes more difficult to reduce. Should this trend hold for π-coordinated arenes with

carbene substituents, the carbene carbon in **A1d** is more stabilised upon substitution of a carbonyl ligand with the more electron-rich dimethylamine ligand.

The compounds formed from **A2** are electronically different from those formed from **A1**. In this case the methoxy substituent is less electron donating (π-resonance) and strongly electron withdrawing (σ-inductive) compared to the dimethylamine substituent. Also, the carbene complexes isolated from the synthesis with **A2** are different, yet their NMR spectra are remarkably similar. The ^{1}H and ^{13}C NMR data of the carbene complexes **A2a** – **A2c** are listed in Table 2.3 and Table 2.4 respectively.

Table 2.3. ^{1}H NMR chemical shift values (ppm) of compounds A2a – A2c in $CDCl_3$ (J/Hz)

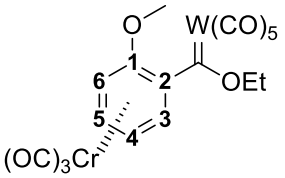

	A2a	A2b	A2c
OCH_3	3.63	3.72	4.50
H_3	5.17 (d, *J*=6.1)	5.29 (dd, *J*=6.2, 1.3)	6.27 (d, *J*=6.3)
H_4	5.00 (d, *J*=6.3)	4.81 (ddd, *J*=6.7, 6.2, 0.8)	4.91 (dd, *J*=6.8, 6.1)
H_5	5.17 (d, *J*=6.1)	5.60 (ddd, *J*=6.8, 6.2, 1.3)	5.78 (dd, *J*=6.8, 6.2)
H_6	–	5.01 (dd, *J*=6.9, 0.5)	5.38 (d, *J*=6.7)
CH_2 (OEt)	5.01-4.93 (m)	4.98 (dq, *J*=7.1, 1.4)	5.01 (dq, *J*=9.7, 7.2)[a]
CH_3 (OEt)	1.76 (t, *J*=7.1)	1.76 (t, *J*=7.1)	1.69 (t, *J*=7.1)

A2a contains two Fischer carbene groups in *o*-positions and because of the molecular symmetry, are identical, yielding a diastereo-isomer without planar chirality which causes simplified NMR spectra. **A2b** and **A2c** give four distinct proton signals for the arene ring, all in a 1:1 ratio – indicating the presence of a single carbene group in the *o*-position relative to the methoxy

substituent. All the synthesised complexes show multiple sets of CH_2-signals representing the ethoxy group which is a substituent to the carbene carbon. The multiplicity observed can be ascribed to planar chirality as a result of the coordination of the ring to the $Cr(CO)_3$ group. **A2c**, because of the chelate ring and the coordination the oxygen, also becomes is chiral. Different conformation of the carbene groups relative to the methoxy substituent of the arene ring is also possible. Figure 2.3 shows the superimposed ^{1}H NMR spectra of **A2b** and **A2c** where the methoxy substituent is uncoordinated and coordinated respectively.

Table 2.4. ^{1}H NMR chemical shift values (ppm) of compounds A2a – A2c in $CDCl_3$ (J/Hz)

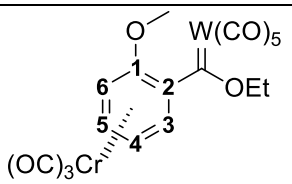

	A2a	A2b	A2c
C (carbene)	315.4	315.7	304.1
OMe	65.0	55.8	67.8
C_1	128.7	136.6	122.7
C_2	119.6*	117.8*	114.7*
C_3	89.3	91.0	88.4
C_4	81.1	81.6	79.6
C_5	89.3	94.6	93.3
C_6	119.6*	71.7	73.4
CH_2 (OEt)	81.2	81.0	84.8
CH_3 (OEt)	14.6	14.5	15.3
$Cr(CO)_3$	232.3	232.6	230.0
$W(CO)_5$	203.5 (*trans*)	203.9 (*trans*)	–
	196.2 (*cis*)	196.6 (*cis*)	
$W(CO)_4$	–	–	219.7
			217.2
			214.2
			210.1

*C_{ipso} to carbene substituent.

A downfield shift of the aromatic protons is observed upon coordination of the methoxy substituent to the tungsten, indicating a reduced amount of electron density present on the arene ring. The protons at the positions of the ring closest to the carbene substituent, show the greatest

downfield shift upon chelation ($\Delta\delta = 0.7$ ppm), thus indicating more electron density was present at these positions prior to chelation. The greatest difference observed in the spectrum is the downfield shift of the methoxy chemical shift value which appears at 3.72 ppm for **A2b** (before chelation) and 4.50 for **A2c** (after chelation). The electron density of the oxygen which initially shielded the methoxyl group, is used for coordination to the tungsten.

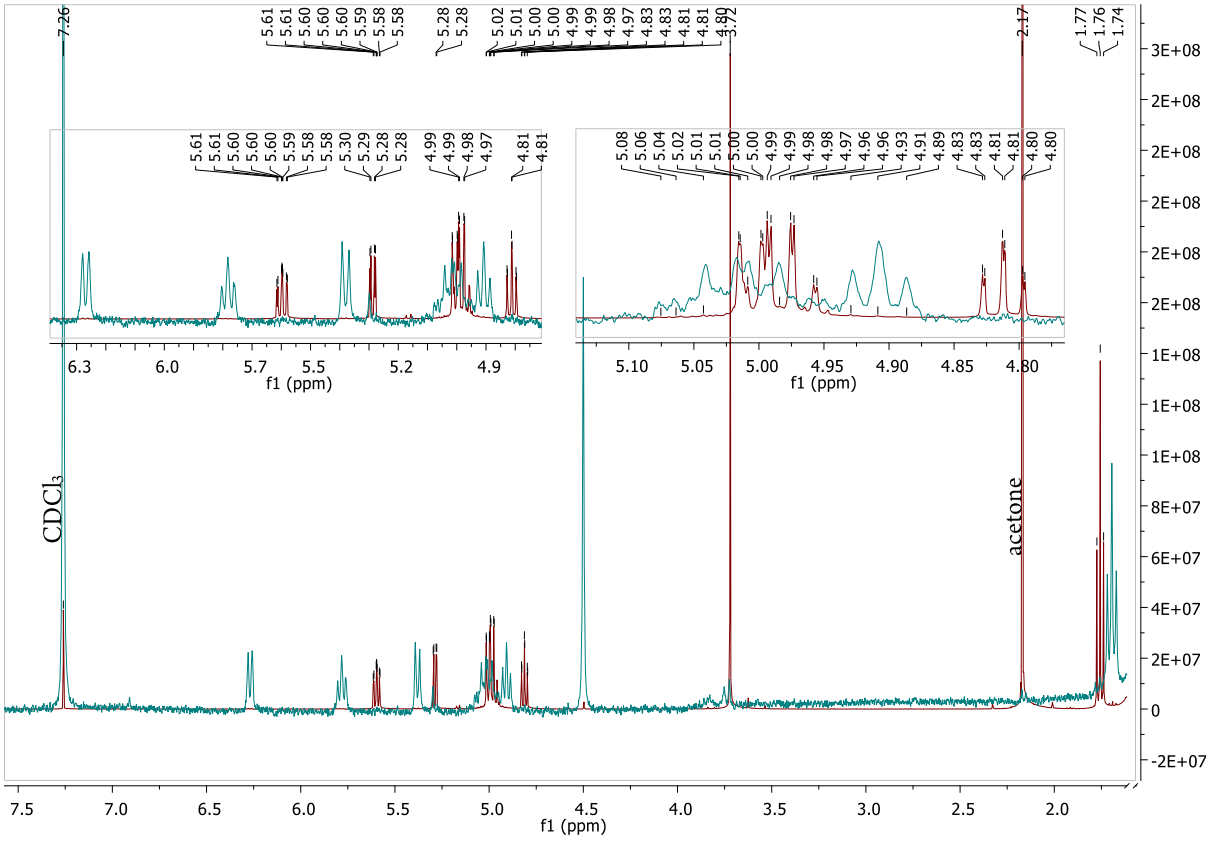

Figure 2.3. ^{1}H NMR spectra of A2b (red) and A2c (blue) in $CDCl_3$ at 298 K

Complex **A2a** represents a symmetrically substituted benzene ring with two carbene moieties adjacent to the methoxy substituent. The complex lacks planar chirality and thus displays well-resolved signals. The arene ring is subjected to the withdrawing of electron density by coordination of the $Cr(CO)_3$ fragment and the electron withdrawing features of two carbene carbons and one methoxy substituent. Thus, the two carbene groups will likely compete.

Furthermore, with two bulky carbene moieties close to each other and adjacent to the methoxy substituent, and a $Cr(CO)_3$ fragment on one side of the ring: steric constraints will undoubtedly lead to molecular distortions which will affect the electronic properties of the arene ring. Unlike **A2a**, complex **A2b** has an unsymmetrically substituted benzene ring which displaying planar chirality (as illustrated for **A1a** in Figure 2.2). It has less electron withdrawing substituents in a less crowded environment and greater freedom of atomic movements in the molecule is possible. For these reasons, it becomes difficult to draw conclusions or compare electronic situations based on chemical shift values in the NMR spectra between **A2a** and **A2b**.

The only comparable difference between **A2a** and **A2b** in the ^{13}C NMR spectra is the 10 ppm downfield shift of the methoxy signal of **A2a** compared to **A2b**. **A2a** further shows increased shielding of the arene carbon carrying the methoxy substituent with a chemical shift value of 128.7 ppm compared to 136.6 ppm for **A2b**. These observations may indicate that the lone pair of electrons present on the oxygen is more delocalised for **A2a** than **A2b**.

A general comparison between the derivatives of **A1** and **A2** can be made in terms of the site reactivity and post-synthetic stabilisation of the carbene complexes. **A2** react such that carbene substituents are found only on the *o*-positions of the arene ring and can accommodate more than one carbene group per complex. The derivatives of **A1** have a single carbene moiety on all the different positions of the ring. By directly comparing the monocarbene derivative in the *o*-position of **A1** (**A1a**) and **A2** (**A2b**), no significant differences are observed within the spectra in terms of increased shielding of the aromatic protons. It is assumed that the dominant interaction is with the $M(CO)_3$ fragment is the same for both complexes as the dimethylamino and methoxy substituents play a less significant role in determining the chemical shifts of the arene protons. It is thus expected that **A1a** and **A2b** will appear similar, as in both cases the proximity to the arene substituent (NMe_2 or OMe) leads to poor orbital overlap between the arene ring and its substituents.

On superimposing the ^{1}H NMR spectra of the chelate complexes synthesised from **A1** (**A1d**, red) and **A2** (**A2c**, blue) it is possible to directly compare coordination effects of the N,N-dimethylamino and methoxy substituents as well as the stabilisation of the carbene substituents (Figure 2.4). There is no significant difference observed in the chemical shift values of the ethoxy substituents of the carbene carbon and the carbene carbons themselves. The greater differences are observed in the chemical shift values of the arene protons where the shielding and deshielding effect is greater for **A2c** than for **A1d**. The *ipso*-carbon carrying the carbene substituent is significantly deshielded in **A1d** compared to that of **A2c** with ^{13}C NMR chemical shift values of 137.3 and 114.7 ppm respectively.

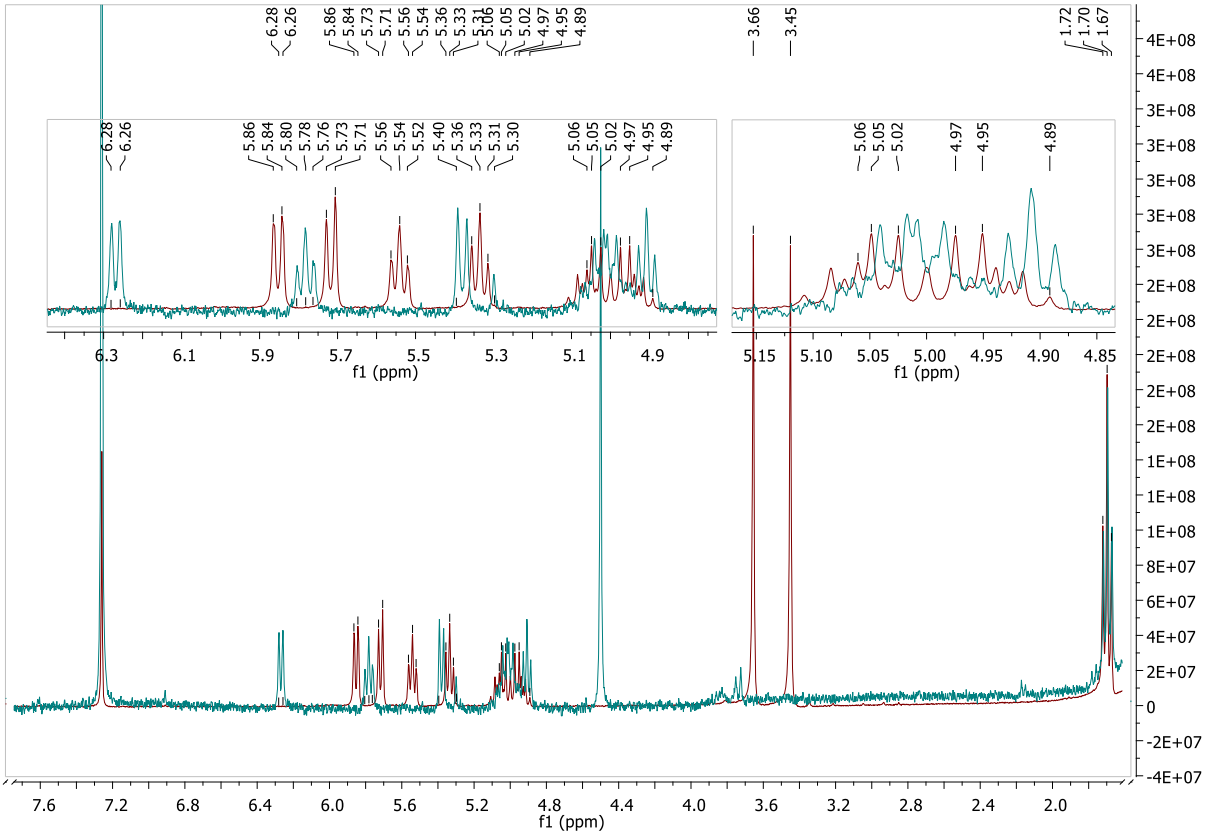

Figure 2.4. ^{1}H NMR spectra of A1d (red) and A2c (blue) in $CDCl_3$ at 298 K

To determine the overall effect that the π-coordination of the N,N-dimethyl aniline and anisole ring to $Cr(CO)_3$ will have on the tungsten Fischer carbene complexes, the complexes with the

carbene substituent in the *o*-position can be compared to the uncoordinated compounds published by Neumann and Dötz respectively.[34,35] The differences on the Fischer carbene complexes and their substituents are listed in Table 2.5.

Table 2.5. ^{13}C chemical shift values of selected carbons of I[34], A1a, A2b and II[35]

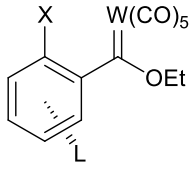

I: X = NMe_2, L = n.a.*
A1a: X = NMe_2, L = $Cr(CO)_3$
A2b: X = OMe, L = $Cr(CO)_3$
II: X = OMe, L = n.a.*

	δ – ^{13}C (ppm)				
	$W{=}C_{carbene}$	*cis*-CO	*trans*-CO	CH_2 (OEt)	CH_3 (OEt)
I[34]	330.4	196.4	203.6	78.1	13.1
A1a	320.5	196.6	203.4	82.2	14.5
II[35]	325.3	197.3	205.4	61.2	14.8
A2b	315.7	196.6	203.9	81.0	14.5

* does not contain $Cr(CO)_3$ group

The overall effect upon π-coordination of the arene ring to $Cr(CO)_3$ leads to shielding of the carbene carbon in the ^{13}C NMR spectra, with chemical shift values moving approximately 10 ppm upfield. There doesn't seem to be any major differences observed in the carbonyl chemical shifts of the metals, but there is a difference in the deshielding of the methylene protons of the ethoxy substituents of the carbene carbons upon π-coordination. It must then be concluded that upon coordination, the ethoxy substituent greatly compensates to a greater extent for electron density at the carbene carbon. Hence, using the π-electron density for the coordination to $Cr(CO)_3$, the carbene carbon must now rely more on the heteroatom for its stabilisation. This study shows that tungsten carbene complexes' stabilisation also occurs from the aromatic ring to which it is a substituent.

2.2.3 *Infrared Spectroscopy*

A prominent feature of any carbonyl system is its carbonyl IR pattern which can be observed and monitored for any metal carbonyl complex or fragment. In this study three different carbonyl patterns are observed for the synthesised complexes: The $W(CO)_5$ groups of the standard carbene complexes, a $W(CO)_4$ group of the chelated compounds (**A1d** and **A2c**) and the $Cr(CO)_3$ group to which all the complexes are π-coordinated. Table 2.6 lists the assigned peaks for all the compounds. **A1d** and **A2c** are listed separately as they contain a $W(CO)_4$ group rather than a $W(CO)_5$ group.

Table 2.6. Carbonyl FTIR assignments of complexes A1a – A1d and A2a – A2c in hexane

	$Cr(CO)_3$, υCO (cm^{-1})		$W(CO)_5$, υCO (cm^{-1})			
	A_1	E	$A_1^{(1)}$	B_1	$A_1^{(2)}$	E
A1a	1982 (s), 1972	1906, 1896	2072	2004 (w)	1960 (m)	1952 (s), 1936 (s)
A1b	1972 (s)	1908 (br)	2068	1984 (w)	1954 (sh)	1944 (s)
A1c	1968 (s)	1896 (s), 1890 (s)	2068	1982 (w)	1948 (s)	1940 (br)
A2a	1983 (w)	1909 (w)	2079	1999 (w)	1955	1969 (vs)
			2073 (w)	1991 (vw)	1918 (w)	1934 (s)
A2b	1979 (s)	1912 (s)	2073	1989 (w)	1936 (s)	1961 (vs)
	$Cr(CO)_3$, υCO (cm^{-1})		$W(CO)_4$, υCO (cm^{-1})			
	A_1	E	$A_1^{(1)}$	$A_1^{(2)}$	B_1	B_2
A1d	1983 (vs)	1926 (s)	2027	1942	1916	1873
A2c	1983 (s)	1908 (br)	2033 (w)	1940 (w)	1919 (br)	1873 (br)
	1974 (w)		2025 (vw)	1932 (w)		

Assignments are complicated by overlapping signals and are made according to the following guidelines: (i) Characteristic peak patterns of metal carbonyl symmetries for $M(CO)_n$ (n = 5, 4, 3) and wavenumbers of similar complexes, (ii) deconvoluted IR spectra (Appendix) to give an idea of overlapping bands and (iii) wavenumber shifts as a result of metal oxidations (*vide infra*) Examples of well-resolved bands and readily assignable spectra are **A1b** and **A1d** (Figure 2.6). In **A1b** the bands of the $W(CO)_5$ fragment are clearly separated from that of the $Cr(CO)_3$ fragment with $A_1^{(1)}$, B_1, $A_1^{(2)}$ and E bands at expected wavenumbers 2068(m), 1984(w), 1954(s,sh) and

1944(vs) cm^{-1} for $W(CO)_5$, respectively, while the A_1 and E bands of $Cr(CO)_3$ are observed at 1972(s) and 1908(s) cm^{-1}, respectively. **A1c** displays the same features but with the intensities of the bands of the $Cr(CO)_3$ fragment much stronger than those of the $W(CO)_5$ fragment. Band assignments in **A1d** are simplified by well resolved bands for both the $Cr(CO)_3$ and $W(CO)_4$ fragments. Some overlapping of the $A_1^{(2)}$ (1942 cm^{-1}) and B_1 (1916 cm^{-1}) bands of the $W(CO)_4$ group with the E band (1926 cm^{-1}) of the $Cr(CO)_3$ group, is evident. In **A2a**, the two $W(CO)_5$ fragments result in a duplication of bands and are much stronger in intensity than the $Cr(CO)_3$ bands which are also duplicated. **A2b** also displays the same features but with the $A_1^{(2)}$ (1961 cm^{-1}) and E (1936 cm^{-1}) bands distorted because of overlapping (Figure 2.7 below).

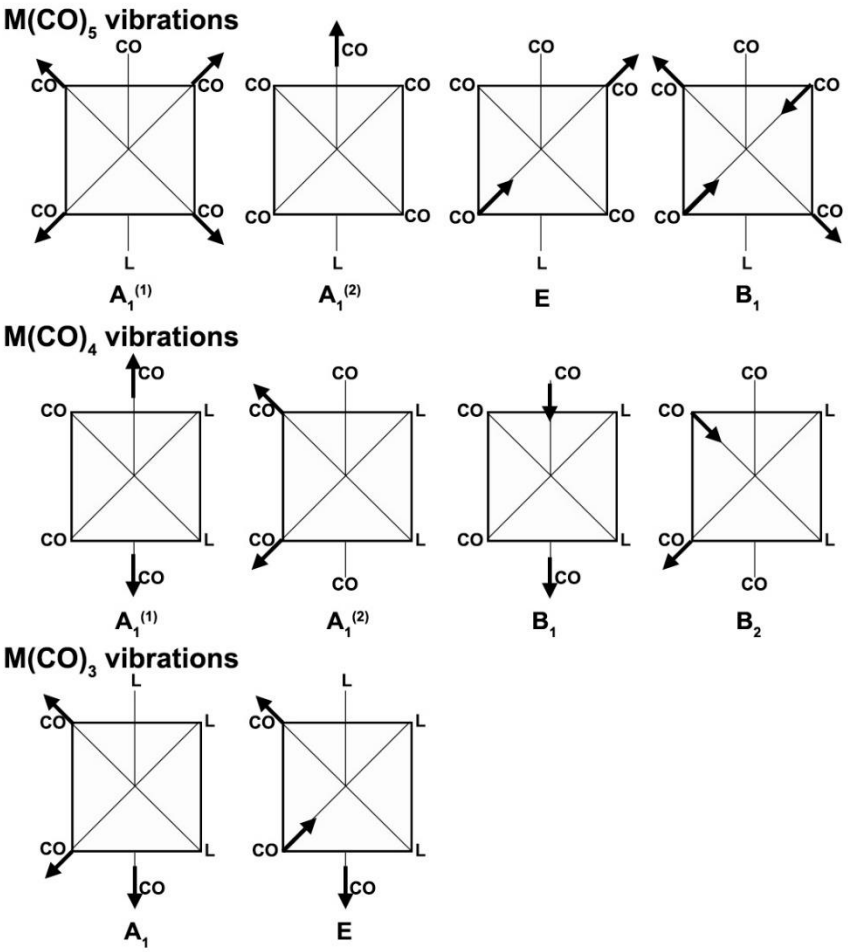

Figure 2.5. Carbonyl IR vibration modes for $M(CO)_5$, *cis*-$M(CO)_4$ and *fac*-$M(CO)_3$ groups

It is necessary to emphasise that the $A_1^{(2)}$ bands and E bands for the $W(CO)_5$ group of **A2a** and **A2b** (Figure 2.7) are assigned in a different order than what is usually expected for $W(CO)_5$ carbene complexes in hexane. Such an assignment takes into consideration relative peak intensity of the overlapping $A_1^{(2)}$ and E bands and poorer π-acceptor ligands such as amines, etc. In literature, support is found in an article by Dötz in 1988 – who synthesised tungsten pentacarbonyl carbene complexes of anisole and measured the IR spectra in pentane.[35]

Figure 2.5 gives the vibrational modes and symmetry assignments of the peaks for each metal carbonyl grouping. The complexes synthesised from **A1** and **A2** will be discussed in terms of the directing properties of the substituents of the arene rings, followed by a general comparison. It is necessary to emphasise that in Fischer carbene complexes, the role of the aryl substituent is generally small compared to that of the metal and ethoxy substituent for the stabilisation of the electrophilic carbene carbon. In all cases the small peak observed for the B_1 band for the $W(CO)_5$ group, which is formally infrared-inactive, becomes visible at times when the asymmetry of the carbene ligand lifts the selection rules.[36]

For the π-coordinated N,N-dimethylamine derivatives (**A1**) it is expected that the $W(CO)_5$ stretching frequencies will be largely influenced by the amount of electron density left available for the stabilisation of the carbene carbon by the arene ring after bonding to the $Cr(CO)_3$ group, on a competitive basis. Based on the IR data of the $W(CO)_5$ fragment, the isomers at the *m*- and *p*-positions (**A1b** and **A1c**) are very similar – the E bands for the respective complexes are observed at 1944 and 1940 cm^{-1}. There is a general move to higher wavenumbers for the $W(CO)_5$ bands in **A1a**, which indicates greater π-backbonding from the metal to the carbene ligand. This is supported by the NMR spectra of the compound which shows decreased stabilisation of the carbene complex by the arene ring. Also, there are differences in the carbonyl vibration frequencies of the $Cr(CO)_3$ group of **A1a** – **A1c**, with wavenumbers decreasing in the same order.

Further, for all the π-coordinated N,N-dimethylaniline carbene derivatives the E band of the $Cr(CO)_3$ group is either broad or split into two separate peaks. This effect has been explained by Orgel who notes that the aromatic system which is coordinated to the $Cr(CO)_3$ is notably different in two mutually perpendicular directions.[37] This effect is further promoted by the presence of planar chirality which exists for **A1a**, **A1b** and **A1d**.

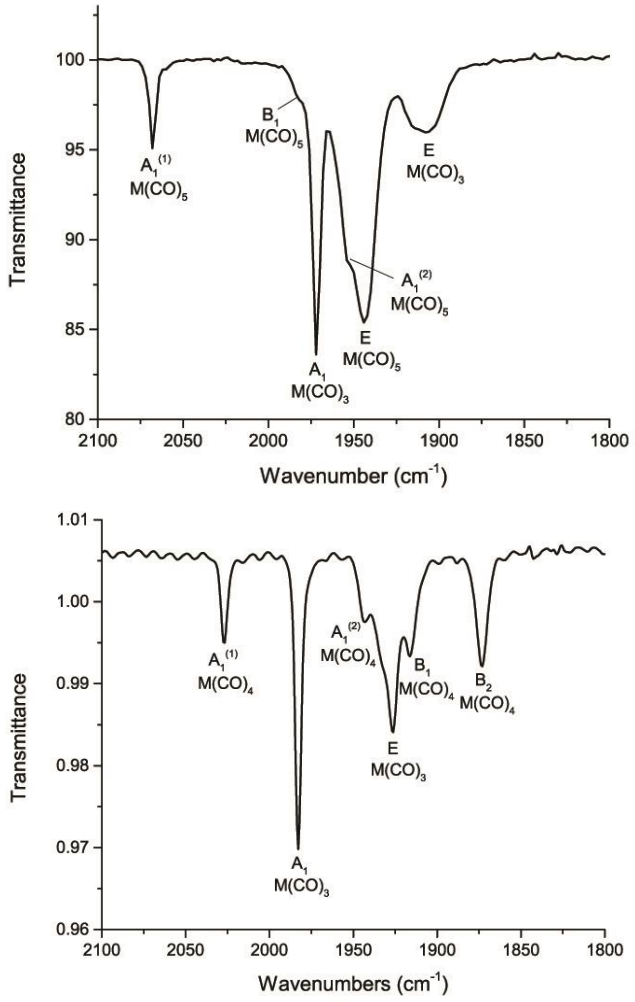

Figure 2.6. FTIR spectra A1b (top) and A1d (bottom) in hexane

There is a significant change in the $Cr(CO)_3$ group vibrational frequencies upon chelation of the nitrogen to the tungsten carbonyl group with a general shift (E-band) of ~20 cm^{-1} to higher wavenumbers, showing that there is less electron density in the arene ring for donation to the $Cr(CO)_3$ fragment. It is clear that the amount of π-electron density donated into the chelate ring by the sharing of an arene double bond, lessens the amount of electron density available for coordination to the $Cr(CO)_3$ fragment. Also, the amount of π-electron density donated into the ring by the dimethylamino substituent significantly decreases when the lone pair is used for the coordination to the tungsten carbonyl group.

The π-coordinated anisole derivatives (**A2**) represents an arene ring with less electron density in the arene ring which can be used for coordination to the $Cr(CO)_3$ group when compared to the

A1 derivatives. There is a clear difference in peak intensity between the compounds: **A2a** has very strong $W(CO)_5$ band intensities compared to its $Cr(CO)_3$ bands. This is expected as there are two carbene moieties on the arene ring which is coordinated to a single $Cr(CO)_3$ group.

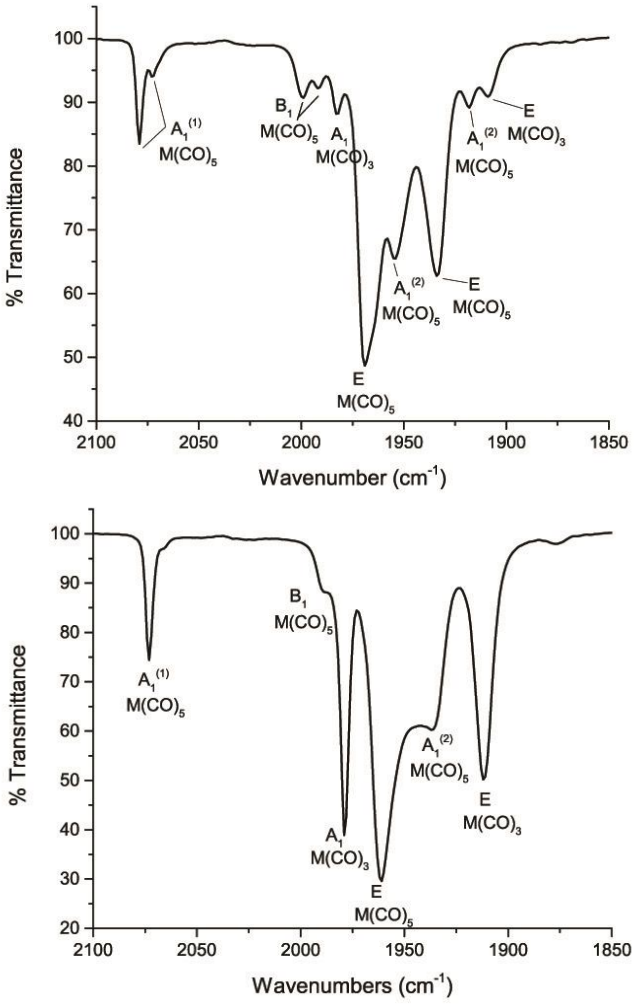

Figure 2.7. FTIR spectra A2a (top) and A2b (bottom) in hexane

There is also a clear presence of two isomers for **A2a** as seen in the bands representing the $W(CO)_5$ group in Figure 2.7 (top). The two possible conformational isomers are shown in Figure 2.8. It is anticipated that the major product will be **A2a(II)** based on steric considerations with the metal carbonyl fragments pointing towards the open side of the arene ring. The symmetry of the complex disallows the existence of planar chirality as well as the existence of two enantiomers.

In conclusion, the IR spectroscopy shows that the aromatic ring of the **A1** derivatives is slightly more electron rich that the **A2** derivatives which leads to an increased stabilisation of the carbene groups of **A1**. For **A1a**, poor orbital overlap – due to steric interactions –does not allow for the ideal alignment of the orbitals and the carbene carbon relies more on the metal and its ethoxy group for stabilisation.

There are very small differences in the IR spectra between the carbene complexes derived from **A2:** the methoxy substituent does not contribute significantly to the delocalization of electron density of the arene ring or to the stabilisation of the carbene carbons. The carbene carbons present in the **A2** derivatives rely largely on the metal to which it is coordinated and its heteroatom for stabilisation.

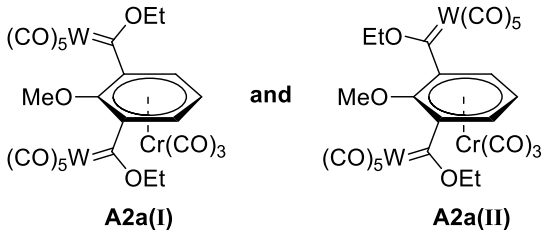

A2a(I) **A2a(II)**

Figure 2.8. Conformational isomers of A2a

2.2.4 Cyclovoltammetry

It has been shown that an aromatic ring which coordinates to $Cr(CO)_3$, does not lose its aromaticity.[38] Further, benzylic cations and anions have also been shown to be significantly stabilised upon η^6-coordination to $Cr(CO)_3$.[39]

Using cyclovoltammetry, the aim is to investigate how the compounds respond to increased or reduced amounts of electron density in the presence of a directing substituent as well as a stabilising group. Two oxidations are expected for both the **A1** and **A2** derivatives as there are numerous examples which show that a reversible oxidation occurs on the $Cr(CO)_3$ group and is largely dependent on the substituent on the arene ring while a second oxidation is possible for the tungsten carbonyl group.[40–42]

The cyclovoltammetry measurements are recorded in DCM with tetrabutylammonium hexafluorophosphate (NBu_4PF_6) as electrolyte. Inspection of the voltammograms reveal that **A1a – A1d** undergo two oxidations of which only the first one is reversible (Figure 2.10, a full analysis at different rates can be found in the Appendix). **A1d** is the only complex that shows a reversible reduction process. The derivatives of **A2** show two irreversible oxidations and one irreversible reduction (Figure 2.9). The half wave potentials of all observed processes for the derivatives of

A1 and **A2** against the ferrocene/ferrocenium or decamethylferrocene/decamethylferrocenium reference are listed in Table 2.7.

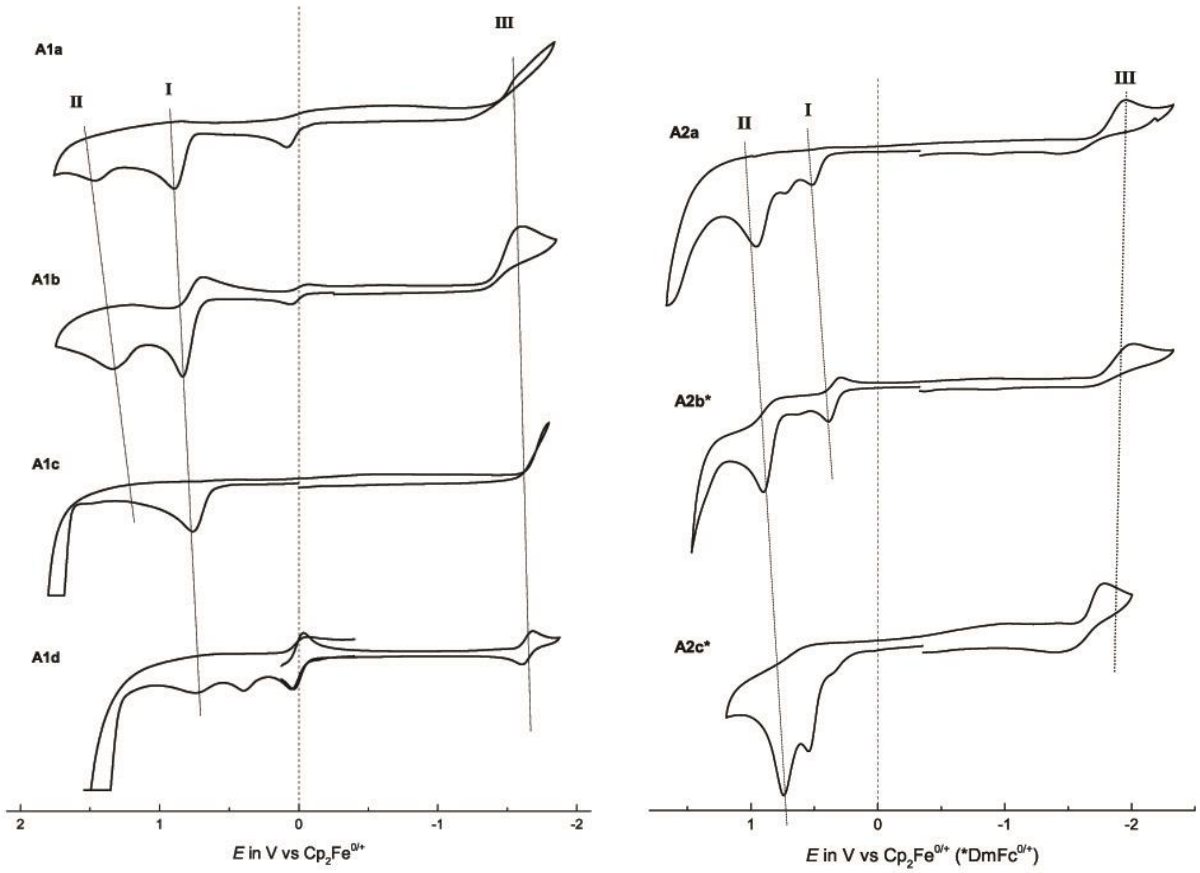

Figure 2.9. Cyclovoltammograms of A1a – A1d (left) and A2a – A2c (right) in CH_2Cl_2/0.1 M NBu_4PF_6 against the ferrocene/ferrocenium (*decamethylferrocene/decamethylferrocenium) standard at 100 mVs/s

At this stage, it is not possible to conclusively state where the oxidation or reduction centres are located within the complexes. The first oxidation potentials of **A1a** – **A1c** remain relatively constant at approximately 0.79 V while all the second oxidation potentials show significant differences between the complexes. By contrast, the second oxidation potential could vary more if dependent on the position and nature of the arene substituents.

Table 2.7. Oxidation and reduction half-wave potentials of complexes A1a – A1d and A2a – A2c in CH_2Cl_2/0.1 M NBu_4PF_6 against the ferrocene/ferrocenium standard

Complex	Ox. 1				Ox. 2	Red.			
	E_{pc}/V [i_{pc}/μA]	E_{pa}/V [i_{pa}/μA]	ΔE/V [i_{pc}/i_{pa}]	E°/V	E°/V [i_{pa}/μA]	E_{pc}/V [i_{pc}/μA]	E_{pa}/V [i_{pa}/μA]	ΔE/V [i_{pc}/i_{pa}]	E°/V
A1a	0.734 [2.00]	0.820 [2.49]	0.088 [0.80]	0.777	1.551* [3.60]	-1.562 [2.28]	–*,b	–*,b	-1.562*,b
A1b	0.725 [3.18]	0.814 [3.18]	0.089 [1.00]	0.772	1.336* [3.70]	-1.602 [3.63]	–*	–*	-1.602*
A1c	0.748 [6.75]	0.864 [6.49]	0.116 [0.96]	0.804	n.o.	-1.669*,b	–*,b	–*,b	-1.669*,b
A1d	0.376 [0.46]	0.441 [0.66]	0.065 [0.70]	0.355	0.737* [0.32]	-1.647 [0.71]	-1.532 [0.43]	0.115 [0.61]	-1.643
A2a	–*	0.519 [2.31] 0.727 [2.71]	–*	0.519* 0.727*	0.960* [5.89]	-1.951 [3.36]	–*	–*	-1.951*
A2b	0.308 [0.88]	0.384 [1.45]	0.761 [0.61]	0.346*,a	0.904*,a,b [3.49]	-2.012 [1.54]	–*	–*	-2.012*,a
A2c	–*	0.545 [2.97]	–*	0.545*,a	0.742*,a [3.79]	-1.781 [1.02]	-1.481 [0.75]	0.300 [0.76]	-1.631*,a

* Peak potential of an irreversible process at υ = 100 mV/s,
[a] against decamethylferrocene/decamethylferrocenium standard
[b] peak on limit of solvent window

It has been established in the discussion of the NMR and IR data, that the position of the carbene substituent influences the amount of electron density which the arene can donate towards the stabilisation of the carbene carbon. The first oxidation observed in the cyclovoltammetry of the **A1a** – **A1c** can be assigned as the $Cr^{0/+}$ oxidation and the second as the $W^{0/+}$ oxidation. As there are no pronounced differences between the first oxidation potentials of **A1a** – **A1c**, it shows that electron donation from the arene ring for coordination to the $Cr(CO)_3$ fragment will not be dramatically affected by substituents on the arene ring and the $Cr(CO)_3$ fragments have very similar electronic environments. In a cyclovoltammetry study of π-coordinated compounds by the research group of Hunter, the $Cr^{0/+}$ oxidation potential of the compounds are used to give an indication as to the electron density present on the $Cr(CO)_3$ group in the complexes.[40] The first oxidation of **A1a** – **A1c** occurs on the $Cr(CO)_3$ group and it is possible to state that for the **A1**

derivatives, the *o*- and *m*-isomers have more electron density present on the $Cr(CO)_3$ group compared to the *p*-isomer with respective first oxidation half wave potentials of 0.777, 0.772 and 0.804 V. From the NMR and IR data, it has been established that the *p*-carbene complex (**A1c**) receives significantly more stabilisation from the dimethylamino substituent and the arene ring. It is likely that the effect is significant enough that a reduced amount of electron density is available for π-bonding to the $Cr(CO)_3$ group as a result of steric congestion. This statement is confirmed by a similar study by Hunter, using electron donating and electron withdrawing substituents at *p*-positions relative to each other on $Cr(CO)_3$ η^6-coordinated arenes.[40] The same would have been expected for the *o*-isomer, however, it has also been determined through other spectroscopic means that the carbene substituent of **A1a** receives less electron density from the aromatic ring than expected due to poor orbital overlap between the arene ring and the carbene carbon as a result of steric congestion.

In Figure 2.10 a small shoulder band is observed for the reversible first oxidation wave of **A1c**. As **A1c** is the only compound of the **A1** derivatives that does not show a second oxidation within the solvent window, it is likely that the first and second oxidation lie over each other. It is expected that the $W^{0/+}$ oxidation will occur at a less positive potential compared to that of **A1a** and **A1b**, as it receives a significant amount of electron density from the arene group and its amino substituent. It is therefore likely that the $W^{0/+}$ and $Cr^{0/+}$ oxidation will occur at similar potentials. Thus, the oxidation potentials of the tungsten centre increase in the order of **A1c** < **A1b** < **A1a** (0.804, 1.337, 1.414 V respectively).

The low half-wave potential for the first oxidation of **A1d** (0.355 V) indicates that the likely site of oxidation is no longer the Cr centre, but rather the amine or the W centre. It is expected that the coordination of the amine to the $W(CO)_4$ group would increase the electron density present on the W centre significantly. The second oxidation potential at 0.740 V can likely be ascribed to the oxidation of the Cr centre and agrees strongly with the assigned oxidation potentials of the Cr centre of the other **A1** derivatives.

The final aspect to consider for the **A1** complexes, is their reduction potentials. The respective reduction potentials for **A1a** – **A1d** is –1.523, –1.602, –1.669 and –1.644 V. The reduction centre is likely present on the carbene carbon itself.[33,43] Assuming that this is the case, the reduction potential is indicative of the amount of electron density present on the carbene carbon – the more negative reduction potential indicates a higher electron density present on the carbene carbon. Thus, the amount of electron density on the carbene carbon increases in the order **A1a**, **A1b** and **A1c**. The carbene carbon of **A1d** has a high electron density, but not as high as that of **A1c**.

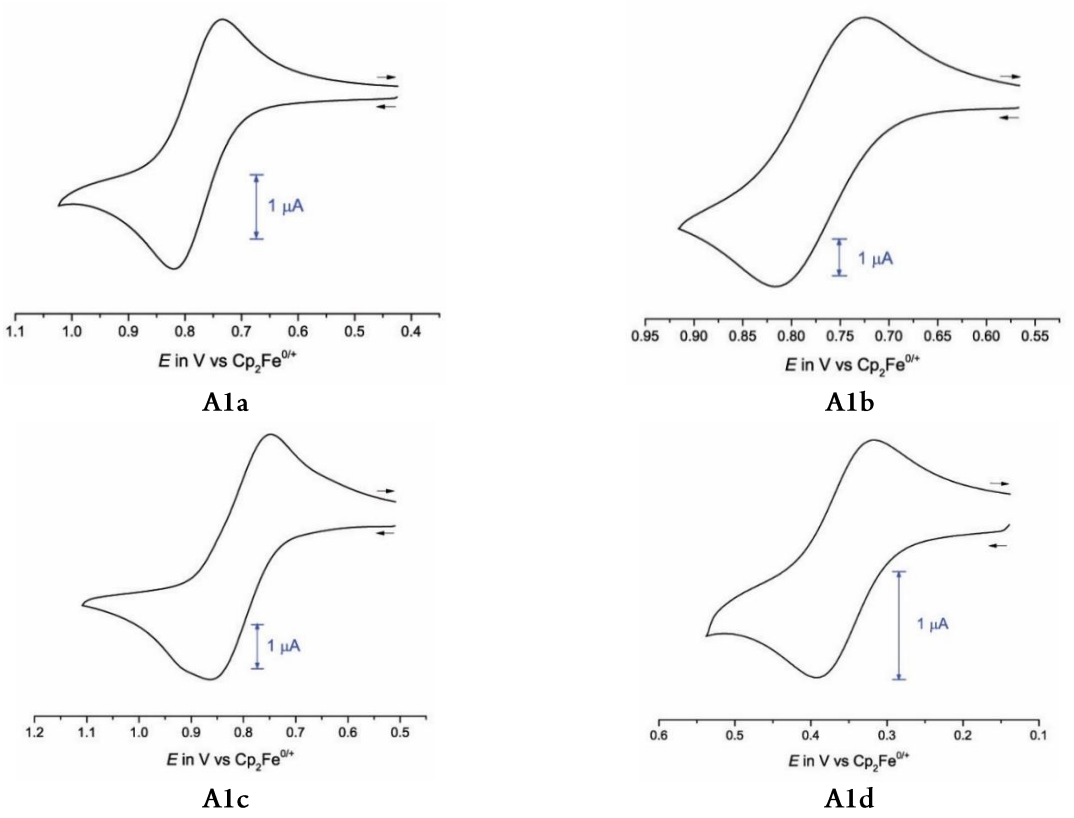

Figure 2.10. Cyclovoltammogram of the reversible oxidation of compounds A1a – A1d in CH_2Cl_2/0.1 M NBu_4PF_6 referenced against a ferrocene/ferrocenium standard

The cyclovoltammetry of the carbene complexes formed from **A2**, reveal multiple irreversible oxidation processes and a single irreversible reduction process. The cyclovoltammogram of **A2a** is shown in Figure 2.9 (top, right) and shows three irreversible oxidation processes at 0.518, 0.728 and 0.956 mV. Although the oxidation of the aromatic ring is possible, it is expected to fall outside

the solvent window.[44] The solvent is oxidised to the end of the cyclovoltammogram. The two oxidations at 0.518 and 0.728 V likely represent a single oxidation process – the $Cr^{0/+}$ oxidation. Two peaks are observed due to the presence of the conformational isomers of **A2a** shown in Figure 2.8. It is then possible to assign multielectron oxidation process at 0.956 V to the oxidation of the two tungsten carbonyl groups ($W^{0/+}$). As it appears that the oxidation processes for both groups occur at the same potential, there is no interaction between the two carbene complexes present within **A2a**. An irreversible reduction process is observed at –1.689 V. The intensity of the peak would suggest a single electron reduction process is being observed. The LUMO and the LUMO+1 orbitals are expected to have similar potentials as they are likely found on the carbene carbons – both of which do not appear to receive electron density from the ring through π delocalisation.[43] Previous studies on the reduction processes for π-coordinated compounds have shown that the LUMO of such complexes is often situated on the arene ring or its substituents, depending on the substituent of the ring.[45] In this case a single electron reduction indicates that the LUMO and LUMO+1 orbitals do not have similar potentials.

For **A2b** and **A2c** the irreversible $Cr^{0/+}$ oxidation occurs at 0.342 and 0.546 V, respectively, indicating that **A2b** is more electron rich at the site of the first oxidation than **A2a** or **A2c**. As the oxidation potential of the Cr atom is influenced by the π-electron density present on the arene ring, it becomes evident that the carbene groups (whether one or two) receive π-electron density from the ring, even if the effect is not necessarily observed in the NMR and IR spectroscopy. As the arene ring of **A2a** carries two electron-withdrawing substituents, the amount of π-electron density on the arene ring available for coordination to the $Cr(CO)_3$ group is reduced. The overall effect of the contribution of the methoxy substituent is also realised as **A2c** has the highest oxidation potential.

Surprisingly, the second oxidation of both **A2b** and **A2c** indicates a multielectron process if the $Cr^{0/+}$ is taken as a one-electron process. The second oxidation for both complexes are expected to

occur on the W atom, thus a one-electron process is expected. Unfortunately, the process is irreversible and makes it impossible to analyse the process by other spectroscopic means.

Comparing the first oxidation potentials of the **A1** and **A2** derivatives, the compounds containing the methoxy substituents are oxidised at slightly lower potentials than the compounds containing the tertiary amine substituents. As the first oxidations of most of the complexes discussed occur on the chromium centre, this would indicate that the **A2** derivatives have a slightly higher electron density present on the chromium carbonyl group than the **A1** derivatives.

2.2.5 IR Spectroelectrochemistry

Because the **A1** derivatives have reversible first oxidations, it is possible to monitor the changes that occur upon oxidation using IR spectroelectrochemistry. This technique does not only allow for the electrochemical process to be followed, but also to determine the site of oxidation.

Figure 2.11 shows the IR spectroscopic changes that occur upon oxidation of the **A1** derivatives. Two sets of IR carbonyl vibration patterns are monitored for each complex: one set representing the tungsten carbonyl group and the other the η^6-bonded $Cr(CO)_3$ group.

Upon oxidation of **A1a** – **A1c**, the bands representing the $Cr(CO)_3$ group for the complexes show a significant shift to higher wavenumbers while the bands representing the $W(CO)_5$ group remain relatively constant. The E bands of the $Cr(CO)_3$ group of **A1a** – **A1c** have values of ~1880 cm^{-1} for the neutral compounds which shift to 1950, 1939 and 1933 cm^{-1}, respectively, upon oxidation ($\Delta\nu$: 50 – 70 cm^{-1}). The same shift is also observed for the group's A_1 bands. The notable shift of the bands representing the $Cr(CO)_3$ group indicates that the oxidation occurs on the metal itself ($Cr^{0/+}$) rather than the aromatic ring or nitrogen present in the compound.[46–48]

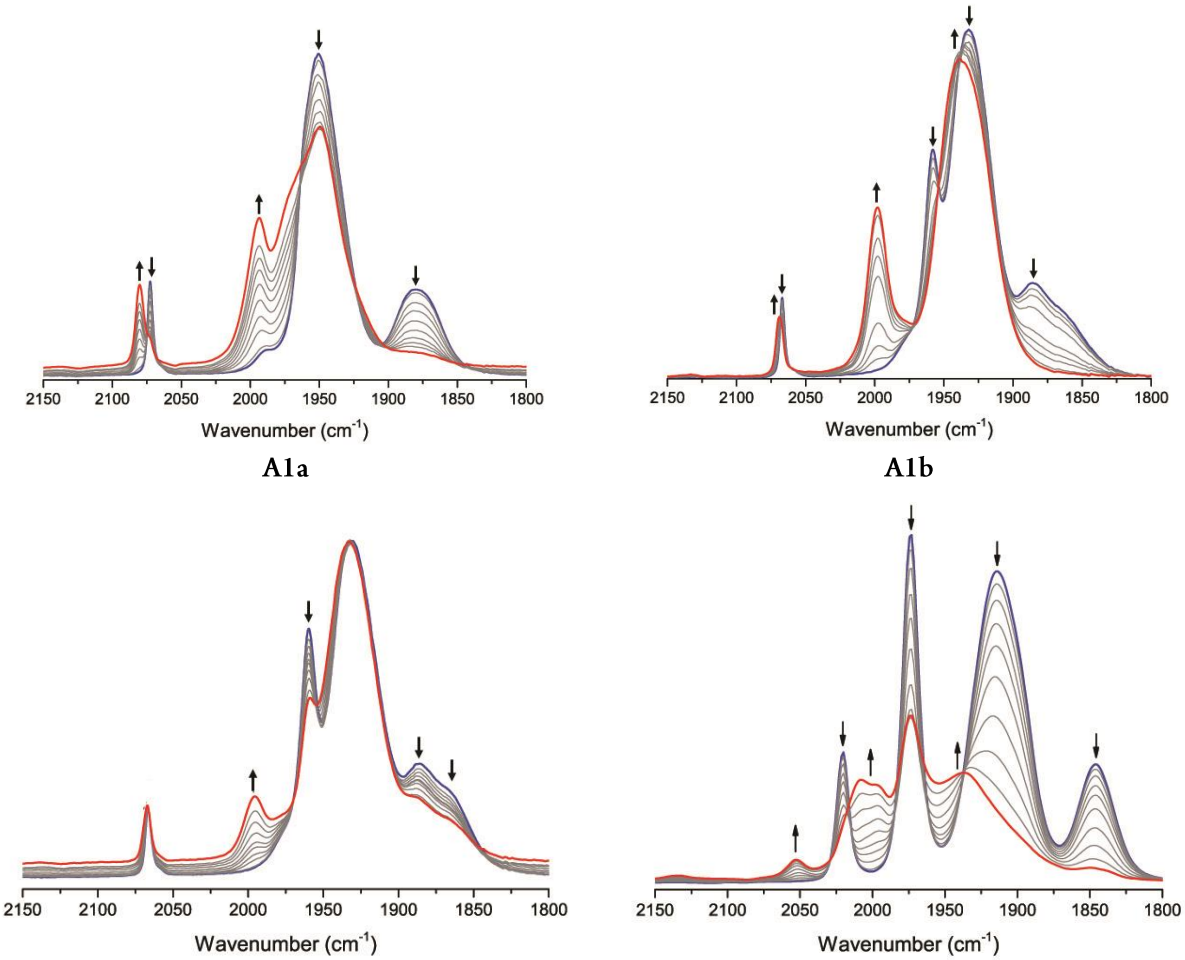

Figure 2.11. IR spectroscopic changes upon the oxidation of complexes A1a – A1d inside a OTTLE cell ($1,2\text{-}C_2H_4Cl_2/NBu_4PF_6$, RT)

Table 2.8. IR band assigments of complexes A1a – A1d (neutral and oxidised) in 1,2-$C_2H_4Cl_2$ with NBu_4PF_6 as electrolyte at 298 K

	υCO/cm^{-1} [Cr(CO)$_3$]		υCO/cm^{-1} [W(CO)$_5$]			
	A_1	E	$A_1^{(1)}$	B_1	$A_1^{(2)}$	E
A1a	1943(vs)	1880(br)	2072	1988(vw)	1943(vs)	1943(vs)
A1a$^+$	1994(s)	1950(vs)	2080	n.o.	1950(vs)	1950(vs)
A1b	1958(s)	1886(br)	2067	1977(w)	1932(vs)	1932(vs)
A1b$^+$	1998(s)	1939(vs)	2068	n.o.	1939(vs)	1939(vs)
A1c	1859(s)	1887(br)	2067	1971(w)	1930(vs)	1930(vs)
A1c$^+$	1996	1933(vs)	2067	1973(w)	1933(vs)	1933(vs)

	υCO/cm^{-1} [Cr(CO)$_3$]		υCO/cm^{-1} [W(CO)$_4$]			
	A_1	E	$A_1^{(1)}$	$A_1^{(2)}$	B_1	B_2
A1d	1973(vs)	1915(vs)	2020	1970	1918	1846
A1d$^+$	1974(vs)	1937(br)	2052	2000	1945	1896(br)

According to a review published by Berger, an electron rich substituent (i.e. NMe_2 or OMe) will donate electron density towards the Cr(CO)$_3$ group through the ring, leading to increased back donation into the π* orbitals present on the CO ligands.[19] On oxidation, the electron density present in the π* orbitals of the CO ligands (Cr(CO)$_3$ group) decreases leading to an increase in the carbonyl bond order present on the chromium. Thus, the carbonyl vibration frequencies move to higher wavenumbers as observed upon oxidation of **A1a** – **A1c** in Figure 2.11.[28] There is no significant change in the bands representing the W(CO)$_5$ group in all three complexes (**A1a** – **A1c**). This observation is unexpected and implies that the oxidation of the Cr(CO)$_3$ group does not influence the carbene moiety present at any position of the ring.

The site of the first oxidation of **A1d** is still unclear as the oxidation pattern in **A1d** is complex. All bands move to higher wavenumbers during the oxidation, but the largest change is that of the bands representing the W(CO)$_4$ group. It is clear that the $A_1^{(1)}$ band of the W(CO)$_4$ group shifts from 2020 to 2052 cm^{-1} on oxidation, while the B_2 band shifts from 1846 to 1937 cm^{-1}. The latter shift is not clear as there is significant overlap with the E band of the Cr(CO)$_3$ group. As there is

not as significant shift upon oxidation of the bands representing the $Cr(CO)_3$ group in **A1d** as there has been observed for the other **A1** derivatives, the first oxidation likely does not occur on the Cr atom. The bands that show a more significant shift are those representing the $W(CO)_4$ group. In the IR spectra of **A1d**, the bands representing the $W(CO)_4$ group show an approximate shift of between 30 – 80 cm^{-1} to higher wavenumbers. As there is no significant shift for the $Cr(CO)_3$ group and a more elaborate shift for the $W(CO)_4$ group, the likely site of oxidation is the amine coordinated to the $W(CO)_4$ group or the W atom itself. This observation corresponds well with what has been postulated for the first oxidation in the cyclovoltammetry of the compound.

2.2.6 DFT calculations

A DFT study was conducted on several of the complexes to gain further insight as to the positions where the electrochemical processes occur and to establish the orbital differences between the positional isomers of the **A1** derivatives. Visual representations of the highest occupied molecular orbital (HOMO) and lowest unoccupied molecular orbital (LUMO) of the neutral complexes of **A1a**, **A1c**, **A2b** and **A2c** are shown in Table 2.9. It is expected that the nature of the HOMO and LUMO will give insight as to where the oxidation or reduction process will occur. Also, included in the table is the visualised HOMO of the oxidised species of the same complexes (except that of **A2b**) to show where the second oxidation is likely to be expected.

Table 2.9. Graphical representations of the HOMO, LUMO and the HOMO of the oxidised complexes for A1a, A1c, A2a and A2c

Complex	HOMO	LUMO	HOMO (oxidised)
A1a	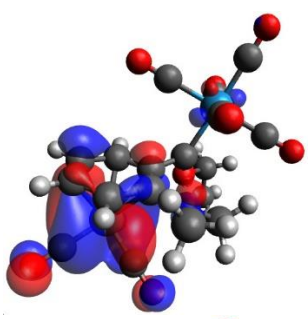	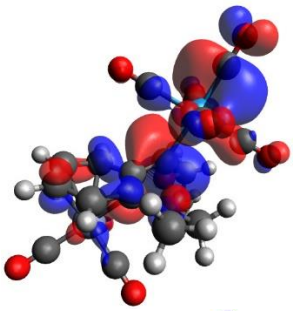	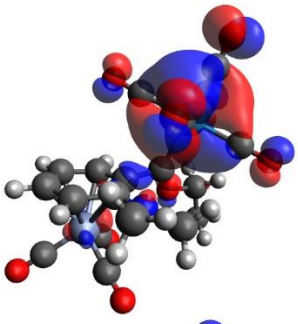
A1c	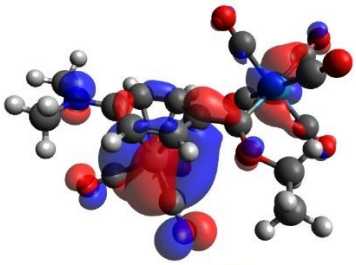	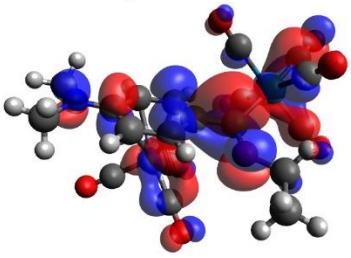	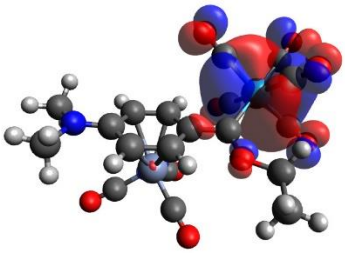
A2b	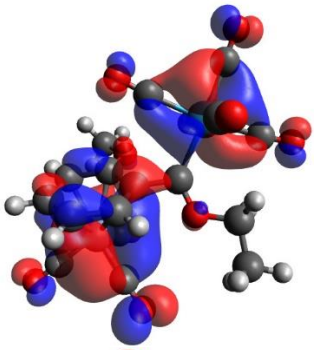	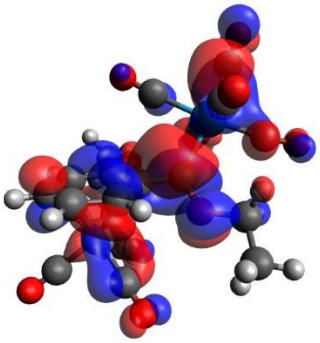	
A2c	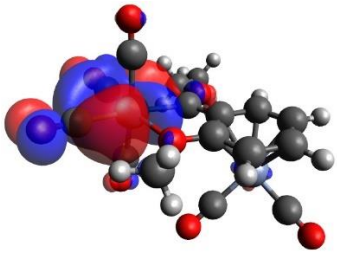	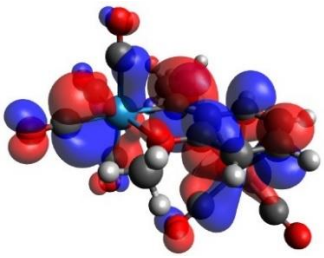	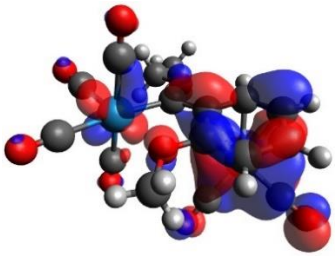

The HOMO and LUMO representations of the **A1** derivatives supports the conclusions reached in the IR-spectroelectrochemistry. The $Cr(CO)_3$ group largely makes up the HOMO in **A1a** with some contribution from the arene ring and is therefore expected to be the site where oxidation occurs. The IR-spectroelectrochemistry confirms this observation as a shift greater than 70 cm^{-1}

is observed for the E band and greater than 45 cm^{-1} for the A_1 band for the carbonyl vibrations of the $Cr(CO)_3$ group of **A1a** – **A1c**, upon oxidation. The same conclusion has been reached for **A1c**, but in this case the tungsten centre also has a small contribution to the HOMO, however, it is largely situated on the Cr atom. The LUMOs for the two neutral **A1** derivatives in Table 2.9 is mainly found on the carbene carbons as has been shown in literature.[43] This observation further supports that the reduction of **A1a**, **A1b** and **A1c** occurs on the carbene carbon as has been postulated in the cyclovoltammetry study of the complexes.

The position of the HOMO of the oxidised species is observed to be solely on the tungsten carbonyl group for **A1a** and **A1c**. This supports the postulation that the second oxidation observed for **A1a** – **A1c** occurs on the W centre.

For the **A2b**, the HOMO has significant contributions from both the Cr and W atoms. This is likely the reason why the first oxidation of the compound is irreversible. The LUMO of the compound is also located over a large section of the molecule of which the carbene carbon seems to have the greatest contribution, indicating that it is the probable site of reduction. For **A2c**, the HOMO is observed solely on the $W(CO)_4$ fragment. In the cyclovoltammetry of the compound, two irreversible oxidation waves at similar potentials were observed for the compound. It is now possible to assume that the first oxidation can be ascribed to the oxidation of the W centre while the second oxidation is likely that of the Cr atom (as the HOMO of the oxidised species is observed on the Cr group). The LUMO of the neutral species is again located largely on the carbene carbon with also a significant contribution from the arene ring.

The DFT calculations can also be used to compare orbital similarities between the positional isomers of **A1a** – **A1c**. In Table 2.10 the energy corresponding to HOMO and LUMO of each neutral complex is listed in comparison with the compounds first oxidation and reduction.

Table 2.10. Energy (eV)of the calculated HOMO and LUMO of the neutral complexes and their corresponding oxidation and reduction half wave potentials (V)

Complex	DFT Energy		Cyclovoltammetry	
	E_{HOMO}/eV	E_{LUMO}/eV	$\Delta E_{1/2}^{0/+}$/V	$\Delta E_{1/2}^{0/-}$/V
A1a	-5.666	-2.588	0.777	-1.562*
A1b	-5.620	-2.831	0.772	-1.602*
A1c	-5.741	-2.675	0.804	-1.669*
A1d	–[b]	–[b]	0.355	-1.643
A2a	–[b]	–[b]	0.519*	-1.951*
			0.727*	
A2b	-6.004	-2.335	0.346*,[a]	-2.012*,[a]
A2c	-5.794	-2.462	0.545*,[a]	-1.631*,[a]

* Peak potential of an irreversible process at υ = 100 mV/s
[a] against decamethylferrocene/decamethylferrocenium standard
[b] no DFT calculations were performed

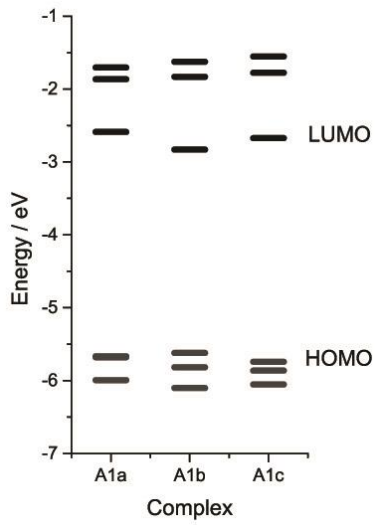

Figure 2.12. Graphical representation of the DFT calculated orbital energy levels for A1a – A1c (B3LYP/6-31G(d,p))

It is expected that the theoretical calculations match that of the physical compound such that the patterns observed during the reduction or oxidation of the complexes match that of the HOMO and LUMO. It is well established that the site of the HOMO represents the valence orbitals of any compound and is therefore also expected to be the site of oxidation. The LUMO is represented by the site of expected reduction of the complexes. A compound with a more stable HOMO (lower energy) is expected to require a more positive potential for oxidation. A LUMO that has a low energy will require a more negative potential for reduction to occur.[49]

An orbital level diagram for **A1a** – **A1c** is shown in Figure 2.12. From the HOMOs displayed for the complexes, it is expected that the *m*-isomer should be oxidised first, followed by the *o*-isomer and then the *p*-isomer. This is the pattern observed in the oxidation of the compounds in the cyclovoltammetry. As the HOMO of all three complexes is found on the Cr atom (Table 2.9), the HOMO of **A1b** is the least stable (more electron density)

and will oxidise at a lower positive potential. As has been previously discussed, this is likely caused by increased electron density on the arene ring and a smaller influence from the carbene substituent of the ring in **A1b**. The pattern does not hold true for the reduction processes. The order of reduction per the DFT calculations should be **A1b**, **A1c** and **A1a**, but the order observed in the reduction during cyclovoltammetry is **A1a**, **A1b** and **A1c**. As the reduction wave of **A1a** and **A1c** has not been clearly observed during the cyclovoltammetry due to the proximity of the solvent's reduction potential (Figure 2.9), it is very likely that this data can be erroneous.

2.2.7 X-Ray Crystallography

Single crystals for all compounds that are discussed in this chapter have been obtained by slow diffusion of hexane into dichloromethane under inert conditions at 5°C. The structures of **A1a**, **A1b** and **A1c**, which form part of this study, have been discussed a previous study.[10] A short summary of the reported data is given below and full data sets can be found in the Appendix. New data and comparative discussions are included in this study. By analysing the bond lengths, bond angles and torsion angles it becomes possible to compare and correlate solid state data with spectroscopically determined data obtained in solution. Of particular interest, are the roles played by the arene directing substituents (NMe_2 or OMe), the carbene substituents, and the $Cr(CO)_3$ fragment, in the electronic and steric properties as indicated by structural features. From the conclusions drawn from the spectroscopic data discussed throughout this part of the thesis, certain trends are expected: For the compounds in which a distant heteroatom lone pair plays a significant role (NMe_2) in the carbene carbon's stabilisation, shorter bonds are expected between the nitrogen atom and the ring as well as the ring and the carbene carbon. In such cases, a greater distance between the plane of the phenyl ring and the coordinated $Cr(CO)_3$ group is expected as there is less π-electron density in the ring to which it can coordinate. Where less stabilisation from the heteroatom is evident (OMe), the opposite is true. For the **A2** derivatives, the bond lengths between the methoxy group and carbene carbon and their corresponding *ipso*-carbons should be longer, more density in the arene ring, and the $Cr(CO)_3$ group should be closer to the plane of

ring. The physical properties of the chelated compounds (**A1d** and **A2c**), in which the distant heteroatom lone pair directly coordinates to the metal complex, are also expected to be significantly different from their uncoordinated analogues.

The bond distances and angles of the arene ring substituents as well as packing are discussed separately for the **A1** and **A2** derivatives, after which an analysis of the bond lengths and angles within the arene rings of all the complexes will follow.

A1 complexes

The three crystal structures of **A1a** – **A1c** are shown in Figure 2.13 and a complete list of their bond lengths and angles can be found in the Appendix as they have appeared in a previous study.[10]

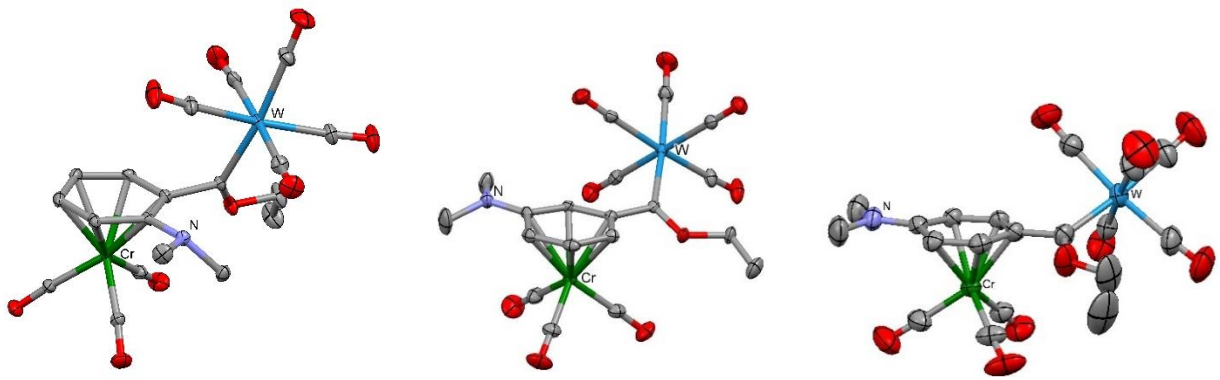

A1a **A1b** **A1c**

Figure 2.13. Solid state structures of A1a, A1b and A1c. Ellipsoids are set at 50% probability. Hydrogen atoms are omitted for clarity[10]

In summary, there were significant differences between **A1a** – **A1c** in bond lengths between the aryl ring and its substituents (as well as within the aryl rings themselves) observed, depending on the amount of electron density delocalised from the nitrogen lone pair to the carbene carbon. The effect was found to be the greatest for **A1c**. The same was expected for **A1a**, but was not observed due to poorer orbital overlap between the carbene carbon and arene ring caused by steric interactions between substituents present in the ring, next to each other. Delocalisation of electron density from the nitrogen to the carbene carbon was observed within the bond lengths

of **A1b**, but not as pronounced as that of **A1c**. For all three complexes the $W(CO)_5$ group as well as the carbene carbon were found to lie above the plane of the ring and the Cr atom was on average 1.714 Å below the plane of the ring.

The crystal structure of **A1d** is shown in Figure 2.14. On the coordination of the nitrogen atom to the tungsten carbonyl group it is expected that the amount of electron density donated towards the ring by the NMe_2 group is significantly reduced. Selected bond lengths and angles of **A1d** is listed in Table 2.11. The same bond lengths and angles of **A1a** have also been included in the table for comparison. The nitrogen lone pair in **A1d** is now involved in the coordination to the W centre and cannot directly contribute electron density to the aryl ring. This is evident from a significantly longer N–C bond distance between the dimethylamine substituent and the phenyl ring for **A1d** compared to that of **A1a** with respective lengths of 1.466(3) and 1.387(2) Å. A second indication is the shorter distance between the Cr atom and the plane of the arene ring with respective values for **A1d** and **A1a** of 1.698 and 1.709 Å.

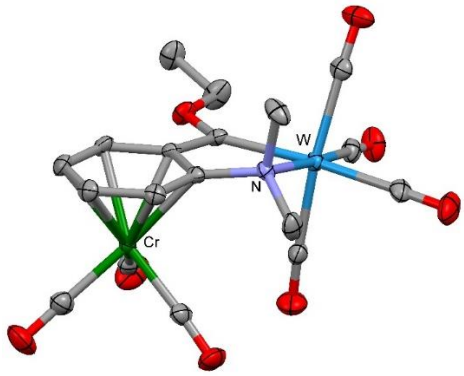

Figure 2.14. Solid state structures of A1d. Ellipsoids are set at 50% probability. Hydrogen atoms are omitted for clarity

It is not possible to accurately determine the effect of the chelation on the stabilisation of the carbene carbon, as many of the bonds within the newly formed chelate ring will be affected by ring strain. The lengths of the C(carbene)–OEt bond will give an indication as to the amount of electron density required from the metal and the arene ring for the stabilisation of the carbene carbon. The respective C–O bond lengths in **A1d** and **A1a** is 1.313(3) and 1.315(1) Å, indicating that the carbene carbon of **A1d** receives a significant amount of electron density from its heteroatom and **A1a** is also highly dependent on its heteroatom for stabilisation. Further, the C_{Ar}–C_{Carb} bond is short for **A1d** (1.482(3) Å) compared to that of the other **A1** derivatives (1.495(2) Å for **A1a**), but this is ascribed to ring strain within the chelate ring.

Table 2.11. Selected bond lengths (Å), bond angles (°) and torsion angles (°) of A1a and A1d

	A1a	**A1d**
Symmetry	P -1	P $2_1/c$
	Bond lengths (Å)	
$N–C_{Ph}$	1.387(2)	1.466(3)
$C_{Ph}–C_{carb}$	1.495(2)	1.482(3)
$C_{carb}–W$	2.167(1)	2.137(2)
$C_{carb}–O_{Et}$	1.315(1)	1.313(3)
$Ph_{plane}–Cr(CO)_3$	1.709	1.698
	Bond Angles (°)	
$C_{Ph}–C_{carb}–O_{Et}$	106.8(1)	107.4(2)
$C_{Ph}–C_{carb}–W$	119.38(8)	116.8(1)
$O_{Et}–C_{carb}–W$	131.57(9)	135.7(2)
$Me_1–N–Me_2$	111.8(1)	107.1(2)
$Me_1–N–C_{Ph}$	118.1(1)	112.6(2)
$Me_2–N–C_{Ph}$	117.3(1)	105.3(2)
$C_{carb}–W–CO_{cis}$	88.68(7)[a]	93.31(9)
$C_{carb}–W–CO_{trans}$	170.55(6)	168.14(9)
	Torsion angles (°)	
$C_{Me(1)}–N–C_{ipso}–C_{Ph}$	129.6(1)	40.9(3)
$C_{Me(2)}–N–C_{ipso}–C_{Ph}$	-8.9(2)	98.2(2)
$C_{Ph}–C_{ipso}–C_{carb}–O_{Et}$	–63.9(1)	7.7(3)
$C_{Ph}–C_{ipso}–C_{carb}–W$	101.1(1)	4.2(3)

[a] average of the four bond angles

The angles surrounding the nitrogen atom is closer to 120 ° for **A1a** and is best described by sp^2-hybridization. This is ideal for π-conjugated resonance interactions. Due to N-coordination to tungsten the angles in **A1d** around the nitrogen are close to 109 ° and best described by sp^3–hybridization with no nitrogen π-interaction. There seems to be no major differences in the angles surrounding the carbene carbon in **A1a** and **A1d**, with the small differences that are observed likely ascribed to strain within the chelate ring of **A1d**. Large differences are observed in the torsion angles around the $N_{NMe2}–C_{Ph}$ and $C_{Ph}–C_{Carb}$ bonds for **A1a** and **A1d**. In **A1a** steric congestion between the dimethylamino group and the metal carbonyl fragment causes some distorsion within both bonds. Upon coordination of the amine to the tungsten, the complex becomes more rigid and it becomes evident that the carbene carbon, its heteroatom and the

tungsten atom lie in the plane of the ring. The torsion angels around the C_{Ph}–C_{Carb} bond are 7.7(3) and 4.2(3) Å, respectively, revealing no steric congestion.

See the arene ring distortion section for a discussion on the bond lengths within the arene rings.

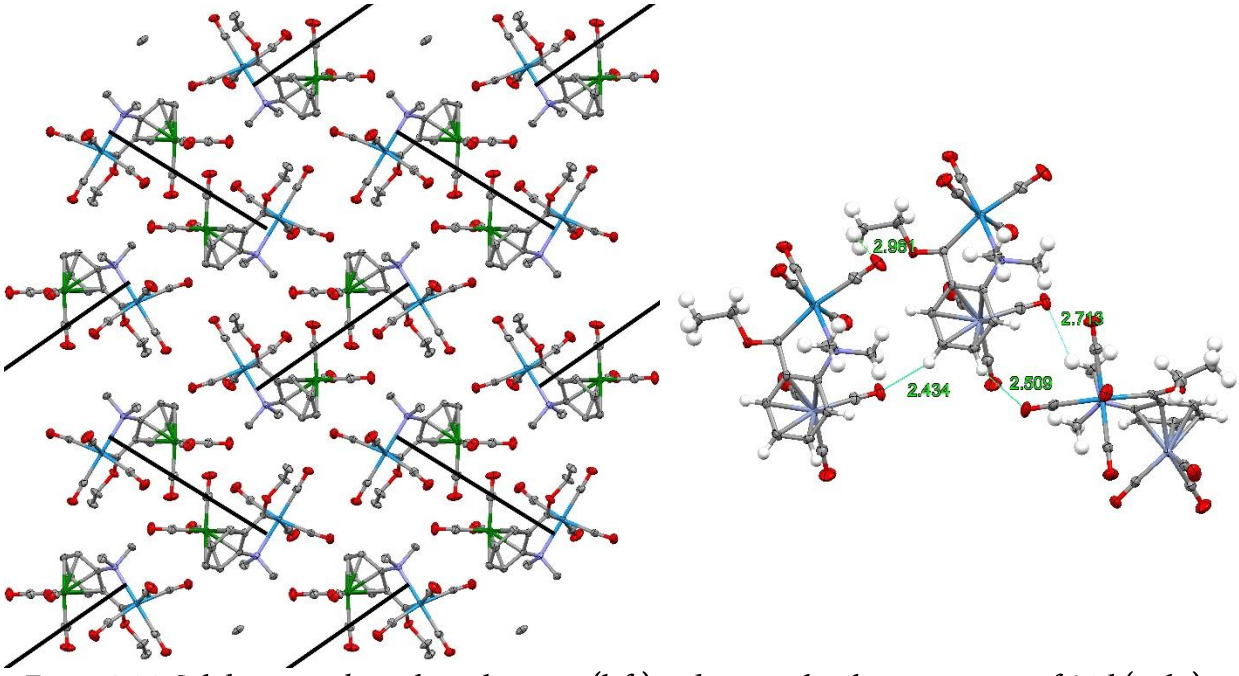

Figure 2.15. Solid-state packing along the a-axis (left) and intermolecular interactions of A1d (right)

The packing of **A1d** along the a-axis indicates that the individual complexes are arranged in paired columns such that the $Cr(CO)_3$ groups are pointing towards each other. When the paired columns are observed as a single unit, each pair of columns is arranged to form parallel units (alternating in direction) along the b- and c-axes as indicated in Figure 2.15 (left). The packing pattern is established by hydrogen bonding. Two molecules are orientated in such a way that the first molecule has H-bonding interactions with the second: a methyl in the dimethylamino group of the first molecule interacts with an oxygen of the $Cr(CO)_3$ fragment (CH_3NCH_2H---$OC(CO)_2Cr$) of the second molecule at 2.719 Å. Further, a *m*-H (relative to the amino substituent of the second molecule) of the arene interacts with a carbonyl of the $W(CO)_4$ unit of the first molecule (PhH---$OCW(CO)_3$ = 2.509 Å). A third molecule interacts with the second through two H---O interactions: the p-H (relative to the amino substituent) of the second

molecule interacts with the oxygen of a carbonyl in the $Cr(CO)_3$ group of the third molecule (2.434 Å), while a methyl-H of the ethoxy substituent in the second molecule interacts with a carbonyl of the $W(CO)_4$ moiety (CH_3NCH_2H---$OCW(CO)_3$ = 2.951 Å) in the third molecule. These interactions are shown in Figure 2.15, right.

A2 complexes

The spectroscopic data of the **A2** derivatives discussed earlier indicate that the carbene groups present in **A2a** and **A2b** are very similar. This is also evident from the single X-Ray structural data of the complexes. Selected bond lengths and angles of the **A2** derivatives are listed in Table 2.12.

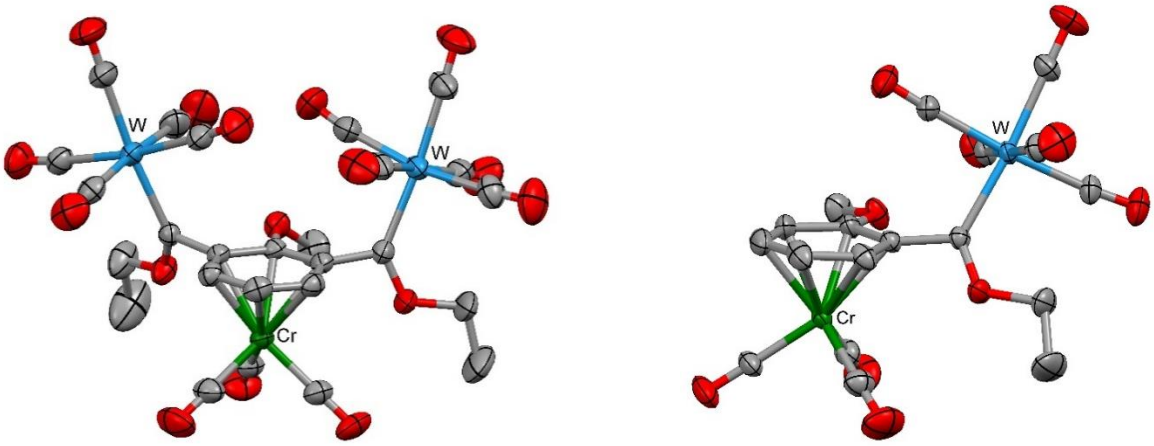

Figure 2.16. Solid state structures of A2a and A2b. Ellipsoids are set at 50% probability. Hydrogen atoms are omitted for clarity

The bond lengths of the C_{Ph}–C_{carb} bonds in **A2a** and A2b have lengths around 1.503 Å. **A2a** and **A2b** display small differences in the C_{carb}–O_{OEt} bond lengths with the two carbene ligands of **A2a** having values of 1.308(3) and 1.301(3) Å, being slightly shorter compared to the corresponding distance of 1.316(2) Å in **A2b**. The same can be said of the C_{carb}–W bond distances of **A2a** with values of 2.144(3) and 2.142(2) Å, again shorter than that of **A2b** (2.169(1) Å).

Table 2.12. Selected bond lengths (Å), bond angles (°) and torsion angles (°) of A2a, A2b and A2c

	A2a	A2b	A2c
Symmetry	P $2_1/n$	P -1	P $2_1/c$
	Bond lengths (Å)		
O_{OMe}–C_{Ph}	1.353(3)	1.346(2)	1.363(3)
C_{Ph}–C_{carb}	1.503(3)	1.502(2)	1.472(3)
	1.504(3)		
C_{carb}–W	2.144(3)	2.169(1)	2.134(2)
	2.142(2)		
C_{carb}–O_{OEt}	1.308(3)	1.316(2)	1.318(3)
	1.301(3)		
Ph_{plane}–$Cr(CO)_3$	1.699	1.693	1.701
	Bond Angles (°)		
C_{Ph}–C_{carb}–O_{OEt}	106.6(2)	105.3(1)	108.3(2)
	107.0(2)		
C_{Ph}–C_{carb}–W	119.5(2)	122.4(1)	116.9(2)
	117.9(1)		
O_{OEt}–C_{carb}–W	133.5(2)	131.3(1)	134.7(2)
	134.8(2)		
C_{carb}–W–CO_{cis}[a]	92.1(1)	92.56(7)	95.7(1)
	90.7(1)		
C_{carb}–W–CO_{trans}	175.0(1)	173.27(7)	166.8(1)
	174.5(1)		
	Torsion angles (°)		
C_{Ph}–C_{ipso}–C_{carb}–O_{OEt}	76.9(3)	54.1(2)	0.5(4)
	-114.0(2)		
C_{Ph}–C_{ipso}–C_{carb}–W	78.2(3)	60.6(2)	6.1(3)
	-102.3(2)		
C_{ipso}–C_{carb}–O_{OEt}–C_{OEt}	-175.5(3)	-170.6(1)	178.4(2)
	-175.3(2)		

[a] average of the four bond angles

The shorter C_{carb}–C_{OEt} and W–C_{Carb} bond distances in **A2a** compared to **A2b** show that the metal and ethoxy substituents play an important role in the stabilisation of biscarbene complex. The C_{Ph}–C_{carb} bond lengths in **A2a** is 1.503(3) and 1.504(3) Å while the corresponding bond in **A2b** is similar. This indicates that there is little or no π electron delocalisation or that **A2b** receives slightly more electron density from the aromatic ring for stabilisation of the single carbene group compared to the two carbene groups of **A2a**. A pronounced feature for both **A2a** and **A2b** is the

larger torsional angles around the C_{Ph}–C_{Carb} bond. The two angles for **A2a** has values of 78.2(3)° and -102.3(2)° while the same bond in **A2b** has a torsional angle of 60.6(2)°. The large torsional angles around these bonds indicate that there is steric congestion present around the methoxy and metal carbene groups present in each arene ring.

In the chelate (**A2c**), the carbene carbon and the tungsten carbonyl group are forced into the plane of the ring through the coordination of the OMe group (Figure 2.17). The whole complex is planar with only the coordinating $Cr(CO)_3$ group lying below the plane of the ring and two *trans* carbonyl ligands which are found perpendicular to the plane (slightly orientated away from the arene ring such that they form an angle of ~84° with the plane). An increase in the O_{OMe}–C_{Ph} bond length is observed in **A2c** compared to that of **A2b** (1.363(3) and 1.346(2) Å respectively). A significant decrease is observed in the bond length between the carbene carbon and the aromatic ring in **A2c** (1.472(3) vs 1.502(2) Å for the same bond in **A2b**). The decrease in the C_{Ph}–C_{carb} bond length is indirectly as a result of restraints caused by the formation and geometry of a five-membered chelate ring. To further support this observation, the bond length between the carbene carbon and the ethoxy group is found to be slightly longer for **A2c** (1.318(3) Å) than for **A2a** (1.308(3) and 1.301(3) Å), but the same as that of **A2b** (1.316(2) Å).

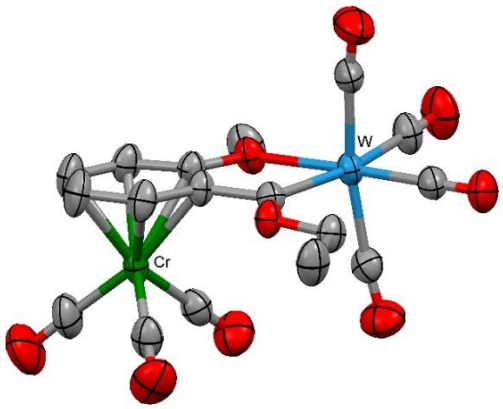

Figure 2.17. Solid state structures of A2c. Ellipsoids are set at 50% probability. Hydrogen atoms are omitted for clarity

See the arene ring distortion section for a discussion on the bond lengths within the arene rings.

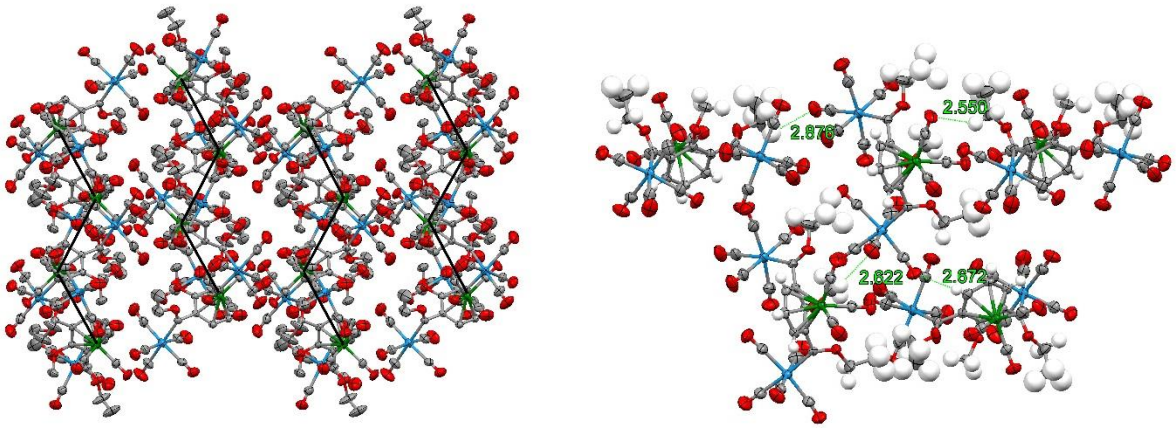

Figure 2.18. Solid-state packing along the a-axis (left) and intermolecular interactions (right) of A2a

A2a, **A2b** and **A2c** pack in space groups of P $2_1/n$, P -1 and P $2_1/c$, respectively. The packing of **A2a** involves the formation of the columns of complexes running in a zig-zag fashion to form a single layer. The columns (viewed along the a-axis) are arranged so that the first compound's $Cr(CO)_3$ group lies on the following compound's $Cr(CO)_3$ group (Figure 2.18, left) with the two $W(CO)_5$ groups pointing in opposite directions. The packing pattern is caused by H-bonding. To simplify the discussion, the interactions of a single molecule with four surrounding molecules will be discussed (Figure 2.18, right). An interaction between an oxygen present in the $Cr(CO)_3$ group and the CH2 in the ethoxy substituent of a carbene carbon in a second complex is observed ($CH_3(O)HCH$---$OCCr(CO)_2$ = 2.550 Å). A similar interaction is observed between an oxygen in one of the $W(CO)_5$ groups with a third complex, such that the $CH_3(O)HCH$---$OCW(CO)_4$ distance is 2.876 Å. The second tungsten pentacarbonyl group interacts with two additional complexes. Thus, the third interaction is between an oxygen of the $W(CO)_5$ group and the methoxy substituent of the arene ring of the other molecule (OCH_2H---$OCW(CO)_4$ = 2.622 Å). The fourth interaction is between a second carbonyl in the same $W(CO)_5$ group with the aromatic hydrogen *para* to the methoxy substituent of a fourth molecule (PhH---$OCW(CO)_4$ = 2.672 Å).

The packing of **A2b** forms layers of complexes along the a-axis, so that all the $Cr(CO)_3$ groups within a layer point in the same direction. Each layer is arranged so that the $Cr(CO)_3$ groups of the layer next to it is pointing in the opposite direction. The complexes are arranged in up-and-

down pairs such that each aromatic *o*-H relative to a methoxy substituent interacts with the partnering oxygen of a carbonyl ligand of the $Cr(CO)_3$ group (PhH---OCCr$(CO)_2$ = 2.702 Å).

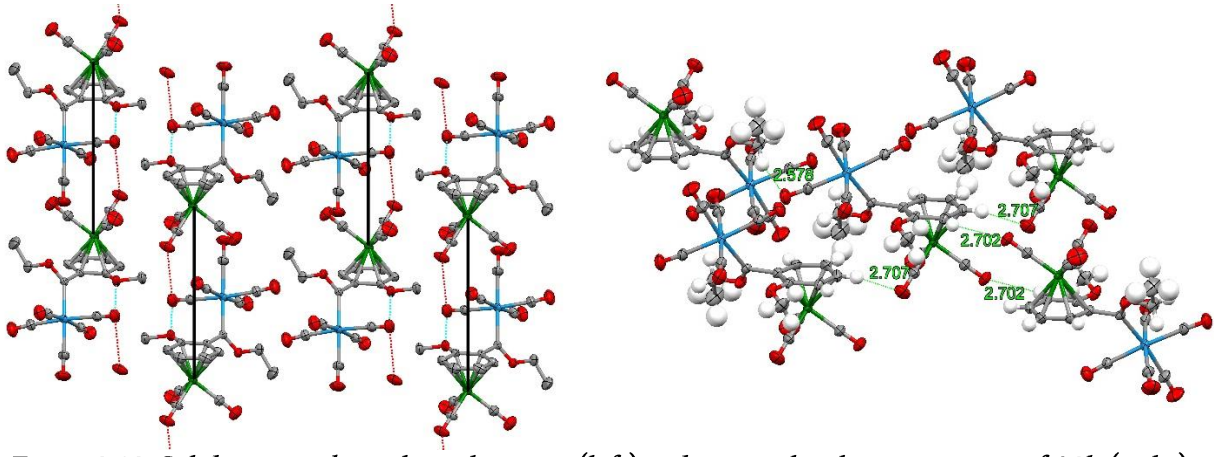

Figure 2.19. Solid-state packing along the a-axis (left) and intermolecular interactions of A2b (right)

Further, the complexes pointing in the same direction interact through an H-bond between the aromatic H in the *p*-position relative to the carbene substituent and a carbonyl oxygen of the $Cr(CO)_3$ group so that they are 2.707 Å apart. Lastly, there are interactions between the carbonyl ligand of a $W(CO)_5$ group and the CH_2 of the ethoxy substituent (CH_3(O)HCH---OCW$(CO)_4$ = 2.578 Å) so that the W centres are pointing towards each other as observed along the a-axis.

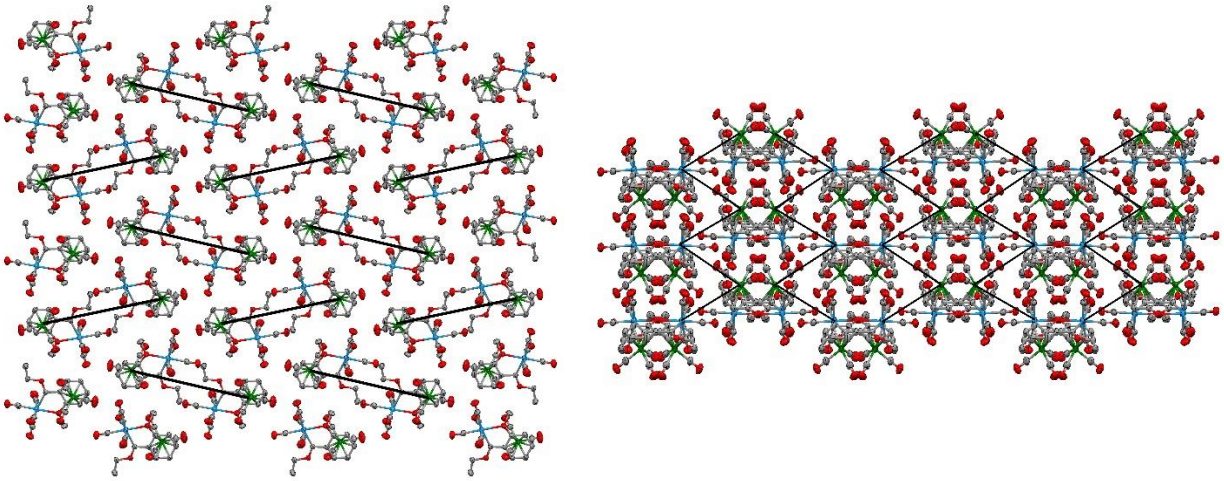

Figure 2.20. Solid-state packing of A2c along the a-axis (left) and c-axis (right)

The overall pattern viewed along the a-axis reveals pairs of complexes arranged in a parallel fashion to form a layer running horizontally across a unit cell. The stacked layers are running in opposite directions. Viewed along the c-axis (Figure 2.20, right) clear horizontal layers are formed between the $W(CO)_4$ groups and the $Cr(CO)_3$ groups pointing towards each other. The complexes marked as pairs viewed along the a-axis has also been marked in the b-axis figure and appear in a zig-zag fashion running vertically down the unit cell, each zig-zag pattern running in the opposite direction from the one next to it. The packing is mainly caused by H-bonding (Figure 2.21) where the aromatic protons at the *p*-position relative to the methoxy substituent interacts with an oxygen of a carbonyl ligand of another molecule's $Cr(CO)_3$ group, each with the other, forming pairs (PhH---$OCCr(CO)_2$ = 2.678 Å): molecule 1 and 2. Further, the aromatic H at the *p*-position relative to the carbene group of molecule 2 interacts with molecule 3's carbonyl ligand present in its $W(CO)_4$ group (PhH---$OCW(CO)_4$ = 2.546 Å). An interaction between the CH_3 of molecule 3's methoxy group and the carbonyl ligand of molecule 1's $Cr(CO)_3$ moiety ($O(CH_2)H$---$OCCr(CO)_3$ = 2.440 Å), creates a group of molecules. Each group of molecules further interact through an H-bond between the CH_2 of the ethoxy group of molecule 1 and the $W(CO)_4$ group of the next group's molecule 1 ($CH_3(O)HCH$---$OCW(CO)_3$ = 2.703 Å).

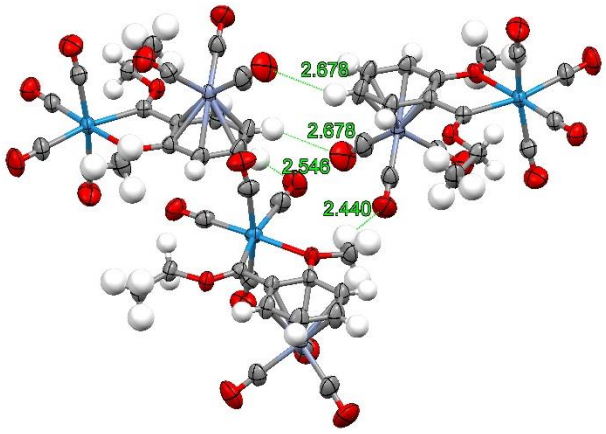

Figure 2.21. Solid-state intermolecular interactions of A2c

*Arene ring distortion and coordination properties of the **A1** and **A2** complexes*

It has been shown through the spectroscopic properties of the two sets of carbene derivatives formed from **A1** and **A2**, that there are significant electronic differences between the N,N dimethylanaline and methoxy complexes. The most pronounced difference is the donation of

electron density into the arene ring by dimethylamine substituent (**A1**) or lack thereof by the methoxy (**A2**) substituent present on the ring. Unlike for **A1c**, **A1a** and **A2b** rely more on carbene carbon stabilization from the metal and ethoxy substituents. The crystal data of the different complexes reveal that the $Cr(CO)_3$ groups are generally found slightly further away from the aromatic rings for the derivatives of **A1** than for those of **A2**. The calculated distances from the aromatic ring to the $Cr(CO)_3$ group in the structures of **A1a** – **A1d** have respective values of 1.709, 1.717, 1.715 and 1.701 Å while those of **A2a** – **A2c** have values of 1.699, 1.693 and 1.701 Å respectively. Cyclic voltammetry and NMR data also indicate more electron density present on the **A1** derivatives compared to the **A2** derivatives.

There have been extensive crystallographic studies done on η^6-coordinated aromatic compounds with different substituents present. An article published by Hunter shows a detailed description as to how single and multiple π-donor and π-acceptor substituents can influence the planarity of the aromatic ring (Scheme 2.6).[50] In general, it is expected that any electron donating substituent will distort the ring so that the electron donating substituent will point away from the $Cr(CO)_3$ group (Scheme 2.6, **A**). The opposite is observed for electron withdrawing substituents, in which case the electron withdrawing substituent will distort the arene ring so that the substituent will point towards the $Cr(CO)_3$ group to which the ring is coordinated (Scheme 2.6, **B**).

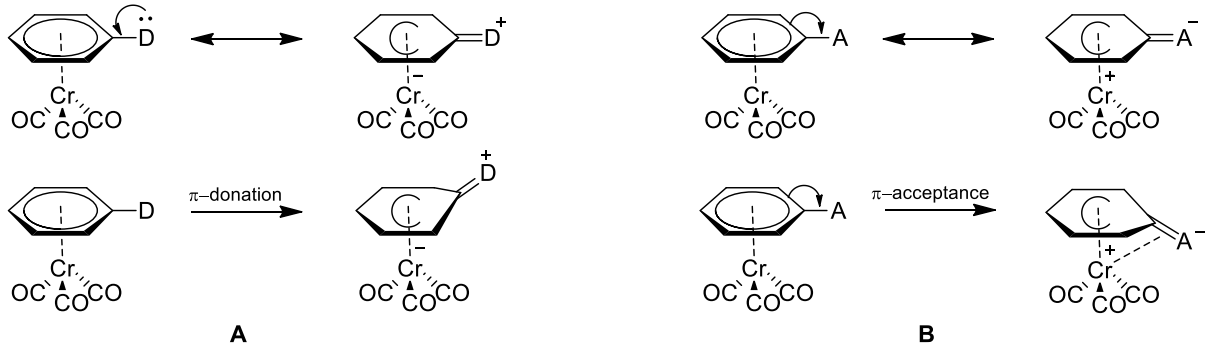

Scheme 2.6. Ring distortions observed for η^6-coordinated aromates to $Cr(CO)_3$ containing an electron donating (A) or electron withdrawing substituent (B)[50]

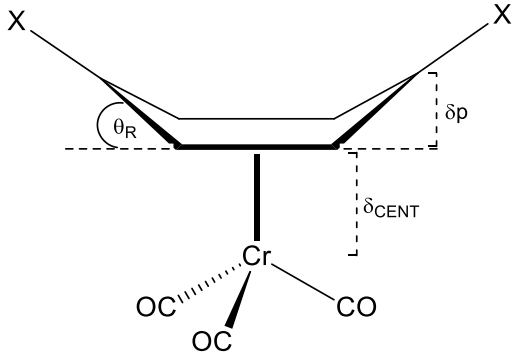

Figure 2.22. Parameters for η⁶-coordinated aromatic compounds defined by Hunter[50]

Even though all the compounds synthesised from **A1** contain an electron donating group, it is not clear how the strong electron withdrawing character of the Fischer carbene will influence the model generalised by Hunter. Analysing compounds **A1a** – **A1c** in the same light it becomes clear that the observations made by the Hunter group seems to be present in some of the complexes. Parameters defined by the Hunter article are depicted in Figure 2.22. Table 2.13 lists the parameters of **A1a** – **A1d** and **A2a** – **A2c** as defined by the Hunter group. It is important to note that not all the parameters are used. The model defined by the Hunter group uses the least squares plane through the four *o*- and *m*-position carbons of the arene ring relative to the NMe_2 or OMe group which do not carry any substituents. Since all but one complex being studied has substituents on the *o*- and *m*-substituents, the ring is likely distorted at the *o*- and *m*-positions and the least squares plane will not be accurately defined and the effect not observed. To solve this problem, the plane through the ring is defined by the four carbons not containing any substituents.

Table 2.13. Aromatic ring distortion parameters defined in Figure 2.22 of complexes A1a-A1d and A2a-A2c

	θ_D (°)	θ_{Carb} (°)	δ_D (Å)	δ_{Carb} (Å)	δ_{CENT} (Å)
A1a	3.49	10.35	0.152	0.135	1.729
A1b	5.30	-0.84	0.098	-0.010	1.735
A1c	5.96	0.60	0.104	0.042	1.738
A1d	0.89	-1.48	0.000	-0.021	1.698
A2a	4.13	7.08, 2.81	0.056	0.084, 0.017	1.691
A2b	0.99	4.10	0.045	0.039	1.707
A2c	2.46	-2.39	0.049	0.010	1.701

Even though the effect is not elaborate, ring distortion is observed for the complexes. If the carbon containing the substituent are distorted so that it lies away from the $Cr(CO)_3$ group, the θ_R and

δp values will be positive. If the carbon is distorted such that it points toward the $Cr(CO)_3$ group, the same variables will have a negative value. These are the only parameters that will be used in this study. In Table 2.13 the parameters are listed such that θ_D represents the θ_R value of the carbon carrying the donating substituent (NMe_2 or OMe) while θ_{Carb} represents the θ_R value of the carbon carrying the carbene substituent. δ_D and δ_{Carb} represents the δp values of the carbons carrying the donating substituent and the carbene substituent respectively. From the proposed model, it is expected that the carbene carbon carrying the NMe_2 or OMe group will lie above the plane of the ring, pointing away from the the $Cr(CO)_3$ group. The carbon carrying the carbene substituent is expected to lie below the plane of the ring, pointing towards the $Cr(CO)_3$ group.

There are several discrepancies where the data do not match the model proposed by the Hunter group. **A1a** shows that both the positions of the ring carrying the amino substituent as well as the carbene substituent is distorted so that these positions lie above the plane of the ring. The carbon carrying the carbene substituent is distorted such that it forms an angle of 10.35° with the plane of the ring, which is significantly large. It is very probable that large distortion is caused by steric interactions between the two substituents themselves. The model holds true for **A1b** with the NMe_2-carbon pointing away from the $Cr(CO)_3$ group while the position carrying the carbene substituent is pointing towards the $Cr(CO)_3$ group. No steric interactions between the substituents are observed. **A1c**, in which the carbene substituent is on the *p*-position relative to the NMe_2 group, does not agree with the model. For this complex, both the ring positions carrying the substituents point away from the $Cr(CO)_3$ group. The chelate, **A1d**, is not expected to match the model as the rigid structure and steric strain of the ring will determine their positions

As most of the compounds do not distort as expected for compounds in which π-resonance effects play a role, it must be assumed that another property cause the ring distortion. Several π-coordinated arene rings carrying an electropositive metal fragment such as titanocene chloride as substituent and smaller substituents (H, F or OMe) have been studied, in which ring distortion

have also been observed. For these compounds distortions within a π-coordinated arene ring is caused by electronegativity of the heteroatom substituent and the σ-inductive effects rather than the π-resonance effects of the substituents of the arene ring.[51] The different bond lengths and internal angles for the arene ring present in the **A1** and **A2** complexes are listed in Table 2.14.

Table 2.14. Bond lengths and angles of the solid-state structure arene rings present in A1a – A1d and A2a – A2c

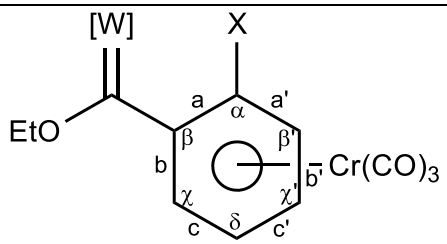

	Arene bond lengths (Å)					
	a	**a'**	**b**	**b'**	**c**	**c'**
A1a	1.421(2)	1.430(2)	1.435(2)	1.404(2)	1.401(2)	1.409(2)
A1b	1.425(5)	1.422(3)	1.411(5)	1.399(3)	1.431(5)	1.392(5)
A1c	1.422(3)	1.422(3)	1.400(3)	1.399(3)	1.421(3)	1.417(3)
A1d	1.418(3)	1.412(3)	1.401(3)	1.418(3)	1.395(3)	1.429(3)
A2a	1.429(3)	1.411(3)	1.398(3)	1.422(3)	1.408(3)	1.390(3)
A2b	1.428(2)	1.414(2)	1.425(2)	1.401(3)	1.409(3)	1.400(4)
A2c	1.414(4)	1.401(4)	1.422(4)	1.405(4)	1.395(4)	1.398(4)
	Arene bond angles (°)					
	α	**β**	**β'**	**γ**	**γ'**	**δ**
A1a	117.7(1)	119.3(1)	121.9(1)	121.9(1)	120.4(1)	118.7(1)
A1b	116.6(3)	122.9(3)	120.8(3)	118.5(3)	121.3(3)	119.4(3)
A1c	116.5(2)	121.4(2)	121.0(2)	121.9(2)	122.2(2)	116.2(2)
A1d	120.3(2)	118.9(2)	119.8(2)	120.7(2)	120.6(2)	119.6(2)
A2a	120.2(2)	119.7(2)	118.2(2)	120.5(2)	121.6(2)	119.6(2)
A2b	120.3(1)	117.9(1)	120.1(2)	121.6(2)	121.0(2)	119.1(2)
A2c	121.8(3)	117.9(2)	118.4(3)	120.9(3)	121.4(3)	119.5(3)

Arene ring distortion is observed for the complexes with the largest distortions observed in the angle and bond distances of the *ipso*-carbon to which the carbene complex is a substituent. A significant increase in bond length is observed for the carbons carrying the carbene substituents while the internal angle decreases compared to the other carbons within the ring. As an example: for **A2b**, the carbene substituent is found on the carbon between the bonds labelled as *a* and *b*

which have lengths of 1.428(2) and 1.425(2) Å while all the other bonds are significantly shorter with average lengths of 1.408 Å. The internal angle of the carbon carrying the carbene substituent is 117.9(1)° and all the other internal angles with values between 119.1 and 121.6°. The same pattern is repeated in all the complexes. For the **A1** derivatives, distortion is also prominent for bonds and angles around the carbon carrying the dimethylamino substituent – much more than for the methoxy group of the **A2** derivatives.

From the internal ring distortion for the complexes, it can be concluded that σ-inductive effects of the substituents are the leading cause for the distortion in the arene ring.

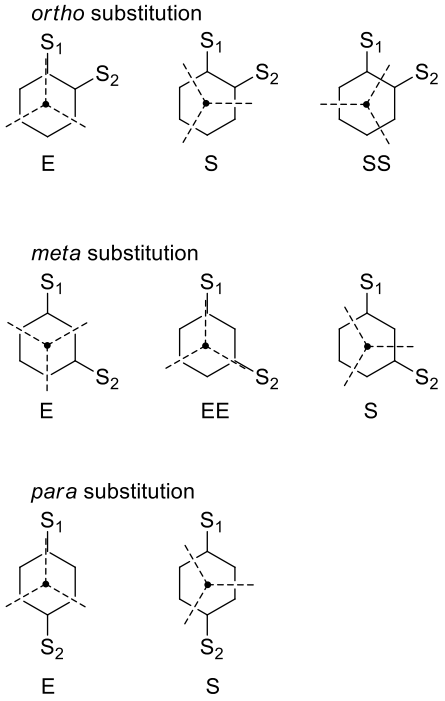

Figure 2.23. Possible orientations of the $Cr(CO)_3$ tripod with two substituents on the arene ring

The final aspect to consider of structural importance of the individual three-legged piano stool molecules, is the orientation of the $Cr(CO)_3$ tripod relative to the ring. For a π-donor substituent the energy of most favoured conformation (EE) is the one where the $Cr(CO)_3$ tripod adopts an orientation so that one of the carbonyl ligands eclipse the donor substituent while the other two will eclipse the carbon atoms in the *m*-position of the arene ring. For a π-acceptor, the favoured conformation (E) is the one where the carbonyl ligands of the $Cr(CO)_3$ tripod eclipses the *o*- and *p*-position of the arene ring. When the benzene ring is fully substituted such as in C_6Me_6 the tripod will adopt a conformation where the carbonyl ligands are staggered (S) between the carbon atoms by bisecting every second C-C bond. The three carbonyls coordinated to the chromium form a tripod which is orientated in an eclipsed (E) or staggered (S) orientation relative to the aromatic ring. The orientation of the chromium-tricarbonyl tripod is solely dependent on the presence of π-donating or π-accepting substituents present on the coordinated aromatic ring. These effects

with reasons are described in a review article by Muetterties and Albright.[45] There are three possible orientations that the $Cr(CO)_3$ tripod can adopt relative to a benzene ring for the *o*- and *m*-conformers, while the symmetrically substituted *p*-conformer has only two. Figure 2.23 describes the different orientations that the chromium-tricarbonyl tripod can adopt relative to the aromatic ring containing two different groups.

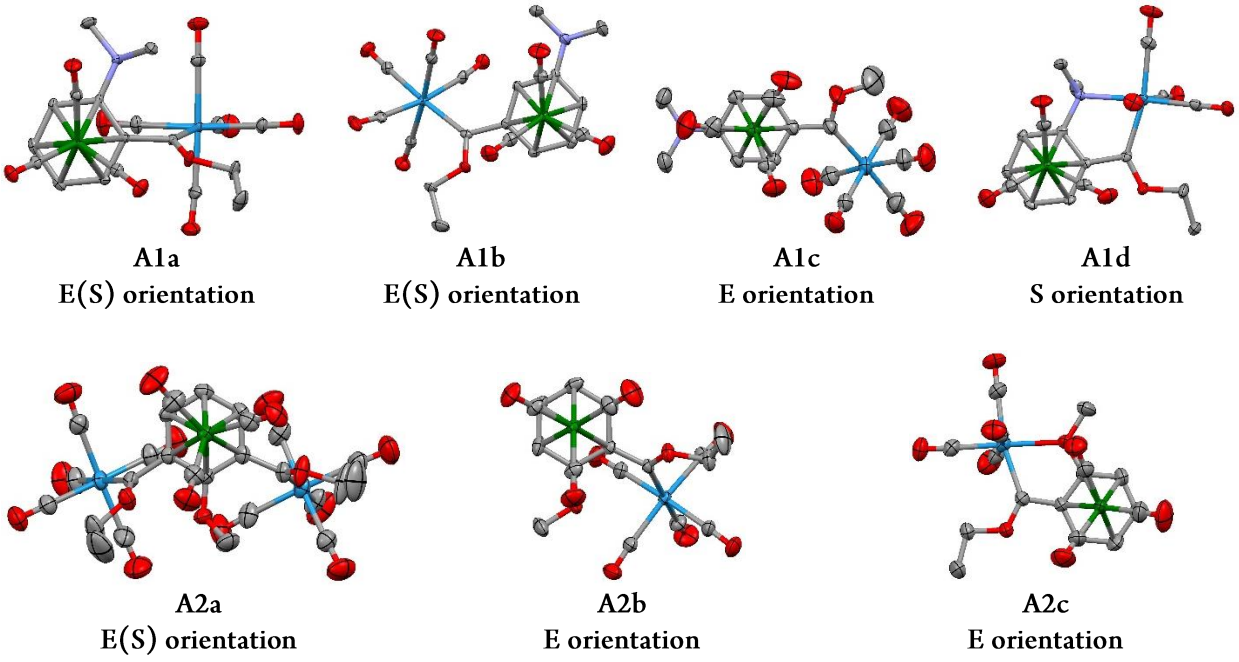

Figure 2.24. Orientation of the $Cr(CO)_3$ tripod relative to the aromatic arene of A1a – A1d and A2a – A2c.

In the complexes, **A1a** and **A2b**, containing two adjacent substituents, the E conformation with a carbonyl ligand eclipsing the NMe_2 or OMe is expected. Both complexes contain electron donating substituents - one strong (NMe_2) the other weak (OMe) – and an electron withdrawing substituent (carbene carbon). The E conformation is observed for **A2b** but deviates slightly for **A1a** because of the bulkiness of the carbene and adjacent NMe_2 substituents. In **A1c** the predicted ideal E conformation is observed with a carbonyl ligand eclipsing the strong π-donor NMe_2 substituent. In **A1b**, with the carbene groups in the *m*-position, two conformers are possible. In the first, an eclipsing NMe_2 conformation is predicted as the NMe_2 is electronically dominant. In

the second, two carbonyl ligands can eclipse the two carbons in the *o*-positions to the carbene substituent in the ring, indicating that the carbene carbon will be electronically dominant. Often with both substituents exerting an electronic role, a staggered conformation is observed. In this case the NMe_2 substituent dominates and determines the structure which is staggered (S), but only slightly deviated from a predicted E-conformation based on NMe_2. Interestingly, the biscarbene trisubstituted arene **A2a** displays a structure with a slight deviation from the ideal E conformation predicted for two electron-withdrawing carbene moieties. Also, as one carbonyl ligand will eclipse the OMe substituent this will correlate with an electron donating OMe substituent. Because of steric interactions the structure does not display an ideal E-conformation.

In **A2c** the chelate ring does not influence the observed conformation that is the predicted (E conformer). By contrast, the bulkier dimethylamine ligand in **A1d** causes a deviation and the structure can best be described as staggered with the carbonyls bisecting the C-C bonds on both sides of the chelate ring.

2.3 Experimental

General

Standard Schlenk techniques under an atmosphere of nitrogen or argon were used for general synthesis. Silica gel 60 (particle size 0.0063–0.200 mm) was used as resin for all separations in column chromatography. THF and hexane were distilled over sodium metal, while CH_2Cl_2 was distilled over CaH_2. All other reagents were used as received from commercial suppliers. NMR spectra were recorded on Bruker Ultrashield Plus 400 AVANCE 3 and Bruker Ultrashield 300 AVANCE 3 spectrometers using $CDCl_3$ as solvent at 25 °C. The NMR spectra were recorded for ^{1}H at 400.13 or 300.13 MHz and ^{13}C at 100.163 or 75.468 MHz. Chemical shifts were recorded in ppm, using the deuterated solvent signal as an internal reference. For $CDCl_3$ δH at 7.2400 and and δC at 77.000 ppm. Infrared spectroscopy was performed on a Bruker ALPHA FT-IR spectrophotometer with a NaCl cell, using hexane as solvent. Xray crystallography was performed

at 20 °C on a Siemens P4 diffractometer fitted with a Bruker 1 K CCD detector using graphitemonochromated, Mo–Kα radiation by means of a combination of phi and omega scans.

Electrochemical and Spectroscopic Measurements.

The electrochemical experiments were performed in a vacuum-tight, one-compartment cell. Pt and Ag wires were used as the counter and reference electrodes, respectively, while a platinum electrode was used as the working electrode. The working electrode was polished with 0.25 μm diamond paste (Buehler-Wirtz) before measurements. NBu_4PF_6 (0.25 mM) was used as the supporting electrolyte. Referencing was done with addition of ferrocene (Cp_2Fe) or decamethylferrocene (DmFc) as an internal standard to the analyte solution after all data of interest had been acquired. Representative sets of scans were repeated with the added standard. Final referencing was done against the $Cp_2Fe^{0/+}$ couple with $E_{½}$ ($DmFc^{0/+}$) = -540 mV *vs.* $Cp_2Fe^{0/+}$ using DCM/TBu_4PF_6 as supporting electrolyte.

Electrochemical data was acquired with a computer-controlled BAS potentiostat. A CaF_2 OTTLE cell was used where Pt-mesh acted as the working and counter electrode and a silver wire as the pseudo-reference electrode. FT-IR spectra were recorded on a Thermo is10 instrument. UV-Vis/NIR spectra were obtained on a TIDAS fiber optic diode array spectrometer (combined MCS UV/NIR and PGS NIR instrumentation) from j&m in HELLMA quartz cuvettes with 0.1 cm 10 optical path lengths.

DFT calculations

The DFT study was conducted using the Gaussian 09 suite of programs[52] with CH_2Cl_2 as solvent. The **A1** derivatives were optimised at the DFT level using the B3LYP functional with the triple-ζ valence basis set 6-31G(d,p)[53,54] on all atoms except W and Cr, where the LanL2DZ[55–57] basis set was used. The **A2** derivatives were optimised using the PBE0 functional[58] with the 6-31G(d)[53,54] basis set on all atoms except W, on which the quasirelativistic Wood–Boring small-core pseudopotentials (MWB) form as well as the corresponding basis set[59] was applied. All

complexes have a positive defined Hessian matrix showing that they are at minima on a potential energy surface.

π-Coordination of N,N-dimethyl aniline to $Cr(CO)_3$

$Cr(CO)_6$ (4.0 g, 18.0 mmol), 5.0 mL THF and 25.0mL N,N-dimethylaniline was dissolved in 60 mL dibutylether and allowed to reflux for 24 hours under an inert atmosphere. The bright yellow solution was allowed to cool to room temperature and the solvent evaporated *in vacuo*. A pure light-yellow product was isolated with silica chromatography using a solvent mixture of hexane: triethylamine (1000mL:2mL). Yield: 3.90 g (15.3 mmol, 85 %).

π-Coordination of anisole to $Cr(CO)_3$

$Cr(CO)_6$ (4.0 g, 18.0 mmol), 5.0 mL THF and 23.0 mL anisole was dissolved in 60 mL dibuthylether. The reaction mixture was allowed to reflux for 48 hours after which the solution was allowed to cool to room temperature. The solvent was evaporated under vacuum. The product mixture was passed through a silica plug using DCM as solvent, removing any decomposed product before the pure product was isolated with silica chromatography using a solvent mixture of hexane: CH_2Cl_2: triethylamine (1000 mL: 62.5 mL: 2.0 mL). Yield: 3.40g (13.1 mmol, 73 %)

*Synthesis of **A1a** and **A1d***

N,N-dimethylaniline(η^6-tricarbonyl chromium) (1.29 g, 5.00 mmol) was dissolved in 10 mL THF. The reaction mixture was lithiated with nBuLi (1.6 M, 3.13 mL) at –40°C and allowed to stir at RT for 60 minutes. The reaction was cooled to –40°C, $W(CO)_6$ (1.76 g, 5.00 mmol) was added and allowed to stir in the cold bath for 30 minutes after which it was removed and allowed to stir at RT until all metal carbonyl was dissolved (60 minutes). The solvent was evaporated and the reaction mixture dissolved in CH_2Cl_2.and cooled to –40°C. Et_3OBF_4 (0.95 g, 5.00 mmol) dissolved in CH_2Cl_2 was added to the cold solution while stirring. After allowing the reaction mixture to heat up, it was passed through a silica plug using CH_2Cl_2 as solvent and the solvent

evaporated. The products were isolated using a silica gel column using hexane and CH_2Cl_2 as solvents. Yield: **A1a** = 2.13 g (66.9 %), **A1d** = 0.283 g (9.3 %).

*Synthesis of **A1b** and **A1c***

N,N-dimethylaniline(η^6-tricarbonyl chromium) (1.29 g, 5.00 mmol) was dissolved in 10 mL THF. The reaction mixture was lithiated with *n*BuLi (1.6 M, 3.13 mL) at –40 °C and allowed to stir in the cold bath for 15 minutes. $W(CO)_6$ (1.76 g, 5.00 mmol) was added and allowed to stir in the cold bath for 30 minutes after which it was removed and allowed to stir at RT until all metal carbonyl was dissolved (60 minutes). The solvent was evaporated and the reaction mixture dissolved in CH_2Cl_2.and cooled to –40°C. Et_3OBF_4 (0.95 g, 5.00 mmol) dissolved in CH_2Cl_2 was added to the cold solution while stirring. After allowing the reaction mixture to heat up, it was passed through a silica plug using CH_2Cl_2 as solvent and the solvent evaporated. The products were isolated using a silica gel column and hexane and CH_2Cl_2 as solvents. Yield: **A1b** = 1.68 g (52.7 %), **A1c** = 0.549 g (17.2 %).

*Synthesis of **A2a**, **A2b** and **A2c***

Anisole(η^6-tricarbonyl chromium) (1.22 g, 5.00 mmol) was dissolved in 10 mL THF. The reaction mixture was lithiated at –40 °C with *n*BuLi (1.6 M, 3.31 mL) and allowed to stir at RT for 60 minutes. After the reaction was cooled to –40°C, $W(CO)_6$ (1.76 g, 5.00 mmol) was added and allowed to stir in the cold bath for 30 minutes after which it was removed and allowed to stir at RT until all metal carbonyl was dissolved (60 minutes). The solvent was evaporated and the reaction mixture dissolved in CH_2Cl_2.and cooled to –40°C. Et_3OBF_4 (0.95 g, 5.00 mmol) dissolved in CH_2Cl_2 was added to the cold solution. After allowing the reaction mixture to reach RT, it was passed through a silica plug using CH_2Cl_2 as solvent and the solvent evaporated. The products were isolated using a silica gel column and hexane and CH_2Cl_2 as solvents. Yield: **A2a** = 0.882 g (23.8 %), **A2b** = 1.44 g (46.1 %), **A2c** = 0.190 g (6.37 %).

Characterisation

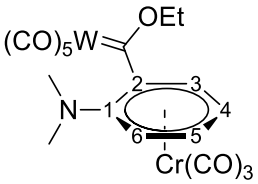

Figure 2.25. NMR spectral assignment of A1a

A1a: $C_{19}H_{15}O_9NCrW$. ^1H NMR ($CDCl_3$, 300 MHz) δ 5.54 (ddd, J = 7.1, 6.1, 1.4 Hz, 1H, H5), 5.31 (d, J = 6.9 Hz, 1H, H3), 5.04 (q, J = 7.1 Hz, 2H, CH_2(OEt)), 4.96 (dd, J = 6.4, 1.4 Hz, 1H, H6), 4.89 (dd, J = 7.0, 6.2 Hz, 1H, H4), 2.71 (s, 6H, NMe_2), 1.78 (t, J = 7.1 Hz, 3H, CH_3 (OEt)). ^{13}C NMR ($CDCl_3$, 75 MHz) δ 320.4 ($^1J_{\{W\}C}$ = 54.5 Hz, C_{carb}), 234.0 ($Cr(CO)_3$), 203.5 ($^1J_{\{W\}C}$ = 56.0 Hz, $W(CO)_5$, *trans*) 196.6 ($^1J_{\{W\}C}$ = 63.3 Hz, $W(CO)_5$, *cis*), 125.8 (C2), 114.9 (C1), 94.6 (C5), 91.6 (C6), 83.1 (C3), 82.2 (C4), 81.2 (CH_2(OEt)), 43.9 (NMe_2), 14.5 (CH_3(OEt)).

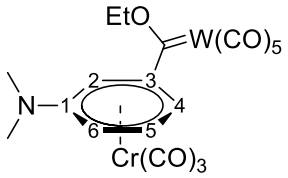

Figure 2.26. NMR spectral assignment of A1b

A1b: $C_{19}H_{15}O_9NCrW$. ^1H NMR ($CDCl_3$, 300 MHz) δ 5.57 (dd, J = 7.3, 6.8 Hz, 1H, H5), 5.53 (s, 1H, H2), 5.48 (d, J = 6.6 Hz, 1H, H4), 5.08 (dq, J = 7.0, 2.3 Hz, 2H, CH_2(OEt)), 5.05 (d, J = 7.0 Hz, 1H, H6), 2.97 (s, 6H, NMe_2), 1.70 (t, J = 7.1 Hz, 3H, CH_3(OEt)). ^{13}C NMR ($CDCl_3$, 75 MHz) δ 311.0 ($^1J_{\{W\}C}$ = 53.7 Hz, C_{Carb}), 234.4 ($Cr(CO)_3$), 202.4 ($^1J_{\{W\}C}$ = 58.4 Hz, $W(CO)_5$, *trans*) 197.0 ($^1J_{\{W\}C}$ = 63.5 Hz, $W(CO)_5$, *cis*), 133.1 (C3), 115.1 (C1), 94.3 (C5), 86.3 (C4), 80.2 (CH_2(OEt)), 78.9 (C2), 75.5 (C5), 40.0 (NMe_2), 14.9 (CH_3(OEt)).

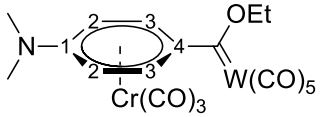

Figure 2.27. NMR spectral assignment of A1c

A1c: $C_{19}H_{15}O_9NCrW$. ^1H NMR ($CDCl_3$, 300 MHz) δ 6.34 (d, J = 7.7 Hz, 2H, H3), 4.93 (q, J = 7.1 Hz, 2H, CH_2(OEt)), 4.87 (d, J = 7.7 Hz, 2H, H2), 3.01 (s, 6H, NMe_2), 1.65 (t, J = 7.0 Hz, 3H, CH_3(OEt)). ^{13}C NMR ($CDCl_3$, 75 MHz) δ 302.9 ($^1J_{\{W\}C}$ = n.o., C_{Carb}), 231.9 ($Cr(CO)_3$), 202.1 ($^1J_{\{W\}C}$ = n.o., $W(CO)_5$, *trans*) 197.3 ($^1J_{\{W\}C}$ = 63.1 Hz, $W(CO)_5$, *cis*), 136.8 (C4), 105.6 (C1), 99.5 (C3), 79.2 (CH_2(OEt)), 73.1 (C2), 40.0 (NMe_2), 15.1 (CH_3(OEt)).

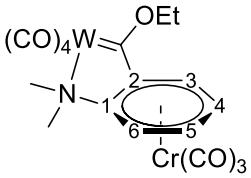

Figure 2.28. NMR spectral assignment of A1d

A1d: $C_{18}H_{15}O_8NCrW$. ^1H NMR ($CDCl_3$, 300 MHz) δ 5.85 (dd, J = 6.7, 0.9 Hz, 1H, H3), 5.72 (d, J = 6.8 Hz, 1H, H6), 5.54 (ddd, J = 7.2, 6.6, 0.9 Hz, 1H, H4), 5.34 (dd, J = 7.1, 6.5 Hz, 1H, H5), 5.04 – 4.89 (m, 2H, CH_2(OEt)), 3.66 (s, 3H, NMe), 3.45 (s, 3H, NMe), 1.70 (t, J = 7.1 Hz, 3H, CH_3(OEt)). ^{13}C NMR ($CDCl_3$, 75 MHz) δ 305.1 ($^1J_{\{W\}C}$ = n.o., C_{Carb}), 230.5 ($Cr(CO)_3$), 222.0 ($^1J_{\{W\}C}$ = n.o., $W(CO)_4$), 213.0 ($^1J_{\{W\}C}$ = n.o., $W(CO)_4$), 205.6 ($^1J_{\{W\}C}$ = n.o., $W(CO)_4$), 203.5 ($^1J_{\{W\}C}$ = n.o., $W(CO)_4$), 137.3 (C2), 110.2 (C3), 91.2 (C5), 90.3 (C1), 84.3 (C6), 83.2 (C4), 79.3 (CH_2(OEt)), 64.2 (NMe), 57.3 (NMe), 15.1(CH_3(OEt)).

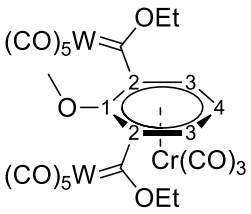

Figure 2.29. NMR spectral assignment of A2a

A2a: $C_{26}H_{16}O_{16}CrW_2$. ^1H NMR ($CDCl_3$, 400 MHz) δ 5.17 (d, J = 6.1 Hz, 2H, H3), 5.11-4.93 (m, 4H, CH_2(OEt)), 5.00 (d, J = 6.3 Hz, 1H, H4), 3.63 (s, 3H, CH_3(OMe)), 1.76 (t, J = 7.1 Hz, 6H, CH_3(OEt)). ^{13}C NMR ($CDCl_3$, 101 MHz) δ 315.4 ($^1J_{\{W\}C}$ = n.o., C_{Carb}), 232.3 ($Cr(CO)_3$), 203.5 ($^1J_{\{W\}C}$ = n.o., $W(CO)_5$, *trans*), 196.2 ($^1J_{\{W\}C}$ = 64.0 Hz, $W(CO)_5$, *cis*), 128.7 (C1), 119.6 (C2), 89.3 (C3), 81.2 (CH_2(OEt)), 81.1 (C4), 65.0 (CH_3(OMe)), 14.6 (CH_3(OEt)).

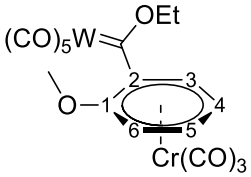

Figure 2.30. NMR spectral assignment of A2b

A2b: $C_{18}H_{12}O_{10}CrW$. ^1H NMR ($CDCl_3$, 400 MHz) δ 5.60 (ddd, J = 6.8, 6.2, 1.3 Hz, 1H, H5), 5.29 (dd, J = 6.2, 1.3 Hz, 1H, H3), 5.01 (dd, J = 6.9, 0.5 Hz, 1H, H6), 4.98 (dq, J = 7.1, 1.1 Hz, 2H, CH_2(OEt)), 4.81 (ddd, J = 6.7, 6.2, 0.8 Hz, 1H, H4), 3.72 (s, 3H, CH_3(OMe)), 1.76 (t, J = 7.1 Hz, 3H, CH_3(OEt)). ^{13}C NMR ($CDCl_3$, 101 MHz) δ 315.7 ($^1J_{\{W\}C}$ = n.o., C_{Carb}), 232.6 ($Cr(CO)_3$), 203.9 ($^1J_{\{W\}C}$ = n.o., $W(CO)_5$, *trans*), 196.6 ($^1J_{\{W\}C}$ = 64.0 Hz, $W(CO)_5$, *cis*), 136.6 (C1), 117.8 (C2), 94.6 (C5), 91.0 (C3), 81.6 (C4), 81.0 (CH_2(OEt)), 71.7 (C6), 55.8 (CH_3(OMe)), 14.5 (CH_3(OEt)).

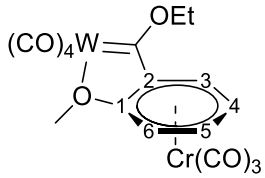

Figure 2.31. NMR spectral assignment of A2c

A2c: $C_{17}H_{12}O_9CrW$. ^{1}H NMR ($CDCl_3$, 400 MHz) δ 6.27 (d, J = 6.3 Hz, 1H, H3), 5.78 (dd, J = 6.8, 6.2 Hz, 1H, H5), 5.38 (d, J = 6.7 Hz, 1H, H6), 5.01 (q, J = 7.2 Hz, 2H, CH_2(OEt)), 4.91 (dd, J = 6.8, 6.1 Hz, 1H, H4), 4.50 (s, 3H, CH_3(OMe)), 1.76 (t, J = 7.1 Hz, 3H, CH_3(OEt)). ^{13}C NMR ($CDCl_3$, 101 MHz) δ 304.1 ($^1J_{\{W\}C}$ = n.o., C_{Carb}), 230.0 ($Cr(CO)_3$), 219.7 ($^1J_{\{W\}C}$ = n.o., $W(CO)_4$), 217.2 ($^1J_{\{W\}C}$ = n.o., $W(CO)_4$), 217.2 ($^1J_{\{W\}C}$ = n.o., $W(CO)_4$), 214.2 ($^1J_{\{W\}C}$ = n.o., $W(CO)_4$), 122.7 (C1), 114.7 (C2), 93.3 (C5), 88.4 (C3), 84.8 (CH_2(OEt)), 73.4 (C6), 73.4 (C4), 67.8 (CH_3(OMe)), 15.3 (CH_3(OEt)).

2.4 References

[1] F. Hein, *Chem. Ber.* **1919**, *52*, 195–196.

[2] R. Meyer, P. L. Wessels, P. H. van Rooyen, S. Lotz, *Inorg. Chim. Acta* **1999**, *284*, 127–132.

[3] K. N. Jayaprakash, D. Hazra, K. S. Hagen, U. Samanta, M. M. Bhadbhade, V. G. Puranik, A. Sarkar, *J. Organomet. Chem.* **2001**, *617–618*, 709–722.

[4] A. Arrais, E. Diana, D. Marabello, G. Gervasio, P. L. Stanghellini, *J. Organomet. Chem.* **2011**, *696*, 2299–2305.

[5] M. F. Semmelhack, G. Clark, *J. Am. Chem. Soc.* **1977**, *99*, 1675–1676.

[6] P. Ricci, K. Krämer, X. C. Cambeiro, I. Larrosa, *J. Am. Chem. Soc.* **2013**, *135*, 13258–61.

[7] P. Ricci, K. Krämer, I. Larrosa, *J. Am. Chem. Soc.* **2014**, *136*, 18082–6.

[8] N. Kuhl, M. N. Hopkinson, J. Wencel-Delord, F. Glorius, *Angew. Chem. Int. Ed.* **2012**, *51*, 10236–54.

[9] C.-L. Ciana, R. J. Phipps, J. R. Brandt, F.-M. Meyer, M. J. Gaunt, *Angew. Chem. Int. Ed.* **2011**, *50*, 458–62.

[10] N. Harris, Piggybacking Fischer Carbene Complexes, University of Pretoria, **2013**.

[11] B. van der Westhuizen, P. J. Swarts, L. M. van Jaarsveld, D. C. Liles, U. Siegert, J. C. Swarts, I. Fernández, D. I. Bezuidenhout, *Inorg. Chem.* **2013**, *52*, 6674–84.

[12] B. van der Westhuizen, J. M. Speck, M. Korb, J. Friedrich, D. I. Bezuidenhout, H. Lang, *Inorg. Chem.* **2013**, *52*, 14253–14263.

[13] P. Veit, C. Förster, S. Seibert, K. Heinze, *Z. Anorg. Allg. Chem.* **2015**, *641*, 2083–2092.

[14] N. Van Order, W. E. Geiger, T. E. Bitterwolf, A. L. Rheingold, *J. Am. Chem. Soc.* **1987**, *109*, 5680–5690.

[15] M. Rosillo, G. Domínguez, J. Pérez-Castells, *Chem. Soc. Rev.* **2007**, *36*, 1589–604.

[16] M. F. Semmelhack, A. Chlenov, *Top. Organomet. Chem.* **2004**, *7*, 21–42.

[17] R. J. Card, W. S. Trahanovsky, *J. Org. Chem.* **1980**, *45*, 2560–2566.

[18] A. R. Lepley, W. A. Khan, A. B. Giumanini, A. G. Giumanini, *J. Org. Chem.* **1966**, *31*, 2047–2051.

[19] A. Berger, J.-P. Djukic, C. Michon, *Coord. Chem. Rev.* **2002**, *225*, 215–238.

[20] M. Fukui, T. Ikeda, T. Oishi, *Tetrahedron Lett.* **1982**, *23*, 1605–1608.

[21] R. J. Salomon, M. A. Todd, M. Sabat, W. H. Myers, W. D. Harman, *Organometallics* **2010**, *29*, 707–709.

[22] B. L. MacLeod, J. A. Pienkos, J. T. Myers, M. Sabat, W. H. Myers, W. D. Harman, *Organometallics* **2014**, *33*, 6286–6289.

[23] Peter M. Graham, Scott H. Meiere, A. Michal Sabat, W. D. Harman, *Organometallics* **2003**, *22*, 4364–4366.

[24] P. M. Graham, D. A. Delafuente, W. Liu, W. H. Myers, M. Sabat, W. D. Harman, *J. Am. Chem. Soc.* **2005**, *127*, 10568–10572.

[25] P. M. Treichel, R. U. Kirss, *Organometallics* **1987**, *6*, 249–254.

[26] S. Lotz, M. van den Berg, J. L. M. Dillen, *Trans. Met. Chem.* **1988**, *13*, 170–175.

[27] W. Strohmeier, *Angew. Chem. Int. Ed.* **1964**, *3*, 730–737.

[28] I. P. Clark, M. W. George, G. M. Greetham, E. C. Harvey, C. Long, J. C. Manton, M. T. Pryce, *J. Phys. Chem. A* **2011**, *115*, 2985–93.

[29] S. Lotz, N. A. van Jaarsveld, D. C. Liles, C. Crause, H. Görls, Y. M. Terblans, *Organometallics* **2012**, *31*, 5371–5383.

[30] N. A. van Jaarsveld, D. C. Liles, S. Lotz, *Dalton Trans.* **2010**, *39*, 5777–5779.

[31] U. Schubert, K. Ackermann, N. H. Tran Huy, W. Röll, *J. Organomet. Chem.* **1982**, *232*, 155–162.

[32] E. O. Fischer, W. Röll, N. H. T. Huy, K. Ackermann, *Chem. Ber.* **1982**, *115*, 2951–2964.

[33] M. Landman, R. Pretorius, R. Fraser, B. E. Buitendach, M. M. Conradie, P. H. van Rooyen, J. Conradie, *Electrochim. Acta* **2014**, *130*, 104–118.

[34] C. Neumann, E. Ionescu, U. Schiemann, M. Schlenker, M. Bode, F. Ruthe, P. G. Jones, R. Streubel, *J. Organomet. Chem.* **2002**, *643–644*, 253–264.

[35] K. H. Dötz, H.-G. Erben, W. Staudacher, K. Harms, *J. Organomet. Chem.* **1988**, *355*, 177–191.

[36] D. M. Adams, *Metal-Ligand and Related Vibrations: A Critical Survey of the Infrared and Raman Spectra of Metallic and Organometallic Compounds*, St. Martin's Press, **1968**.

[37] L. E. Orgel, *Inorg. Chem* **1962**, *1*, 25–29.

[38] P. von Ragué Schleyer, B. Kiran, D. V. Simion, T. S. Sorensen, *J. Am. Chem. Soc.* **2000**, *122*, 510–513.

[39] C. A. Merlic, B. N. Hietbrink, K. N. Houk, *J. Org. Chem.* **2001**, *66*, 6738–6744.

[40] A. D. Hunter, V. Mozol, S. D. Tsai, *Organometallics* **1992**, *11*, 2251–2262.

[41] N. Camire Ohrenberg, L. M. Paradee, R. J. DeWitte, D. Chong, W. E. Geiger, *Organometallics* **2010**, *29*, 3179–3186.

[42] C. G. Zoski, D. A. Sweigart, N. J. Stone, P. H. Rieger, E. Mocellin, T. F. Mann, D. R. Mann, D. K. Gosser, M. M. Doeff, A. M. Bond, *J. Am. Chem. Soc.* **1988**, *110*, 2109–2116.

[43] M. Landman, R. Pretorius, B. E. Buitendach, P. H. van Rooyen, J. Conradie, *Organometallics* **2013**, *32*, 5491–5503.

[44] S. D. Ross, M. Finkelstein, E. J. Rudd, *Anodic Oxidation: Organic Chemistry: A Series of Monographs, Volume 32*, Academic Press, Inc., New York, **1975**.

[45] E. L. Muetterties, J. R. Bleeke, E. J. Wucherer, T. Albright, *Chem. Rev.* **1982**, *82*, 499–525.

[46] E. Bulak, T. Varnali, B. Schwederski, D. Bubrin, J. Fiedler, W. Kaim, *Organometallics* **2011**, *30*, 6441–6445.

[47] J. Handzlik, F. Hartl, T. Szymańska-Buzar, *New J. Chem.* **2002**, *26*, 145–152.

[48] A. M. Bond, P. J. Dyson, D. G. Humphrey, G. Lazarev, P. Suman, *J. Chem. Soc., Dalton Trans.* **1999**, 443–448.

[49] A. Jansen van Rensburg, M. Landman, D. van der Westhuizen, M. M. Conradie, J. Conradie, *Electrochim. Acta* **2015**, *186*, 321–327.

[50] A. D. Hunter, L. Shilliday, W. S. Furey, M. J. Zaworotko, *Organometallics* **1992**, *11*, 1550–1560.

[51] R. Meyer, M. Schindehutte, P. H. van Rooyen, S. Lotz, *Inorg. Chem.* **1994**, *33*, 3605–3608.

[52] Gaussian 09, Revision D.01, M. J. Frisch, G. W. Trucks, H. B. Schlegel, G. E. Scuseria, M.

A. Robb, J. R. Cheeseman, G. Scalmani, V. Barone, B. Mennucci, G. A. Petersson, H. Nakatsuji, M. Caricato, X. Li, H. P. Hratchian, A. F. Izmaylov, J. Bloino, G. Zheng, J. L. Sonnenberg, M. Hada, M. Ehara, K. Toyota, R. Fukuda, J. Hasegawa, M. Ishida, T. Nakajima, Y. Honda, O. Kitao, H. Nakai, T. Vreven, J. A. Montgomery, Jr., J. E. Peralta, F. Ogliaro, M. Bearpark, J. J. Heyd, E. Brothers, K. N. Kudin, V. N. Staroverov, R. Kobayashi, J. Normand, K. Raghavachari, A. Rendell, J. C. Burant, S. S. Iyengar, J. Tomasi, M. Cossi, N. Rega, J. M. Millam, M. Klene, J. E. Knox, J. B. Cross, V. Bakken, C. Adamo, J. Jaramillo, R. Gomperts, R. E. Stratmann, O. Yazyev, A. J. Austin, R. Cammi, C. Pomelli, J. W. Ochterski, R. L. Martin, K. Morokuma, V. G. Zakrzewski, G. A. Voth, P. Salvador, J. J. Dannenberg, S. Dapprich, A. D. Daniels, Ö. Farkas, J. B. Foresman, J. V. Ortiz, J. Cioslowski, and D. J. Fox, Gaussian, Inc., Wallingford CT, **2009**.

[53] G. A. Petersson, A. Bennett, T. G. Tensfeldt, M. A. Al-Laham, W. A. Shirley, J. Mantzaris, *J. Chem. Phys.* **1988**, *89*, 2193–2218.

[54] G. A. Petersson, M. A. Al-Laham, *J. Chem. Phys.* **1991**, *94*, 6081–6090.

[55] P. J. Hay, W. R. Wadt, *J. Chem. Phys.* **1985**, *82*, 270–283.

[56] W. R. Wadt, P. J. Hay, *J. Chem. Phys.* **1985**, *82*, 284–298.

[57] P. J. Hay, W. R. Wadt, *J. Chem. Phys.* **1985**, *82*, 299–310.

[58] J. Paier, R. Hirschl, M. Marsman, G. Kresse, *J. Chem. Phys.* **2005**, *122*, 234102.

[59] D. Andrae, U. Häußermann, M. Dolg, H. Stoll, H. Preuß, *Theor. Chim. Acta* **1990**, *77*, 123–141.

CHAPTER 3

TUNGSTEN CARBONYL FISCHER CARBENE COMPLEXES WITH AROMATIC AMINE SUBSTITUENTS

3.1 Introduction

The electrophilic nature of the carbene carbon in Fischer carbene complexes is stabilized by π-donation of electron density by predominately (i) the transition metal filled d-orbitals and (ii) the lone pair of electrons of the heteroatom substituent (OR, NR_2). The delocalisation of electron density from an electron donating substituent on an aromatic ring towards an electron withdrawing substituent has also been investigated.[1–3] There have been several examples published where this characteristic has been used to play a role in the stabilisation of Fischer carbene complexes.[4,5] In this section of the study several aromatic ethoxy- and aminocarbene complexes are synthesised, all of which display tertiary amine groups, with the amino substituent in the *p*-position relative to the Fischer carbene carbon. It is expected that for all the compounds containing amine substituents, electron density will be donated into the ring through delocalisation (electron donor) towards the carbene substituent (electron acceptor) shown in Figure 3.1. Making use of this characteristic, the amount of electron density donated into the aromatic ring will be investigated by altering the R groups present on the distant nitrogen.

It is further expected that an increase of the electron density at the carbene carbon through aminolysis will directly influence and decrease the amount of electron density required from the aromatic ring towards the stabilisation of the carbene tungsten carbonyl complex.

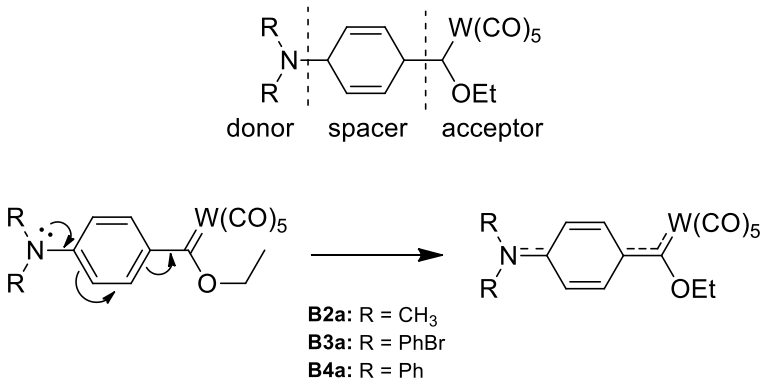

Figure 3.1. Electron delocalisation from the nitrogen through the aromatic ring to the carbene carbon

Unlike for the π-arene$(Cr(CO)_3)$ complexes in Chapter 2, some of the complexes synthesised and discussed are known. The unique electronic properties of these complexes will be used in the synthesis of more complex compounds and will provide the electronic properties and characteristics of the macromolecules. To ensure a better understanding of the individual carbene ligands, a more comprehensive study of these compounds is conducted using spectroscopic methods such as IR, NMR and cyclovoltammetry supported with IR-spectroelectrochemistry techniques.

3.2 Results and Discussion

3.2.1 Synthesis

The synthesis of the compounds is conducted under an inert atmosphere using standard Schlenk techniques. Starting aromatic materials have bromine substituents which are lithiated by lithium-halogen exchange reactions, after which $W(CO)_6$ is added. After formation, the metal acylate is neutralised by alkylation. The compounds are all bright orange of colour and are isolated in sufficient yields as to use for large scale aminolysis and coordination reactions.

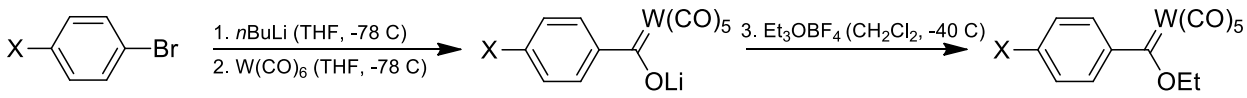

B1a: X = H
B2a: X = NMe_2
B3a: X = $N(PhBr)_2$
B4a: X = NPh_2

Scheme 3.1. Synthesis of ethoxycarbene complexes with aromatic amine substituents[6,7]

A series of aminocarbene complexes are also synthesised to investigate the effect of an increased amount of electron density available at the carbene carbon and the effect on the distant aromatic amino substituent. This synthesis, however, requires that a secondary amine group is used for the aminolysis (Scheme 3.2) as to reduce the potential reactivity of a primary amine group during further reactions of the macromolecules. By making use of the stability of the synthesised aminoaryl-ethoxycarbene complexes, aminolysis by a secondary amine is achieved in quantitative yields of all Fischer carbene complexes in an aqueous environment. Dimethylamine is commercially available in the gas form or as a THF solution which is not ideal to handle or store for long periods of time. Thus, a new method is introduced to indirectly aminolise with dimethylamine: the tungsten carbonyl ethoxycarbene complex, dimethylamine hydrochloride (dimethylammonium chloride) and sodium hydroxide are suspended in THF. A small amount of distilled H_2O is added to the solution until all reagents are dissolved. Upon solvation, the bright orange solution turns bright yellow within seconds.

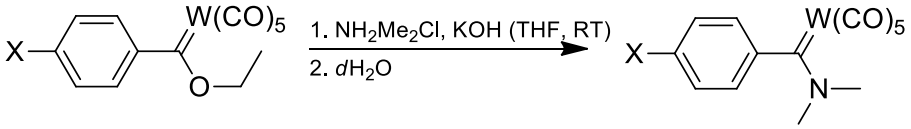

B1a: X = H
B2a: X = NMe_2
B3a: X = $N(PhBr)_2$
B4a: X = NPh_2

B1b: X = H
B2b: X = NMe_2
B3b: X = $N(PhBr)_2$
B4b: X = NPh_2

Scheme 3.2. Synthesis of N,N-dimethylamine carbene complexes through the *in situ* release of dimethylamine

The reaction is based on the release of dimethylamine in an acid-base reaction between the dimethylamine hydrochloride and sodium hydroxide. The reaction requires an aqueous

environment which is why a small amount of H_2O is added to trigger the reaction. The bright orange solution turns bright yellow within seconds to confirm that the aminolysis reaction is complete. The rapid reaction ensures that the Fischer carbene complex survives the harsh environment to which it is exposed.

By synthesising the four different ethoxycarbene complexes and isolating their aminolysis products, eight carbene complexes are synthesised which will be used as reagents in the rest of the project as carbene transfer agents.

3.2.2 NMR Spectroscopy

Table 3.1. Selected ^{1}H and ^{13}C NMR chemical shifts of B1a to B4a in CD_2Cl_2

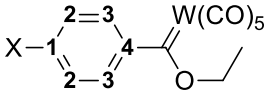

B1a: X = H
B2a: X = NMe_2
B3a: X = $N(PhBr)_2$
B4a: X = NPh_2

^{1}H NMR spectra (ppm), *J* (Hz)	B1a	B2a*	B3a*	B4a*
H_1	7.56 (dd, *J* = 8.4, 8.3)	–	–	–
H_2	7.45 (dd, *J* = 8.0, 8.0)	6.65 (d, *J* = 9.4)	6.94 (d, *J* = 9.0)	6.88 (d, *J* = 9.1)
H_3	7.44 (d, *J* = 8.2)	8.04 (d, *J* = 9.3)	7.79 (d, *J* = 9.0)	7.84 (d, *J* = 9.1)
CH_2 (OEt)	5.06 (q, *J* = 7.1)	5.00 (q, *J* = 7.0)	5.04 (q, *J* = 7.0)	5.02 (q, *J* = 7.0)
CH_3 (OEt)	1.71 (t, *J* = 7.1)	1.65 (t, *J* = 7.0)	1.67 (t, *J* = 7.1)	1.65 (t, *J* = 7.1)
^{13}C NMR spectra (ppm)	**B1a**	**B2a***	**B3a***	**B4a***
C_1	132.0	141.1	146.8	145.5
C_2	128.5	110.5	118.1	132.8
C_3	126.6	134.7	131.6	117.8
C_4	155.9	155.0	151.5	153.3
C_{Carb}	320.5	299.2	308.4	305.8
$C_{W(CO)5}$	204.4	203.8	203.4	203.8
	197.9	199.7	197.9	198.6
CH_2 (OEt)	81.0	78.9	79.6	79.7
CH_3 (OEt)	15.2	13.3	14.8	15.2

*Chemical shifts of substituents not directly bonded to the carbene ligand, but to N, is available in the experimental section

The NMR spectra for all compounds have been recorded in CD_2Cl_2 so that a comparative study can be conducted with less soluble complexes. Selected NMR chemical shift values are shown in Table 3.1 and Table 3.2 for the ethoxy- and aminocarbene complexes respectively. Full NMR spectral assignments for all compounds can be found in the experimental section of the chapter.

Table 3.2. Selected ^{1}H and ^{13}C NMR chemical shift values of compounds B1b to B4b in CD_2Cl_2

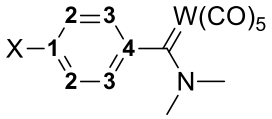

B1b: X = H
B2b: X = NMe_2
B3b: X = $N(PhBr)_2$
B4b: X = NPh_2

^{1}H NMR spectra (ppm), *J* (Hz)	**B1b**	**B2b**	**B3b**	**B4b**
H_1	7.18 (ddd, *J* = 7.8, 7.5, 1.4)	–	–	–
H_2	7.42 (ddd, *J* = 7.8, 7.5, 1.7)	6.74 (d, *J* = 9.1)	6.75 (d, *J* = 8.8)	6.70 (d, *J* = 8.6)
H_3	7.42 (dd, *J* = 7.5, 1.7)	6.69 (d, *J* = 9.1)	7.11 (d, *J* = 8.8)	7.09 (d, *J* = 8.5)
NMe_2	3.93 3.03	3.89 3.04	3.93 3.16	3.91 3.14
^{13}C NMR spectra (ppm)	**B1b**	**B2b**	**B3b**	**B4b**
C_1	126.6	143.5	145.4	146.3
C_2	119.9	112.1	121.6	121.2
C_3	128.8	121.5	125.0	123.4
C_4	153.8	149.4	149.9	148.8
C_{Carb}	256.7	258.2	256.9	257.2
$C_{W(CO)5}$	204.8 199.0	205.1 199.3	205.0 199.2	204.9 199.1
NMe_2	44.8	44.5	45.1	44.9

*Chemical shifts of substituents not directly bonded to the carbene ligand, but to N, is available in the experimental section

A pronounced electronic difference is observed between the ethoxy- and aminocarbene complexes in terms of carbene stabilisation and electron delocalisation by the carbene substituents. Carbene carbons which contain an amine as heteroatom are more stabilised

compared to their ethoxy- or methoxy- analogues.[6,8] When all the different aminocarbene complexes are compared in Table 3.2, there are no significant differences in the chemical shift values of the carbene carbons for **B1b**, **B2b**, **B3b** and **B4b** with respective values of 256.7, 258.2, 256.9 and 257.2 ppm. This is expected as the complexes receive most of their stabilisation from their metal and amino substituents.

Significant differences in the carbene chemical shift values are observed for the ethoxycarbene complexes. The respective chemical shift values of the carbene carbon for complexes **B1a**, **B2a**, **B3a** and **B4a** are 320.5, 299.2, 308.4 and 305.8 ppm. The recorded values are ascribed to the amount of electron density provided indirectly by the distant amine via the benzene spacer and thus reflect the involvement of the aromatic ring in the stabilisation of the ethoxycarbene complexes. The difference between an ethoxy- and its aminolysed analogue is further illustrated in Figure 3.2 which shows the ^{1}H NMR spectra of **B2a** (red) and **B2b** (blue). There is little difference between the four aromatic protons (6.75 – 6.68 ppm) in **B2b** even if there is an electron withdrawing substituent (carbene carbon) directly next to two of the protons. While, for **B2a**, the protons in the *o*-position relative to the carbene substituent are found significantly downfield with a value of 8.04 ppm and the protons at the *m*-positions at 6.65 ppm ($\Delta\delta$ =1.4 ppm). This indicates the effect of shielding of one set of protons from the distant nitrogen and the deshielding effect of the other set from the electron-withdrawing carbene complex.

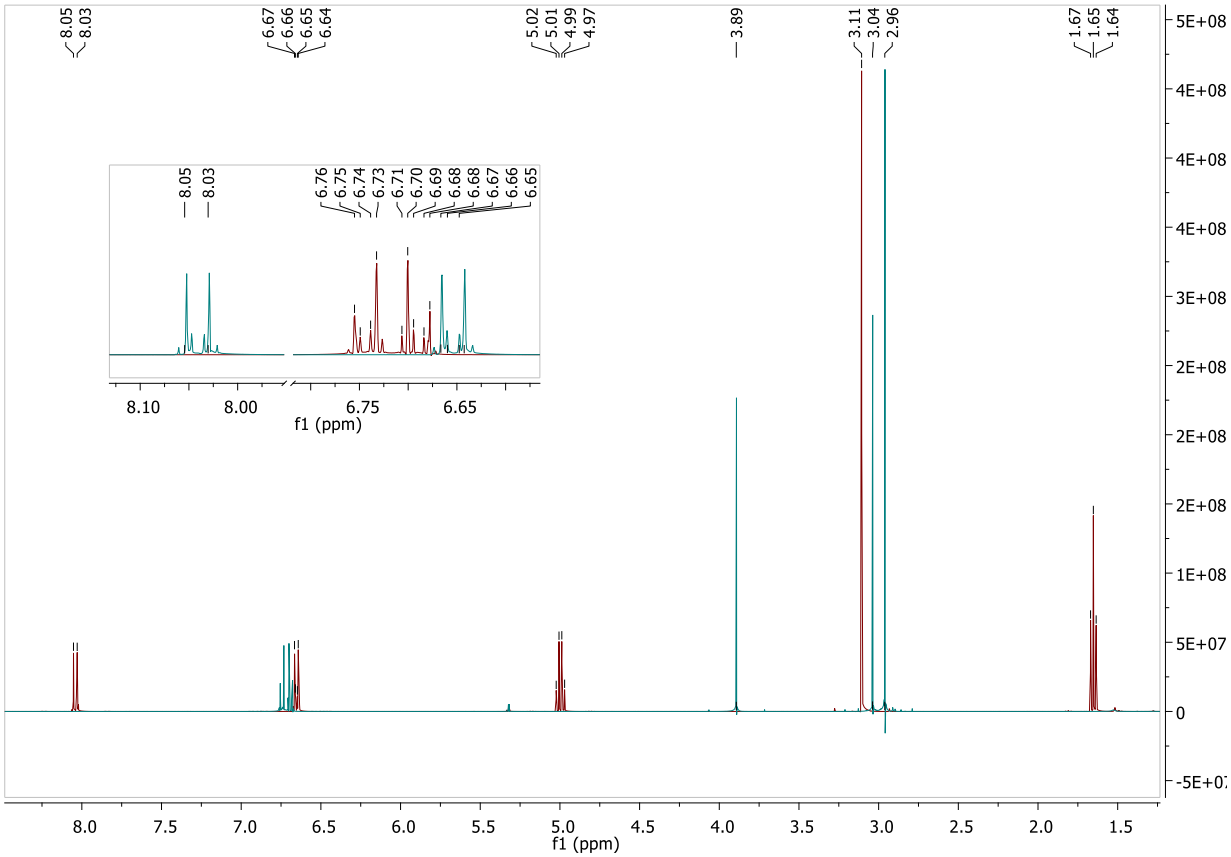

Figure 3.2. ^{1}H NMR spectra of B2a (red) and B2b (blue) in CD_2Cl_2

The known carbene complexes that have been synthesised without aromatic substituents are reactive and less stable.[9–11] For the ethoxycarbene complexes in this study, it is clear that the carbene carbon receives a significant amount of electron density from the aromatic ring as most of the complexes synthesised has a nitrogen atom at the *p*-position relative to the carbene substituent on the ring. It is further expected that as the substituents of the amine change, the amount of electron density donated towards the carbene carbon will also change. **B1a** and **B1b** do not contain an amine that can contribute towards the stabilisation of the carbene carbon, and can therefore be used as references to investigate the effect when a tertiary amine is present.

The NMR spectra of the compounds reveal that the distant amine substituent contributes significantly when it is present (as in **B2a**, **B3a** and **B4a**). For example, overlaying **B1a** (blue) and **B2a** (red) shows the electron donating effect of the distant amine on the aromatic ring (Figure

3.3). In **B2a**, the *o*-protons relative to the carbene carbon are deshielded (8.04 ppm), while the *o*-protons relative to the amine substituent are shielded (6.66 ppm). The aromatic protons for **B1a** are observed between 7.51 and 7.41 ppm, all showing a similar deshielding effect by the carbene carbon. The same pattern is observed for all the other compounds containing a tertiary amine on the *p*-position relative to the carbene complex.

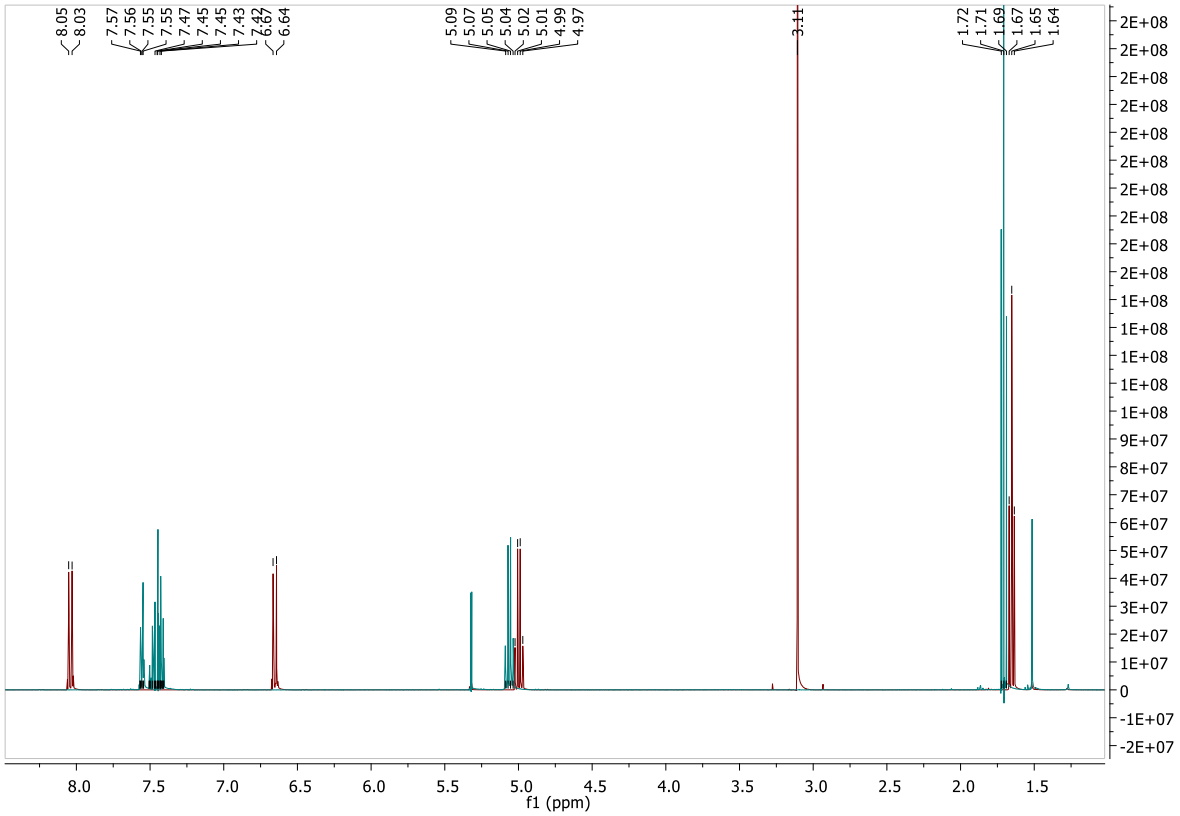

Figure 3.3. ^{1}H NMR spectrum of B1a (blue) and B2a (red) in CD_2Cl_2

Interestingly, a small downfield shift of the methylene protons of the ethoxy substituent is visible for **B1a** to support of the lack of stabilization from the aromatic ring. By comparing the ^{1}H NMR chemical shift value of the CH_2 present in the ethoxy substituent, it is possible to indirectly determine which complex receives the most electron density from the aromatic ring on the premise that the metal contribution, although significant, is more or less constant. When the carbene carbon receives a significant amount of electron density from the aromatic ring, less electron density is displaced from the ethoxy substituent and it will appear more shielded. On this

basis, it is possible to conclude that **B2a** receives the greatest amount of electron density from the aromatic ring as the ^{1}H NMR chemical shift has a value of 5.00 ppm, followed by **B4a** (5.02 ppm), **B3a** (5.04 ppm) and **B1a** (5.06 ppm). The same pattern is observed in the shielding of the carbene carbon: As the carbene carbon receives more electron density from the aromatic ring, it becomes more shielded. Again, **B2a** is the most shielded followed by **B4a**, **B3a** and **B1a** with respective ^{13}C NMR chemical shift values for the respective carbene carbon signals at 299.2, 305.8, 308.4 and 320.5 ppm. The contribution of the amine towards the stabilisation of the carbene complex is evident when **B1a** – which does not contain the amine substituent – is compared to **B2a**, **B3a** and **B4a**. As mentioned earlier, the ^{13}C NMR chemical shift value for the carbene carbon of **B1a** is downfield compared to the other complexes. The carbene carbon also relies more on the metal carbonyl as well as on the ethoxy substituent for its stabilisation.

From these observations, and in the following sections, it is and will become more evident that the aromatic substituent of an aminolysed carbene complex do not play a significant role in the stabilisation of the carbene carbon, but rely greatly on the electron density of the attached nitrogen heteroatom. The opposite is true for the ethoxycarbene complexes, which require the aromatic ring to participate to a much greater extent since their oxygen heteroatoms do not supply enough electron density towards the stabilisation of the carbene carbon

3.2.3 Cyclovoltammetry

The cyclovoltammetry experiments were initially conducted in CH_2Cl_2, but it was found that the reduced species reacted with the solvent to form $[W(CO)_5Cl]^-$. Therefore, the voltammetry measurements of the compounds are conducted in THF at room temperature with NBu_4PF_6 as buffer. All the ethoxycarbene complexes are irreversibly oxidised between 0.3 and 0.7 V and show some form of reversible reduction between –1.8 and –2.1 V when referenced to the oxidation and reduction half wave potential of ferrocene ($FeCp_2$), decamethylferrocene (DmFc) or cobaltocene ($CoCp_2$).

There are two possible sites of oxidation in each complex: the metal to which the carbene carbon is coordinated or the amine present on the aromatic substituent of the carbene carbon. Previous publications on the oxidation and reduction processes that occur in small aromatic carbene complexes (the aromatic rings not containing substituents) of tungsten and chromium show that the metal is oxidised while the reduction occurs on the carbene carbon itself.[12,13] As the complexes under investigation contain tertiary amines that are well known for their electron donating character, the first oxidation is expected on the nitrogen atom itself.[14]

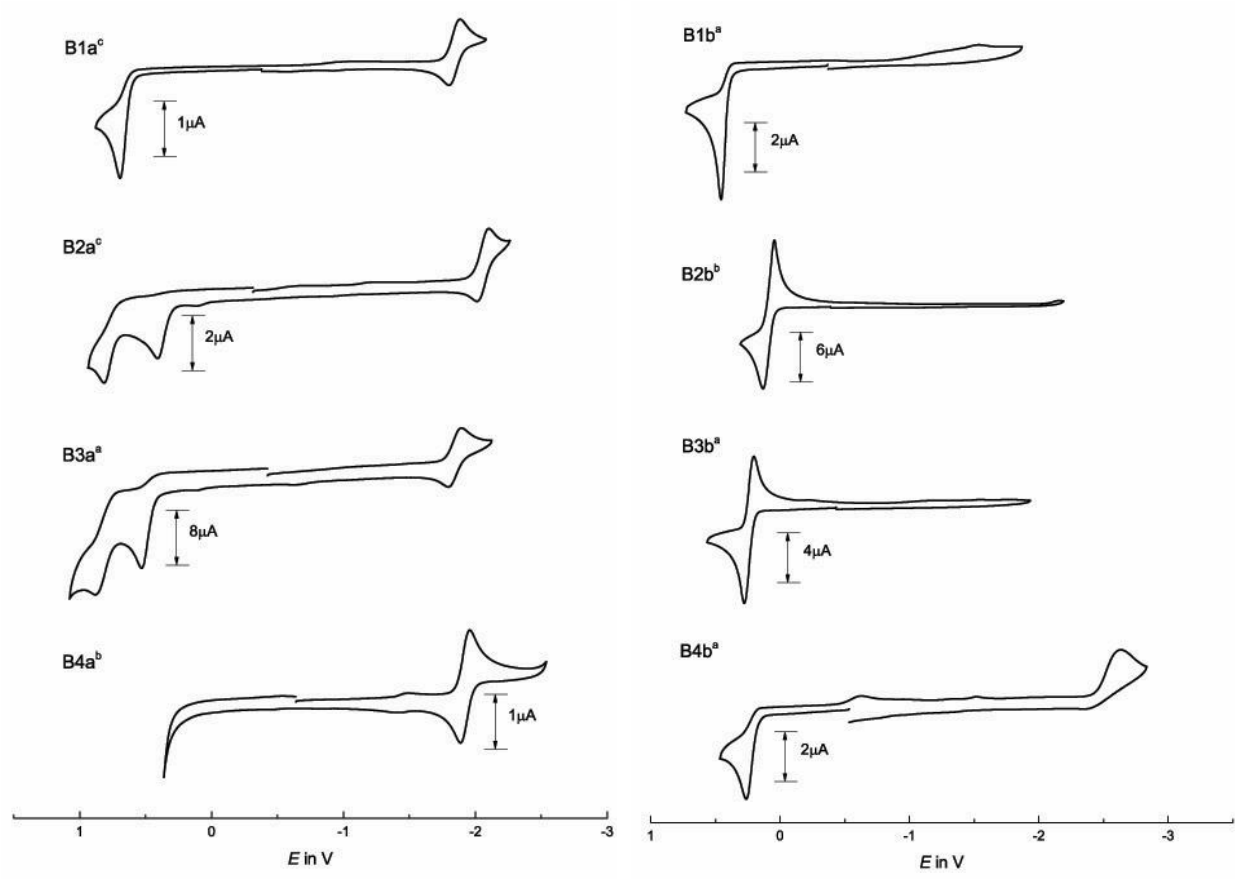

Figure 3.4. Cyclovoltammograms of B1a – B4a (left) and B1b – B4b (right) in THF/0.1 M NBu_4PF_6 buffer at scan rate 100 mV/s referenced against $^{a}FeCp_2^{0/+}$, $^{b}DMFc^{0/+}$ or $^{c}CoCp_2^{0/+}$

The cyclovoltammograms of **B1a** – **B4a** as well as **B1b** – **B4b**, recorded at a scan rate 100 mV/s are shown in Figure 3.4. Each oxidation or reduction process for each complex has been analysed

at different scan rates to conclude whether the processes are reversible, quasi-reversible or irreversible. As examples, the current and peak potentials of the electrochemical processes at different scan rates of **B2a** and **B2b** are listed in Table 3.3 and Table 3.4, respectively, and shown in Figure 3.5 and Figure 3.6, respectively. The analyses of all other complexes can be found in the Appendix of the manuscript. For an oxidation or reduction process to be described as fully reversible, it requires and i_{pc}/i_{pa} value close to 1, a ΔE_p value of ~59 mV for a one electron process and the $E_{1/2}$ value is expected to remain constant. The process must meet the requirements at all scan rates to be described as a reversible process.[15]

Table 3.3. Peak currents and peak current ratios for the reduction of B2a at different scan rates in THF/0.1 M NBu_4PF_6 buffer against a cobaltocene/cobaltocenium standard

Scan rate /mV.s^{-1}	i_{pc} /µA	i_{pa} /µA	i_{pc}/i_{pa}	E_{pc} /V	E_{pa} /V	ΔE_p /V	$E_{1/2}$ /V
50	0.43	0.18	2.36	-2.1097	-2.0092	0.1005	-2.0594
100	0.63	0.35	1.79	-2.1020	-2.0155	0.0865	-2.0588
200	1.09	0.74	1.47	-2.1020	-2.0168	0.0852	-2.0594
400	1.63	1.33	1.23	-2.0996	-2.0258	0.0738	-2.0627
600	2.13	1.76	1.21	-2.1007	-2.0270	0.0738	-2.0638
800	2.50	2.11	1.19	-2.0996	-2.0232	0.0764	-2.0614
1000	2.80	2.48	1.13	-2.1033	-2.0245	0.0789	-2.0639
1500	3.64	3.23	1.13	-2.1033	-2.0232	0.0802	-2.0633
2000	4.31	3.76	1.15	-2.1046	-2.0181	0.0865	-2.0614

In general (from Figure 3.4), the ethoxycarbene complexes show reversible reductions or reductions that have some degree of reversibility while their oxidations are irreversible. The aminocarbene complexes all show irreversible reductions and only **B2b** and **B3b** appears to have reversible oxidations. Upon the analysis of peak currents and potentials of all complexes, it is evident that the reduction processes of all the ethoxycarbene complexes show ΔE_p values that increase above 59 mV as the scan rate of the reduction process in each case is increased. The compounds meet all the other requirements for a reversible process. As the reduction and reoxidation of the ethoxycarbene complexes are dependent on the scan rate of the experiment,

the reduction processes for all complexes are therefore quasi-reversible. The oxidation of **B2b** is assigned as quasi-reversible as it too, shows dependence on the scan rate of the process while the oxidation of **B3b** is irreversible as it does not meet any of the criteria for a reversible process.

Table 3.4. Peak currents and peak current ratios for the reduction of B2b at different scan rates in THF/0.1 M NBu_4PF_6 buffer against a decamethylferrocene/decamethylferrocenium standard

Scan rate /mV.s^{-1}	i_{pc} /µA	i_{pa} /µA	i_{pc}/i_{pa}	E_{pc} /V	E_{pa} /V	ΔE_p /V	$E_{1/2}$ /V
50	3.96	4.19	0.95	0.0616	0.1205	0.0589	0.0911
100	7.50	6.12	1.22	0.0536	0.1241	0.0705	0.0888
200	9.26	8.12	1.14	0.0476	0.1284	0.0808	0.0880
400	13.22	11.54	1.15	0.0463	0.1314	0.0851	0.0888
600	15.44	13.70	1.13	0.0418	0.1357	0.0940	0.0887
800	17.22	15.70	1.10	0.0403	0.1357	0.0955	0.0880
1000	18.39	17.20	1.07	0.0403	0.1416	0.1013	0.0909
1500	21.89	20.49	1.07	0.0374	0.1431	0.1057	0.0902
2000	24.59	22.73	1.08	0.0329	0.1489	0.1160	0.0909

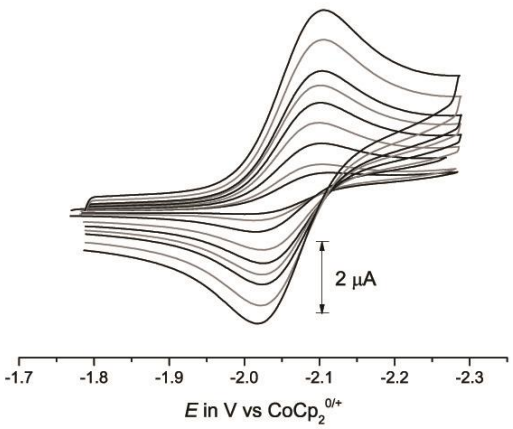

Figure 3.5. Reduction of B2a in THF/0.1 M NBu_4PF_6 at scan rates of 50, 100, 200, 400, 600, 800, 1000, 1500 and 2000 mV/s referenced against $CoCp_2^{0/+}$

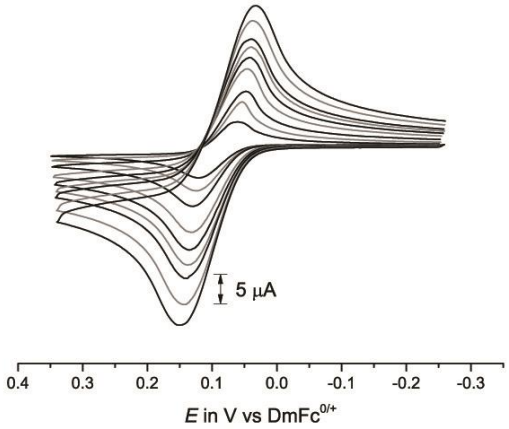

Figure 3.6. Oxidation of B2b in THF/0.1 M NBu_4PF_6 at scan rates of 50, 100, 200, 400, 600, 800, 1000, 1500 and 2000 mV/s referenced against $DmFc^{0/+}$

By using internal standards and their oxidation potentials against free ferrocene it is possible to compare the oxidation and reduction potentials of the carbene complexes. The oxidation and

reduction half wave potentials for the complexes are recorded in Table 3.5. In Figure 3.4, the reduction potentials of **B1b**, **B2b** and **B3b** are not recorded as the complexes are very reactive upon reduction and delivers unusable data when reduced.

Table 3.5. Oxidation and reduction half wave potentials for B1a – B4a and B1b – B4b in THF/0.1 M NBu_4PF_6 at scan rate of 100 mV/s against a $^{a}Cp_2Fe^{0/+}$, $^{b}Cp_2Co^{0/+}$ or $^{c}DmFc^{0/+}$ internal standard

Compound	Oxidation $E_{1/2}$ /V	Reduction $E_{1/2}$ /V
B1a[b]	0.696*	-1.838
B2a[b]	0.416*	-2.058*
B3a[a]	0.538*	-1.841*
B4a[c]	0.359*	-1.919
B1b[a]	0.455*	n.o.[a]
B2b[a]	0.089	n.o.[a]
B3b[c]	0.240*	n.o.[a]
B4b[a]	0.224*	-2.635*

* Irreversible oxidation or reduction, [a] Reduction falls outside solvent window

Comparing the ethoxycarbene complexes in Figure 3.4, a single oxidation process is observed for **B1a**, which has a phenyl as an aromatic substituent of the carbene carbon. It is expected that the oxidation of **B1a** will occur on the W(0) centre as the HOMO is commonly found on the metal for small aromatic Fischer carbene complexes of Group VI metals.[12,13] **B2a** – **B4a** are expected to show two one-electron oxidation processes: one for the W(0) centre and the other for the tertiary amine present in the aromatic substituent of the carbene carbon. This is indeed observed for **B2a** and **B3a** which show two irreversible oxidation processes. **B4a** however, shows only a single oxidation at which the compound readily reacts or decomposes. This is expected as there are numerous examples which show that the oxidation of a triphenylamine compound without protection at the *p*-positions of the aromatic rings relative to the amine lead to intermolecular reactions upon oxidation.[14,16,17] As immediate decomposition is observed for **B4a** upon oxidation, it is expected that the HOMO for the compound is found on the tertiary amine present

in the aromatic substituent of the carbene carbon rather than the metal centre present in the complex. An irreversible anodic wave, rather than immediate decomposition would have been expected should the metal be oxidised first. The HOMOs for both **B2a** and **B3a** are expected to reside on the tertiary amine of the carbene substituent as the two complexes show similar oxidation patterns. Further, it has been previously shown through DFT calculations that the HOMO resides on the tertiary amine of **B3a.**[7,18,19] Thus, to summarise, a single irreversible oxidation of **B1a** is observed and occurs on the metal. Two irreversible oxidations are observed for **B2a** and **B3a**, the first which occurs on the tertiary amine of the carbene substituent and the second which occurs on the metal. **B4a** decomposes upon the first oxidation of the tertiary amine.

Comparing the compounds containing the tertiary amines, **B4a** is oxidised at the lowest potential followed by **B2a** and finally by **B3a** with respective oxidation potentials of 0.359, 0.416 and 0.538 V. It is evident that the bromine substituents of the aromatic rings have a significant electron withdrawing effect on the amount of electron density present on the nitrogen atom when the first oxidation potentials of **B3a** and **B4a** are compared (0.538 and 0.359 V, respectively). The oxidation of **B2a** occurs at a higher potential than that of **B4a**, which is unexpected as its amine is electron rich compared to **B4a**. Two effects that may cause the difference in oxidation potential is the extensive electron delocalisation from the amine to the carbene carbon in **B2a**. Another aspect to consider is the stabilisation of the formed radical upon oxidation which may also influence the oxidation potential. A more stabilised radical will allow for oxidation at lower potentials.[20] Both effects need to be considered.

All reduction processes are expected to occur on the carbene carbon for all the complexes.[21] For the ethoxycarbene complexes the series can then be arranged in the following order of decreasing electron density on comparison of their reduction potentials: **B2a**, **B4a**, **B3a** and **B1a** with respective reduction half-wave potentials of –2.058, –1.919, –1.841 and –1.838 V. The order of the series corresponds directly with what has been observed in the NMR spectroscopy for the compounds.

Comparing the oxidation and reduction potentials of the ethoxy- and aminocarbene complexes, it is evident that the oxidation of the aminocarbene complexes occur at much lower potentials than those of the ethoxycarbene complexes. From the NMR spectra, it has been established that the aromatic ring of any of the aminolysed carbene complexes do not contribute significantly to the stabilisation of the carbene carbons themselves. Assuming the HOMO remains on the nitrogen and the aromatic ring for the aminocarbene complexes, the aromatic ring will be significantly more electron rich than that of the ethoxycarbene complexes. This is confirmed with the significantly lower oxidation potentials of the aminocarbene complexes compared to the analogous ethoxycarbene complexes. The oxidation potentials correlate well to what has been predicted from the NMR analysis. **B2b** is oxidised at the lowest potential (0.089 V), while **B3b** and **B4b** are oxidised at 0.240 and 0.224 V, respectively. The irreversible oxidation of **B4b** is expected.

The irreversible oxidation of **B1b** occurs at a much higher potential of 0.457 V because it has been previously shown that it is the metal being oxidised rather than the aromatic group, in small aromatic aminolysed carbene complexes.[12]

3.2.4 IR-spectroscopy and IR-Spectroelectrochemistry

As some of the complexes can undergo reversible or quasi-reversible redox processes, it is possible to measure the changes in IR-vibration frequencies during these processes. This is achieved through a technique known as spectroelectrochemistry (SEC). All the spectra are analysed in THF as to ensure that the reduced species of the complexes do not react with the solvent.

The IR peak assignments of the neutral species of the complexes in the IR region are listed in Table 3.6. The ethoxycarbene carbon, receiving the greater amount of electron density from the aromatic substituent, requires less backbonding from the metal carbonyl group. As a result, with more electron density on the tungsten, more π back-bonding to the five carbonyl ligands are required leading to a decrease in carbonyl bond order. Thus, for the more electron donating

aromatic groups, the carbonyl vibration pattern is found at lower wavenumbers. The series for the most to the least electron donating aromatic group is again confirmed by what is observed in the IR spectra of the carbonyl vibrations for the ethoxycarbene complexes: **B2a** > **B4a** > **B3a** > **B1a**. As anticipated, the position of the bands correlate directly with the observations made for the carbene carbon's chemical shifts in the ^{13}C NMR section of this study.

From the data, the bands of the ethoxycarbene complexes are found at higher wavenumbers than those of the aminocarbene complexes. For these complexes, the carbene carbon receives a greater amount of electron density from its heteroatom substituent, and therefore require less back-bonding from the tungsten which will have a higher residual electron density. It is further observed that there is no difference in the vibration frequencies of the aminocarbene complexes. This shows that the carbene carbon and its coordinated metal carbonyl moiety can function electronically independently from the aromatic substituent. This is supported by the ^{13}C NMR spectral data.

Table 3.6. IR spectral assignments of the carbonyl region of B1a – B4a and B2b – B4b in THF at RT

	$A_1^{(1)}$	B_1	E	$A_1^{(2)}$
B1a	2068	1983	1940	n.o.
B2a	2060	1973	1929	n.o.
B3a	2064	1977	1934	n.o.
B4a	2063	1976	1933	n.o.
B2b	2060	1968 (w)	1924 (vs)	1903 (sh)
B3b	2060	1969 (w)	1925 (vs)	1904 (sh)
B4b	2060	1969 (w)	1925 (vs)	1906 (sh)

The IR-SEC allows for the indirect identification of the site of oxidation or reduction and the influence of the process on the tungsten carbonyl group. As discussed in an earlier part of the study, for a pentacarbonyl system, four allowed bands are expected: $A_1^{(1)}$, B_1, E and $A_1^{(2)}$ bands. Upon reduction of a compound, an increase of electron density is expected on either the metal carbonyl or the aromatic group to which the carbene carbon is a substituent. Should the reduction occur on the metal itself, a large shift to lower wavenumbers is expected (normally greater than 70 cm^{-1} in either direction).[22,23]

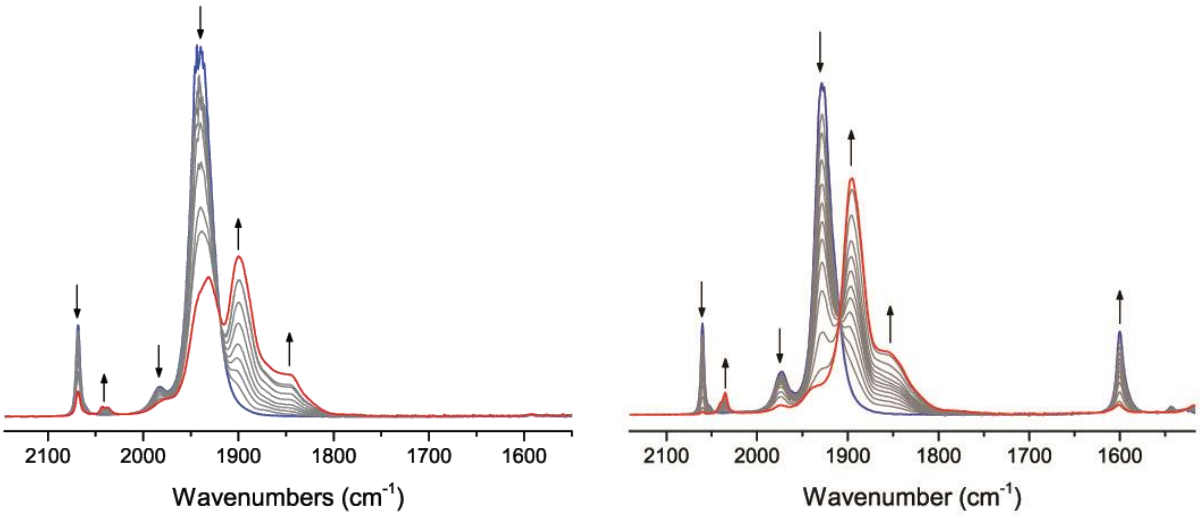

B1a **B2a**

Figure 3.7. IR-SEC spectra of the carbonyl region of complexes B1a and B2a upon reduction in THF /1.5 M NBu_4PF_6

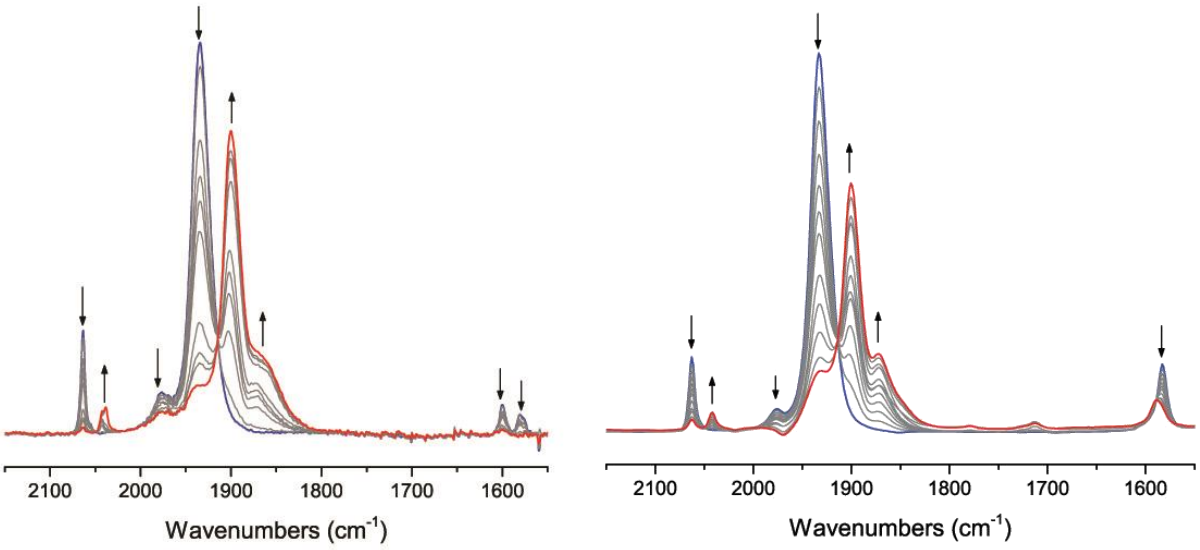

B3a **B4a**

Figure 3.8. IR-SEC spectra of the carbonyl region of complexes B3a and B4a upon reduction in THF /1.5 M NBu_4PF_6

The IR-SEC spectra of **B1a** – **B4a** are shown in Figure 3.7 and Figure 3.8 for the reduction processes of the ethoxycarbene complexes. All the reductions of **B1a** – **B4a** have been assigned as

quasi-reversible. The carbonyl vibration bands for the neutral and reduced species of the ethoxycarbene complexes are listed in Table 3.7.

Table 3.7. $W(CO)_5$ IR vibrational bands for B1a – B4a before and after reduction in THF /1.5 M NBu_4PF_6

	$A_1^{(1)}$	B_1	E	$A_1^{(2)}$
B1a	2068	1983	1940	n.o.*
B1a$^-$	2040	n.o.*	1900	1844
B2a	2060	1973	1929	n.o.*
B2a$^-$	2035	1940	1896	1852
B3a	2064	1977	1934	n.o.*
B3a$^-$	2039	1938	1900	1864
B4a	2063	1976	1933	n.o.*
B4a$^-$	2043	n.o.*	1900	1871

* Overlap with E band

From the spectra, it is evident that it is not the metal being reduced. In general, a clear shift of the E band of about 40 cm^{-1} is observed to lower wavenumbers. In the spectra for all complexes, the $A_1^{(2)}$ band which is not generally observed before reduction, becomes visible as a shoulder band of the E band. In all cases the B_1 band is no longer observed upon oxidation and the $A_1^{(1)}$ band moves approximately 30 cm^{-1} to lower wavenumbers. (Table 3.7). As the centre of reduction is not the metal itself, it is evident that the reduction is ligand based. The site of reduction is on the carbene carbon rather than the aromatic groups to which the carbene carbon is a substituent as has been shown is several cases in literature (Scheme 3.3).[21,24]

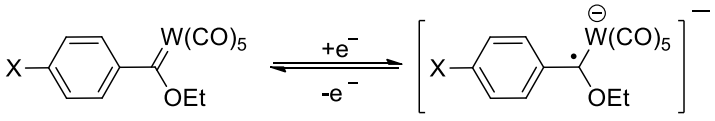

B1a: X = H
B2a: X = NMe_2
B3a: X = $N(PhBr)_2$
B4a: X = NPh_2

Scheme 3.3. Quasi-reversible reduction of the ethoxycarbene complexes

It is also necessary to state that the nitrogen atoms present in the tertiary amine carbene complexes are not sites that will easily reduce as the amines are well known for their orbital saturating character (i.e. hole-transport capabilities). As none of the ethoxycarbene complexes show any form of reversible oxidation, it was not possible to investigate the effect of the oxidation on the tungsten carbonyl group.

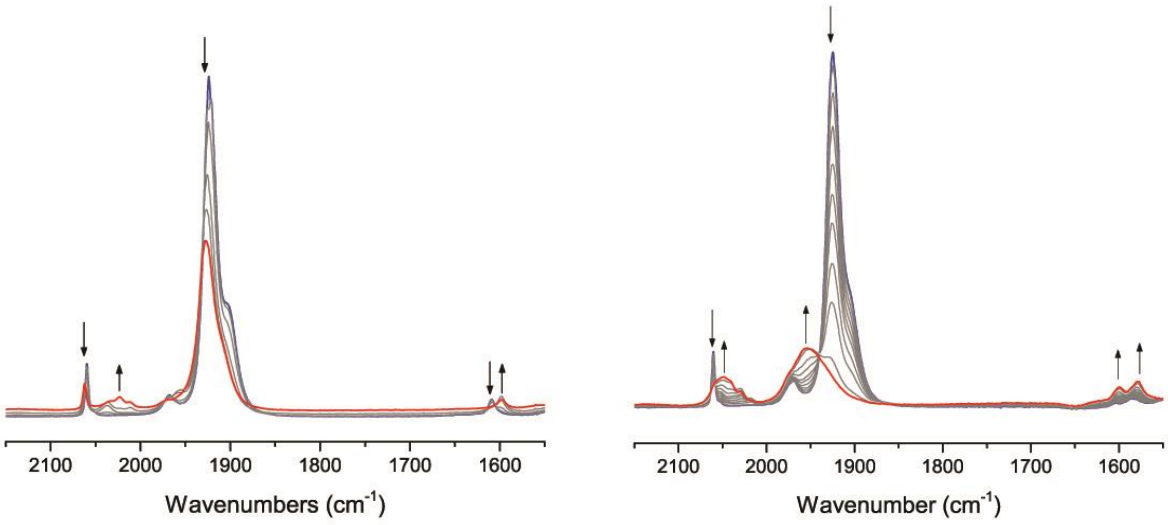

B2b **B3b**

Figure 3.9. IR-SEC spectra of the carbonyl region of complexes B2b and B3b upon oxidation in THF /1.5 M NBu_4PF_6

As stated in the cyclovoltammetry section, only **B2b** shows a fully reversible oxidation while the oxidation of **B3b** has formally been assigned as irreversible although it does show some degree of reversibility. Upon oxidation, the E-band of **B3b** shifts from 1925 cm^{-1} to 1950 cm^{-1}, indicating that the oxidation does not occur on the metal, but is found on the ligand (Figure 3.9). The SEC spectra of the two compounds are shown in Figure 3.9. Both the spectra reveal that the formed oxidised species are quite reactive as both compounds show some decomposition upon oxidation of the compounds. It is likely that the timescale on which the SEC takes place is much slower than that of the CV, thus allowing the oxidised species to react while the measurement is in progress. The only observation that can be made from the two spectra is the clear shift of the E band to higher wavenumbers.

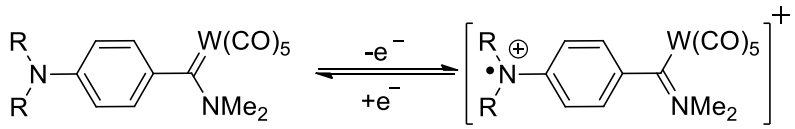

B2b: R = Me
B3b: R = PhBr

Scheme 3.4. Oxidation of the aminocarbene complexes, affording the oxidised species

3.2.5 X-Ray Crystallography

The crystal structure of **B1a** was published before and will be used to compare structural properties of the amino-arylcarbene complexes of this study.[25] Complex **B3a** has recently been published, but forms part of this project.[7] Selected bond lengths and angles for **B1a**, **B3a** and **B4a** are listed in Table 3.8 while that of **B2a** are listed in Table 3.9. The solid state structures of **B2a** is shown in Figure 3.11 and that of **B3a** and **B4a** are shown in Figure 3.10.

Table 3.8. Selected bond lengths and bond angles for the crystal structures of B1a, B3a and B4a

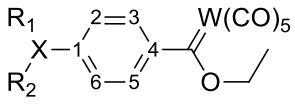

B1a: X = H, R_1 and R_2 = 0
B2a: X = N, R_1 and R_2 = Me
B3a: X = N, R_1 and R_2 = PhBr
B4a: X = N, R_1 and R_2 = Ph

	B1a[25]	**B3a**[7]	**B4a**
Symmetry	P $2_1/c$	C 2/c	P -1
Bond lengths (Å)			
X–C_1	0.96(4)	1.398(4)	1.379(4)
C_4–C_{carb}	1.60(3)	1.482(5)	1.471(4)
C_{carb}–O_{OEt}	1.30(3)	1.317(4)	1.325(3)
C_{carb}–W	2.20(2)	2.221(3)	2.235(3)
Bond angles (°)			
R_1–X–C_1	–	119.6(3)	2.235(3)
R_2–X–C_1	–	123.9(3)	122.7(3)
R_1–X–R_2	–	116.6(3)	116.5(2)
C_4–C_{Carb}–O_{OEt}	105(2)	106.0(3)	106.8(2)
C_4–C_{Carb}–W	125(1)	127.0(2)	126.6(2)
W–C_{Carb}–O_{OEt}	130(2)	127.0(2)	126.5(2)
Torsion angles (°)			
R_1–X–C_1–C_2	–	15.6(5)	-3.8(4)
R_2–X–C_1–C_6	–	17.6(5)	-13.2(4)
W–C_{Carb}–C_4–C_3	8(3)	11.2(4)	2.0(4)
O_{OEt}–C_{Carb}–C_4–C_5	11(3)	8.6(4)	-1.3(4)

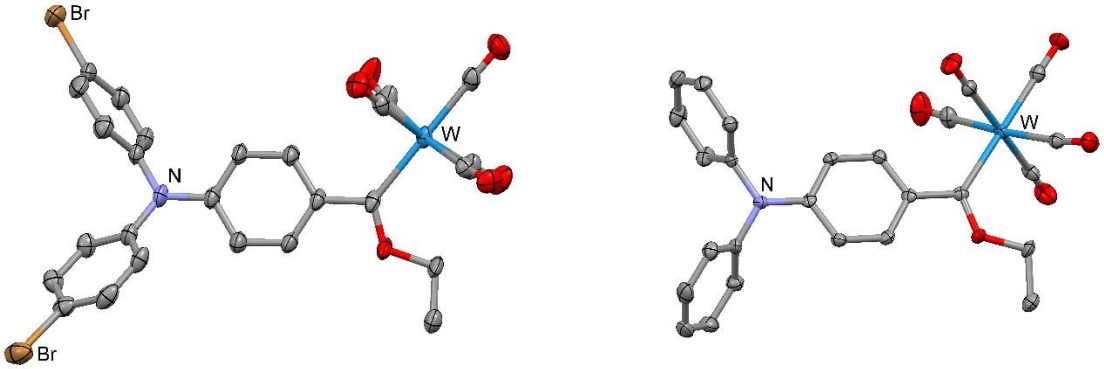

Figure 3.10. Solid state structures of B3a[7] and B4a. Ellipsoids are set at 50% probability. Hydrogen atoms are omitted for clarity

The bond length between the carbene carbon and the aromatic ring for each complex is indicative as to the amount of electron density received from the distant nitrogen towards the stabilisation of the carbene carbon. Hence, with no amino-substituent present on the aromatic ring which can contribute to the stabilisation of the carbene complex, the C_{carb}–C_{ipso} bond length is the longest for **B1a**. Upon the introduction of a distant nitrogen at the *p*-position of the ring relative to the carbene carbon, the length of the C_{carb}–C_{ipso} bond decreases significantly. In accordance, as more electron density is received from the aromatic ring, less electron density is required from the ethoxy and metal substituents of the carbene carbon. This is seen for both **B2a** (which receives the greatest amount of electron density from the distant nitrogen) and **B4a**, where the bond lengths of C_{ipso}–C_{Carb} bonds have respective values of 1.463(3) and 1.471(4) Å, while the C_{carb}–O_{OEt} bonds have respective bond lengths of 1.336(3) and 1.325(3) Å. The delocalisation of the electron density present on the nitrogen atom is also realised when the bond lengths of the N–C_{ipso} bonds are compared with respective lengths for **B2a** and **B4a** of 1.355(3) and 1.379(4) Å. The significantly shorter bond for **B2a** indicates a greater delocalisation of the electron density present on the nitrogen towards the aromatic ring.

Although the effect is not pronounced, the two bromine atoms present on the phenyl groups of **B3a** have an electron withdrawing effect as the delocalisation of the electron density from the

nitrogen towards the carbene carbon is reduced for **B3a** compared to **B4a** ($N–C_{ipso}$ bond length of 1.398(4) and 1.379(4) Å for **B3a** and **B4a**, respectively).

The torsion angles around the $N–C_{ipso}$ and $C_{carb}–C_{ipso}$ bonds further reveal the contribution of the nitrogen lone pair to the stabilisation of the carbene via the phenyl ring. Should the torsion angles be close to 0 ° or 180 ° it indicates that the substituents of the nitrogen are approximately in the same plane as the phenyl ring and carbene carbon. This will also indicate sp^2 hybridization at the nitrogen. A significant deviation from planarity such that the substituents around the nitrogen will form a cone angle, indicates greater p-orbital contribution and a movement away from sp^2 to sp^3 hybridization on the nitrogen and imply poorer π-overlap with the phenyl ring and less delocalisation of the electron lone pair over the ring.

For **B2a**, the torsion angles around the $N-C_{ipso}$ bond is smaller (0.1(3) ° and –3.1(4) °) compared to **B3a** (15.6(5) ° and 17.6(5) °) and **B4a** (–3.8(4) ° and –13.2(4) °) indicating increased planarity (greater delocalisation of nitrogen lone pair or less steric strain) for **B2a** compared to the other complexes. Further, the torsion angle around the $C_{ipso}–C_{Carb}$ bond gives an indication as to the contribution of the ethoxy group to the stabilisation of the carbene carbon. **B2a** (20.5(3) ° and 15.8(3) °) shows the greatest deviation from planarity, followed by **B3a** (11.2(4)° and 8.6(4)°) then **B4a** (2.0(4) ° and -1.3(4) °).

Throughout this study, it is evident that there are significant differences between the tungsten ethoxy- and aminocarbene complexes. From the discussion: the carbene carbons of the ethoxycarbene complexes rely strongly on their aromatic substituents rather than solely on the ethoxy heterogroup and their coordinated tungsten carbonyl fragment. In contrast, the aminocarbene complexes rely largely on its amino heterogroup for stabilisation with a much smaller contribution from the tungsten carbonyl fragment. This is evident from the carbene carbon chemical shift value in the ^{13}C NMR NMR data as well as the carbonyl vibrational data in the IR spectroscopy. It therefore comes as no surprise that upon investigation of the crystal

structures of **B2a** and **B2b** to find that there are significant differences between the structures of the two complexes in the solid state.

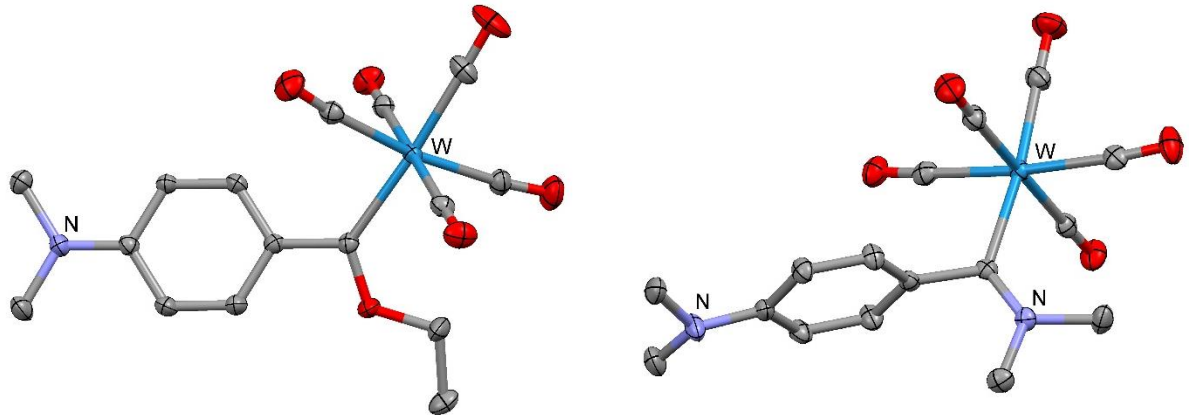

Figure 3.11. Solid state structures of B2a (left) and B2b (right). Ellipsoids are set at 50% probability. Hydrogen atoms are omitted for clarity

In the molecular structure of **B2a**, the carbene carbon, its coordinated tungsten carbonyl, the ethoxy group and the distant NMe_2 group all lie in the same plane. These observations are confirmed by the small torsion angles around the N–C_{ipso} bond and the C_{Carb}–C_{ipso} bond which have values slightly larger than 0 °. The opposite is true for **B2b**, in which the C_{carb}–W bond is perpendicular to the plane of the ring with torsion angles around the C_{Carb}–C_{ipso} bond and values of approximately 90 °. This suggests that there is little, if any, π-orbital overlap between aromatic ring and the carbene carbon in **B2b**. Table 3.9 lists selected bond lengths and bond angles while Figure 3.12 illustrates the differences in the bond lengths of the arene rings between the ethoxy- and aminocarbene complex.

Table 3.9. Selected bond length and bond angles of B2a and B2b

	B2a	B2b
Symmetry	P n a 2_1	P 2_1/c
	Bond lengths (Å)	
C_{Ph}–NMe_2	1.355(3)	1.379(4)
C_{Ph}–C_{carb}	1.463(3)	1.504(4)
C_{carb}–R*	1.336(3)	1.303(4)
C_{carb}–W	2.226(2)	2.251(3)
	Bond angles (°)	
$Me_{(1)}$ –N–$Me_{(2)}$	118.1(2)	116.8(3)
$Me_{(1)}$ –N–C_{Ph}	120.6(2)	119.6(3)
$Me_{(2)}$ –N–C_{Ph}	121.2(2)	119.7(3)
W–C_{Carb}–C_{Ph}	126.5(2)	116.9(2)
W–C_{Carb}–R*	127.0(2)	129.1(2)
C_{Ph}–C_{Carb}–R*	106.3(2)	113.9(3)
	Torsion angles (°)	
$N_{Me(1)}$ –N–C_{ipso}–C_{Ph}	0.1(3)	-8.1(5)
$N_{Me(2)}$ –N–C_{ipso}–C_{Ph}	-3.1(4)	15.9(5)
R*–C_{Carb}–C_{ipso}–C_{Ph}	15.8(3)	90.3(3)
W–C_{Carb}–C_{ipso}–C_{Ph}	20.5(3)	90.0(4)

*R = OEt (**A2a**) and NMe_2 (**A2b**)

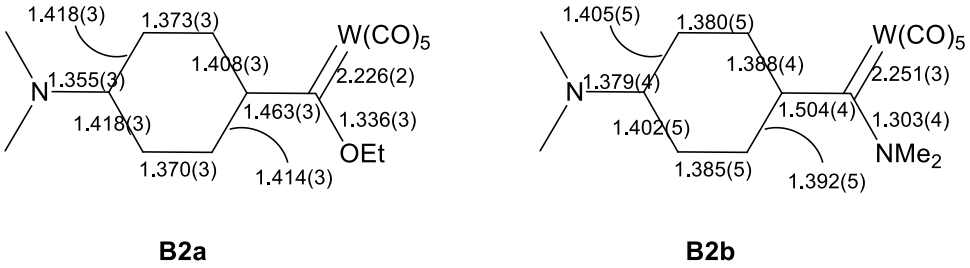

B2a **B2b**

Figure 3.12. Selected bond lengths (Å) of B2a (left) and B2b (right)

Comparing the bond lengths of the aromatic rings between **B2a** and **B2b**, it is possible to illustrate the effect that distant nitrogen has when it contributes to the stabilisation of the carbene carbon. For **B2a** the N–C_{ipso} and C_{carb}–C_{ipso} bonds are significantly shorter (1.355(3) and 1.463(3) Å, respectively) than those of **B2b** (1.379(4) and 1.504(4) Å, respectively). Further, each bond in the arene ring of **B2a** is alternatively longer and shorter, while those of **B2b** do not show the same pattern. The effect is clearly illustrated in Figure 3.1. It is evident that the arene ring and its amino

substituent play a significant role in the stabilisation of the carbene carbon through electron delocalisation over the arene ring. For **B2b**, the $C_{carbene}$–W and $C_{carbene}$–C_{ipso} bonds are much longer than **B2a**, indicating that it receives most of the required electron density from the amine heteroatom and the π-electron density of the aromatic ring does not contribute to the stabilisation of the carbene carbon. The stabilisation of the carbene carbon by its amine substituent in **B2b** is evident by the short $C_{carbene}$–N bond with a length of 1.303(4) Å.

The packing for both the complexes are due to the many H-bonding interactions that exist between the molecules.

Molecules of **B2a** interact through an H-bond between the proton at the *o*-position of the arene ring relative to the carbene substituent with a carbonyl ligand of the $W(CO)_5$ moiety of a neighbouring complex (PhH---OCW$(CO)_4$ = 2.876 Å). Thus, the molecules are arranged in a zig-zag fashion so that the ethoxy groups and are pointing towards each other. Another interaction exists between a carbonyl ligand of the $W(CO)_5$ moiety and the methylene protons present in the dimethylamino substituent of the arene ring such that the atoms are between 2.72 and 2.83 Å apart.

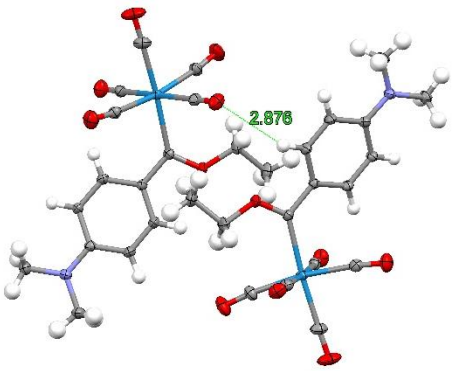

Figure 3.13. Solid state intermolecular interactions of B2a

A single molecule of **B2b** interacts with eight other surrounding molecules to form the packing pattern. The carbonyl ligands in the $W(CO)_5$ group has four different H-bonding interactions with surrounding molecules while the dimethylamino and phenyl protons make up the rest of the interactions. An oxygen of a carbonyl ligand interacts with a phenyl proton such that the distance between the two atoms is 2.571 Å. All the other interactions are between the protons present in the two dimethylamino substituents of the carbene carbon and the arene ring. These interactions place the H and O atoms approximately 2.691 Å apart.

3.3 Experimental

General

Standard Schlenk techniques were used, under an atmosphere of nitrogen or argon, for general synthesis. Silica gel 60 (particle size 0.0063–0.200 mm) was used as resin for all separations in column chromatography. THF and hexane were distilled over sodium metal, while CH_2Cl_2 was distilled over CaH_2. All other reagents were used as received from commercial suppliers. NMR spectra were recorded on Bruker Ultrashield Plus 400 AVANCE 3 and Bruker Ultrashield 300 AVANCE 3 spectrometers using CD_2Cl_2 as solvent at 25 °C. The NMR spectra were recorded for ^1H at 400.13 or 300.13 MHz and ^{13}C at 100.163 or 75.468 MHz. Chemical shifts were recorded in ppm, using the deuterated solvent signal as an internal reference. For CD_2Cl_2 δH at 5.3400 and and δC at 53.840 ppm. Infrared spectroscopy was performed on a Bruker ALPHA FT-IR spectrophotometer with a NaCl cell, using hexane as solvent. Xray crystallography was performed at 20 °C on a Siemens P4 diffractometer fitted with a Bruker 1 K-αCCD detector using graphitemonochromated, Mo–Kα radiation by means of a combination of phi and omega scans.

The starting materials were used as received from Sigma Aldrich. Et_3OBF_4 was synthesised according to the published procedure by Meerwein.[26] The cyclovoltammetry was performed in a vacuum-tight one-compartment cell. A Pt working electrode was used with Pt and Ag wires as counter and reference electrodes, respectively. NBu_4PF_6 (0.25 mM) was used as the supporting electrolyte in THF. Referencing was done with addition of ferrocene (Cp_2Fe), decamethylferrocene (DmFc) or cobaltocene (Cp_2Co) as an internal standard to the analyte solution after all data of interest had been acquired. Representative sets of scans were repeated with the added standard. Final referencing was done against the ferrocene/ferrocenium ($Cp_2Fe^{0/+}$) couple with $E_{½}$ ($DmFc^{0/+}$) = -540 mV vs. $Cp_2Fe^{0/+}$ and $E_{½}$ ($Cp_2Co^{0/+}$) = -1330 mV vs. $Cp_2Fe^{0/+}$ using THF/NBu_4PF_6 as supporting electrolyte. Electrochemical data was acquired remotely with a BAS CV50 potentiostat. The IR-SEC measurements were conducted using an

OTTLE cell with Pt-mesh as working and counter electrodes while silver wire was used as the reference electrode in a standard CaF_2 liquid IR cell.

Synthesis of B1a – B4a

The brominated starting substrate (R - Table 3.10) was dissolved in 30 ml THF and cooled to -78 °C. *n*BuLi was added to the cold solution and thereafter $W(CO)_6$ while stirring. The reaction mixture was allowed to stir at –70° C for 30 minutes and then at room temperature until all metal carbonyl was dissolved (60 minutes). The solvent was removed under vacuum and the remaining residue dissolved in 30 ml CH_2Cl_2. The solution was cooled to -40 °C and Et_3OBF_4, dissolved in CH_2Cl_2, was added to the cold reaction mixture. The dark reaction mixture was allowed to stir for 30 minutes at room temperature and was then filtered through a silica plug. The orange product was isolated using silica column chromatography with *n*-hexane and CH_2Cl_2 as solvents.

Table 3.10. Synthesis of B1a – B4a, experimental variables and yields

Complex	R (structure)	R	*n*BuLi	$W(CO)_6$	Et_3OBF_4	Yield
B1a	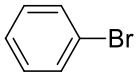	1.65 mL 10.0 mmol	7.50 mL 12.0 mmol	3.52 g 10.0 mmol	1.90 g 10.0 mmol	2.06 g (45.0 %)
B2a	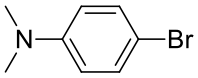	3.00 g 15.0 mmol	9.38 mL 15.0 mmol	5.28 g 15.0 mmol	2.85 g 15.0 mmol	2.87 g (38.2 %)
B3a	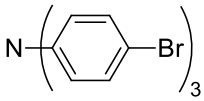	4.82 g 10.0 mmol	6.60 mL 10.0 mmol	3.52 g 10.0 mmol	1.89 g 10.0 mmol	1.23 g (15.7 %)
B4a	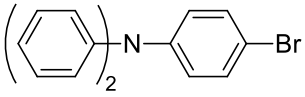	3.24 g 10.0 mmol	6.60 mL 10.0 mmol	3.52 g 10.0 mmol	1.89 g 10.0 mmol	2.37g (37.9 %)

Synthesis of B1b – B4b

An ethoxycarbene complex, **B1a** – **B4a**, was dissolved in 10 ml THF. Excessive amounts of dimethylamine hydrochloride and KOH were suspended in the reaction mixture. Distilled H_2O was added dropwise until all the suspended salts were dissolved. The reaction immediately changed from bright orange to bright yellow. The reaction mixture was placed under vacuum until

the yellow product that formed, formed a solid in the remaining H_2O. Et_2O (15 ml) was added to the reaction vessel, dissolving the yellow solid. The organic phase was washed three times with distilled H_2O saturated with $NHMe_2$.HCl. The organic phase was isolated, dried over $MgSO_4$ and filtered. The bright yellow product was filtered through a silica plug using *n*-hexane and CH_2Cl_2 as solvents.

Table 3.11. Aminolysis of B1a – B4b, experimental variables and yields

Complex		KOH	$NHMe_2$.HCl	Yield
B1b	**B1a** 0.94 g (2.1 mmol)	1.12 g (20.0 mmol)	1.63 g (20.0 mmol)	0.77 g (80.2 %)
B2b	**B2a** 2.09 g (4.42 mmol)	2.24 g (40.0 mmol)	3.26 g (40.0 mmol)	1.88 g (85.1 %)
B3b	**B3a** 0.481 g (0.613 mmol)	0.34 g (6.00 mmol)	0.49 g (6.00 mmol)	0.480 g (100 %)
B4b	**B4a** 0.253 g (0.404 mmol)	0.224 g (4.04 mmol)	0.33 g (4.04 mmol)	0.253 g (100 %)

Characterisation

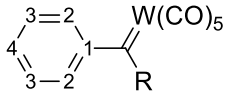

B1a: R = OEt
B1b: R = NMe_2

Figure 3.14. NMR assignments of B1a and B1b

B1a: $C_{14}H_{10}O_6W$. ^{1}H NMR (CD_2Cl_2, 400 MHz) δ 7.56 (dd, *J* = 8.4, 8.3 Hz, 1H, H4), 7.45 (dd, *J* = 8.0, 8.0 Hz, 2H, H3), 7.44 (d, *J* = 8.2 Hz, 2H, H2), 5.06 (q, *J* = 7.1 Hz, 2H, H_{CH2}), 1.71 (t, *J* = 7.1 Hz, 3H, H_{CH3}). ^{13}C NMR (CD_2Cl_2, 101 MHz) δ 320.5 ($^1J_{\{W\}C}$ = n.o., C_{Carb}), 204.4 ($^1J_{\{W\}C}$ = n.o., $C_{W(CO)5}$, *trans*), 197.9 ($^1J_{\{W\}C}$ = 64.2 Hz, $C_{W(CO)5}$, *cis*), 155.9 (C1), 132.0 (C4), 128.5 (C3), 126.6 (C2), 81.0 (C_{CH2}), 15.2(C_{CH3}). ESI-MS (2.8 V, positive mode, *m/z*): calcd for $[M]^+$ 458.0013; found 458.0387.

B1b: $C_{14}H_{11}O_5NW$. ^{1}H NMR (CD_2Cl_2, 300 MHz) δ 7.42 (ddd, *J* = 7.8, 7.5, 1.7 Hz, 2H, H2), 7.18 (ddd, *J* = 7.8, 7.5, 1.4 Hz, 1H, H4), 6.80 (dd, *J* = 8.3, 1.2 Hz, 2H, H3), 3.93 (s, 3H, H_{NMe}), 3.03 (s, 3H, H_{NMe}). ^{13}C NMR (CD_2Cl_2, 75 MHz) δ 256.7 ($^1J_{\{W\}C}$ = 46.0 Hz, C_{Carb}), 204.8 ($^1J_{\{W\}C}$ = 63.5

Hz, $C_{W(CO)5}$, *trans*), 199.0 ($^1J_{\{W\}C}$ = 63.7 Hz, $C_{W(CO)5}$, *cis*), 153.8 (C1), 128.8 (C2), 126.6 (C4), 119.9 (C3), 44.8 (C_{NMe2}).

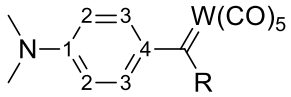

B2a: R = OEt
B2b: R = NMe_2

Figure 3.15. NMR assignments of B2a and B2b

B2a: $C_{16}H_{15}O_6NW$. ^{1}H NMR (CD_2Cl_2, 400 MHz) δ 8.04 (d, 9.3 Hz, 2H, H3), 6.65 (d, 9.4 Hz, 2H, H2), 5.00 (q, 7.0 Hz, 2H, H_{CH2}), 3.11 (s, 6H, H_{NMe2}), 1.65 (t, 7.0 Hz, 3H, H_{CH3}). ^{13}C NMR (CD_2Cl_2, 101 MHz) δ 299.2 ($^1J_{\{W\}C}$ = 50.1 Hz, C_{Carb}), 203.8 ($^1J_{\{W\}C}$ = 60.2 Hz, $C_{W(CO)5}$, *trans*), 199.7 ($^1J_{\{W\}C}$ = 64.1 Hz, $C_{W(CO)5}$, *cis*), 155.0 (C4), 141.1 (C1), 134.7 (C3), 110.5 (C2), 78.9 (C_{CH2}), 40.3 (C_{NMe2}), 13.3 (C_{CH3}). ESI-MS (2.8 V, positive mode, *m/z*): calcd for $[M + H]^+$ 502.0487; found 502.0453.

B2b: $C_{16}H_{16}O_5N_2W$. ^{1}H NMR (CD_2Cl_2, 400 MHz) δ 6.74 (d, *J* = 9.1 Hz, 2H, H3), 6.69 (d, *J* = 9.1 Hz, 2H, H2), 3.89 (s, 3H, H_{NMe}), 3.04 (s, 3H, H_{NMe}), 2.96 (s, 6H, H_{NMe2}). ^{13}C NMR (CD_2Cl_2, 101 MHz) δ 258.2 ($^1J_{\{W\}C}$ = n.o., C_{Carb}), 205.1 ($^1J_{\{W\}C}$ = 63.7 Hz, $C_{W(CO)5}$, *trans*), 199.3 ($^1J_{\{W\}C}$ = 64.1 Hz, $C_{W(CO)5}$, *cis*), 149.4 (C4), 143.5 (C1), 121.5 (dd, *J* = 157.9, 6.8 Hz, C3), 112.1 (dd, *J* = 157.9, 6.8 Hz, C2), 44.5 (q, *J* = 140.5 Hz, NMe_2), 40.6 (q, *J* = 135.3 Hz, NMe_2). ESI-MS (2.8 V, positive mode, *m/z*): calcd for $[M + H]^+$ 501.0647; found 501.0657.

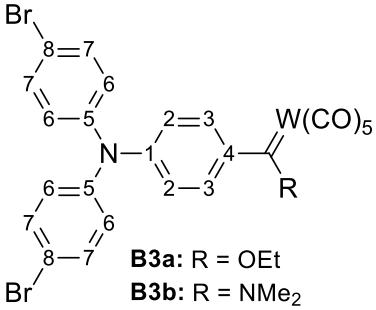

B3a: R = OEt
B3b: R = NMe_2

Figure 3.16. NMR assignments of B3a and B3b

B3a: $C_{26}H_{17}O_6NBr_2W$. ^{1}H NMR (CD_2Cl_2, 300 MHz) δ 7.79 (d, *J* = 9.0 Hz, 2H, H3), 7.47 (d, *J* = 8.8 Hz, 4H, H7), 7.05 (d, *J* = 8.8 Hz, 4H, H6), 6.94 (d, *J* = 9.0 Hz, 2H, H2), 5.04 (q, *J* = 7.0 Hz, 2H, H_{CH2}), 1.67 (t, *J* = 7.1 Hz, 3H, H_{CH3}). ^{13}C NMR (CD_2Cl_2, 75 MHz) δ 308.4 ($^1J_{\{W\}C}$ = n.o., C_{Carb}), 203.4 ($^1J_{\{W\}C}$ = n.o., $C_{W(CO)5}$, *trans*), 197.9 ($^1J_{\{W\}C}$ = n.o., $C_{W(CO)5}$, *cis*), 151.5 (C4), 146.8 (C1), 144.9 (C5), 132.8 (C7), 131.6 (C3), 127.6 (C6), 118.9 (C8), 118.1 (C2), 79.6 (C_{CH2}) 14.8 (C_{CH3}). ESI-MS (2.8 V, positive mode, *m/z*): calcd for $[M]^+$ 782.8966; found 782.9845.

B3b: $C_{26}H_{18}O_5N_2Br_2W$. ^{1}H NMR (CD_2Cl_2, 400 MHz) δ 7.37 (d, J = 8.9 Hz, 4H, H7), 7.11 (d, J = 8.8 Hz, 2H, H3), 6.96 (d, J = 8.9 Hz, 4H, H6), 6.75 (d, J = 8.8 Hz, 2H, H2), 3.93 (s, 3H, H_{NMe}), 3.16 (s, 3H, H_{NMe}). ^{13}C NMR (CD_2Cl_2, 101 MHz) δ 256.9 ($^1J_{\{W\}C}$ = n.o., C_{Carb}), 205.0 ($^1J_{\{W\}C}$ = 63.0 Hz, $C_{W(CO)5}$, *trans*), 199.2 ($^1J_{\{W\}C}$ = 62.8 Hz, $C_{W(CO)5}$, *cis*), 149.9 (C4), 147.0 (C5), 145.4 (C1), 132.9 (C7), 126.0 (C6), 125.0 (C3), 121.6 (C2), 116.1 (C8), 45.1 (C_{NMe2}).

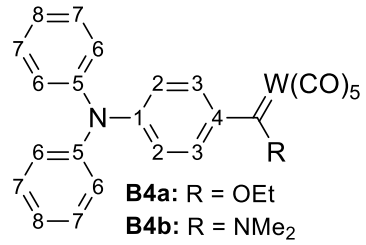

Figure 3.17. NMR assignments of B4a and B4b

B4a: $C_{26}H_{19}O_6NW$. ^{1}H NMR (CD_2Cl_2, 400 MHz) δ 7.84 (d, J = 9.1 Hz, 2H, H3), 7.37 (ddd, J = 8.0, 6.4, 2.4 Hz, 4H, H7), 7.21 (m, 2H, H8), 7.20 (d, J = 7.9 Hz, 4H, H6), 6.88 (d, J = 9.1 Hz, 2H, H2), 5.02 (q, J = 7.0 Hz, 2H, H_{CH2}), 1.65 (t, J = 7.1 Hz, 3H, H_{CH3}). ^{13}C NMR (CD_2Cl_2, 101 MHz) δ 305.8 ($^1J_{\{W\}C}$ = n.o., C_{Carb}), 203.8 ($^1J_{\{W\}C}$ = n.o., $C_{W(CO)5}$, *trans*), 198.6 ($^1J_{\{W\}C}$ = 64.4 Hz, $C_{W(CO)5}$, *cis*), 153.3 (C4), 146.2 (C5), 145.5 (C1), 132.8 (C3), 130.2 (C7), 127.0 (C6), 125.9 (C8), 117.8 (C2), 79.7 (C_{CH2}), 15.2 (C_{CH3}). ESI-MS (2.8 V, positive mode, *m/z*): calcd for $[M+H]^+$ 626.0800; found 626.0856.

B4b: $C_{26}H_{20}O_5N_2W$. ^{1}H NMR (CD_2Cl_2, 300 MHz) δ 7.26 (dd, J = 8.4, 7.4 Hz, 4H, H7), 7.09 (d, J = 8.5 Hz, 2H, H3), 7.08 (dd, J = 8.5, 1.2 Hz, 4H, H6), 7.03 (dd, J = 7.9, 7.4 Hz, 2H, H8), 6.70 (d, J = 8.6 Hz, 2H, H2), 3.91 (s, 3H, H_{NMe}), 3.14 (s, 3H, H_{NMe}). ^{13}C NMR (CD_2Cl_2, 75 MHz) δ 257.2 ($^1J_{\{W\}C}$ = 45.9 Hz, C_{Carb}), 204.9 ($^1J_{\{W\}C}$ = 62.9 Hz, $C_{W(CO)5}$, *trans*), 199.1 ($^1J_{\{W\}C}$ = 64.1 Hz, $C_{W(CO)5}$, *cis*), 148.8 (C4), 148.1 (C5), 146.3 (C1), 129.7 (C7), 124.6 (C6), 124.0 (C8), 123.4 (C3), 121.2 (C2), 44.9 (C_{NMe2}). ESI-MS (2.8 V, positive mode, *m/z*): calcd for $[M+H]^+$ 625.0960; found 625.0912.

3.4 References

[1] C.-P. Hsieh, H.-P. Lu, C.-L. Chiu, C.-W. Lee, S.-H. Chuang, C.-L. Mai, W.-N. Yen, S.-J. Hsu, E. W.-G. Diau, C.-Y. Yeh, *J. Mater. Chem.* **2010**, *20*, 1127–1134.

[2] L. Hagopian, G. Koehler, R. I. Walter, *J. Phys. Chem.* **1967**, *71*, 2290–2296.

[3] M. Kuss-Petermann, O. S. Wenger, *J. Am. Chem. Soc.* **2016**, *138*, 1349–1358.

[4] Z. Lamprecht, N. A. van Jaarsveld, D. I. Bezuidenhout, D. C. Liles, S. Lotz, *Dalton Trans.* **2015**, *44*, 19218–19231.

[5] S. Lotz, N. A. van Jaarsveld, D. C. Liles, C. Crause, H. Görls, Y. M. Terblans, *Organometallics* **2012**, *31*, 5371–5383.

[6] U. Klabunde, E. O. Fischer, *J. Am. Chem. Soc.* **1967**, *89*, 7141–7142.

[7] N. Weststrate, I. Fernández, D. C. Liles, N. van Jaarsveld, S. Lotz, *Organometallics* **2015**, *34*, 696–710.

[8] N. A. van Jaarsveld, D. C. Liles, S. Lotz, *Dalton Trans.* **2010**, *39*, 5777–5779.

[9] R. W. Alder, M. E. Blake, *Chem. Commun.* **1997**, 1513–1514.

[10] R. A. Moss, G. J. Ho, S. Shen, K. Krogh-Jespersen, *J. Am. Chem. Soc.* **1990**, *112*, 1638–1640.

[11] X. Cattoën, K. Miqueu, H. Gornitzka, D. Bourissou, G. Bertrand, *J. Am. Chem. Soc.* **2005**, *127*, 3292–3293.

[12] M. Landman, R. Pretorius, B. E. Buitendach, P. H. van Rooyen, J. Conradie, *Organometallics* **2013**, *32*, 5491–5503.

[13] I. Hoskovcová, J. Roháčová, D. Dvořák, T. Tobrman, S. Záliš, R. Zvěřinová, J. Ludvík, *Electrochim. Acta* **2010**, *55*, 8341–8351.

[14] E. T. Seo, R. F. Nelson, J. M. Fritsch, L. S. Marcoux, D. W. Leedy, R. N. Adams, *J. Am. Chem. Soc.* **1966**, *88*, 3498–3503.

[15] A. J. Bard, L. R. Faulkner, *Electrochemical Methods: Fundamental and Applications, 2nd Edition*, John Wiley & Sons, Inc., New York, **2001**.

[16] O. Yurchenko, D. Freytag, L. zur Borg, R. Zentel, J. Heinze, S. Ludwigs, *J. Phys. Chem. B* **2012**, *116*, 30–39.

[17] K. Sreenath, C. V. Suneesh, V. K. R. Kumar, K. R. Gopidas, *J. Org. Chem.* **2008**, *73*, 3245–3251.

[18] M. A. Sierra, M. Gómez-Gallego, R. Martínez-Alvarez, *Chem. Eur. J.* **2007**, *13*, 736–44.

[19] W. I. Dzik, X. P. Zhang, B. de Bruin, *Inorg. Chem.* **2011**, *50*, 9896–903.

[20] R. I. Walter, *J. Am. Chem. Soc.* **1966**, *88*, 1923–1930.

[21] P. J. Krusic, U. Klabunde, C. P. Casey, T. F. Block, *J. Am. Chem. Soc.* **1976**, *98*, 2015–2018.

[22] J. Handzlik, F. Hartl, T. Szymańska-Buzar, *New J. Chem.* **2002**, *26*, 145–152.

[23] B. van der Westhuizen, J. Matthäus Speck, M. Korb, D. I. Bezuidenhout, H. Lang, *J. Organomet. Chem.* **2014**, *772*, 18–26.

[24] K. Fuchibe, N. Iwasawa, *Chem. Eur. J.* **2003**, *9*, 905–14.

[25] R. J. Staples, D. M. Potts, J. C. Yoder, *Z. Krist.* **1995**, *210*, 381.

[26] H. Meerwein, *Org. Synth.* **1966**, *46*, 113–114.

CHAPTER 4

MONONUCLEAR Pt(II) FISCHER MULTICARBENE COMPLEXES: SYNTHESIS AND PHOTOPHYSICS

4.1 Introduction

Extensive research is being conducted in the fields of Ru(II), Ir(III) and Pt(II) photophysics as these transition metals are known for their fast intersystem crossing (ISC) properties upon excitation. Organometallic compounds containing these metals are known for their high quantum yields of long-lived triplet excited states which can provide controlled phosphorescence and are currently known as some of the best compounds for organic light emitting diodes (OLEDs) and photoactive materials.[1–3]

In this study, Pt(II) is chosen as the transition metal to which several carbene ligands will be coordinated through transmetallation. Pt(II) complexes with heteroatom substituents on carbene ligands (mostly NHC ligands) have recently made contributions in the fields of catalytic, biological and photochemical research because of the unique properties of the carbene carbon atoms.[4] Until now, reports of Fischer carbene ligands in materials, where their electron accepting character is exploited, are scarce. It is for this reason that the synthesis of mononuclear ethoxy- and aminocarbene complexes through transmetallation reactions to Pt(II) is investigated. In this study, the focus will remain on the synthesis as well as the photophysical properties of the compounds.

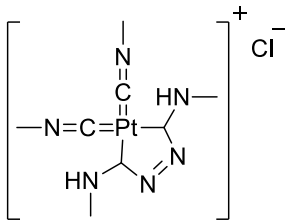

Figure 4.1. Revised structure of Chugaev's salt as published by Rouschias and Shaw[5]

The first Pt(II) aminocarbene complex was synthesised by Chugaev and co-workers in 1925, but it was not until 1973 that the compound was structurally characterised by Rouschias and Shaw (Figure 4.1). The aminocarbene ligand was part of a chelating ring of a bidentate ligand in the complex.[5,6] Since 1968, several examples of small Pt(II) Fischer carbene complexes have been prepared by mainly four methods. The first method, published by Chatt and co-workers in 1969, was the modification of Pt(II) isocyanide precursors with alcohols and amines (Scheme 4.1).[7] This method has been widely used to make Pt(II)-N*C*N- or Pt(II)-N*C*O carbene(*C*) complexes.[8]

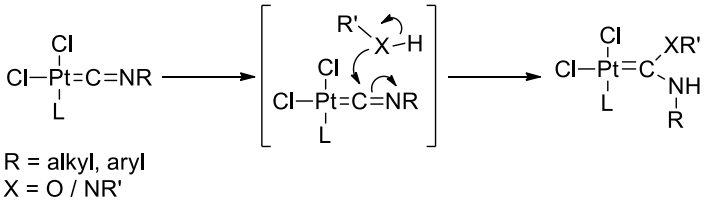

Scheme 4.1. Modification of Pt-isocyanides into Fischer carbene complexes

Shortly afterwards, Chisholm and Clark reported the reaction of $PtClCH_3(P(CH_3)_2C_5H_5)_2$ with a terminal alkyne and $AgPF_6$ in methanol or ethanol.[9] In 1972 they showed that the mechanism of formation proceeded via a carbonium ion (Scheme 4.2).[10]

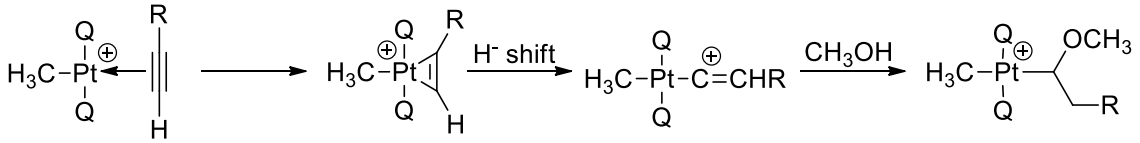

Scheme 4.2. Mechanism of formation of a Pt(II) carbene on reaction of a terminal alkyne with $PtClCH_3(P(CH_3)_2C_5H_5)_2$. Q= $P(CH_3)_2C_5H_5$ or $As(CH_3)_3$.[10]

In 1979 a crystal structure of the first Pt(II) bisalkoxy carbene complex was published by Struchkov and Aleksandrov.[11] Their method of synthesis was refined in more recent years by the research group of Steinborn: hexachloroplatinic

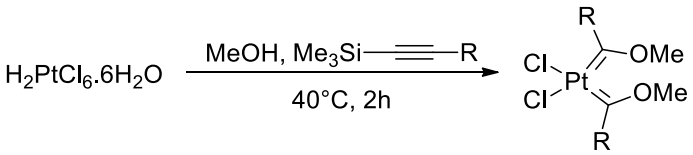

Scheme 4.3. Synthesis of Pt(II) biscarbene complexes via a trimethylsilyl-substituted alkyne[11,12]

acid reacted with trimethylsilyl-substituted alkynes in an alcohol to form Pt(II) biscarbene complexes (Scheme 4.3).[12] Based on these methods several other Pt(II) carbene complexes have also been published.[13–16] A number of other Pt(II) carbenes exist that make use of intermediates in the reactions mentioned above or forms from interesting ligand based reactions or interactions.[17–20]

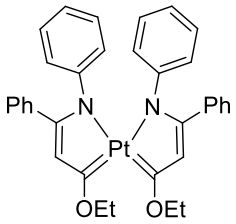

Figure 4.2. Mononuclear alkoxy biscarbene complex reported by Sierra[21]

It was however, the synthesis of Pd(II) and Pt(II) biscarbene complexes reported by Sierra and his co-workers in 2009, with the objective to trap the key intermediates of the well-known self-dimerisation reactions of coordinated carbene ligands in the presence of Pd(0), that the potential of transmetallation reactions was realised.[21,22] The complexes were prepared through the transmetallation of Cr(0) carbene complexes containing a distant coordinating nitrogen atom which trapped and stabilized the carbene ligand in a chelate ring as part of a bidentate ligand as shown in Figure 4.2. This complex is, as far as we are aware, the only example of a mononuclear alkoxy multicarbene complex which has been transmetallated to Pt(II).

The Fischer carbene complexes discussed in this study are not the first examples of mononuclear multicarbene complexes. There are examples of NHC Pt(II) tetracarbene complexes reported and studies further describe their use as phosphorescent emitters (Figure 4.3).[23–26] There are also very popular pincer-type chelating ligands with multiple NHC or MIC (mesoionic carbene) ligands coordinated to Pt(II) centres which show significant photophysical applications.[27–29]

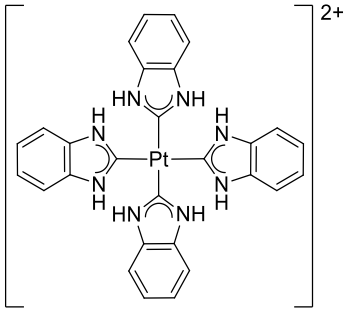

Figure 4.3. NHC tetracarbene Pt(II) complex synthesised by Hahn and co-workers[26]

Having identified that it is possible for Group 6 carbene ligands to be transmetallated to a Pt(II) centre, the aim is to synthesise a series of Pt(II) multicarbene complexes through a carbene transfer reaction. The ethoxy- and aminocarbene complexes of W(0) with organic amine substituents in Chapter 3, will be the compounds used in the synthesis of the Pt(II) carbene complexes. In the synthesis, it will first be necessary to establish that it is possible to form stable independent multi-Pt(II) carbene complexes, without them necessarily participating in carbene-carbene C–C coupling reactions which has been reported for smaller Pt(II) biscarbene complexes.[30] Secondly, once formed, it is necessary to determine how the carbene(s) will influence the electronic and steric properties around the Pt(II) centre. These properties will be investigated using UV/VIS, emission and ultrafast transient absorption spectroscopy (TAS).

4.2 Results and Discussion

4.2.1 Synthesis

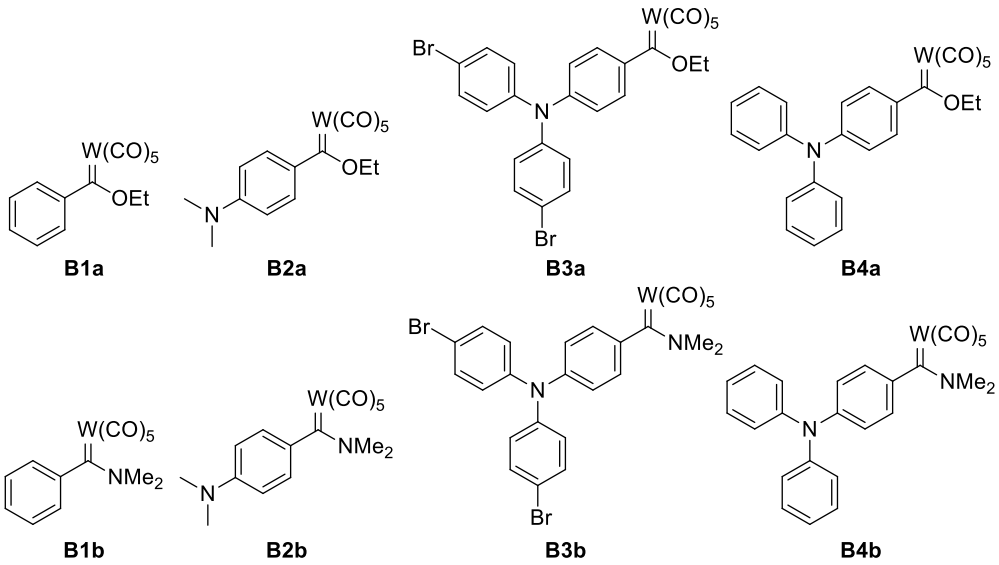

Figure 4.4. W(0) carbene complexes used in the synthesis of the Pt(II) multicarbene complexes

Synthesis of the Pt(II) multicarbene complexes is achieved through a transmetallation reaction of W(0) carbene complexes to a Pt(II) centre. For the synthesis, $[Pt(COD)Cl_2]$ has been chosen as the starting complex due to the readily displaceable COD ligand and ease of product isolation after the reaction. The tungsten carbene complexes used, are those that have been discussed Chapter 3 and are listed in Figure 4.4.

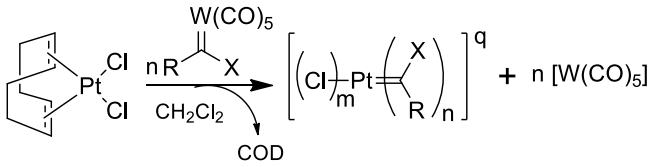

X = OEt, n = 2, m = 2, q = 0
X = NMe_2, n = 3, m = 1, q = +1
R = aryl

Scheme 4.4. Synthesis of mononuclear carbene complexes of Pt(II)

Although the synthesis of the Pt(II) Fischer carbene complexes are reasonably simple, the most challenging aspect is the purification of the final complexes. The products are insoluble in many solvents except dichloromethane and cannot be isolated once exposed to any form of chromatographic material. The synthesis of the desired complexes involves the stirring of a tungsten carbene complex (Figure 4.4) and $Pt(COD)Cl_2$ in anhydrous dichloromethane for approximately 24 hours as shown in Scheme 4.4.

This method leads to the formation of Pt(II) carbene complexes, however, the isolation of a pure product is difficult as traces of unreacted $Pt(COD)Cl_2$ cannot be removed if present after the reaction. It is therefore important to drive the reaction to completion. Optimally, a pure product can be isolated through repeated crystallisation. This is possible for only two of the compounds (**C1a** and **C1b**). To ensure that all the COD has been replaced with carbene ligands, the reaction mixtures are allowed to reflux at 50 °C for at least 24 hours. The time required for a particular carbene complex to react is dependent on the size of the carbene ligand being transmetallated – the larger complexes require a longer reaction time.

All products isolated are brown-yellow solids and when dissolved, a concentrated solution will appear black due the compounds' significant light absorbance. All the mononuclear Pt(II)

carbene complexes are largely insoluble in many solvents except dichloromethane and even then, precipitates out as a powder when the temperature decreases slightly. The complex that forms in the reaction between $[W\{C(OEt)Ph\}(CO)_5]$ (**B1a**) and $[Pt(COD)Cl_2]$ is an unstable complex which decomposes on light exposure. The analogous complex that forms in the reaction between $[W\{C(NMe_2)Ph\}(CO)_5]$ (**B1b**) and $[Pt(COD)Cl_2]$ is more stable, but still decomposes on exposure to light. This observation highlights the importance of the distant nitrogen atom in the aryl substituent, however, the two compounds will not be discussed further.

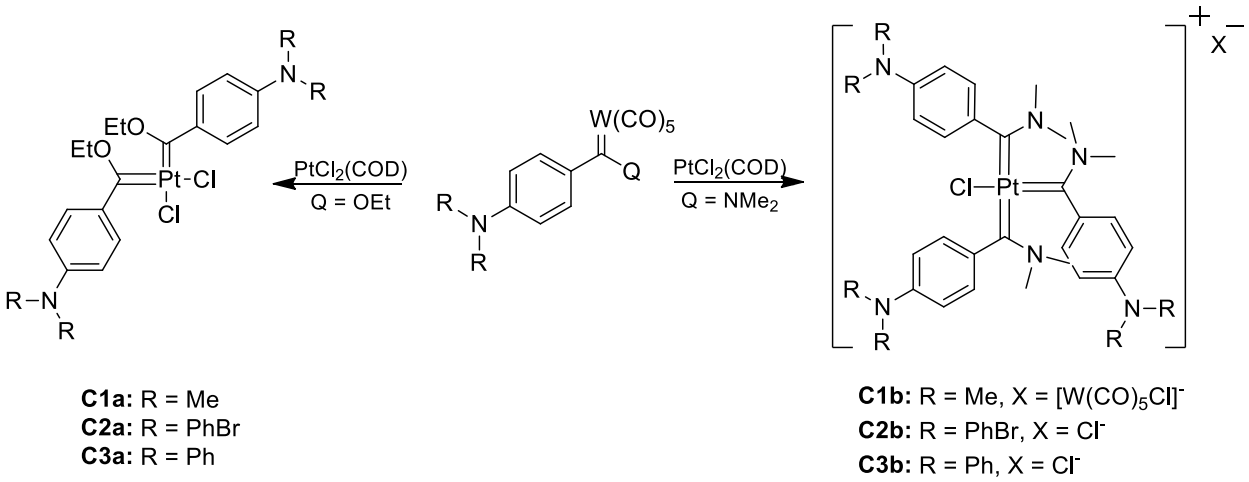

C1a: R = Me
C2a: R = PhBr
C3a: R = Ph

C1b: R = Me, X = $[W(CO)_5Cl]^-$
C2b: R = PhBr, X = Cl^-
C3b: R = Ph, X = Cl^-

Scheme 4.5. Mononuclear Pt(II) complexes synthesised through transmetallation of W(0) ethoxy- and aminocarbene complexes

The major product that forms from the reaction between $[W\{C(OEt)\text{-}p\text{-}C_6H_4NMe_2\}(CO)_5]$ (**B2a**) and $[Pt(COD)Cl_2]$ is the neutral bis-ethoxycarbene complex, **C1a**. The product is isolated after repeated crystallation from dichloromethane and hexane mixtures. The bright yellow product is stable, but reacts with H_2O on exposure to air. The reaction of the analogous aminolysed W(0) carbene complex (**B2b**) with $[PtCl_2(COD)]$ forms a cationic mononuclear triscarbene complex with a $[W(CO)_5Cl]^-$ counter ion. To confirm that a cationic complex is indeed formed, an anion exchange reaction is performed using KPF_6. The anion's presence is confirmed with NMR spectroscopy. After characterisation of all the compounds synthesised, it is clear that all the ethoxycarbene complexes of W(0) react with $[PtCl_2(COD)]$ to form neutral

biscarbene complexes while their aminolysed analogues react to form cationic triscarbene complexes with Cl^- counter ions (with the exception of **C1b** which has a $[W(CO)_5Cl]^-$ counter ion).

It is unclear why, in the case of the aminolysed carbene ligands, the biscarbene complexes proceed to react further to form the triscarbene complexes. The key to a probable explanation lies in the increased electron density available to the carbene carbon for the aminolysed ligands and the stronger Pt(II)–C(carbene) bonds because of the positive charge on the complex. The $[W(CO)_5Cl]^-$ counter ion that has been isolated in **C1b** also gives a further clue as to the mechanism of the reaction. It appears that upon coordination of the third carbene ligand, the $W(CO)_5$ and Cl^- is being simultaneously released to form the counter ion. The identity of the counter ion was confirmed using NMR, IR and X-Ray crystallography. A carbene transfer reaction was previously reported between $W(CO)_5$ carbene complex and AuCl.HCl by Aumann and co-workers.[31] Their carbene transfer reaction generates a Au(I) carbene complex which represents a redox reaction, unlike for the Pt(II) complexes reported in this study. We did not investigate the mechanism.

Surprisingly, after complete analyses of all compounds, for any ethoxycarbene complex, an exclusive neutral Pt(II) bis-ethoxycarbene is obtained while aminocarbene complexes form positively charged triscarbene complexes of Pt(II). Even upon exposure of the $[Pt(COD)Cl_2]$ and the W(0) ethoxycarbene complex to longer reaction times and increased temperature, the biscarbene complex is still exclusively formed.

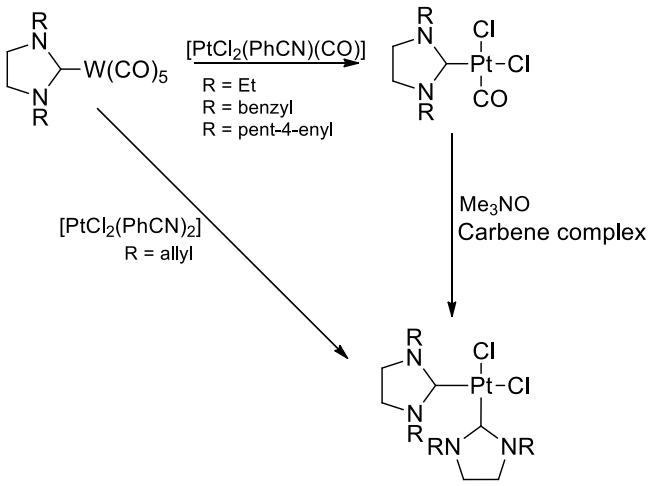

Scheme 4.6. Synthesis of NHC mono- and biscarbene complexes of Pt(II) via transmetallation[32]

As far as the author is aware, there are no examples of Fischer carbene complexes that can be used as references in regard to transmetallation reactions to Pt(II), however, there are NHC complexes reported that can give an indication as to why the observed compounds are obtained. A review by Liu and Reddy describe several NHC ligands which are transmetallated from $W(CO)_5$ to a Pt(II) centre (Scheme 4.6).[32] For most complexes, the carbene ligand as well as a carbonyl ligand is transferred to the Pt(II) centre and only by oxidising and eliminating the CO ligand with Me_3NO, can a second NHC ligand coordinate. When the NHC ligand contains an allyl substituent on the two nitrogen atoms in the NHC ring, it is possible for two carbene ligands to coordinate directly to the Pt(II) centre without the coordination of a carbonyl ligand. In a publication by Voutchkova and Crabtree, the coordination of three small, electron rich NHC ligands to a single Pt(II) centre, through the reaction of NHC-CO_2 with K_2PtCl_4 is observed. The product is a positively charged Pt(II) triscarbene complex with a single chloro-ligand.[33] By taking these aspects into account and the products that formed, it becomes clear that the number of carbenes that coordinate to the Pt(II) centre, is dependent on the characteristics of the carbene ligand – steric and electronic properties.

For a biscarbene Pt(II) complex to form via the substitution of a COD ligand, a stepwise mechanism is likely followed. Initially, after the introduction of the first carbene ligand, the COD ligand remains partially coordinated to stabilize the metal centre, allowing two coordination sites to open.[33,34] The COD ligand is then completely displaced by the coordination of a second carbene ligand leading to the final product. The substitution of the two olefinic moieties of a COD

ligand by electronically similar alkoxycarbene ligands, support the formation and stabilisation of the biscarbene complexes of Pt(II). It is likely that the alkoxycarbene ligands display similar σ-donor, π-acceptor bonding properties than that of olefins, unlike chloro-ligands which only participates in σ-bonding. In the case of aminocarbene complexes, a third ligand is displaced to give a cationic triscarbene complex of Pt(II). The substitution of the chloride atom by an additional aminolysed carbene ligand would suggest that this step follows the substitution step of the COD by two aminocarbene ligands. The substitution of the chloro ligand by a carbene ligand greatly alters the electronic environment in the Pt coordination sphere compared to the alkoxycarbene ligands. Hence, the carbene carbon bonding properties changes drastically on replacing an alkoxy with an amino substituent: The carbene carbon becomes a poorer π-acceptor ligand (from the Pt) which will have a *trans* influence on the opposite Pt–Cl bond. Thus, the chloro-ligand *trans* to an aminocarbene ligand becomes more labile compared to the chloro-ligand *trans* to an alkoxycarbene ligand and is more readily displaced.[35] As theoretically proven by Voutchkova, the substitution of a chloro-ligand is possible in polar solvents, creating a vacant coordination site which is temporarily stabilised by a solvent molecule.[33] However, since this is only the case for the aminolysed carbene complexes, it must be assumed that it is a consequence of electronic effects whereby three aminocarbene ligands stabilises cationic Pt(II) centres more effectively.

4.2.2 NMR Spectroscopy

The ^{1}H NMR spectra of the carbene complexes are complicated by peak broadening ascribed to small differences in chemical shift of protons. This is a direct result of the presence of more than one of the same carbene ligands in a macromolecular complex and results in poorly resolved signals. Bulky carbene substituents, as is the case for **C2** and **C3**, cause broadened and overlapping of aryl peaks due to restricted rotations in the molecules. Furthermore, in **C2** and **C3** (containing triaryl amines), one of the aryl groups will be attached to a Fischer carbene functionality while the other two have a different substituent in the *para*-positions of the other rings. These aryl

resonances differ but are very close to each other and are better observed in the ^{13}C NMR than in the ^{1}H NMR spectra.

Due to the low solubility of the complexes, spectra are recorded at low concentration levels in CD_2Cl_2. Even after long collection times the carbene carbon and aryl *ipso*-carbon atoms are often not observed in the ^{13}C NMR spectra. In fact, the methylene signals of the ethoxy subsituents on the carbene carbon in the ^{1}H NMR spectra are also not observed in some cases because of peak broadening.

The complexes displaying three carbene ligands in a square-planar structure will have two types of carbene ligands, i.e. a carbene *trans* to a chloro ligand and two carbene ligands opposite each other. Peak intensities are helpful to discriminate between resonances and to determine the number of carbene ligands in a complex. In the case of two carbene ligands, the *cis*-conformation is exclusively observed.

^{1}H NMR Spectroscopy

The ^{1}H NMR spectra of all the compounds give an indication as to the electronic contribution of the aromatic substituents towards the stabilisation of the carbene carbon. This does not only show how the electron density from the distant nitrogen atom is delocalised over an aromatic ring towards the carbene carbon, but also the amount of electron density received from the stabilising heteroatom (OEt/NMe_2) carbene substituents.

The chemical shifts in the ^{1}H NMR spectra of the bis-ethoxycarbene complexes reveal downfield shifts representing a significant shift of electron density from the aromatic substituent towards the carbene carbon. This is clearly illustrated in the ^{1}H NMR spectrum of **C1a** is shown in Figure 4.5.

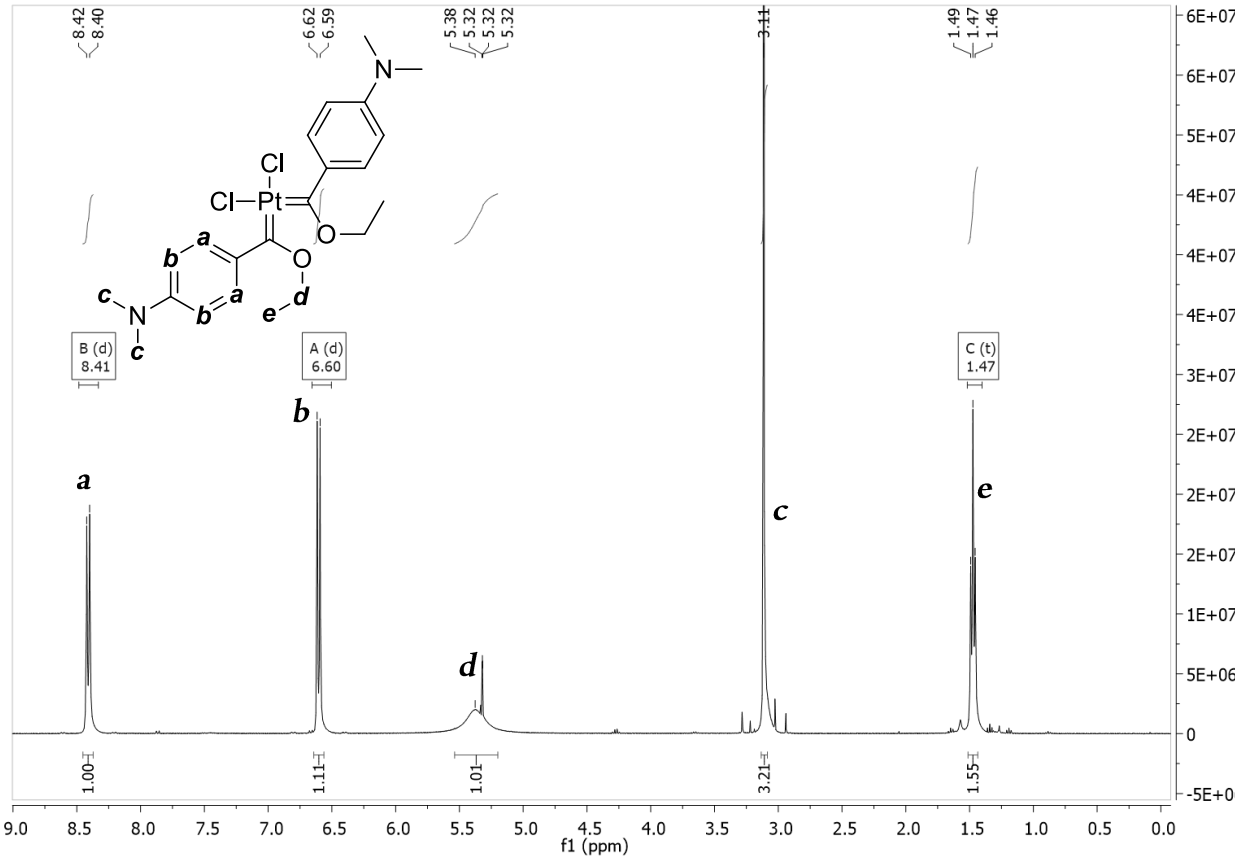

Figure 4.5. ^{1}H NMR spectrum of C1a in CD_2Cl_2 at ambient temperature

The large chemical shift difference between the *o*-protons closest to the carbene carbon (8.41 ppm) and those closest to the dimethylamine fragment (6.60 ppm) emphasise this fact. For **C2a** and **C3a**, difficulty is experienced in assigning aryl resonances as peak overlap and peak broadening is observed. This is ascribed to the formation of conformers of the complexes containing the carbene ligands with the larger substituents. For **C1a** the N,N-dimethylaniline ligand is small enough for spatial rearrangements to occur and the two ligands present in the complex are exactly the same. This is not the case for **C2a** and **C3a** in which the ligands are too large to allow for any spatial rearrangements to occur. In Figure 4.6 the ^{1}H NMR spectrum of **C2a** is shown. The spectrum in the aromatic region reveals four signals for the carbene-carrying benzene ring, two each for the protons *ortho* to the carbene carbon (7.58 and 7.51 ppm) and two for the protons *ortho* to the nitrogen atom (7.27 and 7.13 ppm). We ascribe the chemical shift

differences between the two *ortho*-protons of the carbene ligand to hydrogen bond interaction of the oxygen (OEt) with one of the benzene *o*-protons, an interaction which should be more pronounced for bulky carbene substituents with greater restricted rotations in solution (see solid state structures). The four signals with double the intensities are assigned to the protons of the remaining two benzene rings in the carbene ligand. Two of these overlap (7.06 ppm) and the two more downfield resonances are ascribed to protons α to the bromo substituent while two upfield resonances are assigned to the protons α to the nitrogen atoms. Figure 4.6 further displays significantly broadened peaks representing each proton. This is ascribed to *cis*/*trans* isomers which can exist in solution for Pt(II) complexes. Even though the *trans* isomer may be observed, the preferred *cis* isomer is often more stable upon solvation in a polar solvent. This is due to the increased dipole moment. It has also been confirmed that the more π-accepting ligand will be *trans* to a more σ-donating ligand (in this case a carbene ligand *trans* to a chloro ligand).[36,37] For this reason and the confirmation of the solid state structure of **C1a** (*vide infra*), the *cis* isomer is taken as the preferred isomer for all biscarbene complexes of Pt(II).

The spectrum further reveals the presence of an additional aromatic compound which is observed in most cases during NMR measurements and its peak intensity increases over time. This compound is assigned as the free olefin that forms upon carbene-carbene coupling when the compound is in solution. As mentioned in the introduction, this is possible when two carbene ligands are coordinated to a Pt(II) centre.[30] Although the olefin is observed, it is also clear that the compound forms very slowly and only upon solvation. It is only observed for the ethoxycarbene complexes.

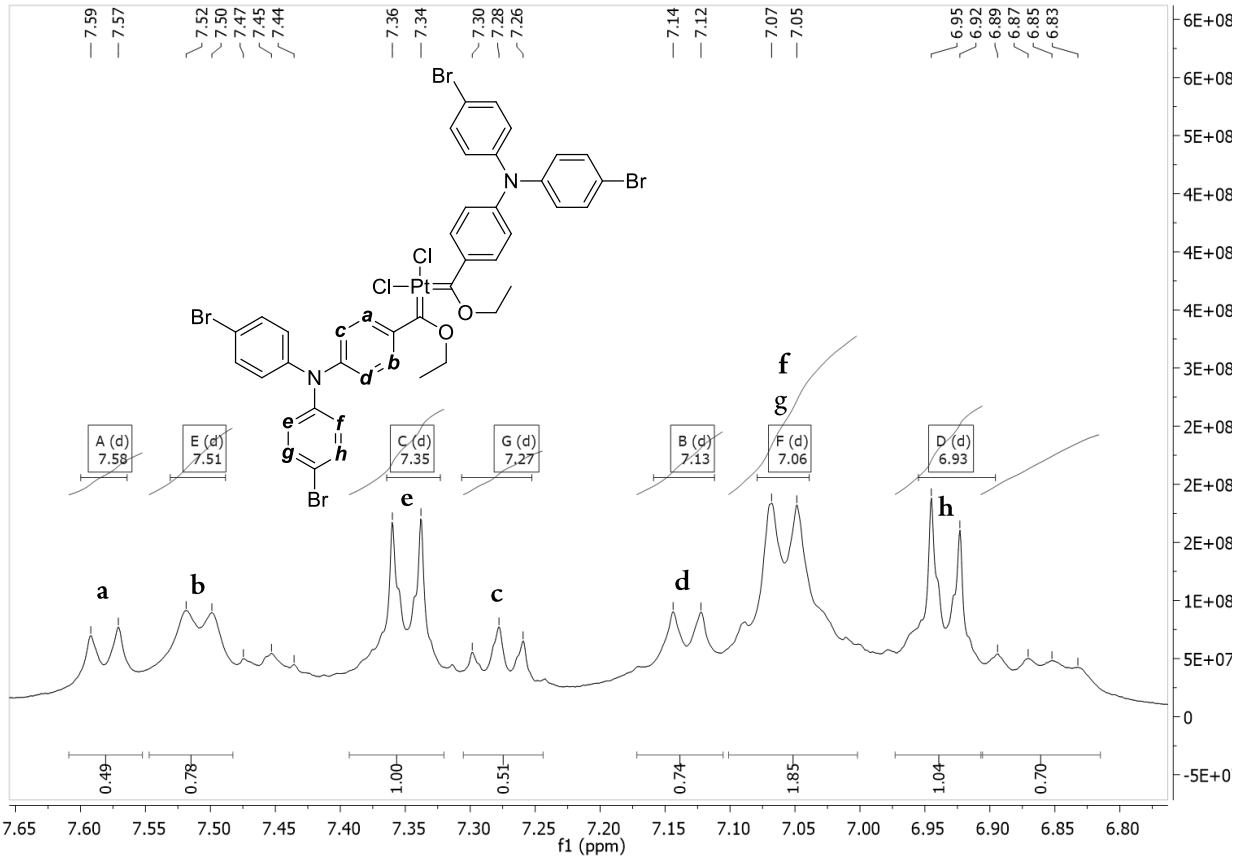

Figure 4.6. ^{1}H NMR spectrum of C2a in CD_2Cl_2 at ambient temperature

When the neutral Pt(II) bisethoxycarbene complexes are compared to their aminolysed conformers, there are important differences in the ^{1}H NMR spectra in terms of sets of signals observed for the ligands. Figure 4.7 shows the ^{1}H NMR spectrum of **C1b** in CD_2Cl_2.

Unlike the corresponding ethoxycarbene complex (**C1a**) there is only a small difference between the two sets of aromatic protons ($\Delta\delta$ = 1.79 ppm for **C1a** compared to $\Delta\delta$ = 0.34 ppm for **C1b**). This is ascribed to the strong involvement of the NMe_2 substituent in the stabilisation of the carbene carbon atom and a far smaller contribution from the aromatic substituent. The resonances of the two different dimethylamine groups of **C1b** are clearly visible in Figure 4.7. The methyl substituents which are in the *p*-position (not attached to the carbene carbon) appears upfield at 3.01 ppm compared to the two methyl groups on the aminocarbene substituent at 3.87 and 3.26 ppm. Two different chemical shift values are observed for this group as electron density

from the nitrogen atom is donated to the carbene carbon, forming a partial double bond. This will lock the two methyl groups in specific positions, one closer to the metal carbonyl moiety and the other further away.

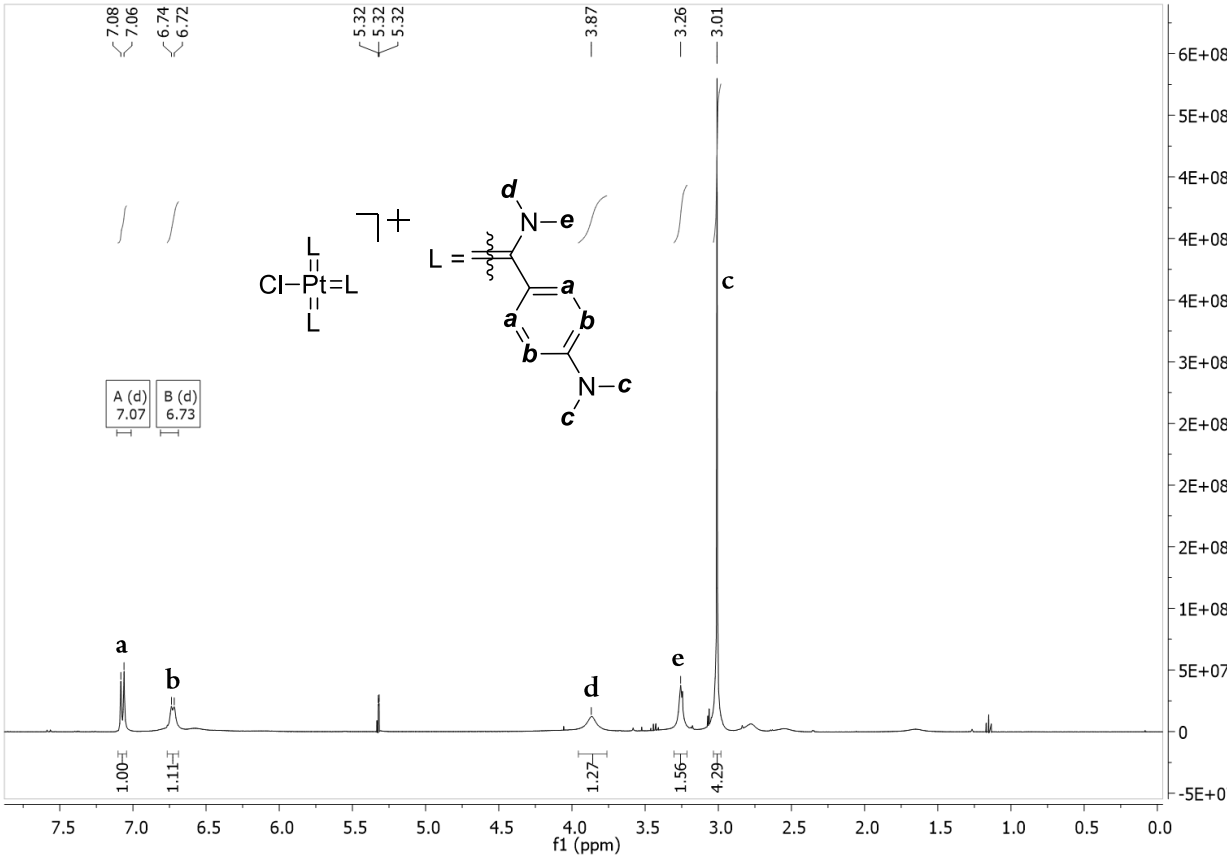

Figure 4.7. ^{1}H NMR spectrum of C1b in CD_2Cl_2 at ambient temperature

The three ligands in **C1b** are very similar in the aromatic region of their ^{1}H NMR spectrum and only a broadening of the *o*-position signal at 6.73 ppm is observed. One would have expected the *trans* influence of the ligands would have caused a more significant difference such that the ligand *trans* to the chloride would be different from the ligands *trans* to each other. This data therefore gives no indication that the complex is a triscarbene complex. The proton NMR spectra of **C2b** and **C3b** show different sets of signals for the different ligands. However, since these sets of signals can also be observed for the different conformers of the biscarbene complexes, it still does not give an indication of the number of carbene ligands present in each complex. It is for this reason that

elemental analysis and high resolution mass spectroscopy measurements are required to confirm the composition of the complexes.

Table 4.1. Selected ^{1}H NMR chemical shifts of C1a – C3a recorded in CD_2Cl_2 at room temperature

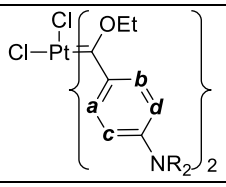

C1a: R = Me
C2a: R = PhBr
C3a: R = Ph

	Aromatic protons (ppm)				Ethoxy protons (ppm)	
	a	***b***	***c***	***d***	CH_2	CH_3
C1a	8.41 d, *J* = 9.1 Hz	8.41 d, *J* = 9.1 Hz	6.60 d, J = 9.4 Hz	6.60 d, J = 9.4 Hz	5.38 s, *br*	1.47 t, J = 7.1
C2a	7.58 d, *J* = 8.5 Hz	7.51 d, *J* = 7.9 Hz	7.27 dd, *J* = 8.2, 7.2 Hz	7.13 d, *J* = 8.6 Hz	n.o.	1.69 t, *J* = 7.0 Hz 1.53, s (*br*)
C3a	7.48 d, *J* = 7.4 Hz	7.45 d, *J* = 7.9 Hz	7.42 d, *J* = 8.1 Hz	7.37 d, *J* = 8.1 Hz	n.o.	1.67, 1.51 t, *J* = 7.1 Hz

Table 4.1 and Table 4.2 shows the ^{1}H NMR chemical shifts for selected protons of the aromatic regions for ethoxy- and aminocarbene complexes, respectively. Peak overlapping and poor resolution complicated the assignments of the signals. Relative peak intensities and repeating patterns were used in making the assignments as well as non-aromatic proton resonances.

In comparing the different sets of complexes, the aromatic rings of the ethoxycarbene ligands are expected to appear downfield compared to their aminolysed analogues. This is simply because the amino- substituent will provide more electron density towards the stabilisation of the carbene carbon than an ethoxy substituent can provide. The increased donation of electron density from the amine heteroatom will reduce the amount of electron density required from the aromatic ring to which the carbene is a substituent. All the aminocarbene ligands are coordinated to a positively charged Pt(II) atom. Although it will not be possible to directly compare a neutral Pt(II) biscarbene complex with a positively charged Pt(II) triscarbene complex, the ligands in the two respective groups can nevertheless be compared.

Table 4.2. Selected ^{1}H NMR chemical shifts of C1b – C3b recorded in CD_2Cl_2 at room temperature

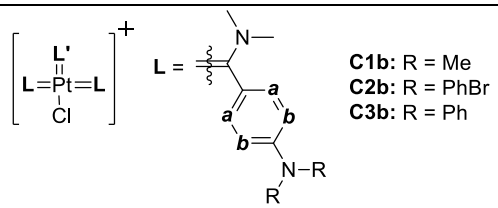

		Aromatic protons (ppm)		Dimethylamine protons (ppm)	
		a	***b***	CH_3	CH_3
C1b	**L**	6.73	7.07	3.87	3.26
		d (*br*), *J* = 7.4 Hz	d, *J* = 8.8 Hz	s	s
	L′	6.73	7.07	3.87	3.26
		d (*br*), *J* = 7.4 Hz	d, *J* = 8.8 Hz	s	s
C2b	**L**	6.99	7.17	3.70	3.49
		d, *J* = 8.8 Hz	d, *J* = 8.8 Hz	s	s
	L′	7.07	7.09	4.20-4.10	3.21-3.13
		d, *J* = 7.2 Hz	d, *J* = 7.3 Hz	m	m
C3b	**L**	7.10	7.22	4.12	3.53
		d (br), *J* = 8.7 Hz	d, *J* = 8.8 Hz	s	s
	L′	7.10	7.20	3.76	3.17
		d (br), *J* = 8.7 Hz	dd, *J* = 8.7, 2.4 Hz	s	s

The bisethoxycarbene complexes show a significant difference in the position of the chemical shift values for the protons in the aromatic rings. For **C1a** the proton in the *o*-position relative to the carbene substituent appears downfield (8.41 ppm) compared to those of **C2a** and **C3a** (at approximately 7.45 ppm). The *m*-proton relative to the carbene substituent for **C1a** appears upfield (6.60 ppm) compared to the same aromatic protons of **C2a** or **C3a** (with an approximate value of 6.9 ppm). This observation shows that the electron density from the external nitrogen in **C1a** is delocalised significantly more towards the carbene carbon compared to that found for **C2a** and **C3a**. The effect is still observed, but to a lesser extent for **C2a** and **C3a**. This can be expected as phenyl rings are generally known for their "electron sink" character and will thus not allow all the electron density which is present on the nitrogen to be delocalised towards the carbene substituent.[38] The chemical shift values of the protons *ortho* to the external tertiary amine in **C2a** appear slightly downfield compared to that of **C3a**. This effect is very small and is likely due to the

electron withdrawing character of the bromine atoms. A final aspect to consider for the three ethoxycarbene ligands is the carbene stabilisation effect from the external nitrogen. The order of carbene stabilisation by external nitrogen lone pair electrons for the ethoxycarbene ligands are **C1a** >> **C3a** > **C2a**.

The delocalisation of the electron density from the external nitrogen towards the carbene substituent observed in the ethoxycarbene complexes is not observed for the aminolysed complexes. The aromatic rings to which the carbene carbon is a substituent does not seem to play a role in its stabilisation as all the protons have chemical shift values between values of 6.7 and 7.2 ppm. From these results, it is evident that the aminocarbene substituent provides sufficient electron density towards to the stabilisation of the carbene carbon such that electron density from the aromatic ring is not required.

Although there are no large differences in electronic properties of the aromatic rings of the Pt(II) aminocarbene complexes, there are significant differences in the proton chemical shift values of the amine substituents of the carbene carbons. For the Pt(II) aminocarbene complexes of **C2b** and **C3b**, two sets of NMe_2 proton chemical shift values are observed. Since only one set of NMe_2 proton chemical shift values is observed for **C1b**, it must be assumed that steric interactions or orientation is the leading cause for the differences observed in the positions of NMe_2 substituent signals.

^{13}C NMR spectroscopy

The first triscarbene complex which was isolated in this study was **C1b**. The initial aim was to replace the COD ligand of $[Pt(COD)Cl_2]$ with two Fischer carbene ligands. It came as a surprise then, when the ^{13}C NMR spectrum shown in Figure 4.8 was obtained.

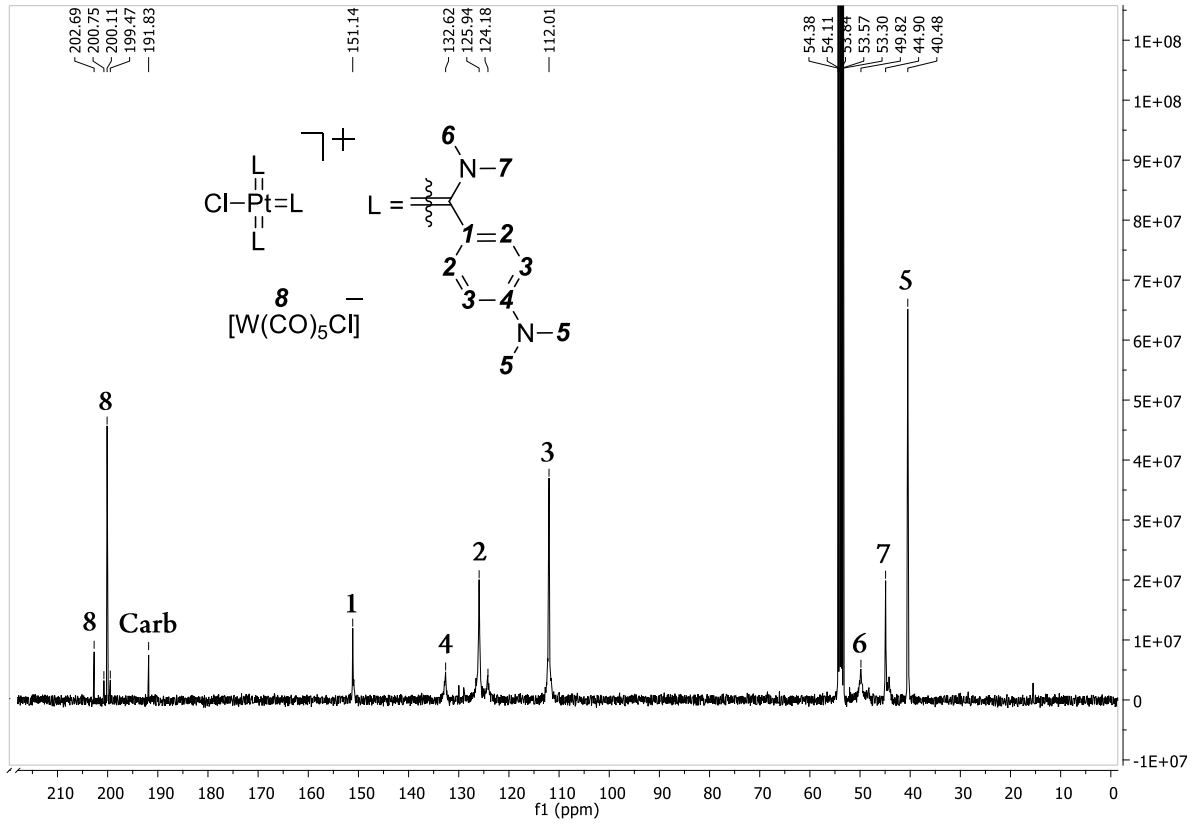

Figure 4.8. ^{13}C NMR spectrum of C1b in CD_2Cl_2 at ambient temperature

It was unclear, at the time, why even after several attempts of purification, the tungsten carbonyl chemical shift values observed at 202.7 and 200.1 ppm were still present. It was only after the crystal structure (discussed in the crystallography section of this chapter) was obtained for this compound that all the peaks could be unambiguously assigned. The tungsten pentacarbonyl group remained present within the complex, as it is part of the anionic counter ion to pair with the positively charged Pt(II) triscarbene complex.

In Figure 4.8 all the peaks assigned to the carbene ligands are broadened except those of the carbene carbon (191.8 ppm) and the tungsten pentacarbonyl chloride anion (202.7 and 200.1 ppm). The peak broadening suggests the presence of more than one ligand coordinated to the Pt(II) centre, but this in effect means that each ligand is almost identical. Once again, the lack of any additional sets of peaks is surprising.

Table 4.3. Selected ^{13}C NMR chemical shifts (ppm) of C1a – C3a recorded in CD_2Cl_2 at room temperature

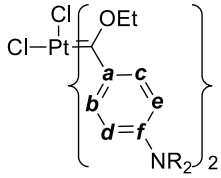

C1a: R = Me
C2a: R = PhBr
C3a: R = Ph

	Carbene	Aromatic carbons						Ethoxy carbons	
		a	***b***	***c***	***d***	***e***	***f***	CH_2	CH_3
C1a	238.5	156.1	137.4	137.4	110.8	110.8	132.7	77.5	14.7
C2a	n.o.	157.0	133.9	133.6	130.0	129.1	154.5	n.o.	15.5
									14.6
C3a	n.o.	147.9	130.1	130.1	127.6	127.0	147.9	n.o.	14.3
									14.1

Table 4.4. Selected ^{13}C NMR chemical shifts (ppm) of C1b – C3b recorded in CD_2Cl_2 at room temperature

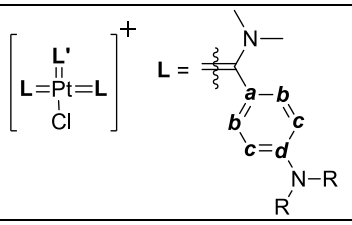

C1b: R = Me
C2b: R = PhBr
C3b: R = Ph

		Carbene	Aromatic carbons				Dimethylamine carbons	
			a	***b***	***c***	***d***	CH_3	CH_3
C1b	**L**	191.8	151.1	125.9	112.0	132.6	49.8	44.9
	L′	191.8	151.1	125.9	112.0	132.6	49.8	40.3
C2b	**L**	213.1	155.7	127.7	121.8	146.2	52.5	44.8
	L′	203.0	149.8	125.1	123.1	147.8	49.8	46.9
C3b	**L**	n.o.	148.3	121.7	119.1	146.2	n.o.	n.o.
	L′	n.o.	n.o.	121.7	120.0	n.o.	n.o.	n.o.

The ^{13}C NMR spectrum of **C1b** is in fact the only spectrum of the aminolysed Pt(II) triscarbene complexes that does not show the presence of two different sets of chemical shifts for the ligands. Figure 4.9 displays the ^{13}C NMR spectrum of **C2b** which clearly shows the two different sets of ligand signals for the compound.

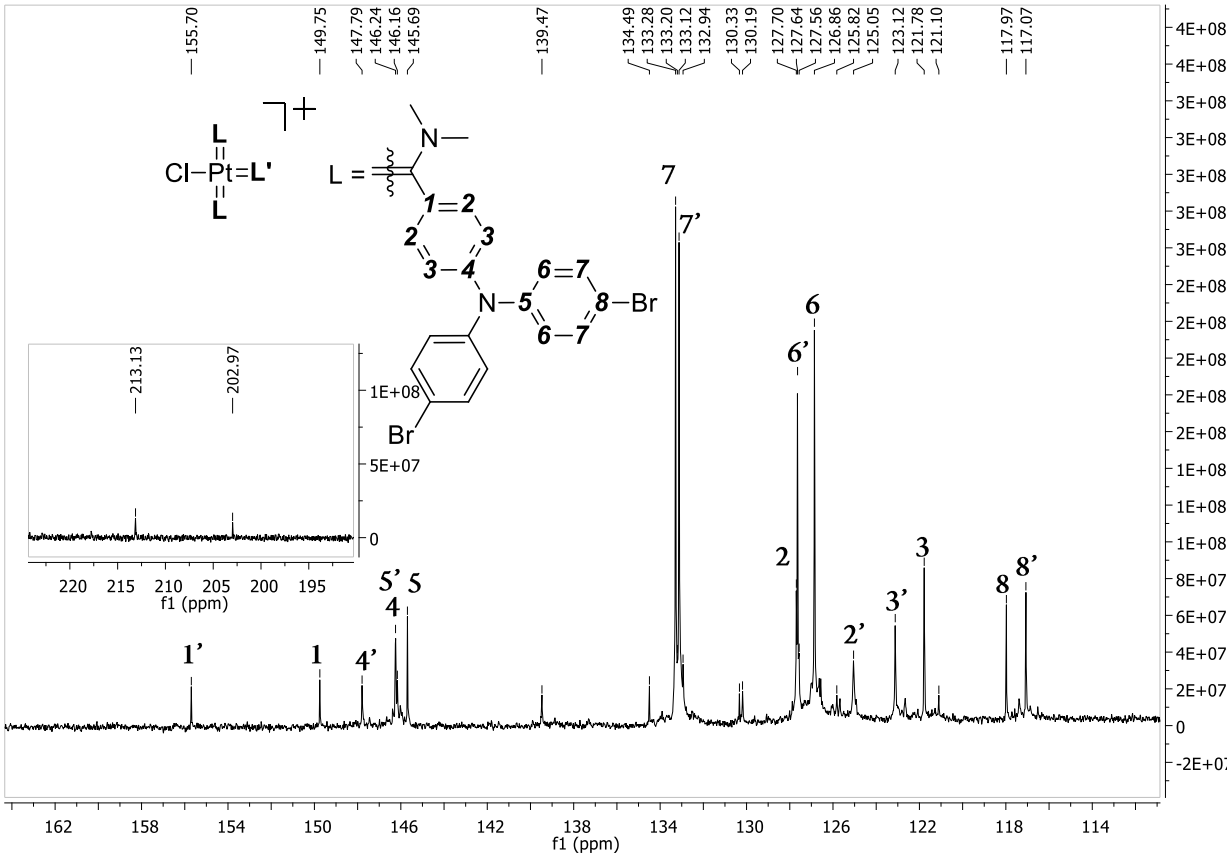

Figure 4.9. ^{13}C NMR spectrum of C2b in CD_2Cl_2 at room temperature

For any carbon bonded directly to a Pt atom one would expect Pt{C} coupling. The coupling is shown in Figure 4.10 which is the ^{13}C NMR spectrum for the Pt(II) bisethoxycarbene complex, **C1a**. The coupling is clearly seen for the carbene carbon with a chemical shift value of 238.5 ppm as well as for the CH_2-unit in the ethoxycarbene substituent at 77.5 ppm. Unfortunately, **C1a** is the only complex in which the coupling is clearly observed due to the high signal to noise ratio which is prevalent for these complexes. For some of the large ligands, the carbene carbon is not visible due to the low solubility of the complexes in CD_2Cl_2.

It is expected that the chemical shifts for the carbene carbons of the ethoxy complexes will appear downfield compared to their aminolysed analogues. The fact that the aminocarbene complexes are positively charged must be considered when making this statement.

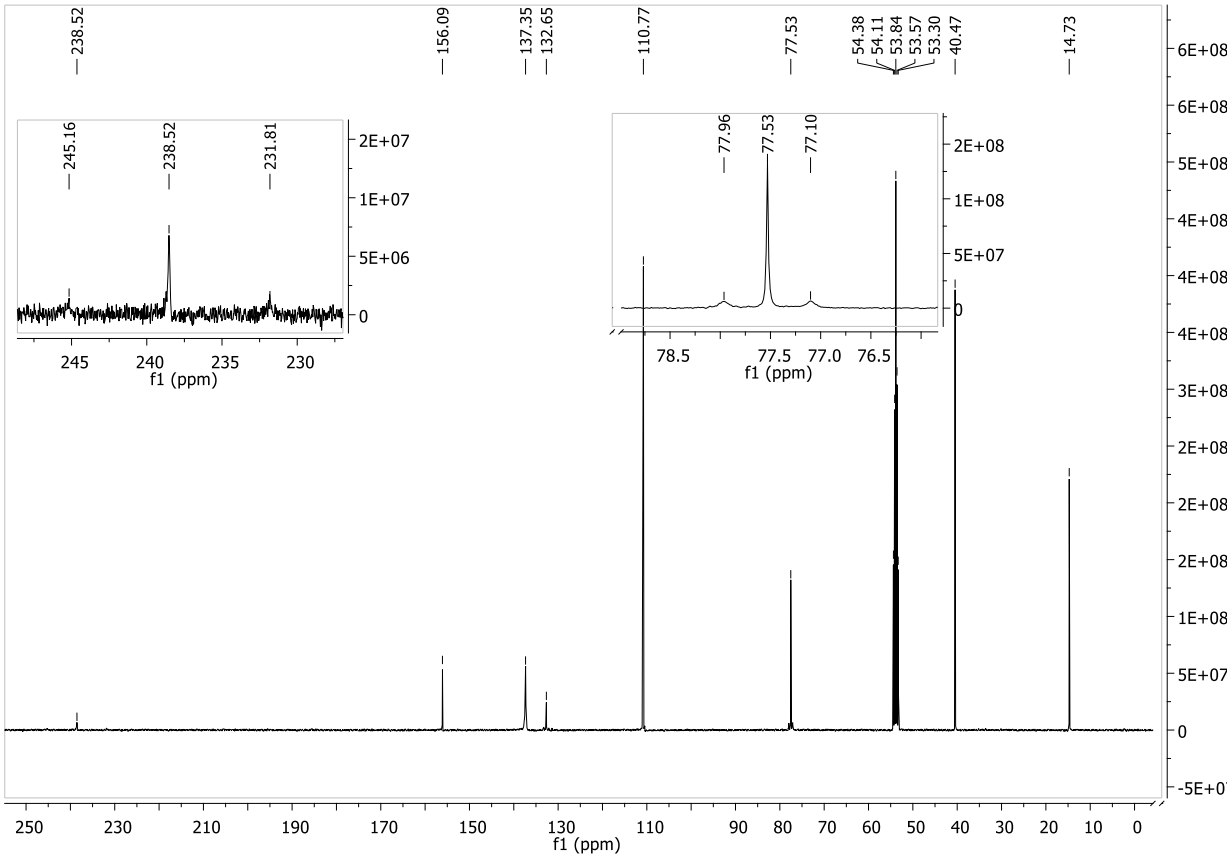

Figure 4.10. ^{13}C NMR spectrum of C1a in CD_2Cl_2 at 298 K

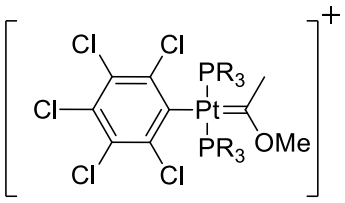

Figure 4.11. Mononuclear methoxycarbene complex synthesized Wada and Koyama[14]

As mentioned in the introductory section of this chapter, there are only a few Fischer Pt(II) alkoxy carbene complexes that exist. An example of a neutral bis-ethoxycarbene complex synthesised by Sierra and co-workers, has a ^{13}C NMR carbene chemical shift that appears upfield (~ 198 ppm) compared to the ^{13}C NMR values for the carbene carbons of **C1a** with a carbene chemical shift value at 238.5 ppm.[21] The upfield carbene position of their complex is likely caused by increased electron density on the metal provided by the amido ligand and the chelating effect of the coordinating nitrogen atom present in the ligand. Either way, the complex synthesized by the group is rich in electron density which allows for the pronounced shielding of the carbene carbon in their synthesized complexes (Figure 4.2). An example of a cationic Pt(II)

monocarbene complex, synthesized by Wada and Koyama (Figure 4.11),[14] has a carbene chemical shift value of 310.1 ppm. The wide range of chemical shift values for the carbene carbons (the complexes under investigation included) coordinated to Pt(II) shows that the electron density provided by the carbene's substituents as well as the charge of the Pt(II) centre determines the stability of the carbene carbon.

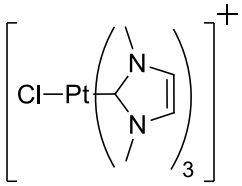

Figure 4.12. Structure of $[Pt(NHC)_3Cl]^+$ complex[33]

A triscarbene complex (three NHC ligands of 1,3-dimethylimidazole-2-ylidene as well as a chloro ligand coordinated to a Pt(II) centre) of similar nature to the aminolysed Pt(II) triscarbene complexes in this study, was synthesised by the group of Crabtree (Figure 4.12).[33] The single carbene chemical shift value in the ^{13}C NMR spectrum is found at 146.4 ppm in CD_3CN, approximately 50 ppm upfield from the carbene signal observed for **C1b** in CD_2Cl_2, giving an indication as to the significant contribution to the stabilisation of the carbene carbon by its two amino substituents in the ring of an NHC.

The NMR spectroscopy gives some indication as to the electronic arrangements of the ligands present in each complex. It is unfortunately not possible to determine whether the compound is a bis- or triscarbene complex from its NMR spectra alone. For some of the triscarbene complexes there are differences between the two carbene ligands *trans* to each other and *trans* to the chloride, but this is not always the case (**C1b**). Another clear example is **C2a**, which has been established as a biscarbene through other analytical methods. It shows different sets of signals for carbene ligands which should theoretically be exposed to the same environment. These different sets of chemical shift values observed are assigned to steric conformers: carbene ligands orientated in different positions relative to each other.

4.2.3 *Mass Spectrometry*

High resolution mass spectrometry (HRMS) was further used to establish the identity of the complexes. Table 4.5 lists the mass to charge ratio (m/z) for some fragments isolated during the analysis.

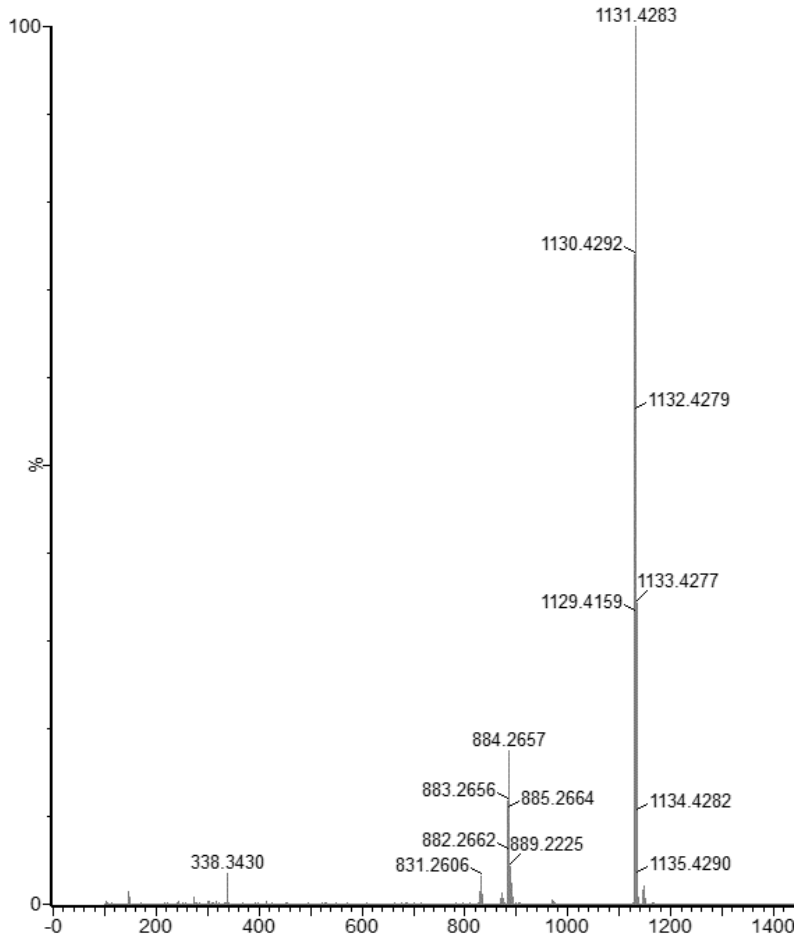

Figure 4.13. MS spectrum of C3b

One of the most problematic complexes is **C2a** as it shows greater reactivity to water and shows different sets of signals for each carbene ligand in its NMR spectroscopy. The mass spectrometry measurement of **C2a** shows a compound with two carbene ligands and two chlorides attached to the central Pt(II) metal centre, thus indicating a complex of neutral charge. The elemental analysis also supports the formation of this sole product.

An ester decomposition product is present in the MS spectra for the Pt(II) ethoxycarbene complexes (**C1a** – **C3a**), indicating the pronounced difference in reactivity of the ethoxycarbene complexes compared to that of the aminocarbene complexes in which no such product is observed.

Table 4.5. Mass spectral data for C1a – C3a and C1b – C3b

Complex	Structure	Fragment	MS (m/z) Calc	Found
C1a	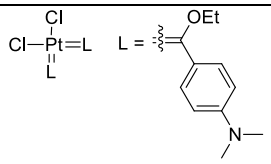	$[M + H]^+$	620.1410	620.1449
C1b	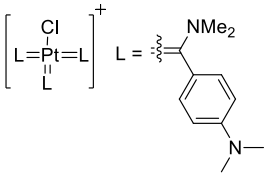	$[M]^+$	759.3278	759.3279
C2a	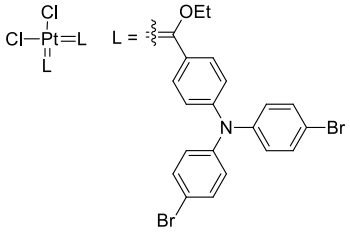	$[M + Na]^+$	1206.8236	1206.8271
C2b	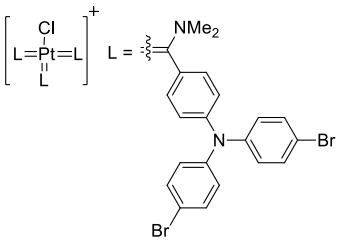	$[M]^+$	1604.8786	1604.8789
C3a	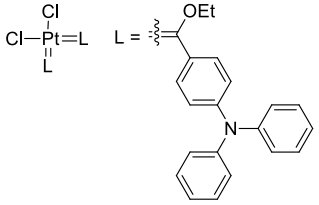	$[M–L]^+$	833.2271	833.2268
C3b	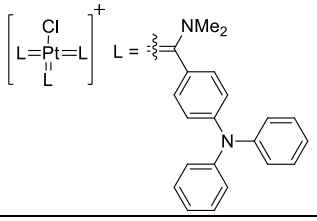	$[M]^+$	1131.4217	1131.4283

For all the aminocarbene complexes the M^+ peaks are always present indicating the reduced reactivity of these complexes even under harsh conditions. Figure 4.13 is the MS spectrum of **C3b**. It shows that there is relatively little decomposition of the product on exposure to the harsh conditions and the product remains intact to give an isotopic mass of 1131.4283 m/z for **C3b**.

4.2.4 *Infrared Spectroscopy*

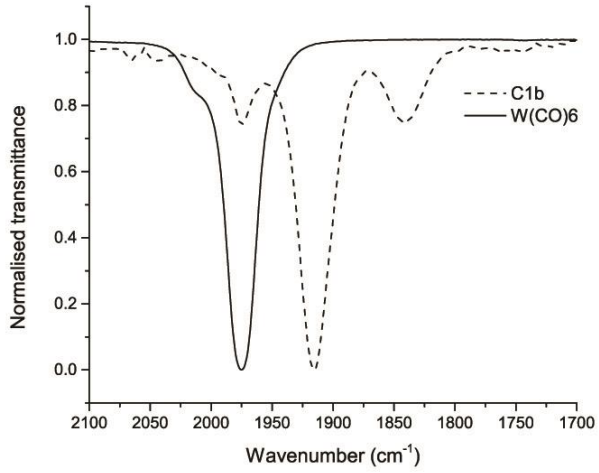

Figure 4.14. FT-IR spectrum of C1b and $W(CO)_6$ in CH_2Cl_2 at ambient temperature

Infrared spectroscopy played an important role in the identification of **C1b**. During its analysis, the presence of the tungsten carbonyl complex is observed in the ^{13}C NMR spectrum. The single X-Ray structure of the compound originally indicated that the compound was a tungsten hexacarbonyl containing a charge. It has been previously reported that it is possible for the wrong identification of elements from single X-Ray crystallography.[39,40] This error resulted from the fact that the crystallographic position of the chloro ligand at more than one of the carbonyl sites dilutes its effect. The IR spectroscopy was the key to determine that the counter ion was in fact a $[W(CO)_5Cl]^-$ ion. The FT-IR spectrum of **C1b** against $W(CO)_6$ in CH_2Cl_2 is shown in Figure 4.14, showing the vast difference between the two compounds.

The solid-state FT-IR spectrum for **C1b** shows three distinct peaks at 1988, 1893 and 1831 cm^{-1}. For $W(CO)_6$ a single stretching frequency is expected at approximately 1980 cm^{-1}, thus eliminating the possibility that the $W(CO)_6$ is present.[41] The solid state (KBr pellets) IR stretching frequencies of the tetraalkylammonium salts with the tungsten pentacarbonyl chloride anion are reported as three distinct peaks at 2061(w), 1904(s) and 1869(m) cm^{-1} for the A^{1b}, E and A^{1a} stretching frequencies respectively.[42] Since the obtained IR spectrum closely matches the pattern as well as the approximate frequencies of vibration for the tetraalkylammonium tungsten pentacarbonyl chloride, it has been concluded that the anion of the **C1b** complex is the $[W(CO)_5Cl]^-$ ion.

4.2.5 X-Ray Crystallography

The crystal structures for **C1a** and **C1b** (with different counter-ions) have been obtained through the slow diffusion of *n*-hexane into dichloromethane.

C1a

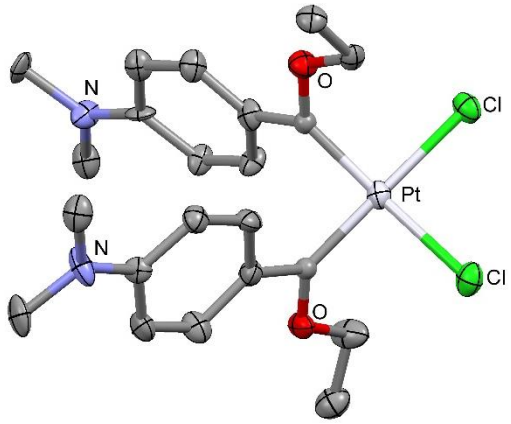

Figure 4.15. Solid state structure of C1a. Ellipsoids are set at 50% probability; hydrogen atoms are omitted for clarity

C1a crystallises in the P-1 space group. The crystal data collection and refinement details can be found in the Appendix. The molecular structure for the compound is shown in Figure 4.15 and a selection of bonding data is shown in Table 4.6.

The two carbene ligands present in the compound are bonded to a square planar Pt(II) centre in the *cis*-configuration. The data reveals that there are small differences between the two carbene ligands in **C1a**. The Pt–C_{Carb} bonds (1.935(15) Å) and the C–C bonds in the benzene rings have the same length. One carbene ligand seems to rely more on the ethoxy group for the stabilisation of its carbene carbon as the C_{Carb}–O_{OEt} bond is shorter than the other (1.29(2) and 1.36(2) Å respectively). The chlorine atoms *trans* to the carbene ligands have slightly different bond lengths of 2.392(5) and 2.377(4) Å, the shorter bond lying *trans* to the carbene ligand having a shorter C_{Carb}–O_{OEt} bond.

Table 4.6. Selected bond lengths, bond angles and torsion angles of C1a

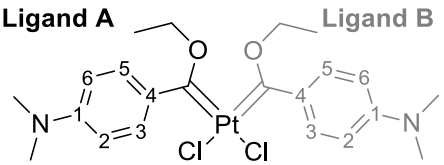

Bond Length (Å)			Bond Angle (°)		
	Ligand A	Ligand B		Ligand A	Ligand B
Pt–$C_{carbene}$	1.935(16)	1.935(15)	O_{OEt}–C_{carb}–C_{Ar}	109.3(14)	108.3(14)
$C_{carbene}$–O_{OEt}	1.36(2)	1.29(2)	Pt–C_{carb}–O_{OEt}	120.1(11)	124.6(11)
$C_{carbene}$–C4	1.46(2)	1.48(2)	Pt–C_{carb}–C_{Ar}	130.4(12)	126.9(12)
N–C1	1.36(2)	1.36(2)	C_{Me1}–N–C_{Ar}	122.6(15)	122.6(15)
C1–C2	1.40(3)	1.43(2)	C_{Me2}–N–C_{Ar}	119.7(14)	117.9(15)
C2–C3	1.40(2)	1.36(2)	C_{Me1}–N–C_{Me2}	117.6(14)	119.2(15)
C3–C4	1.41(2)	1.43(2)	C_{carb}–Pt–Cl	89.2(5)	90.2(5)
C4–C5	1.42(2)	1.43(2)			
C5–C6	1.39(2)	1.37(2)	**Torsion Angle (°)**		
C6–C1	1.41(2)	1.42(2)		Ligand A	Ligand B
Pt–Cl_{trans}	2.392(5)	2.377(4)	Pt–C_{carb}–C4–C3	-16(2)	-2(2)
N–CH_3	1.45(2)	1.43(2)	O_{OEt}–C_{carb}–C4–C5	-8(2)	-9(2)
	1.50(2)	1.49(2)	C_{Me1}–N–C1–C2	-3(3)	-1(3)
			C_{Me2}–N–C1–C6	-3(3)	-10(3)

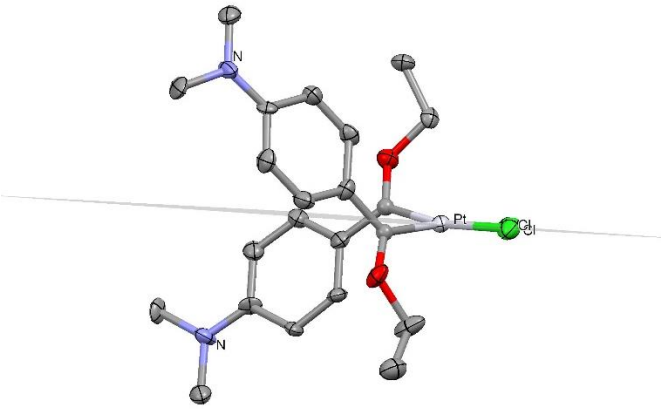

Figure 4.16. Solid state structure of C1a with a plane throug the Pt(II) metal and chloride atoms.

The ethoxy and phenyl group are on opposite sides of a plane through the Pt atom and the chloro ligands (Figure 4.16). By constructing a visible plane of the rings that bisects the Pt centre, a slight distortion of the square planar complex is observed with each carbene carbon lying slightly above or below the plane (Figure 4.16). Further examination reveals that each carbene ligand, including its ethoxy substituent, lies in the plane of the aromatic ring which is not necessarily the case for the analogous tungsten pentacarbonyl carbene complex (**B2a**) discussed in Chapter 3. For **B2a** the nitrogen, the aromatic group and the carbene carbon all lie in

the same plane while the metal and ethoxy groups lie on opposite sides, out of the plane. The planarity of each ligand indicates significant π-conjugation and electron delocalisation that extends from the nitrogen atom of the NMe_2 moiety to the carbene carbon and its ethoxy substituent.

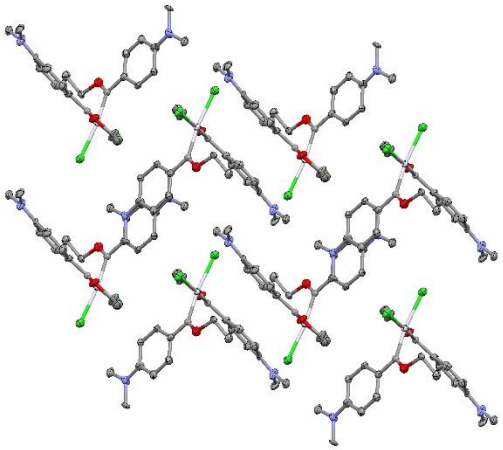

Figure 4.17. Crystal packing of C1a along the a-axis

The packing of **C1a** along the three different axes are shown in Figure 4.17. The packing pattern is established by hydrogen bonding between the two chloro ligands and two protons of one carbene ligand. The unit motif is clearly shown along the a-axis. A Pt and one of its carbene ligands intermolecularly interacts with a second Pt and carbene ligand in a head to tail fashion. One chloro ligand of Pt(1) interacts with a proton of a methyl substituent of NMe_2 of a carbene ligand (PtCl---H(CH_2)NMe = 2.708 Å) of Pt(2), while the second chloro ligand interacts with a benzene proton of the same carbene ligand which is α to the NMe_2 substituent (PtCl---H(Bz) = 2.778 Å) of the same Pt(2). The same applies for Pt(1) and its chloro ligands with one of Pt(2)'s carbene ligands.

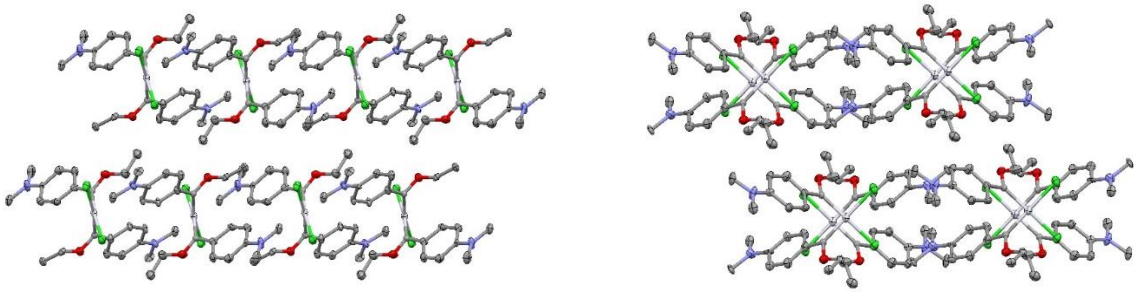

Figure 4.18. Crystal packing of C1a along the b-axis (left) and c-axis (right)

The packing along the b-axis shows clear layers or bands that form in the structure, each a single Pt complex thick (Figure 4.18). Along this axis, it is also clear that the Pt(II) centres are far apart, thus, no metal-metal interactions are involved in the packing of the compound. For Pt---Pt

interactions to exist, the distance between the Pt atoms is in the range of 3.3 and 4.5 Å.[43,44] The packing along the c-axis again shows the clear formation of layers. The metal centres of the individual complexes are not aligned in a straight line, but rather arranged in a zig-zag fashion. Every carbene complex has its two chlorine atoms pointing in the opposite direction than that of the complex next to it. This allows for the OEt and NMe_2 groups to be far enough apart such as not to cause repulsion between the groups.

By comparing selected bond lengths and bond angles of the two carbene ligands in **C1a** with those of **I** – the Pt(II) bis-ethoxycarbene complex isolated by Steinborn and co-workers (Figure 4.19) and **II** – Pt(II) bis-ethoxycarbene complex isolated by Sierra and co-workers (Figure 4.20), it is possible to investigate the effect that different ligands have in the complexes.

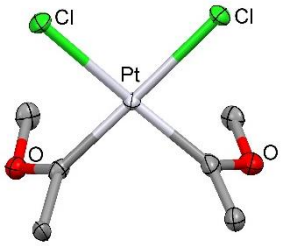

Figure 4.19. Solid state structure of I, published by Steinborn and co-workers. Ellipsoids are set at 50% probability; hydrogen atoms are omitted for clarity[12]

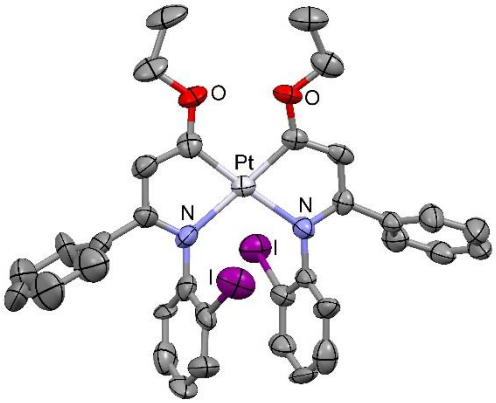

Figure 4.20. Solid state structure of II, published by Sierra and co-workers. Ellipsoids are set at 50% probability; hydrogen atoms are omitted for clarity[21]

Table 4.7. Selected bond lengths in C1a, I and II

Bond	C1a R = N,N-dimethylaniline		I[12] R = Methyl		II[21] R = Amide	
	Carbene 1	Carbene 2	Carbene 1	Carbene 2	Carbene 1	Carbene 2
Pt–$C_{carbene}$	1.935(16)	1.935(15)	1.932(7)	1.956(7)	1.93(1)	1.94(1)
$C_{carbene}$–O_{OEt}	1.36(2)	1.36(2)	1.282(9)	1.278(9)	1.35(1)	1.35(1)
$C_{carbene}$–C_R	1.46(2)	1.48(2)	1.51(1)	1.48(1)	1.39(1)	1.37(1)
Pt–Cl	2.392(5)	2.377(4)	2.374(2)	2.378(2)	–	–

From the data listed in Table 4.7 there are no pronounced differences between the metal-carbene bonds of **C1a**, **I**, and **II**, which have lengths of approximately 1.93 Å. This is interesting as the substituents which provide some of the electronic stabilisation for the carbene carbon is remarkably different between the three complexes. Another solid-state structure of a Pt(II) mono-ethoxycarbene complex published by Anderson and co-workers in 1979 has a Pt–$C_{carbene}$ bond length of 1.920(9) Å, which also fits the trend previously observed in the above mentioned carbene complexes.[15] In the Anderson structure, the Pt–Cl bond *trans* to the carbene ligand has a reported length of 2.375(3) Å which also fits the trend for Pt–Cl bond lengths *trans* to ethoxycarbene ligands. A structure published in 1976 by Badley shows the exact same pattern with a Pt–$C_{carbene}$ bond length of 1.962(18) Å and a *trans* Pt–Cl bond length of 2.361(5) Å.[45] The data shows that Pt ethoxycabene complexes and the chlorides coordinated *trans* to them have lengths of around 1.93 and 2.37 Å, respectively.

C1b

Two crystal structures are obtained for **C1b**: one with a $[W(CO)_5Cl]^-$ counter ion and the other with a PF_6^- counter ion which will, in this section, be referred to as **C1b(I)** and **C1b(II)** respectively. The crystal data collection and refinement details for both the crystal structures are available in the Appendix. The bright yellow, rod-like crystals were obtained by the slow diffusion of hexane into a dichloromethane solution.

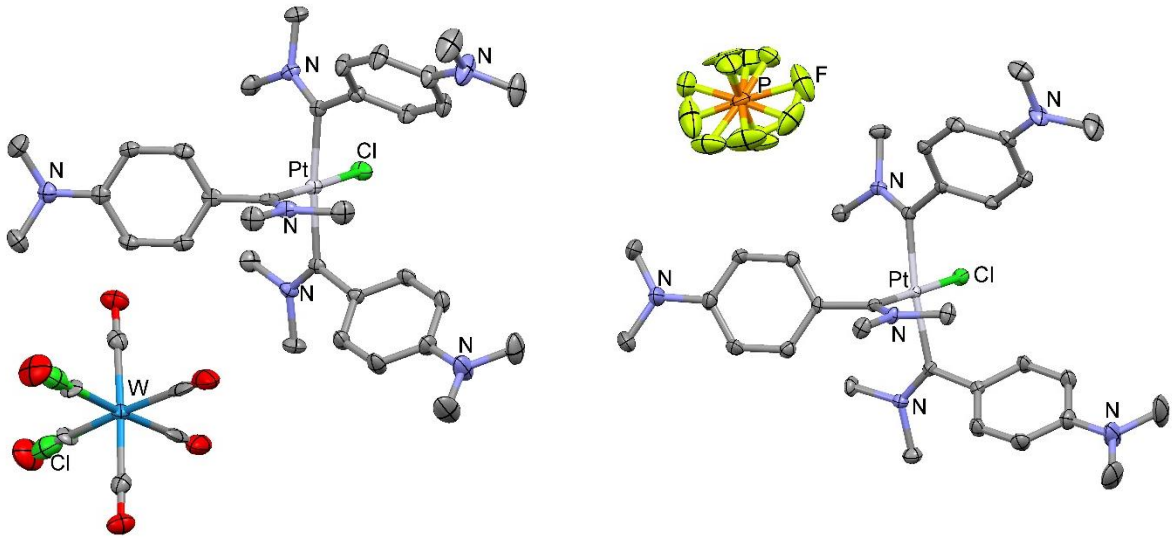

Figure 4.21. Solid-state structures of C1b(I) (left) and C1b(II) (right). Ellipsoids are set at 50% probability; hydrogen atoms are omitted for clarity

Table 4.8. Selected bond lengths (Å) of C1b(I) and C1b(II)

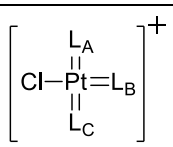

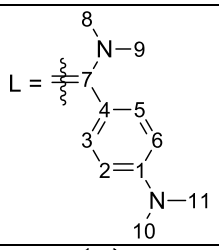

	C1b(I) Carbene Ligands			C1b(II) Carbene Ligands		
Bond	**A**	**B**	**C**	**A**	**B**	**C**
Pt–Cl	2.3804(15)			2.3798(10)		
Pt–C7	2.053(4)	1.975(6)	2.053(4)	2.059(4)	1.973(4)	2.051(4)
N2–C1	1.382(6)	1.376(9)	1.382(6)	1.368(5)	1.385(6)	1.382(6)
N2–C10	1.438(7)	1.457(6)	1.438(7)	1.451(7)	1.436(6)	1.442(7)
N2–C11	1.425(7)	1.457(6)	1.425(7)	1.462(6)	1.450(6)	1.429(7)
N1–C7	1.311(5)	1.318(8)	1.311(5)	1.308(5)	1.307(5)	1.382(6)
N1–C8	1.467(6)	1.476(9)	1.467(6)	1.476(5)	1.469(5)	1.429(7)
N1–C9	1.480(6)	1.477(8)	1.480(6)	1.477(5)	1.484(5)	1.442(7)
C1–C2	1.412(7)	1.414(6)	1.412(7)	1.412(6)	1.402(6)	1.401(6)
C1–C6	1.390(7)	1.414(6)	1.390(7)	1.404(6)	1.404(6)	1.408(6)
C2–C3	1.369(6)	1.385(6)	1.369(6)	1.386(6)	1.376(6)	1.373(6)
C3–C4	1.398(6)	1.401(6)	1.398(6)	1.412(6)	1.389(6)	1.394(6)
C4–C5	1.394(6)	1.401(6)	1.394(6)	1.404(6)	1.398(6)	1.395(6)
C4–C7	1.490(6)	1.473(9)	1.490(6)	1.462(6)	1.494(5)	1.487(6)
C5–C6	1.375(6)	1.385(6)	1.375(6)	1.382(6)	1.391(6)	1.372(6)

Table 4.9. Selected bond angles (°) and torsion angles (°) of C1b(I) and C1b(II)

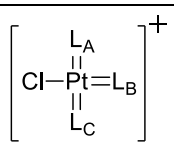

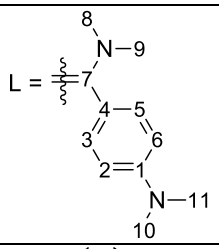

	C1b(I) Carbene Ligands			C1b(II) Carbene Ligands		
	A	B	C	A	B	C
Bond Angles (°)						
C1–N2–C10	120.8(5)	119.7(3)	120.8(5)	120.2(4)	119.9(4)	121.5(5)
C1–N2–C11	120.5(5)	119.7(3)	120.5(5)	119.9(4)	119.2(4)	120.8(5)
C10–N2–C11	118.6(5)	116.1(6)	118.6(5)	118.6(4)	115.6(4)	117.6(4)
C7–N1–C8	120.8(4)	123.0(6)	120.8(4)	125.6(4)	122.6(3)	122.4(4)
C7–N1–C9	125.7(4)	124.5(6)	125.7(4)	122.0(3)	125.0(4)	125.7(4)
C8–N1–C9	113.4(4)	112.5(5)	113.4(4)	112.3(3)	112.3(3)	111.9(3)
Pt–C7–N1	124.3(3)	125.5(5)	124.3(3)	122.3(3)	125.2(3)	124.4(3)
C4–C7–Pt	116.0(3)	117.9(4)	116.0(3)	118.1(3)	117.4(3)	117.4(3)
C4–C7–N1	119.7(4)	116.6(6)	119.7(4)	119.5(4)	117.4(3)	118.2(4)
AC7–Pt–BC7	91.09(11)			95.03(16)		
AC7–Pt–CC7	91.09(11)			90.15(16)		
BC7–Pt–Cl	89.10(11)			85.28(11)		
CC7–Pt–Cl	89.10(11)			89.76(11)		
Torsion angles (°)						
C2–C1–N2–C10	5.3(9)	14.1(8)	5.3(9)	-6.2(7)	16.7(7)	2.2(9)
C6–C1–N2–C11	1.7(9)	-14.1(8)	1.7(9)	6.9(7)	-12.7(8)	-0.9(9)
C8–N1–C7–Pt	3.4(6)	0.0	3.4(6)	10.3(5)	5.5(6)	-2.3(6)
C9–N1–C7–C4	4.7(6)	0.0	4.7(6)	9.7(6)	1.1(6)	-6.8(6)
C3–C4–C7–Pt	47.8(5)	92.0(5)	47.8(5)	38.9(5)	-71.1(4)	-50.1(5)
C5–C4–C7–N1	56.2(6)	88.0(5)	56.2(6)	48.4(6)	-70.3(5)	-55.5(6)

Three carbene ligands are coordinated to the square planar Pt(II) centre in both **C1b(I)** and **C1b(II)**. The fourth position, occupied by a chloro ligand, is crowded by the surrounding carbene ligands. There is chemically no significant difference between the two single crystal structures except for the different counter ions. The counter ion for each complex is distorted in both structures. In **C1b(I)**, the counter ion can lie in any position relative to the positively charged Pt(II) carbene complex, thus the average structure is displayed and for **C1b(I)** in which the chlorine atom is orientated in one of two positions relative to the large Pt(II) complex and that is

why two of the counter ion bonds in the $[W(CO)_5Cl]^-$ anion is represented by both a W–CO bond and a W–Cl bond.

The data listed in Table 4.8 and Table 4.9 demonstrates the similarities between the different carbene ligands within the two crystal structures of **C1b(I)** and **C1b(II)**, which have different counter ions. The three individual carbene ligands present in each structure are marked as *A*, *B* and *C*. The values for *B* represents the carbene ligand *trans* to the chloro ligand, while *A* and *C* are the ligands *trans* to each other.

The two *trans* carbene ligands in **C1b(I)** are the same (refined symmetrically equivalent) while the carbene ligand *trans* to the chloro ligand is different. The same is not true for **C1b(II)** with differences in the bond lengths of all three different carbene ligands. The bond lengths for the different carbene ligands are visually represented in Figure 4.22 and Figure 4.23. The Pt–carbene bond is significantly shorter in **C1b(I)** in the *B*-carbene ligand (1.975(6) Å) than the other two carbene ligands with both bonds having a length of 2.053(4) Å. The Pt–$C_{carbene}$ distance for the *B*-ligand (*trans* to the Cl atom) in **C1b(II)** is also observed as the shortest bond (1.973(4) Å), when the three ligands are compared. All corresponding benzene C–C bond distances of the carbene ligands in **C1b(I)** and **C1b(II)** are the same with one important observation: There are pronounced differences in C–C bond distances in the benzene ring when delocalisation of electron density is viewed. Delocalisation is evident within the ligands from the dimethylamine substituent on the aromatic ring towards the carbene carbon. The localisation of electron density by conjugation is clear with a shortening and lengthening of the alternate bonds in the aromatic ring. Further, the plane of the aromatic group is perpendicular to the plane of the dimethylaminocarbene substituent for the *B*-ligand (**C1b(I)**) with the torsion angle of 92.0(5) ° while that for the *A*- and *C*-ligands have values of 47.8(5) °. Orbital overlap between the π electron cloud of the aromatic ring and the dimethylamine of the *B*- ligand will consequentially lead to localized conjugation, but is not aligned with the empty p-orbital of the carbene carbon. The latter is aligned for π-conjugation with the dimethylaminocarbene substituent. Support for this is also

found in a much shorter C(carbene)–NMe_2 distance, 1.31(1) Å compared with a C(phenyl)–NMe_2 distance of 1.38(1) Å. Thus, the analine substituent cannot contribute to the stabilisation of the carbene carbon by π-resonance effects.

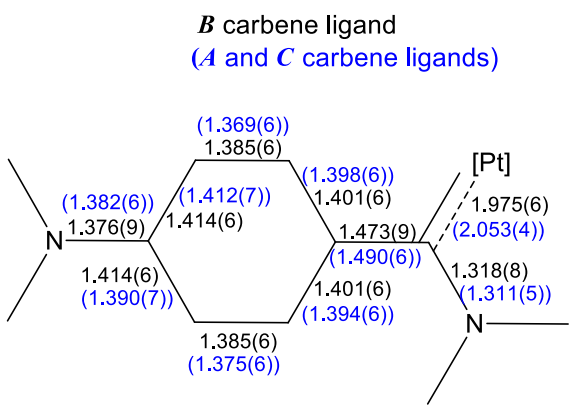

Figure 4.22. Carbene ligand bond lengths (reported in Å) in C1b(I)

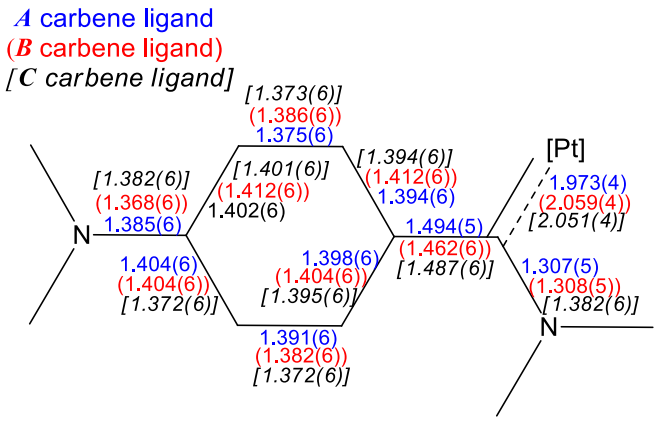

Figure 4.23. Carbene ligand bond lengths (reported in Å) in C1b(II)

In the ^{13}C NMR this is the carbene carbon found more upfield compared to the other two carbene ligands in the complex. This observation corresponds well to the structural data as the carbene stabilisation from the aromatic ring and nitrogen heteroatom is less pronounced as is the case of the ethoxycarbene complexes.

Although **C1b(I)** and **C1b(II)** are essentially the same compounds, the exchange of the counter ion influences the packing of the complexes remarkably. **C1b(I)** crystallises in a *Pbcm* space group with a cell volume of 4207.82 $Å^3$ while **C1b(II)** crystallises in a *Pbca* space group with a unit cell volume of 7424.84 $Å^3$. The packing of the complexes themselves illustrate the complexity of the networks and the beauty of the symmetric packing patterns observed along different axes. The shortest hydrogen bonding contacts are between the carbonyl oxygens and protons of methyl substituents of both amino substituents in carbene ligands and hydrogen of the benzene moiety (*ortho* to carbene substituent). The packing patterns are determined by the counter ion $[W(CO)_5Cl]^-$ and these H-bonding interactions. Three different carbonyl oxygens of a $[W(CO)_5Cl]^-$ will show interactions with three hydrogens on one carbene ligand, i.e., unlike for

the chloro ligands of the biscarbene complex, the chloro ligand in **C1b(I)** are shielded by the three bulky carbene ligands.

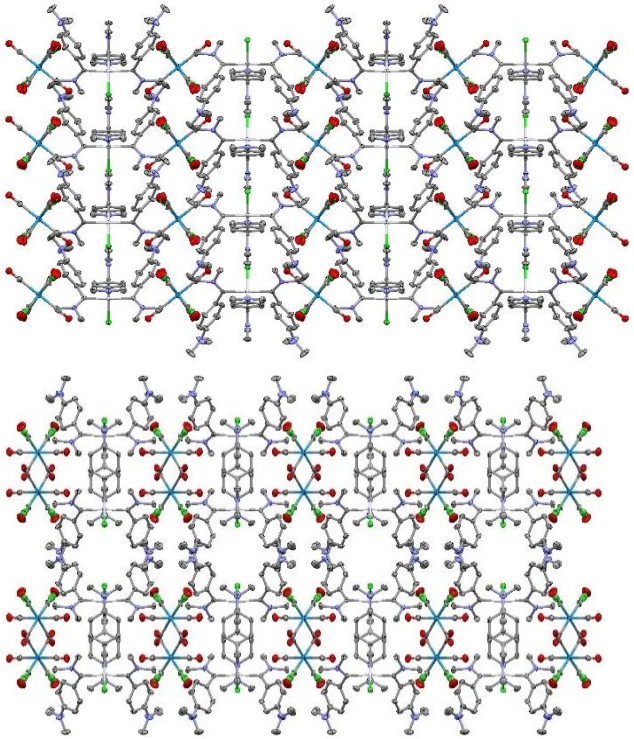

Figure 4.24. Packing of C1b(I) along the a-axis (top) and b-axis (bottom)

In Figure 4.24 the packing of **C1b(I)** is illustrated which shows the Pt–Cl bonds all lying in the same direction within a column, but each alternate column, separated by a $[W(CO)_5Cl]^-$ counter ion, has the Pt–Cl bond lying in opposite directions (Figure 4.24, top). By looking down the column (Figure 4.24, bottom), the staggering of each complex between the rings can be observed. Distinct tunnels throughout the complex is formed between the chlorides of two complexes and their *A*- and *C*-carbene ligands' dimethylaniline substituent groups.

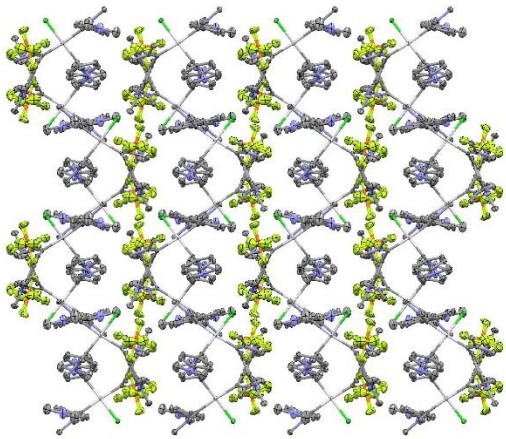

Figure 4.25. Packing of C1b(II) along the c-axis

The packing of **C1b(II)**, which consists out of a larger unit cell than **C1b(I)**, is significantly more complex and dense. A clear pattern forms within the crystal lattice which can be viewed along its c-axis (Figure 4.25) and takes the form of parallel sigmoidal curves. Hydrogen bonding between the chloro ligand and hydrogens of methyl groups of both dimethyl amino substituents are in the range 2.78 – 2.91 Å (2.783, 2.916, 2.896 and 2.912 Å). This type of interaction was present in **C1a** but not in **C1b(I)**. Numerous F---H interactions in

the range 2.45 – 2.65 Å are present between counter ion flourines and hydrogens of the methyl groups of the distant NMe_2 substituent and hydrogens of the benzene ring (α to distant NMe_2 substituent).

Table 4.10. Pt–Pt distances in the crystal structures of C1a(I), C1b(I) and C1b(II)

Complex	Pt–Pt distance (Å)
C1a	6.210
C1b(I)	8.979
C1b(II)	8.031

The possibility of metal-metal interactions in Pt-complexes exist and need to be investigated. These interactions can influence the photophysical properties of the compounds at different temperatures and concentrations within solution. Since the crystal structures of **C1a** and two different crystal structures for **C1b** are obtained it is possible to investigate possible interactions of Pt(II) metal centres with each other in the solid state (listed in Table 4.10).

The intermolecular distances between Pt(II) metal centres of **C1a** and **C1b** are large (~6.210 Å). Examples of significant metal–metal interactions will allow for distances between the two metals to range between 3.358 and 4.489 Å, thus indicating that there is no metal-metal interaction in the solid state of **C1a**, **C1b(I)** and **C1b(II)**.[43,44] The most prominent contribution to the packing of the crystal structures is the hydrogen bonding interactions involving the chloro ligand and carbene amino hydrogens (**C1a** and **C1b(II)**) and counter ion interactions with carbene hydrogens.

4.2.6 UV/Vis Spectroscopy

This study will be focused on the identification of the $\pi \rightarrow \pi^*$ and charge transfer (CT) bands present in the UV/Vis absorption spectra of the synthesised complexes. There are numerous examples where ligand field (LF) and metal to ligand charge transfer (MLCT) bands are observed in Fischer carbene complexes.[46,47]

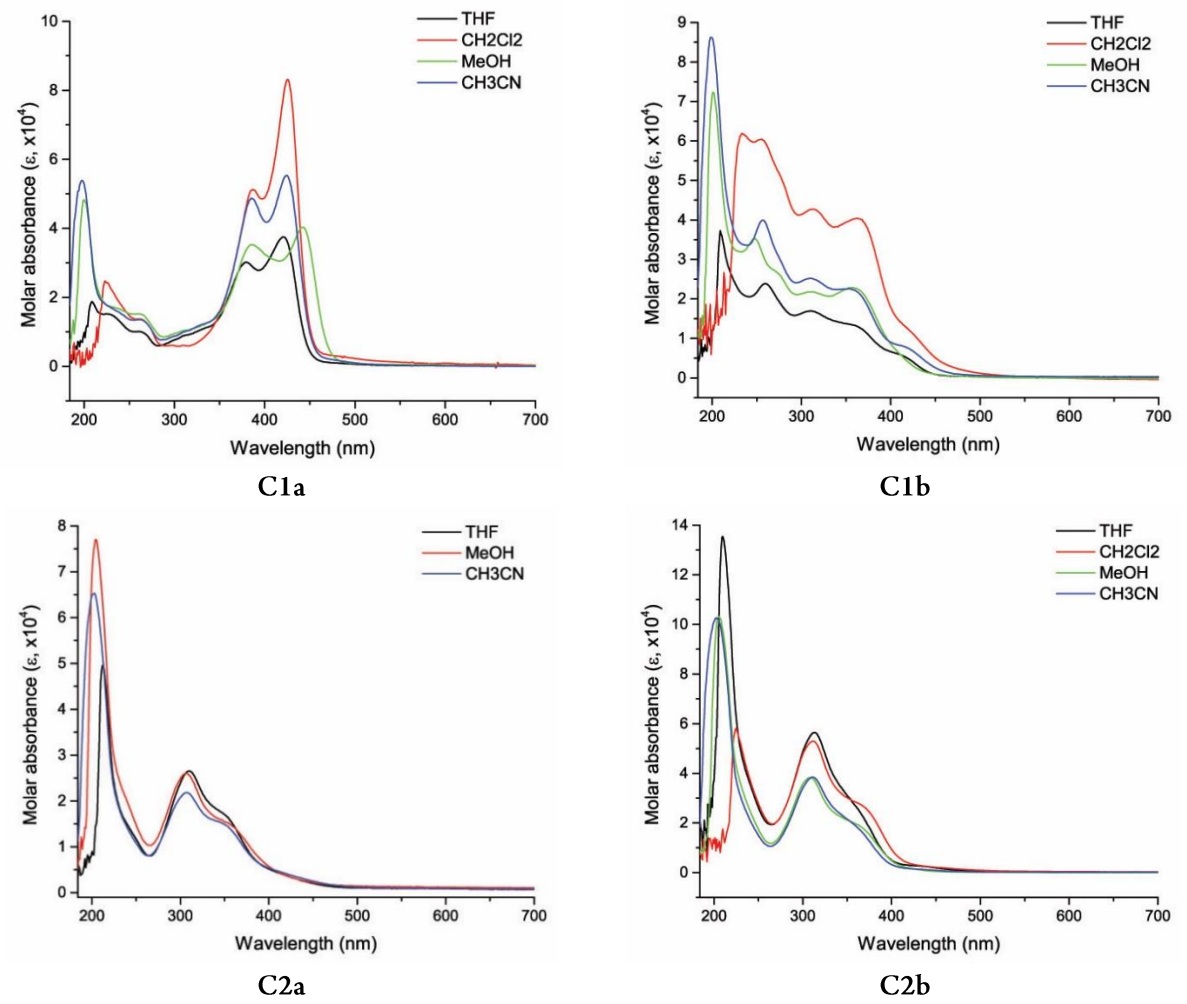

Figure 4.26. UV/Vis spectra of the ethoxy- and aminocarbene complexes of C1 and C2 in different solvents at 298 K

In theory, a UV/Vis peak shift that occurs in solvents of different polarity or polarizability indicates a dipole moment is formed or destroyed on excitation of the complex. This means that when a dipole moment is formed upon excitation of a complex, the more polar or polarised solvent will interact with the compound in such a way that the HOMO-LUMO gap is decreased and the peak will show a bathochromic shift. In general, it has been found that positive solvatochromism (red shift) is observed for a compound which has an increase in its dipole moment on photoexcitation.[48]

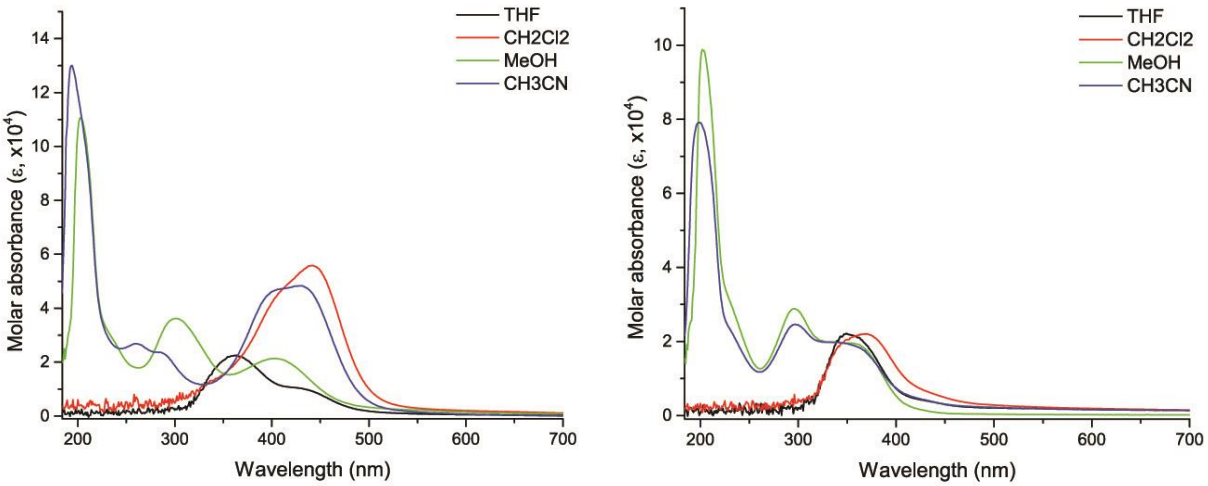

C3a C3b

Figure 4.27. UV/Vis spectra of the ethoxy- and aminocarbene complexes of C3 in different solvents at 298 K

The solvatochromism of the complexes has been conducted solely to identify the CT bands of the complexes. No further analysis of peak positions and dipole effects in the different solvents will be investigated. By comparing reported carbene ligands to those synthesized in this section of the study, it becomes possible to identify which peaks can be assigned to π–π^* transitions. The UV/Vis absorption peaks of known tungsten carbonyl complexes with similar carbene ligands to the those under investigation in this study show that the LF transitions are observed at lower wavelengths compared to the CT bands.[47,49] The UV/Vis spectra of the complexes in different solvents are shown in Figure 4.26 and Figure 4.27 and the data listed in Table 4.11. The physical positions of the different orbitals in the complexes are not currently known and will require DFT and TD-DFT calculations to make such assignments. As it is not possible to determine whether the CT bands observed are metal to ligand or ligand to ligand CT bands, they will only be referred to as CT bands for this part of the study.

Table 4.11. UV/Vis absorption energies (nm) of C1–C3 in THF, CH_3CN, CH_3OH and CH_2Cl_2

	Solvent	Wavelength (nm)				
		$\pi \rightarrow \pi^*$	$\pi \rightarrow \pi^*$/LF	$\pi \rightarrow \pi^*$/LF	CT	CT
C1a	THF	209	231	262	380	420
	CH_3CN	197	230	262	386	424
	CH_3OH	200	232	265	385	442
	CH_2Cl_2	-	223	261	387	425
C1b	THF	209	260	311	362	413
	CH_3CN	199	258	310	355	415
	CH_3OH	201	248	310	358	-
	CH_2Cl_2	-	233	313	363	422
C2a	THF	212	-	309	351	-
	CH_3CN	202	-	308	352	-
	CH_3OH	204	-	307	357	-
C2b	THF	210	-	313	355	-
	CH_3CN	202	-	311	353	-
	CH_3OH	205	-	308	366	-
	CH_2Cl_2	225	-	312	368	-
C3a	THF	-	-	-	360	437
	CH_3CN	194	261	288	402	430
	CH_3OH	203	-	299	403	-
	CH_2Cl_2	-	-	-	401	441
C3b	THF	-	-	-	349	-
	CH_3CN	199	-	297	359	-
	CH_3OH	202	-	295	361	-
	CH_2Cl_2	-	-	-	371	-

There is no clear trend observed in the energy of charge transfers for the different complexes. In general, the peaks at shorter wavelengths (high energy) are assigned as π–π^* transitions. These peaks have a high molar absorbance (ε/L.mol^{-1}.cm^{-1}) and have a shoulder band present. The bands observed above 300 nm are assigned as CT bands, are predominantly broad, and have a molar absorbance close to or higher than 30 000 L.mol^{-1}.cm^{-1}. These bands show the greatest differences in absorbance band-position in the different solvents, thus indicating that a dipole moment is formed upon excitation at the specific wavelength and influenced by the solvent.

4.2.7 *Steady State Emission Spectroscopy*

Emissive Pt(II) complexes are well-known and are currently under investigation for their uses in organic light emitting diodes (OLEDs) and as bio-imaging agents.[28,50–53] Many of these complexes are being explored because of their marked ability to purely show phosphorescence thus harvesting both singlet and triplet excitons resulting in 100% internal quantum efficiency.[54] Pt(II) square planar complexes are especially attractive in phosphorescent photophysical applications because the metal centre enables an intersystem crossing (ISC) from an excited singlet state to a triplet state and are also well-known for metal-metal interactions either in the ground or excited state due to their square planar molecular conformation.[55,56] A particular trait for all these multidentate, large conjugated systems are their prolonged phosphorescence lifetimes and impressive quantum yields.[2,52]

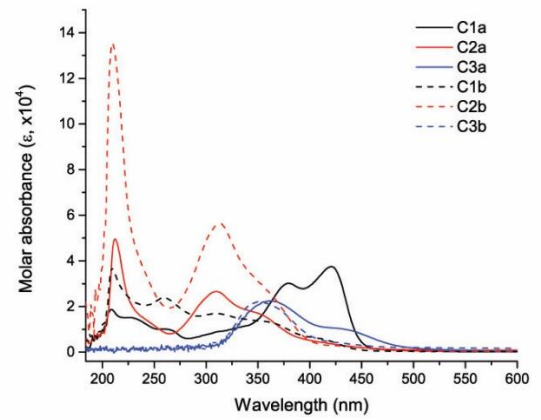

Figure 4.28. Molar absorbance of the ethoxy- and amincarbene complexes C1 – C3 in THF at 298 K

Due to the Pt(II) metal centre's high spin-orbit coupling constant (χ = 4481 cm^{-1}), which promotes rapid intersystem crossing from singlet to triplet states, it is expected that emission of any Pt(II) complex would originate from the triplet state unless the excited state of the complex is far removed from the metal centre.[57] It is also for this reason that most luminescent Pt(II) complexes are phosphorescent emitters that show emission from around 500 nm into the near-infrared region with long lifetimes on a μs timescale.[58]

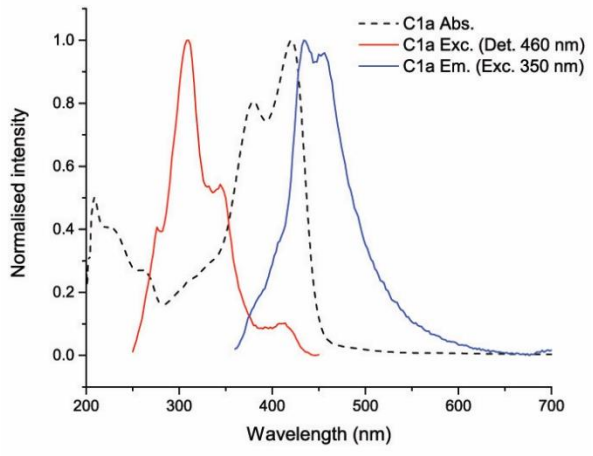

C1a

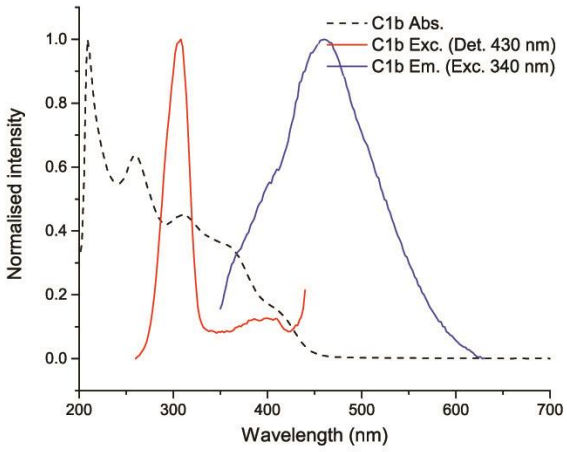

C1b

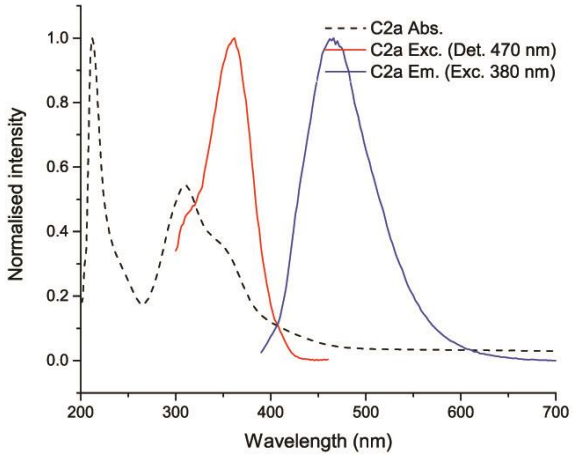

C2a

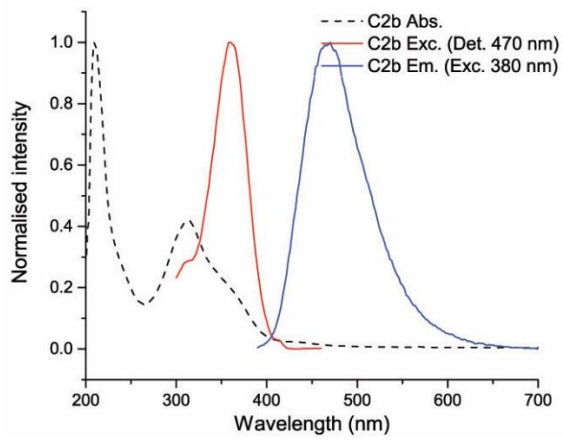

C2b

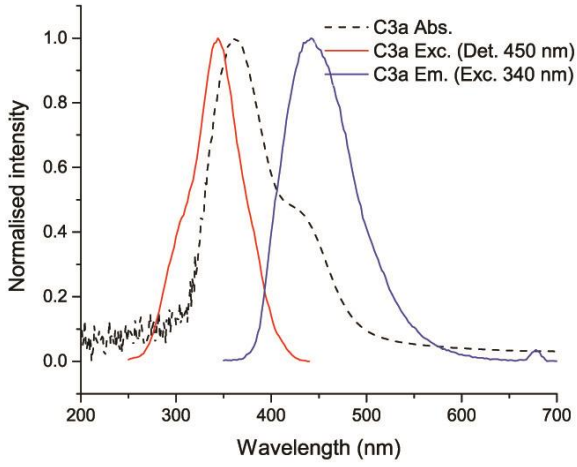

C3a

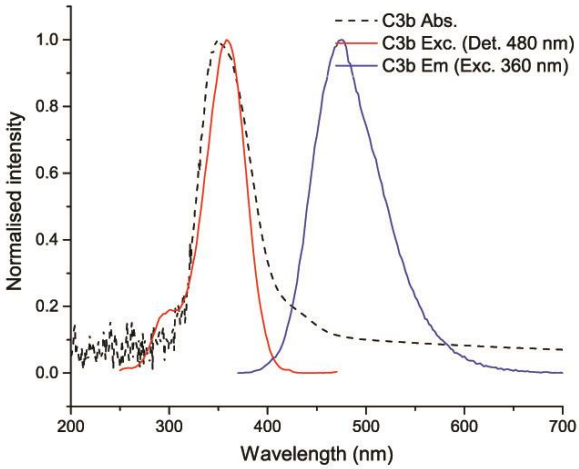

C3b

Figure 4.29. Absorbance (Abs.), excitation (Exc.) and emission (Em.) spectra of ethoxy- and aminocarbene complexes of C1 – C3 in THF at 298 K

The molar absorbance and steady state emission measurements of the complexes discussed in this part of the study are conducted at room temperature in degassed tetrahydrofuran (THF) and 2-methyltetrahydrofuran (MeTHF) at 77 K. The more non-polar solvents are chosen because polar solvents are known to lead to the quenching of emissive processes.[59] $\pi \rightarrow \pi^*$ transitions for the complexes are observed between 200 and 275 nm while the CT bands for all complexes occur between 300 nm and 450 nm as shown in Figure 4.28. Figure 4.29 shows the absorbance, emission and excitation spectra of all Series C compounds in THF at 298 K.

A summary of the absorbance, excitation and emission at 298 K and 77 K, as well as the quantum yields (Φ) recorded at 298 K are listed in Table 4.12. The 77 K excitation and emission spectra can be found in the Appendix. The Stokes shift (between excitation and emission spectra) for the 298 K measurements are also shown in wavenumbers. The table further lists the multicomponent lifetime (τ) of the emission (determined by fitting a time-dependent exponential decay function to the emission at a certain wavelength), and the fractional intensities of the decay components; thus, it is possible to determine which emission is the largest contributing component to the peak observed. The quantum yield of the complexes is determined at ambient temperature in THF making use of a calibrated integrating sphere. For more information on the functioning of a calibrated integration sphere please see the publication by the research group of Pålsson and Beeby.[60]

Table 4.12. Absorbance, excitation and emission data for C1 – C3 at 298 K (THF) and 77 K (MeTHF)

	Abs CT λ_{maz}/nm	Excitation λ_{maz}/nm	Emission (298 K) λ_{maz}/nm (Stokes shift/cm^{-1})	τ/ns [%][a]	Emission (77 K) λ_{maz}/nm	τ [%][a]	Φ 298 K
C1a	318	310	434 (9216)	7.33 [89]	534	0.38 ms [46]	0.003
	378			1.08 [11]		0.17 ms [54]	
	421						
C2a	312	362	466 (6165)	7.69 [16]	480	4.43 ns [55]	0.001
	357			2.78 [49]		1.61 ns [45]	
				0.82 [35]	514	8.02 ms [59]	
						0.35 ms [41]	
C3a	355	344	442 (6445)	11.03 [32]	414	5.65 ns [3]	0.062
				1.57 [68]		1.09 ns [97]	
					440	3.56 ns [23]	
						1.09 ns [77]	
					560	3.56 ns [100]	
C1b	309	308	460 (10728)	13.21 [32]	508	0.30 ms [43]	0.011
	353			4.33 [45]		0.13 ms [57]	
				1.01 [23]	508	11.34 ns [61]	
						1.91 ns [39]	
C2b	362	358	470 (6656)	5.83 [22]	480	3.38 ns [71]	0.029
	436			2.55 [76]		0.84 ns [29]	
				0.19 [2]	502	0.97 ms [46]	
						0.41 ms [54]	
C3b	311	358	476 (6924)	9.33 [100]	420	16.40 ns [66]	0.013
	365					2.93 ns [34]	
	414				484	5.49 ns [44]	
						1.37 ns [56]	
					504	5.49 ns [79]	
						1.37 ns [21]	

[a]Fractional intensities of decay components

Broad emission peaks are observed for all the compounds with peak maxima observed between 400 and 450 nm, thus the emission observed for all the compounds is blue. Although blue emission in Pt(II) complexes to date is rare, there recently has been success in isolating compounds which can be used as blue OLED devices.[61] In Pt(II) compounds there also have been positive results of late by synthesising large tetradentate ligands which coordinate to a Pt(II) metal centre.[53,62–64] Fleetham and co-workers found that the breaking of the conjugation present in ligands which are usually used, achieves blue emission rather than green emission.[53] One of

the major drawbacks of blue-light emitting Pt(II) complexes are the low quantum yields observed for the compounds. The efficiency of blue light emission in any Pt(II) complex depends on the size of the energy gap between the emitting triplet state and the metal centred d–d* states that lie at a higher energy level. The d–d* orbitals are responsible for the quenching of emission when the gap is too small.[65]

The lifetimes (τ) of **C1** – **C3** for the emission at room temperature is long for fluorescence and very short for phosphorescence. This specific characteristic will be discussed below. All the complexes except **C3b**, have multi-exponential decay functions for the emission observed, thus showing multiple emissive processes within the compounds. The excitation spectra (red spectra in Figure 4.29) does not exactly match that of the absorbance spectra (dashed black spectra in Figure 4.29). This indicates that not all absorbance bands result in emission – thus not all excitations lead to emission. There is, however, a clear overlap between the absorbance measured for each complex and the excitation band that leads to the emission observed for all complexes. The determined quantum yields (Φ) for all complexes, are low with values between 0.3 % and 6.2 %, compared to Pt(II) complexes studied for their use in OLEDs.[52] The emission at 77 K is generally red-shifted relative to the emission measured at room temperature and consists out of multiple emissive processes. At 77 K, phosphorescence is observed (as determined from the lifetime of the emission) for most complexes with lifetimes on the ms timescale. The emission at 77 K will not be fully analysed as different and other photophysical measurements are required to fully assign all the emissive processes observed. The 77 K measurements will be used to analyse the emission processes observed at room temperature.

Most complexes in which Pt(II) centres have an orbital contribution in the ground and excited states show that an intersystem crossing (ISC) occurs such that the emission observed originates from a long-lived triplet state.[66] Dual emissive complexes give an indication as to the size of the Stokes shift for both fluorescence and phosphorescence in Pt(II) complexes. Several examples show that the fluorescence is observed with a Stokes shift between 400 and 3000 cm^{-1}, while

phosphorescence has a Stokes shift anywhere above 5000 cm^{-1}.[67–70] Based on this trend, the emission observed for the complexes in this study points to phosphorescence with very short lifetimes (the Stokes shifts for the complexes are noted in Table 4.12 and are between 6 000 and 10 000 cm^{-1}). The author is not aware of any examples of phosphorescence emission of Pt(II) complexes where the emission lifetime is below 100 ns. Thus, it is not possible to state whether the emission observed originates from an excited singlet (fluorescence) or triplet (phosphorescence) energy level without further investigation.

To usually determine whether emission is fluorescence or phosphorescence, the emission of a complex is tested in the presence and absence of triplet O_2 in solution at room temperature. The triplet state of the oxygen will react with the formed triplet state upon excitation of the complex and no phosphorescence will be observed.[70] This technique, however, does not work for the complexes under investigation as the emission observed has too short lifetime for any $^3O_2$ in solution to react with a formed triplet state of the complexes.

For **C1a** (Graph **I**, Figure 4.29), the two-component emission (lifetimes of 7.33 and 1.08 ns) between 400 and 550 nm is caused by excitation between 280 to 450 nm (measured by monitoring emission at 460 nm). The emission is caused largely by the shoulder (~280 – 350 nm) to the two intense absorbance peaks at ~380 and ~420 nm. The two intense absorbance peaks also cause some of the emission observed, but the contribution is small compared to that of the shoulder band. **C1b** has a single excitation peak which leads to three-component emission (lifetimes of 13.21, 4.33 and 1.01 ns). The excitation peak matches one of the peaks in the absorbance spectrum of **C1b** (dashed black line) at ~300 nm. A small degree of excitation is also observed at ~400 nm. For both **C1a** and **C1b** there is overlap observed between the absorbance and emission bands. When this is observed, it can be assigned as a $0 \rightarrow 0$ transition or (HOMO $\rightarrow$ LUMO transition) where the compound is excited into the first singlet state which leads to

prompt fluorescence.[71] The 0 → 0 transition as well as other possible transitions are described in Figure 4.30.

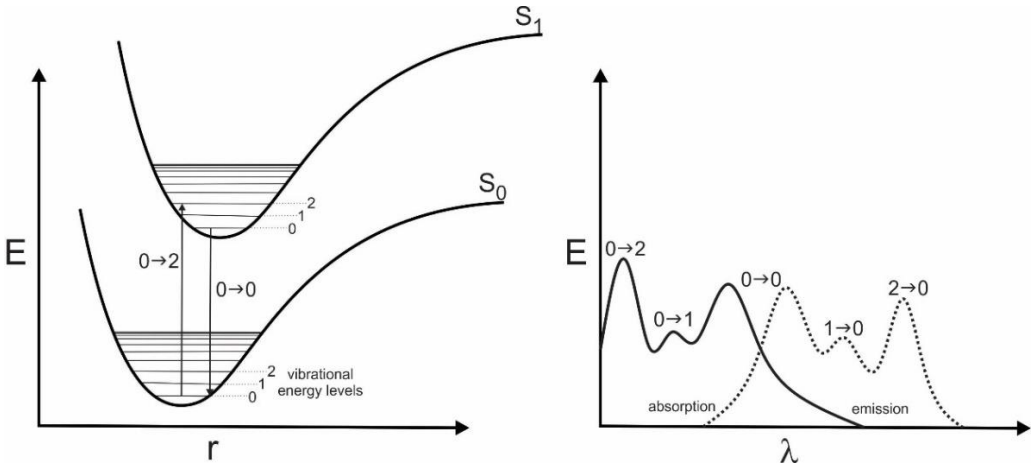

Figure 4.30. Potential energy scheme and vibronic structure in absorption and fluorescence spectra. Modified from figure by Michl[72]

It is evident that the 0 → 0 transition is the smallest component that contributes to the emission observed for both **C1a** and **C1b** with respective lifetimes of 1.08 and 1.01 ns, and can be assigned to fluorescence from the S_1 state.[69,70] It is evident however, that the excitation for the observed emission occurs from the ground state (S_0) to a higher singlet state (S_n) than the first excited state (S_1). This shows that the compound is excited to S_n, reach S_1 via an internal conversion, from where the prompt fluorescence is observed. This would explain the large Stokes shift.

In **C1a** the other component with the largest contribution to the emission and a lifetime of 7.33 ns, originates from the same or a similar energy level than that of S_1 and is unlikely to originate from a triplet state as the lifetime for the component is too short. For **C1b**, the shortest and smallest component of the observed emission (1.01 ns – 23 %) has been assigned as fluorescence from the S_1 state. The origin for two larger contributions to the emission with lifetimes of 4.33 and 13.21 ns and respective contributions of 45 and 32 %, are not currently known. For both the complexes, the emission components lie over each other thus indicating that the emission originates from similar or the same excited singlet state.

Emission for **C2a** and **C2b** is observed between 400 and 600 nm. The compounds show excitation between 300 and 400 nm which overlaps with a shoulder peak in the absorbance spectra of both complexes in THF. Both complexes show three-component emission of which the shortest component is assigned as prompt fluorescence from S_1 while the two longer components are assigned as fluorescence originating from S_1 or a similar energy level after internal conversion. The complexes show some overlap between the absorbance and emission spectra at ~400 nm which supports that prompt fluorescence from S_1 contribute to the observed emission. In **C2a** the prompt fluorescence has a lifetime of 0.82 ns and contributes to 35 % of the emission observed. The other two emissive components with lifetimes of 7.69 and 2.78 ns has respective contributions of 16 and 49 % to the observed emission, and the origin of these components are not currently known. The three components that contribute to the emission of **C2b** have lifetimes of 0.19, 2.55 and 5.83 ns with respective contributions of 2, 76 and 22 % and is similarly assigned as the three components of **C2a**.

Upon excitation between 280 and 400 nm, **C3a** and **C3b** show emission between 390 and 600 nm. Some degree of overlap is observed between the excitation and emission wavelengths of **C3a** at ~400 nm, but not for **C3b**. Two-component emission is observed for **C3a** while only single component emission is observed for **C3b**. The two components which make up the emission of **C3a** have lifetimes of 11.03 and 1.57 ns with respective contributions to the emission of 32 and 68 %. The prompt fluorescence originates from the S_1 state while the longer component likely originates upon internal conversion from a higher energy level to an emissive state at a similar energy level than S_1. In this case, the prompt fluorescence has the greatest contribution to the observed emission. For **C3b**, no prompt fluorescence is observed as for the other complexes, but only emission with a longer excited state which is expected to originate from a higher singlet state.

The organic carbene ligands studied in this project individually are well-known electron donor compounds. N,N-dimethylaniline will not readily show any emission without a luminophore present to which a charge can be transferred and emission can be observed by its excited state

relaxation.[73,74] For triphenylamine and its derivatives it is possible to show fluorescence as an organic molecule without any luminophore present especially in the solid state. In THF however, the triphenylamine has an absorbance at 300 nm and show weak fluorescence at 360 nm.[75] It can thus be concluded that the emission observed for the complexes studied in this chapter are not solely observed due to the presence of the individual aromatic ligands, but also with a contribution of the Pt(II) centre or their proximity to each other.

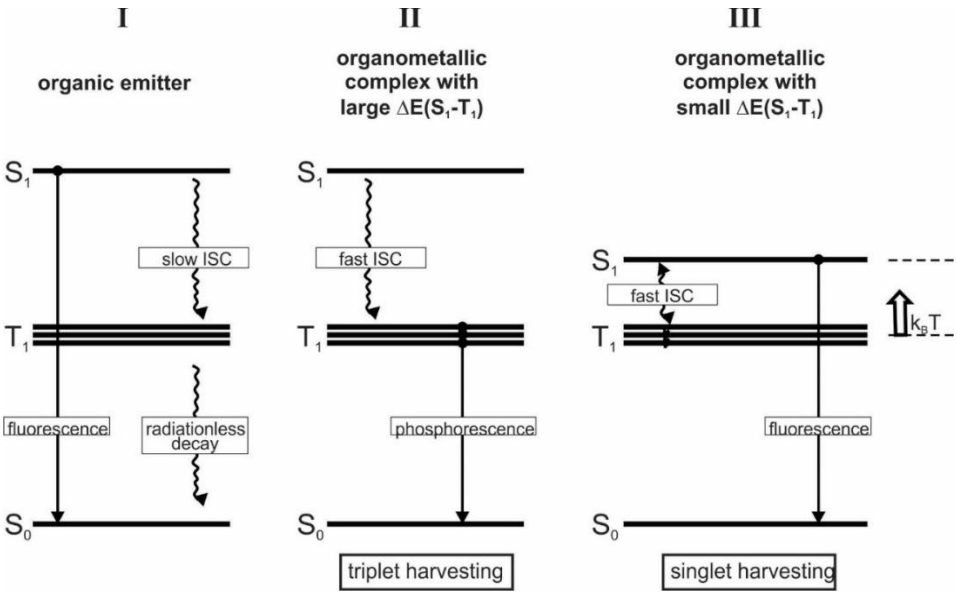

Figure 4.31. A diagram displaying the difference between triplet and singlet harvesting in organometallic compounds[65]

As the assigned emission originates from very similar energy levels, the possibility of delayed fluorescence must also be considered for these complexes. Examples where delayed fluorescence is observed show that both prompt and delayed fluorescence are expected to occur at the same wavelengths.[76,77] In a schematic representation of the different types of emission by Yersin and co-workers, delayed fluorescence can be described as excitons that go through an intersystem crossing to access a slightly lower triplet excited state. Through an energy donating process, it re-enters the ISC process to return to the slightly higher-in-energy singlet state and then falls to the ground state via emission (reverse ISC). Figure 4.31 is a schematic adaptation of a summary between fluorescence, phosphorescence and delayed fluorescence by the research group of

Yersin. In organic emitters (**I**) only singlet excitations omit light (fluorescence), triplet excitation releases heat (radiationless decay). In **II**, organometallic complexes with a fast ISC, singlet excitations fall to the lowest triplet state and emit as phosphorescence. For complexes with small ΔE(S1-T1) (**III**) fast forward and reverse ISC processes can occur which lead to thermally activated fluorescence.[65] Keivanidis clearly states that delayed fluorescence couples directly with the longer lived triplet excited state and delayed fluorescence has a lifetime in the same order expected of phosphorescence.[78] Thus, should delayed fluorescence be observed, long lifetimes are expected.

According to the research group of Stang, it is possible to distinguish between thermally activated delayed fluorescence and normal fluorescence by decreasing the temperature of the emission experiment. Should thermally activated delayed fluorescence be observed, the emission will decrease with a decrease of temperature.[79] It is for this reason that emission spectra of the compounds at different temperatures are shown in Figure 4.32. Generally, a blue shift is expected from the triplet state at cold temperatures.[80,81]

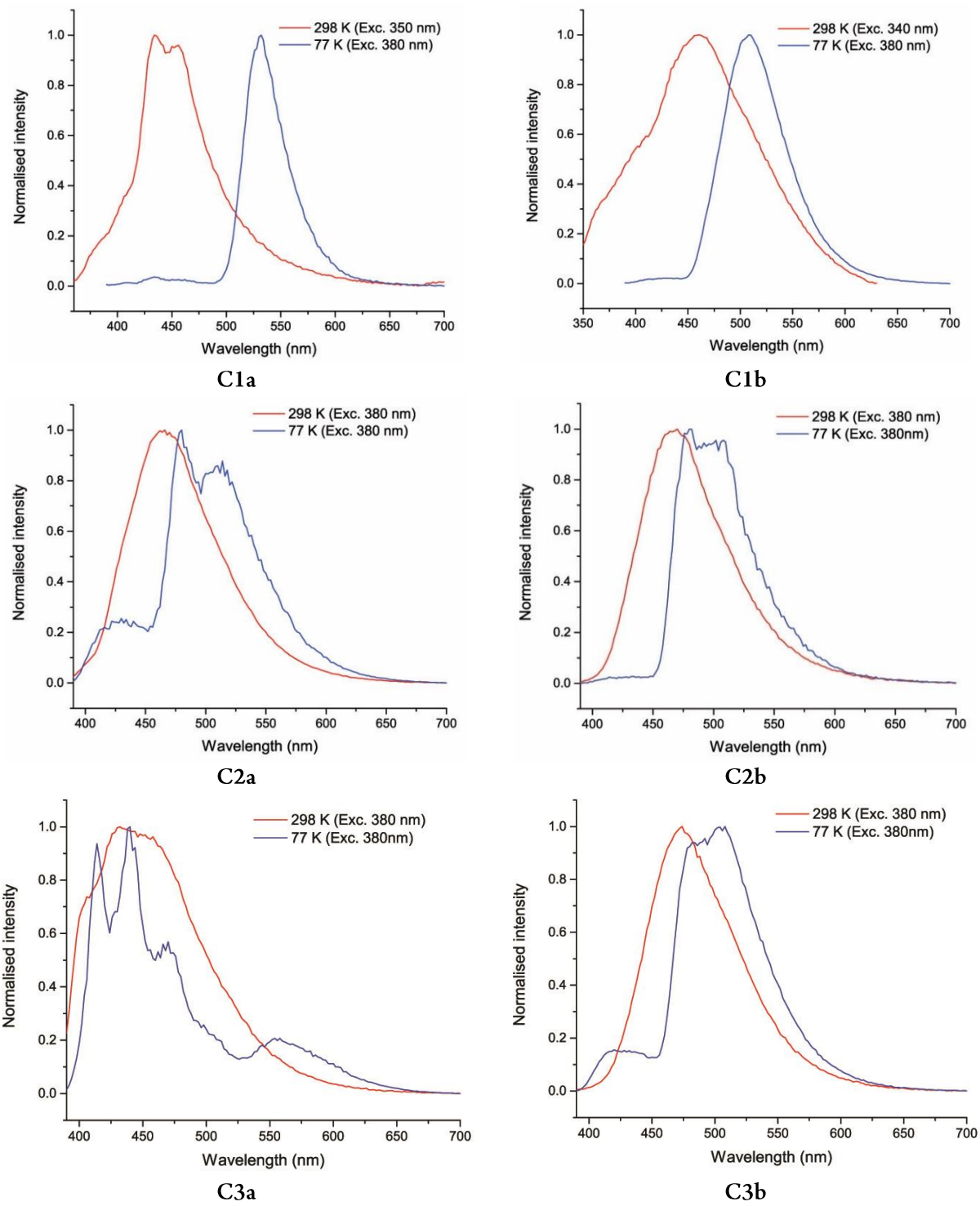

Figure 4.32. Emission spectra for complexes C1 – C3 at 298 K (THF) and 77 K (MeTHF)

A clear red shift is observed in the emission for all complexes or rather, emission maxima observed at 298 K is no longer observed at 77 K. This shows that some of the longer components of the

emission observed at room temperature for the complexes being studied can possibly be assigned as delayed fluorescence. For most complexes (except **C3a**), there is a clear decrease in the intensity of emission at shorter wavelengths at 77 K compared to 298 K. It is the emission at these wavelengths that can possibly be assigned as delayed fluorescence. Since there are no significant differences in emission upon the decrease of temperature for **C3a**, it is likely that the emission observed for the compound at 77 K and 298 K is temperature independent and thus cannot be assigned as delayed fluorescence caused by thermal activation.

The emission at 77 K further shows the presence of phosphorescence at longer wavelengths which appear as shoulder peaks to the fluorescence being observed. **C1a** is the only compound that shows pure phosphorescence at 77 K while all the other compounds show phosphorescence is addition to the multicomponent fluorescence. No phosphorescence is observed for **C3a** – the only compound which emission also remains independent of temperature.

A summary of the kinetic parameters for each complex is shown in Table 4.13. The radiative rate constant has been determined from the Φ value and the lifetime determined for the emission observed. As the emission observed at room temperature originates from more than one process the Φ value will also represent the emission of more than one process. In this case τ_{comp} has been determined from the relative intensities of the different components making up the observed emission. Ideally, emission should be made up of a single component, but this will allow for an estimated radiative and nonradiative rate constant to be determined. The nonradiative rate constants for all complexes are much larger than that of the radiative rate constants. This indicates that there is a dominant nonradiative process or processes by which the excitons return to the ground state.[82]

Table 4.13. Luminescence properties of C1 – C3 at 298 K in THF

	λ_{max}[a] (nm)	Φ[b]	τ_{comp}[c] (ns)	k_r[d] (s^{-1})	k_{nr}[e] (s^{-1})
C1a	434	0.003	6.64	$4.52x10^5$	$1.50x10^8$
C2a	466	0.001	2.88	$3.47x10^5$	$3.47x10^8$
C3a	442	0.062	4.60	$1.35x10^7$	$2.04x10^8$
C1b	460	0.011	6.41	$1.72x10^6$	$1.54x10^8$
C2b	470	0.029	3.22	$9.01x10^6$	$3.02x10^8$
C3b	476	0.013	9.33	$1.93x10^6$	$1.06x10^8$

[a] Emission maximum. [b] Quantum yield at 298 K in THF. [c] Average emission lifetimes. [d] Radiative rate constant calculated with $k_r = \Phi/\tau_{comp}$. [e] Nonradiative rate constant was calculated using $k_{nr} = k_r(1 - \Phi)/\Phi$

In summary, all synthesised mononuclear Pt(II) carbene complexes show emission. The emission observed at 298 K is assigned as fluorescence and possibly delayed fluorescence. It has earlier been established that all the ethoxycarbene complexes are biscarbene complexes while the aminocarbene complexes form triscarbene complexes. The emission for the ethoxycarbene complexes are generally found at slightly lower wavelengths than their amino analogues, thus indicating that the emission of the ethoxycarbene complexes generally originates from a slightly higher energy level compared to that of the aminocarbene complexes. A general trend is not observed in the quantum yields of the complexes. **C1a** and **C2a** have very low quantum yields while that of **C3a** is the highest recorded for all the complexes. **C3a** is also the only compound which does not show a temperature dependence for its emission. Treating **C3a** as an outlier, it becomes possible to state that the Φ values for the ethoxycarbene complexes are significantly lower than those of the aminocarbene complexes. The reason for this observation is unclear and will likely become more evident with DFT calculations as there are two significant differences between the groups: the aminocarbene complexes contain a more electron-rich carbene carbon and contain an additional carbene ligand which can contribute significantly to the emission. Still treating **C3a** as an outlier, the greatest differences between the ethoxy- and aminocarbene complexes is realised when the radiative (k_r) and nonradiative (k_{nr}) rate constants are compared. The k_r values for the aminocarbene complexes are an order of magnitude larger than those of the

ethoxycarbene complexes indicating that the emission of aminocarbene complexes are significantly more efficient. The nonradiative decay rates of both the ethoxy- and aminocarbene complexes fall in the range of $1x10^8$ and $3.5x10^8$ s^{-1} with the nonradiative decay rates of **C2a** and **C2b** being the greatest.

4.2.8 Femtosecond Transient Absorption Spectroscopy (TAS)

From the emission spectroscopy of **C1** – **C3**, it has been established that the compounds show multicomponent emission, but the quantum yields are low in all cases and the nonradiative rate constant for all the compounds are much larger than the radiative rate constant. By making use of femtosecond TAS, more clarity will be afforded as to what processes occur upon excitation of the complexes on a femtosecond timescale.[83]

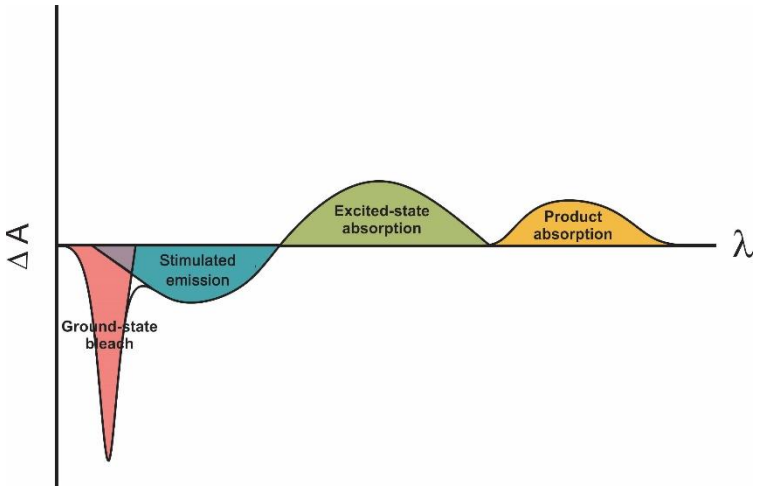

Figure 4.33. A graphical illustration of a pump-probe TAS spectrum

To give some background in regards to TAS, a summary of possible processes which can be observed using the technique is discussed as described by Berera and co-workers.[84] Figure 4.33 is a simplified graphical illustration as to a possible pump-probe TAS spectrum. There are mainly four different processes which can be followed with the technique: A fraction of the molecules in the sample is excited to an electronically excited state by a "pump" pulse. A much less intense "probe" pulse is then passed through the sample at a time delay, τ, after the pump-pulse. A difference absorption spectrum is generated (absorbance of excited sample minus absorbance of ground state), ΔA. Changing the time delay between the pump and probe pulse and measuring the ΔA spectrum at each time delay,

allows for the dynamic processes that occur upon excitation of the compound to be examined. A ground state bleach (GSB) – a negative peak in the spectrum – is observed when a fraction of the molecules has been excited to a higher energy state and the overall absorbance of the sample being analysed is less after the pump pulse than before it. This trough usually corresponds with the absorbance spectrum of any given complex at the wavelengths where the excited state has ground state absorption. Secondly, stimulated emission (SE) – also a trough – will roughly have the Stokes shift of a fluorescence spectrum. This is observed for processes where an excited electron (excited by the pump-pulse) falls back to the ground state as emission through stimulation by the probe pulse. Both the probe pulse as well as the emission are detected and will thus appear as a negative peak. Thirdly, excited state absorption (ESA) can be observed. In this process the fraction of excited chromophores can be further excited to optically allowed higher excited-states by the probe pulse. This will mean that the probe pulse will be absorbed and the signal will appear as a positive peak in the spectrum. Lastly product absorption (PA) is possible. After the excitation of the complex in question, a long-lived or transient state (triplet states or charge-separated states) may exist which will absorb the probe pulse and will also appear as a positive peak in the ΔA spectrum. PA is often accompanied by a GSB where the chromophore on which the product is present has ground-state absorption.

For the complexes being investigated in this section, some have a clear trend towards being more photoactive than others. Although the biscarbene complexes show emission at ambient temperature, there are not many indications that there are significant photophysical processes occurring within these complexes upon excitation. The same cannot be said of the tris-aminocarbene complexes. They are the series of complexes easily synthesised and isolated, they are very photoactive, and show an increased quantum yield compared to their ethoxy analogues. Using femtosecond pump-probe TAS it becomes possible to investigate the dynamic processes that occur upon excitation of the complexes on an ultra-fast timescale. All the samples are analysed in THF at ambient temperature. All the complexes are excited with a 387.5 nm pump pulse and

analysed within a window 440 to 680 nm. Due to time constraints and availability of the instrumentation, all the samples have been analysed with a 387.5 nm excitation pump pulse only.

As an immense amount of data is generated by the technique, a kinetic compartmental model can be used to describe the data. This makes it possible to easily determine how many "transients" as well as their corresponding lifetimes, are present upon excitation of a compound. For this investigation, Glotaran[85] (a graphical interface to the R package TIMP), is used to fit superposition models to the data. The global fit analysis (using a sequential model) will be discussed in general for the complexes being investigated. The evolution associated difference spectra (EADS), generated from the global fit analysis by using a sequential model, describe transients that will decay into each other. Thus, the first transient represents processes at τ_0 with a lifetime of τ_1. The second transient grows from τ_1 and has a lifetime of τ_2. The EADS and time traces at specific wavelengths for each complex can be found in the Appendix.

The TAS spectra of **C1a** and **C1b** do not show any distinguishable processes that occur. This is likely because the excitation of their photoactive processes occur at shorter wavelengths, as is observed in the emission spectroscopy. They will not be discussed.

Selected traces at different time delays for **C2a** and **C2b** are shown in Figure 4.34 (not analysed using global fit analysis) while their global fit analyses (EADS) are shown in Figure 4.35

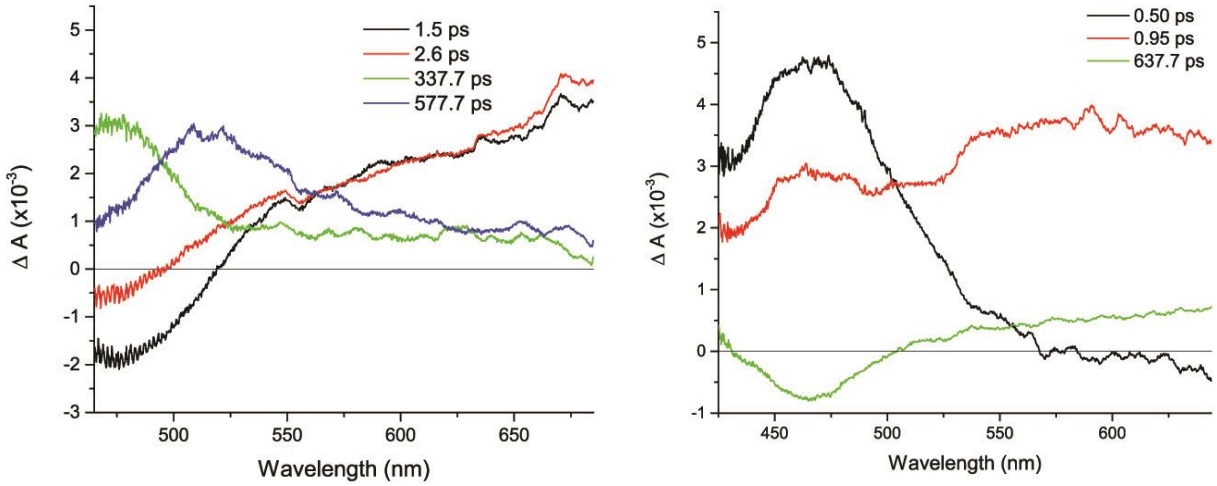

C2a C2b

Figure 4.34. Femtosecond TAS of C2a and C2b recorded in THF at ambient temperature with an excitation wavelength of 387.5 nm

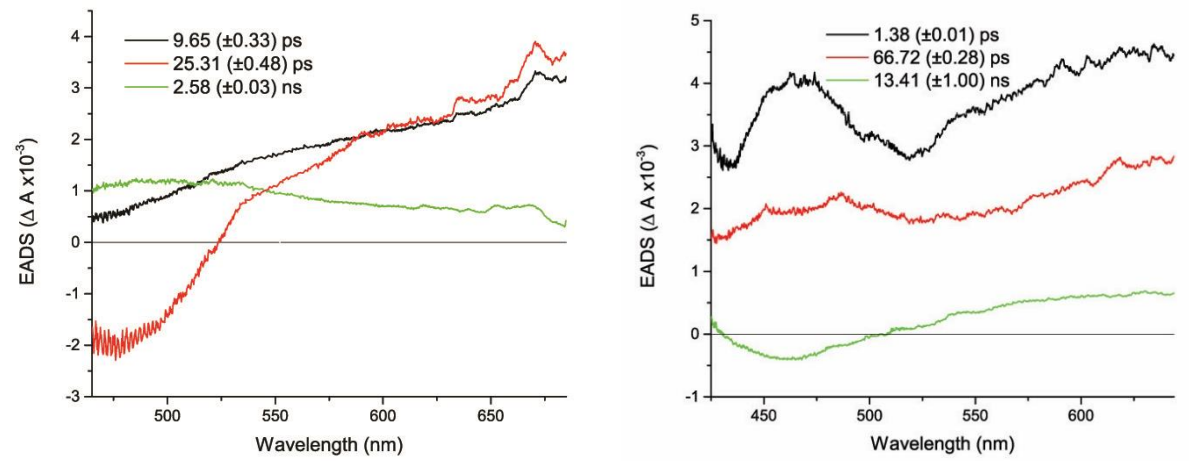

C2a C2b

Figure 4.35. EADS for C2a and C2b, obtained from global fit analysis using a sequential model, in THF at 298 K

The excited state processes of **C2a** can be described by three unique transients (Figure 4.35, left). In the first transient – at a time delay of 0 ps between the pump and probe pulse (τ_0) – absorbance across the whole window of analysis is observed. This is often the case with ESA as many different excited states are populated. The ESA has a lifetime of 9.65 (±0.33) ps. With compounds containing a Pt(II) atom, it is likely that some, if not all, excited state processes occur in the triplet

state because the atom facilitates a fast intersystem crossing (ISC). Numerous examples in literature place the lifetime of ESA after an ISC for Pt(II) compounds between 0.15 and 10 ps.[86–90] From this, the assumption is made that the first transient is the ESA of populated triplet states. The second transient is observed from a time delay of 9.65 ps and has a lifetime of 25.31 (±0.48) ps. In this transient, a GSB is observed between 465 and 525 nm ($\Delta A<0$) while broad, featureless PA is observed between 425 and 684 nm ($\Delta A>0$). The GSB corresponds with ground state absorption for **C2a** (as determined by the UV/Vis spectroscopy for the complex). The "chromophore" thus, is formed upon ground state absorption at ~470 nm. The PA of the second transient can likely be assigned as a charge transfer (CT) state, as the product decays into the final transient which has a lifetime of 2.58 (±0.03) ns and displays broad featureless absorption with λ_{max} at ~504 nm. Possible products may include a stable triplet state, charge separated state or an isomerised state.[84]

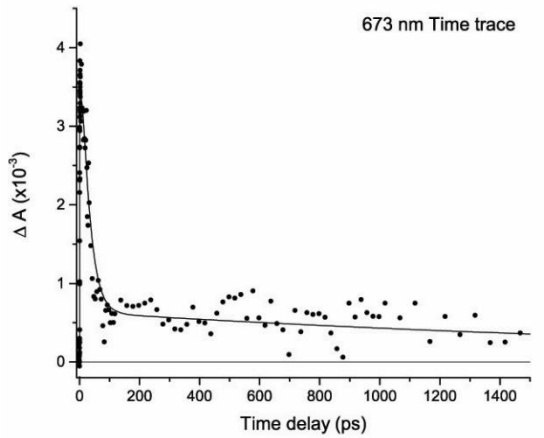

Figure 4.36. C2a TAS 673 nm time trace recorded in THF at 298 K with a 387.5 nm excitation pulse

A time trace at of **C2a** at 673 nm (Figure 4.36) shows the absorbance of the compound at short delays and how this absorption decreases as the time delays become longer between the pump and the probe pulse. It is evident that the complex still shows absorbance at longer time delays (> 200 ps). The global fit analysis of the data is also shown which is indicative of how well the calculated model matches the data.

The EADS of **C2b** reveal that similar processes occur upon photoexcitation as have been observed for **C2a**. It displays ESA at τ_0 with a lifetime of 1.38 (±0.01) ps, followed by PA in its second transient with a lifetime of 66.72 (±0.28) ps. The final transient displays weak SE between 431 and 505 nm, and PA between 506 and 643 nm that has a calculated lifetime of 13.41 (±1.00) ns.

Both **C2a** and **C2b** display properties like long lifetime excited state products and ESA lifetimes expected for Pt(II) complexes showing triplet state absorption. This claim is further supported by the presence of phosphorescence which is observed in the emission spectroscopy at 77 K. This confirms that an ISC process takes place and the triplet manifold of the compounds are accessed. It is evident that there are products that form upon photoexcitation at 387.5 nm, but the identity of these can only be speculated.

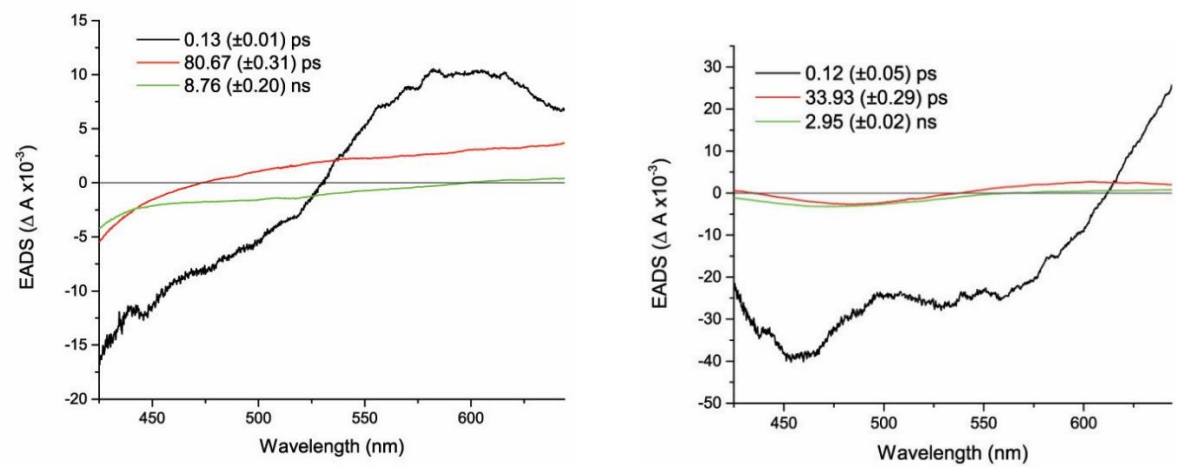

C3a **C3b**

Figure 4.37. EADS for C3a (left) and C3b (right), obtained from global fit analysis using a sequential model, in THF at 298 K

C3a and **C3b** differs from **C2a** and **C2b** in that a GSB and ESA are observed in their EADS (Figure 4.37) at τ_0 that have very short lifetimes (~0.13 ps), likely indicating the excitation and absorption of singlet excited states. The second transients of both complexes reveal the formation of a second more stable product with respective lifetimes of 80.67 (±0.31) and 33.93 (±0.29) ps. In their third transients, SE for both complexes are observed with lifetimes in the nanosecond timescale. The two complexes display no indication that their triplet manifolds are accessed upon photoexcitation at 387.5 nm. This statement is further supported by the absence of phosphorescence at 77 K for both **C3a** and **C3b** (which is observed for all other compounds).

4.3 Experimental

UV/Vis absorption and Emission spectroscopy

UV/Vis absorption spectroscopy was measured on a TIDAS fibre-optic diode array spectrometer MCS from j&m in HELLMA quartz cuvettes with 1 cm optical path lengths.

Luminescence spectra and lifetimes of the complexes were recorded in THF on a PicoQuant FluoTime 300 spectrometer. Quantum yields were measured in degassed THF at 298 K using a Hamamatsu Absolute PL Quantum Yield Measurement System C9920-02 equipped with an integrating sphere.

Femtosecond transient absorption spectroscopy (TAS)

TAS measurements were recorded in degassed THF at 298 K on a Ti:Sapphire amplified laser system (150 fs pulse duration and 775 nm peak wavelength at 1 kHz repetition rate, Clark-MXR 2110*i*). An output of 850 mW was split into two beams (30% pump and 70% probe). The pump beam was directed into a β-barium borate crystal for frequency doubling to produce a beam of 387.5 nm with a FWHM bandwidth of ~6 nm. The pump beam was focussed into the sample using a telescope and neutral density filters were used to attenuate the pump power. A chopper was inserted into the pump beam and the pump pulses were estimated to have a pulse duration of 200 femtoseconds. Different pump-probe delay times were obtained by passing the probe beam through a motorised translation stage where a maximum probe delay of 2 nanoseconds can be achieved. After the delay line, the probe beam is attenuated and focussed into a sapphire crystal to produce a white light continuum which was split using a 50/50 beam splitter. One part of the supercontinuum was used as the probe beam (focussed into the sample to temporally and spatially overlap with the pump beam) while the other part was used as the reference beam (directed through the sample, but not overlapping with the pump beam). The reference is used to account for fluctuations occurring in the probe beam. The pump beam has a diameter of 500 μm while the probe beam has a diameter of ~300 μm. Beyond the sample both the reference and the probe

beams were focussed into optical fibres and directed onto a grating which dispersed the beams into a photodiode array to measure the spectra. ExciPro was used for further processing of data. Global fit analysis was performed on all data sets using the free Glotaran software package.[85]

General synthesis

All syntheses were conducted using standard Schlenk techniques under an atmosphere of argon or nitrogen. Anhydrous THF and hexane were distilled over sodium metal while DCM was prepared by distillation over CaH_2. All other reagents were used as received from commercial suppliers. NMR spectra were recorded on a Varian Unity Inova 400, a Bruker Avance III DRX 400, Bruker Avance DRX 600, a Bruker Ultrashield Plus 400 AVANCE 3 or a Bruker Ultrashield 300 AVANCE 3 spectrometer. ^{1}H and ^{13}C NMR spectra were recorded in ppm and referenced to the CD_2Cl_2 solvent signal.

Synthesis of Pt(COD)Cl_2[91]

2.04 g K_2PtCl_4, 4.00 ml cyclooctadiene (COD) and 0.034 g $SnCl_2.2H_2O$ was allowed to stir in a solution of 36 ml distilled H_2O and 25 ml *n*-propanol for 48 hours after which a cream coloured precipitate was isolated with suction filtration followed by repeated washing with distilled H_2O and then ethanol. The product was air-dried. Yield: 80 – 85 %

Synthesis of W carbene complexes ***B1(a,b) – B4(a,b)***

Please refer to Chapter 3 for the synthesis of all tungsten carbene complexes.

Synthesis of complexes ***C1(a,b) – C3(a,b)***

There are two different methods used in the synthesis of the above-mentioned complexes. Please refer to Table 4.14 for the specified method used in the synthesis, amounts of reagents as well as the product yield of each complex.

Method 1

Excess (n mmol) of a specified tungsten carbene complex was dissolved in 20 ml dried dichloromethane. Pt(COD)Cl_2 (m mmol) was suspended in the same mixture and allowed to stir

at room temperature under an inert atmosphere for 24 hours. During the reaction, the bright orange or yellow (tungsten ethoxy- or aminocarbene complex, respectively) darkened and later became a black-yellow solution. The solvent was evaporated, redissolved in a minimal amount of dichloromethane and then cannula filtered. The formed Pt(II) carbene complex was triturated into *n*-hexane (for tungsten ethoxycarbene complexes) or diethylether (for tungsten aminocarbene complexes) and repeatedly washed with the same solvent until the solvent remained colourless. The product was dried *in vacuo* and characterised.

Method 2

Excess (n mmol) of a specified tungsten carbene complex and m mmol $Pt(COD)Cl_2$ were dissolved in 20 ml dried dichloromethane and allowed to reflux under an inert atmosphere at 50 °C for 24 to 30 hours. The solvent was evaporated and the reaction mixture redissolved in a minimal amount of dichloromethane. The product was cannula filtered and triturated into *n*-hexane (for tungsten ethoxycarbene complexes) or diethyl ether (for tungsten aminocarbene complexes) and repeatedly washed with the same solvent until the solvent remained colourless. The product was allowed to dry under vacuum and fully characterised.

Table 4.14. Experimental data for Series C synthesis

Product	Method	W carbene complex (mmol)	$Pt(COD)Cl_2$ (mmol)	Reaction time (hours)	Yield (mmol)	% Yield
C1a	1	2.96 g (5.91)	0.75 g (2.00)	30	0.947 g (1.53)	76.3 %
C1b	1/2	2.84 g (6.02)	0.611 g (1.63)	24	1.347 g (1.204)	73.9 %
C2a	2	0.47 g (0.60)	0.067 g (0.18)	24	0.125 g (0.106)	58.6 %
C2b	2	0.365 g (0.47)	0.043 g (0.12)	24	0.179 g (0.109)	93.2 %
C3a	2	0.20 g (0.32)	0.03 g (0.08)	27	0.040 g (0.034)	43 %
C3b	2	0.20 g (0.32)	0.03 g (0.08)	27	0.038 g (0.032)	41 %

Characterisation

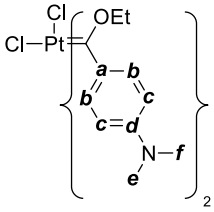

Figure 4.38. NMR assignments of C1a

C1a: $C_{22}H_{30}O_2N_2PtCl_2$. ^{1}H NMR (CD_2Cl_2, 400 MHz) δ 8.41 (d, *J* = 9.1 Hz, 2H, H***b***), 6.60 (d, J = 9.4 Hz, 2H, H***c***), 5.38 (s, 2H, CH_2 (OEt)), 3.11 (s, 6H, H***e*** and H***f***), 1.47 (t, J = 7.1 Hz, 3H, CH_3 (OEt)). ^{13}C NMR (CD_2Cl_2, 101 MHz) δ 238.5 (C_{carb}), 156.1 (C***a***), 137.4 (C***b***), 132.7 (C***d***), 110.8 (C***c***), 77.5 (CH_2 (OEt)), 40.5 (C***e*** and C***f***), 14.7 (CH_3 (OEt)). ESI-MS (2.8eV, positive mode, *m/z*): calcd for $[M+H]^+$ 620.1410, found 620.1449.

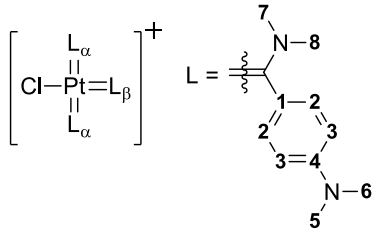

Figure 4.39. NMR assignments of C1b

C1b: $C_{38}H_{48}N_6O_6WPtCl_2$. ^{1}H NMR ($CD_2Cl_2$, 400 MHz) δ 7.07 (d, *J* = 8.8 Hz, 6H, H***α*2** and H***β*2**), 6.73 (d (*br*), *J* = 7.4 Hz, 6H, H***α*3** and H***β*3**), 3.87 (s, 9H, H***α*7** and H***β*7**), 3.26 (s, 9H, H***α*8** and H***β*8**), 3.01 (s, 18H, H***α*5**, H***α*6**, H***β*5** and H***β*6**). ^{13}C NMR (CD_2Cl_2, 101 MHz) δ 202.7 ($^1J_{\{W\}C}$ = n.o., $[W(CO)_5Cl]^-$, *trans*), 200.1 ($^1J_{\{W\}C}$ = 63.9 Hz, $[W(CO)_5Cl]^-$, *cis*), 191.8 (Cα_{carb} and Cβ_{carb}), 151.1 (*br*, C***α*1** and C***β*1**), 132.6 (*br*, C***α*4** and C***β*4**), 125.9 (*br*, C***α*2** and C***β*2**), 112.0 (*br*, C***α*3** and C***β*3**), 44.9 (C***α*7** and C***β*7**), 40.5 (C***α*5**, C***α*6**, C***β*5**, C***β*6**, C***α*8** and C***β*8**). ESI-MS (2.8eV, positive mode, *m/z*): calcd for $[M^*]^+$ 759.3278; found 759.3279. [* M = $C_{33}H_{48}N_6PtCl^+$ (without counter-ion)].

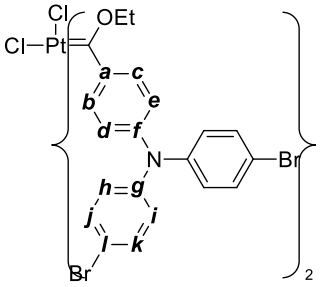

Figure 4.40. NMR position assignments of C2a

C2a: $C_{42}H_{34}O_2N_2Br_4PtCl_2$. ^{1}H NMR ($CD_2Cl_2$, 400 MHz) δ 7.58 (d, *J* = 8.5 Hz, 1H, H***b***), 7.51 (d, *J* = 7.9 Hz, 1H, H***c***), 7.35 (d, *J* = 8.8 Hz, 2H, H***j***), 7.27 (dd, *J* = 8.2 7.2 Hz, 1H, H***d***), 7.13 (d, *J* = 8.6 Hz, 1H, H***e***), 7.06 (d, *J* = 7.8 Hz, 4H, H***h*** and H***k***), 6.93 (d, *J* = 8.8 Hz, 2H, H***i***), (CH_2 (OEt), n.o.), 1.69 (t, *J* = 7.0 Hz, 3H, CH_3 (OEt)), 1.53 (s, 3H, CH_3 (OEt)). ^{13}C NMR (CD_2Cl_2, 101 MHz) δ (C_{carb}, n.o.), 157.0 (C***a***), 154.5 (C***f***), 147.0 (C***g***), 133.9 (C***b***), 133.6 (C***c***), 132.6 (C***j***), 130.0 (C***d***), 129.1 (C***e***), 128.6 (C***k***), 125.8

(C***h***), 125.1 (C***i***), 115.6 (C***l***), (CH_2 (OEt), n.o.), 15.5 (CH_3 (OEt)), 14.6 (CH_3 (OEt)). ESI-MS (2.8eV, positive mode, *m/z*): calcd for $[M + Na]^+$ 1206.8236; found 1206.8271. EA: calcd C = 42.59 %, H = 2.89 %, N = 2.37 %; found C = 42.67 %, H = 2.99 %, N = 2.47 %.

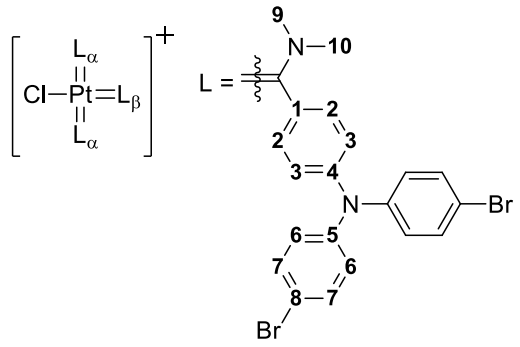

Figure 4.41. NMR assignments of C2b

C2b: $C_{63}H_{54}N_6Br_6PtCl_2$. ^{1}H NMR ($CD_2Cl_2$, 400 MHz) δ 7.45 (d, *J* = 8.9 Hz, 8H, H***α*7**), 7.43 – 7.41 (m, 4H, H***β*7**), 7.17 (d, *J* = 8.8 Hz, 4H, H***α*2**), 7.09 (d, *J* = 7.3 Hz, 2H, H***β*2**), 7.07 (d, *J* = 7.2 Hz, 2H, H***β*3**), 7.04 (d, *J* = 8.9 Hz, 8H, H***α*6**), 6.99 (d, *J* = 8.8 Hz, 8H, H***α*3** and H***β*6**), 4.20 – 4.10 (m, 6H, H***α*9**), 3.70 (s, 3H, H***β*9**), 3.49 (s, 3H, H***β*10**), 3.21 – 3.13 (m, 6H, H***α*10**). ^{13}C NMR (CD_2Cl_2, 101 MHz) δ 213.1 (Cα_{Carb}), 203.0 (Cβ_{Carb}), 155.7 (C***α*1**), 149.8 (C***β*1**), 147.8 (C***α*4**), 146.2 (C***β*5**), 146.2 (C***β*4**), 145.7 (C***α*5**), 133.3 (C***α*7**), 133.1 (C***β*7**), 127.7 (C***α*2**), 127.6 (C***α*6**), 126.9 (C***α*3**), 125.1 (C***β*6**), 123.1 (C***β*2**), 121.8 (C***β*3**), 118.0 (C***α*8**), 117.1 (C***β*8**), 52.5 (C***β*9**), 49.8 (C***β*10**), 46.9 (C***α*9**), 44.8 (C***α*10**). ESI-MS (2.8eV, positive mode, *m/z*): calctd for $[M]^+$ 1604.8786; found 1604.8789. EA: calctd C = 46.12%, H = 3.32 %, N = 5.13%; found C = 46.00 %, H = 3.34 %, N = 4.35 %.

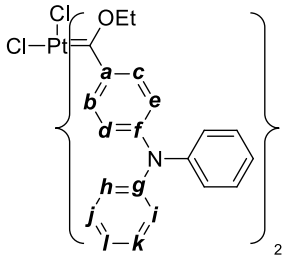

Figure 4.42. NMR position assignments of C3a

C3a: $C_{42}H_{38}O_2N_2PtCl_2$. ^{1}H NMR (CD_2Cl_2, 300 MHz) δ 7.48 (d, *J* = 7.4 Hz, 1H, H***b***), 7.45 (d, *J* = 7.9 Hz, 1H, H***c***), 7.42 (d, *J* = 8.1 Hz, 1H, H***d***), 7.37 (d, *J* = 8.1 Hz, 1H, H***e***), 7.32 – 7.26 (m, 2H, H***j***), 7.22 (dd, *J* = 7.5, 4.4 Hz, 2H, H***k***), 7.07 – 6.99 (m, 4H, H***h*** and H***i***), 6.81 (dd, *J* = 9.8, 9.5 Hz, 2H, H***l***), (CH_2 (OEt), n.o.), 1.67 (t, *J* = 7.1 Hz, 3H, CH_3 (OEt)), 1.51 (t, *J* = 7.1 Hz, 3H, CH_3 (OEt)). ^{13}C NMR (CD_2Cl_2, 75 MHz) δ ($C_{Carbene}$, n.o.), 147.9 (C***a***), 147.9 (C***f***), 143.8 (C***g***), 130.2 (C***j***), 130.1 (C***b***), 130.1 (C***c***), 129.2 (C***k***), 127.6 (C***d***), 127.2 (C***h***), 127.0 (C***e***), 124.1 (C***i***), 116.5 (C***l***), (CH_2 (OEt), n.o.), 14.3 (CH_3 (OEt)), 14.1 (CH_3 (OEt)). ESI-MS (2.8eV, positive mode, *m/z*): calcd

for $[M - L]^+$ where L = $C_{21}H_{19}NO$: 833.2271; found 833.2268. Calcd: C: 64.67 %, H: 4.91 %, N: 3.59 %. Found: C: 64.38 %, H: 5.15 %, N: 3.81 %.

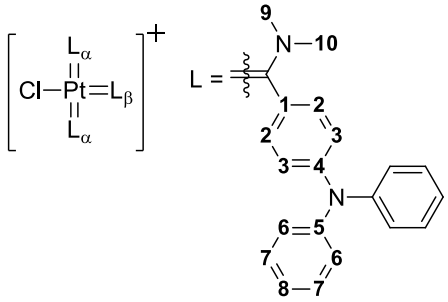

Figure 4.43. NMR assignments of C3b

C3b: $C_{63}H_{60}N_6PtCl_2$. ^{1}H NMR (CD_2Cl_2, 300 MHz) δ 7.42 – 7.48 (m, 2H, H**β7**), 7.36 (dd, *J* = 11.5, 7.4 Hz, 4H, H**α7**), 7.22 (d, *J* = 8.8 Hz, 2H, H**β2**), 7.20 (dd, *J* = 8.7, 2.4 Hz, 4H, H**α2**), 7.15 (d (br), *J* = 7.2 Hz, 12H, H**α6** and H**β6**), 7.10 (d (br), *J* = 8.7 Hz, 6H, H**α3** and H**β3**), 7.05 – 7.00 (m, *J* = 8.9 Hz, 6H, H**α8** and H**β8**), 4.12 (s, 3H, H**β9**), 3.76 (s, 6H, H**α9**), 3.53 (s, 3H, H**β10**), 3.17 (s, 6H, H**α10**). ^{13}C NMR (CD_2Cl_2, 75 MHz) δ (C**α**$_{Carb}$, n.o.), (C**β**$_{Carb}$, n.o.), 148.3 (C**α1**), (C**β1**, n.o.), 146.9 (C**α5**), 146.8 (C**β5**), 146.2 (C**α4**), (C**β4**, n.o.), 129.7 (C**β7**), 129.5 (C**α7**), 126.4 (C**β6**), 125.5 (C**β8**), 125.1 (C**α6**), 123.9 (C**α8**), 121.7 (C**β2**), 121.7 (C**α2**), 120.0 (C**β3**), 119.1 (C**α3**), (C**α9**, C**α10**, C**β9** and C**β10**, n.o.). ESI-MS (2.8eV, positive mode, *m/z*): calcd for $[M]^+$ 1131.4217; found 1131.4283. EA: calctd C = 64.83 %, H = 5.18 %; found C = 64.62%, H = 4.94 %.

4.4 References

[1] W. M. Campbell, A. K. Burrell, D. L. Officer, K. W. Jolley, *Coord. Chem. Rev.* **2004**, *248*, 1363–1379.

[2] P.-K. Chow, G. Cheng, G. S. M. Tong, W.-P. To, W.-L. Kwong, K.-H. Low, C.-C. Kwok, C. Ma, C.-M. Che, *Angew. Chem. Int. Ed.* **2015**, *54*, 2084–9.

[3] P. Du, K. Knowles, R. Eisenberg, *J. Am. Chem. Soc.* **2008**, *130*, 12576–7.

[4] R. H. Crabtree, D. M. P. Mingos, *Comprehensive Organometallic Chemistry III, Volumes 1 - 13*, Elsevier, **2007**.

[5] G. Rouschias, B. L. Shaw, *Chem. Commun.* **1970**, 183.

[6] L. Chugaev, M. Skanavy Grigorieva, A. Posniak, *Z. Anorg. Chem.* **1925**, *148*, 37.

[7] E. M. Badley, J. Chatt, R. L. Richards, G. A. Sim, *J. Chem. Soc., Chem. Commun.* **1969**,

1322–1323.

[8] P. de Frémont, N. Marion, S. P. Nolan, *Coord. Chem. Rev.* **2009**, *253*, 862–892.

[9] H. C. Clark, M. H. Chisholm, *Inorg. Chem.* **1971**, *10*, 1711–1716.

[10] M. H. Chisholm, H. C. Clark, *J. Am. Chem. Soc.* **1972**, *94*, 1532–1539.

[11] Y. T. Struchkov, G. G. Aleksandrov, V. B. Pukhnarevich, S. P. Sushchinskaya, M. G. Voronkov, *J. Organomet. Chem.* **1979**, *172*, 269–272.

[12] M. Werner, T. Lis, C. Bruhn, R. Lindner, D. Steinborn, *Organometallics* **2006**, *25*, 5946–5954.

[13] M. Wada, Y. Koyama, K. Sameshima, *J. Organomet. Chem.* **1981**, *209*, 115–121.

[14] M. Wada, Y. Koyama, *J. Organomet. Chem.* **1980**, *201*, 477–491.

[15] G. K. Anderson, R. J. Cross, L. Manojlović-Muir, K. W. Muir, R. A. Wales, *J. Chem. Soc., Dalton Trans.* **1979**, 684–689.

[16] G. K. Anderson, R. J. Cross, *J. Chem. Soc., Dalton Trans.* **1979**, 690.

[17] T. Kluge, M. Bette, T. Rüffer, C. Bruhn, C. Wagner, D. Ströhl, J. Schmidt, D. Steinborn, *Organometallics* **2013**, *32*, 7090–7106.

[18] T. Mihály, M. Bette, B. Mihály, J. Schmidt, H. Schmidt, D. Steinborn, *J. Organomet. Chem.* **2013**, *739*, 57–62.

[19] G. W. V. Cave, A. J. Hallett, W. Errington, J. P. Rourke, *Angew. Chem. Int. Ed.* **1998**, *37*, 3270–3272.

[20] Michelina. Rino A., A. J. L. Pombeiro, M. F. C. Guedes da Silva, *Coord. Chem. Rev.* **2001**, *218*, 75–112.

[21] M. P. López-Alberca, M. J. Mancheño, I. Fernández, M. Gómez-Gallego, M. A. Sierra, R. Torres, *Chem. Eur. J.* **2009**, *15*, 3595–3603.

[22] M. P. López-Alberca, M. J. Mancheño, I. Fernández, M. Gómez-Gallego, M. A. Sierra, R. Torres, *Org. Lett.* **2007**, *9*, 1757–1759.

[23] Y. Unger, A. Zeller, S. Ahrens, T. Strassner, *Chem. Commun.* **2008**, 3263–5.

[24] Y. Unger, A. Zeller, M. A. Taige, T. Strassner, *Dalton Trans.* **2009**, 4786–94.

[25] Y. Unger, D. Meyer, T. Strassner, *Dalton Trans.* **2010**, *39*, 4295–301.

[26] F. E. Hahn, V. Langenhahn, T. Lügger, T. Pape, D. Le Van, *Angew. Chem. Int. Ed.* **2005**, *44*, 3759–3763.

[27] S. Fuertes, H. García, M. Perálvarez, W. Hertog, J. Carreras, V. Sicilia, *Chem. Eur. J.* **2015**, *21*, 1620–1631.

[28] R. Visbal, M. C. Gimeno, *Chem. Soc. Rev.* **2014**, *43*, 3551–74.

[29] Y. Maeda, H. Hashimoto, I. Kinoshita, T. Nishioka, *Inorg. Chem.* **2015**, *54*, 448–59.

[30] R. C. Klet, J. A. Labinger, J. E. Bercaw, *Organometallics* **2012**, *31*, 6652–6657.

[31] R. Aumann, E. O. Fischer, *Chem. Ber.* **1981**, *114*, 1853–1857.

[32] S.-T. Liu, K. R. Reddy, *Chem. Soc. Rev.* **1999**, *28*, 315–322.

[33] A. M. Voutchkova, M. Feliz, E. Clot, O. Eisenstein, R. H. Crabtree, *J. Am. Chem. Soc.* **2007**, *129*, 12834–12846.

[34] F. Hanasaka, Y. Tanabe, K. Fujita, Y. Ryohei, *Organometallics* **2006**, *25*, 826–831.

[35] J. Cooper, T. Ziegler, *Inorg. Chem.* **2002**, *41*, 6614–6622.

[36] J. N. Harvey, K. M. Heslop, A. G. Orpen, P. G. Pringle, *Chem. Commun.* **2003**, 278–279.

[37] J. Chatt, R. G. Wilkins, *J. Chem. Soc.* **1952**, 4300–6.

[38] H. A. Smith, R. R. Myers, *J. Am. Chem. Soc.* **1942**, *64*, 2362–2365.

[39] A. F. Greene, P. Chandrasekaran, Y. Yan, J. T. Mague, J. P. Donahue, *Inorg. Chem.* **2014**, *53*, 308–17.

[40] B. M. Segal, H. R. Hoveyda, R. H. Holm, *Inorg. Chem.* **1998**, *37*, 3440–3443.

[41] L. Rivera-Rivera, F. Colón-Padilla, A. Del Toro-Novalés, J. E. Cortés-Figueroa, *J. Coord. Chem.* **2001**, *54*, 143–151.

[42] E. W. Abel, I. S. Butler, J. G. Reid, *J. Chem. Soc.* **1963**, 2068.

[43] S. Delahaye, C. Loosli, S. X. Liu, S. Decurtins, G. Labat, A. Neels, A. Loosli, T. R. Ward, A. Hauser, *Adv. Func. Mater.* **2006**, *16*, 286–295.

[44] S.-W. Lai, M. C.-W. Chan, T.-C. Cheung, S.-M. Peng, C.-M. Che, *Inorg. Chem.* **1999**, *38*, 4046–4055.

[45] E. M. Badley, K. W. Muir, G. A. Sim, *J. Chem. Soc., Dalton Trans.* **1976**, 1930–1933.

[46] G. M. Chu, A. Guerrero-Martínez, C. Ramírez de Arellano, I. Fernández, M. A. Sierra, *Inorg. Chem.* **2016**, *55*, 2737–47.

[47] N. Weststrate, I. Fernández, D. C. Liles, N. van Jaarsveld, S. Lotz, *Organometallics* **2015**, *34*, 696–710.

[48] S. Barlow, H. E. Bunting, C. Ringham, J. C. Green, G. U. Bublitz, S. G. Boxer, J. W. Perry, S. R. Marder, *J. Am. Chem. Soc.* **1999**, *121*, 3715–3723.

[49] R. Ganesamoorthi, A. Thakur, D. Sharmila, V. Ramkumar, S. Ghosh, *J. Organomet. Chem.* **2013**, *726*, 56–61.

[50] R. C. Evans, P. Douglas, C. J. Winscom, *Coord. Chem. Rev.* **2006**, *250*, 2093–2126.

[51] V. W.-W. Yam, V. K.-M. Au, S. Y.-L. Leung, *Chem. Rev.* **2015**, *115*, 7589–7728.

[52] K. Li, G. S. Ming Tong, Q. Wan, G. Cheng, W.-Y. Tong, W.-H. Ang, W.-L. Kwong, C.-M. Che, *Chem. Sci.* **2016**, *7*, 1653–1673.

[53] T. B. Fleetham, L. Huang, K. Klimes, J. Brooks, J. Li, *Chem. Mater.* **2016**, *28*, 3276–3282.

[54] H. Ohara, A. Kobayashi, M. Kato, *Dalton Trans.* **2014**, *43*, 17317–23.

[55] A. Bossi, A. F. Rausch, M. J. Leitl, R. Czerwieniec, M. T. Whited, P. I. Djurovich, H. Yersin, M. E. Thompson, *Inorg. Chem.* **2013**, *52*, 12403–15.

[56] J. Kalinowski, V. Fattori, M. Cocchi, J. A. G. Williams, *Coord. Chem. Rev.* **2011**, *255*, 2401–2425.

[57] J. A. G. Williams, S. Develay, D. L. Rochester, L. Murphy, *Coord. Chem. Rev.* **2008**, *252*, 2596–2611.

[58] S. B. Piepho, P. N. Schatz, A. J. McCaffrey, *J. Am. Chem. Soc.* **1969**, *91*, 5994–6001.

[59] J. A. Zuleta, J. M. Bevilacqua, J. M. Rehm, R. Eisenberg, *Inorg. Chem.* **1992**, *31*, 1332–1337.

[60] L. Porrès, A. Holland, L.-O. Pålsson, A. P. Monkman, C. Kemp, A. Beeby, *J. Fluoresc.* **2006**,

16, 267–273.

[61] J. Lee, H.-F. Chen, T. Batagoda, C. Coburn, P. I. Djurovich, M. E. Thompson, S. R. Forrest, *Nat. Mater.* **2016**, *15*, 92–8.

[62] T.-T. Feng, F.-Q. Bai, L.-M. Xie, Y. Tang, H.-X. Zhang, *RSC Adv.* **2016**, *6*, 11648–11656.

[63] K.-Y. Liao, C.-W. Hsu, Y. Chi, M.-K. Hsu, S.-W. Wu, C.-H. Chang, S.-H. Liu, G.-H. Lee, P.-T. Chou, Y. Hu, N. Robertson, *Inorg. Chem.* **2015**, *54*, 4029–38.

[64] X.-C. Hang, T. Fleetham, E. Turner, J. Brooks, J. Li, *Angew. Chem. Int. Ed.* **2013**, *52*, 6753–6.

[65] H. Yersin, A. F. Rausch, R. Czerwieniec, T. Hofbeck, T. Fischer, *Coord. Chem. Rev.* **2011**, *255*, 2622–2652.

[66] S. Archer, J. A. Weinstein, *Coord. Chem. Rev.* **2012**, *256*, 2530–2561.

[67] Y. Cao, M. O. Wolf, B. O. Patrick, *Inorg. Chem.* **2016**, *55*, 8985–8993.

[68] Y. Wang, J. Fan, T. Li, Q. Wang, J. Shi, Z. Qu, H. Tan, Y. Liu, W. Zhu, *RSC Adv.* **2016**, *6*, 45864–45872.

[69] P. Irmler, R. F. Winter, *Dalton Trans.* **2016**, *45*, 10420–10434.

[70] F. Geist, A. Jackel, R. F. Winter, *Inorg. Chem.* **2015**, *54*, 10946–10957.

[71] P. D. Harvey, N. Proulx, G. Martin, M. Drouin, D. J. Nurco, K. M. Smith, F. Bolze, C. P. Gros, R. Guilard, *Inorg. Chem.* **2001**, *40*, 4134–4142.

[72] J. Michl, V. Bonačić-Koutecký, *Electronic Aspects of Organic Photochemistry*, Wiley, **1990**.

[73] P. Kumar Bera, D. Nath, A. Misra, M. Chowdhury, *J. Photochem. Photobiol. A* **1996**, *95*, 127–136.

[74] M. R. Wasielewski, D. W. Minsek, M. P. Niemczyk, W. A. Svec, N. C. C. Yang, *J. Am. Chem. Soc.* **1990**, *112*, 2823–2824.

[75] J.-H. Wu, W.-C. Chen, G.-S. Liou, *Polym. Chem.* **2016**, *7*, 1569–1576.

[76] K. Masui, H. Nakanotani, C. Adachi, *Org. Electron.* **2013**, *14*, 2721–2726.

[77] Z. Yang, Z. Mao, Z. Xie, Y. Zhang, S. Liu, J. Zhao, J. Xu, Z. Chi, M. P. Aldred, *Chem. Soc. Rev.* **2017**, *46*, 915–1016.

[78] P. E. Keivanidis, S. Baluschev, G. Lieser, G. Wegner, *Chem. Phys. Chem.* **2009**, *10*, 2316–2326.

[79] J.-S. Chen, G.-J. Zhao, T. R. Cook, K.-L. Han, P. J. Stang, *J. Am. Chem. Soc.* **2013**, *135*, 6694–6702.

[80] W. Wu, H. Guo, W. Wu, S. Ji, J. Zhao, *Inorg. Chem.* **2011**, *50*, 11446–11460.

[81] I. E. Pomestchenko, F. N. Castellano, *J. Phys. Chem. A* **2004**, *108*, 3485–3492.

[82] B. Valeur, *Molecular Fluorescence: Principles and Applications*, Wiley, **2002**.

[83] J. Zhao, W. Wu, J. Sun, S. Guo, *Chem. Soc. Rev.* **2013**, *42*, 5323–5351.

[84] R. Berera, R. van Grondelle, J. T. M. Kennis, *Photosynth. Res.* **2009**, *101*, 105–118.

[85] J. J. Snellenburg, S. P. Laptenok, R. Seger, K. M. Mullen, I. H. M. van Stokkum, *J. Stat. Softw.* **2012**, *49*, 1–22.

[86] R. M. van der Veen, A. Cannizzo, F. van Mourik, A. Vlček, M. Chergui, *J. Am. Chem. Soc.* **2011**, *133*, 305–15.

[87] E. O. Danilov, I. E. Pomestchenko, S. Kinayyigit, P. L. Gentili, M. Hissler, R. Ziessel, F. N. Castellano, *J. Phys. Chem. A* **2005**, *109*, 2465–2471.

[88] S. E. Brown-Xu, M. S. J. Kelley, K. A. Fransted, A. Chakraborty, G. C. Schatz, F. N. Castellano, L. X. Chen, *J. Phys. Chem. A* **2016**, *120*, 543–550.

[89] S. Cho, M. W. Mara, X. Wang, J. V. Lockard, A. A. Rachford, F. N. Castellano, L. X. Chen, *J. Phys. Chem. A* **2011**, *115*, 3990–3996.

[90] F. N. Castellano, *Acc. Chem. Res.* **2015**, *48*, 828–39.

[91] H. C. Clark, L. E. Manzer, *J. Organomet. Chem.* **1973**, *59*, 411–428.

CHAPTER 5

BINUCLEAR Pt(II) FISCHER MULTICARBENE RODS: SYNTHESIS AND PHOTOPHYSICS

5.1 Introduction

In recent years more attention has been given to larger molecules of Pt(II) complexes as they become more prominent in the fields of solar energy,[1] organic light emitting diodes (OLEDs),[2,3] bio-agents[4,5] and even molecular machines.[6] There are several known bimetallic, rod-like Pt(II) compounds, most of which are used in OLEDs or solar cell devices.[7–11] Several examples show that upon introducing multiple metal centres or a bridging ligand between two Pt(II) centres allows for the manipulation of the physical or photophysical properties which are observed for similar mononuclear complexes.[9,12–14]

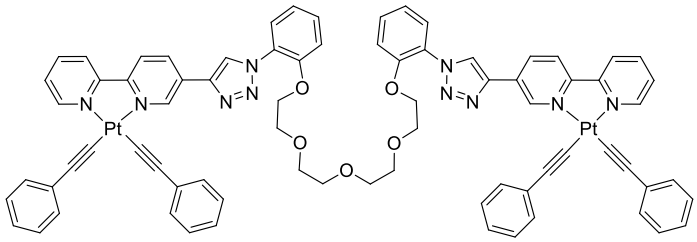

Figure 5.1. Binuclear Pt(II) complexes with a polyethylene glycol bridging unit[15]

The research group of Bäuerle published an electronic study on binuclear Pt(II) complexes containing polyethylene glycol bridging units where clear metal-metal interactions are present upon excitation of the compounds that enhances the compounds' emission.[15] The linkers allow for intramolecular eximer formation through Pt-Pt and π-π interactions which leads to ground state coupling

between the metal centres. The proximity interactions between the metal centres permits an alteration of photophysical and electrochemical properties and can be further influenced by altering solvents.

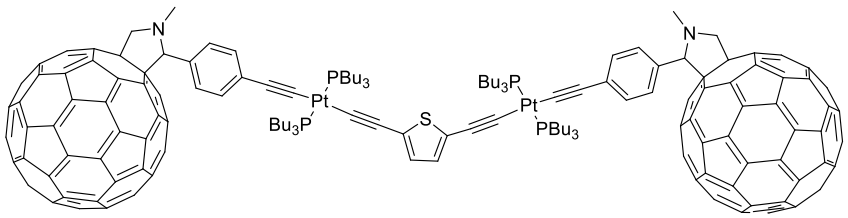

Figure 5.2. The symmetrical platinum-acetylide with end-capped fulleropyrolidine[16]

Another example of a bimetallic Pt(II) rod has been published by Schanze in which an end-capped platinum acetylide donor–acceptor triad (donor, bridge, acceptor) assembly was synthesized.[16] The compound showed photoinduced charge transfer processes and good charge carrier transport properties which could be used in solar cells.

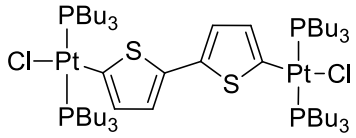

Figure 5.3. A binuclear platinum rod with a thiophene linker[17]

Kotani and co-workers use thiophene and bithiophene to link two Pt(II) moieties together. They use 2,5-bis-trimethyl-stannylthiophene or 2,5'-bis-trimethylstannylbithienyl as precursors that is reacted with [Pt(COD)Cl_2] whereby trimethyltin chloride is eliminated affording the thiophene-bridged diplatinum rod. They go further to replace the labile cyclooctadiene (COD) ligands with tertiary phosphines (Figure 5.3).[17]

In Chapter 4 it has been established that several Fischer carbene ligands can be coordinated to a single Pt(II) centre via a transmetallation reaction. The number of Fischer carbene ligands that coordinated to the metal centre depend on the amount of electron density available to the carbene carbon through its aromatic and heterogroup substituents. Further the compounds show emission upon excitation albeit in low quantum yields. The possibility for intermolecular metal-metal interactions and the formation of eximers – unique to Pt(II) square planar complexes – are eliminated by the bulky character of the carbene ligands.

In this study, the aim is to synthesise several rod-like binuclear Pt(II) compounds containing multiple Fischer carbene ligands. A binuclear complex where two Pt(II) centres, each containing a chloro ligand and a labile bidentate ligand, and are bridged by a bithienylene linker, is chosen as macromolecular starting material. The synthesis of the precursors follows Sonagashira's method by making use of a Stille-like reaction. From a synthetic perspective, the binuclear Pt(II) bridge provides a rigid structure which should be able to easily accommodate multiple carbene ligands.

Aspects to consider include how many ligands coordinate in each case and whether the number of ligands that coordinate can be controlled. Also, whether intermolecular communication between the two Pt(II) centres exists and if so, investigate the photophysical properties by means of steady state absorbance, emission spectroscopy and ultra-fast transient absorption studies. The photophysical studies will also reveal whether there is potential use for such compounds in the never-ending race after improved OLED or solar cell devices.

5.2 Results and Discussion

5.2.1 Synthesis

To synthesise large, electron-rich Pt(II) rods, two Pt $(COD)Cl_2$ complexes are linked with a bithienylene bridge (Scheme 5.1).[17] In this case Pt(COD)Cl fragments replaces trimethyltin on 5,5'-bis(trimethylstannyl)-2,2'-bithiophene to form trimethyl-tinchloride and two platinum metal centres linked with a bithienylene bridge (Scheme 5.1).

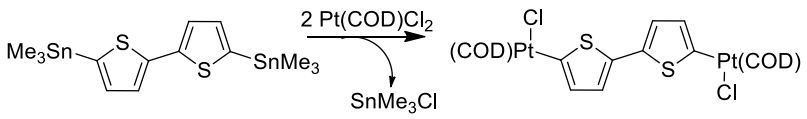

Scheme 5.1. Synthesis of binuclear Pt(II) bithienylene precursors

As in Chapter 4, the synthesis of the binuclear Fischer multicarbene complexes are achieved through a carbene transfer reaction of tungsten pentacarbonyl carbene complexes to Pt(II) centres by readily replaceable COD ligands. It is anticipated that both COD ligands will be replaced by four Fischer carbene ligands. However, as seen in Chapter 4, the number of carbene ligands that will

coordinate to a diplatinum rod is influenced by the coordinating properties and steric constraints of the carbene ligands. The tungsten carbonyl carbene precursors used for the substitution reaction are the complexes discussed in Chapter 3 (Figure 5.4).

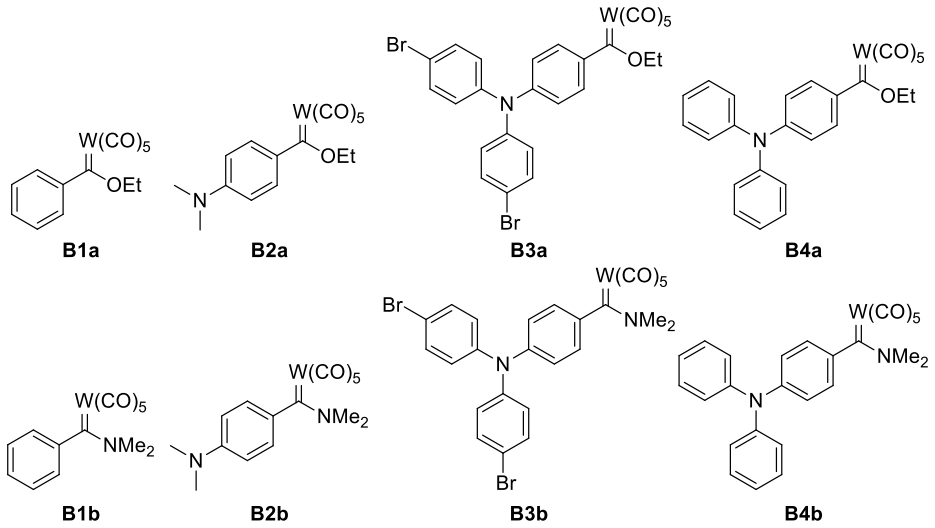

Figure 5.4. W(0) carbene complexes used in the synthesis of the Pt(II) rod multicarbene complexes

Considering the results obtained for the mononuclear Pt(II) carbene complexes, KPF_6 is added to the reaction mixture should any counter ion be needed. Thus, a tungsten pentacarbonyl carbene complex is refluxed in DCM in the presence of the binuclear Pt(II) dithienylene rod and anhydrous KPF_6 for at least 24 hours. The completion of a reaction is monitored by NMR spectroscopy. Once it has been established that the reaction has been completed (no more coordinated cylcooctadiene is observed in the NMR spectroscopy), the product is canula-filtered under inert conditions and triturated several times into *n*-hexane or diethylether. *n*-Hexane is used for the ethoxycarbene complexes while diethylether is used for the aminocarbene complexes as the solubility of the aminolysed tungsten carbene complexes are poor in hexane. All possible unreacted reagents or products can be dissolved by the respective solvents except for the product and any unreacted binuclear Pt(II) bithienylene starting material.

A general reaction scheme is shown in Scheme 5.2. The substitution reactions afford Pt(II) multicarbene binuclear rods that are stable under irradiation and can be stored under inert

conditions. In all cases the yields are average ranging between 30 and 60%, depending on the size of the carbene ligand being coordinated, and form brown-yellow powders or bright pink powders for the ethoxy- and aminocarbene complexes, respectively. The complexes show high solubility in DCM and to a lesser extent in THF. Once dissolved in DCM the solution appears black due to the high light absorbance of the complexes. **D1a**, **D3a** and **D4a** are more prone to undergo reduction of the Pt(II) to form Pt black which can cause the dimerization of the carbene ligands.[18]

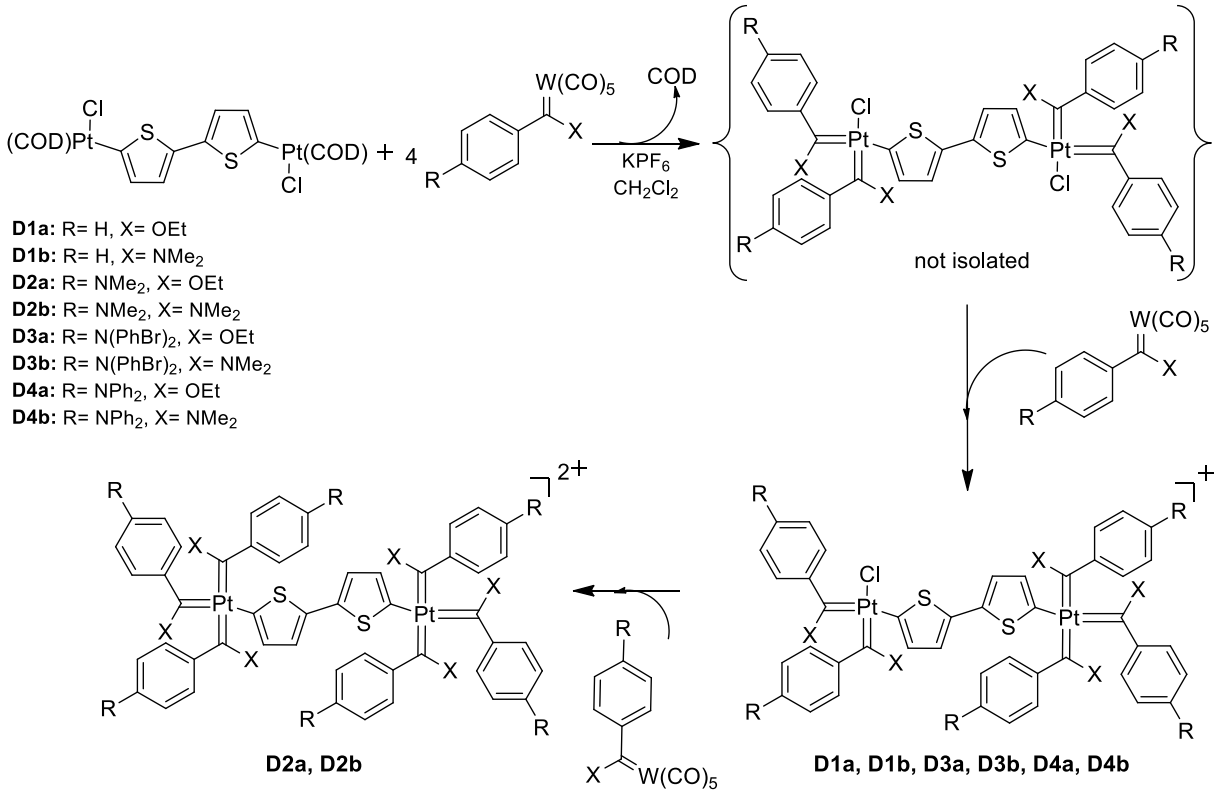

Scheme 5.2. Synthesis of D1 – D4

All the complexes have five carbene ligands coordinated to the Pt(II) rod except **D2a** and **D2b** which are dicationic and have six coordinated carbene ligands. In Chapter 4, the products that was formed in the synthesis of the mononuclear multicarbene Pt(II) complexes was influenced by three factors: The electron density available on the carbene carbon of a particular ligand, the electron density available on the Pt(II) centre after the substitution of the COD ligand by two of

the carbene ligands, and the net charge of the complex ion. Thus, the mononuclear Pt(II) aminocarbene ligands coordinated to form cationic triscarbene complexes while the ethoxycarbene ligands formed neutral biscarbene complexes.

In Chapter 3 it has further been shown that the carbene carbon of the aminocarbene complexes receives a substantial amount of electron density from its amino substituent and depends less on the electron density provided by the phenyl substituent. Thus, the products expected from the transmetallation of the aminocarbene ligands will be influenced by steric factors and electronic effects. The formation of monocationic pentacarbene products from the transmetallation of the large triphenylamine aminocarbene ligands (**D3b** and **D4b**) are expected to be significantly influenced by steric interactions. The reason why a mono-cationic pentacarbene product is obtained for **D1b** rather than a di-cationic hexacarbene product as for **D2b** must relate to the large electronic difference between the two phenyl carbene substituents and a H (**D1b**) vs a NMe_2 (**D2b**) substituent in the *p*-position.

The mechanism whereby a neutral Pt biscarbene fragment is converted into a cationic Pt triscarbene fragment is important. No mechanistic study was undertaken, but from literature examples and observations during the reactions, a feasible mechanism can be proposed. It is postulated that the tertiary amine present in the aromatic substituent of the carbene carbon contributes to reactivity by interacting with a Pt centre. Thus, the tungsten carbene bond is activated due to less stabilization of the carbene carbon by the distant nitrogen substituent. The activated W–C(carbene) bond coordinates to a second Pt biscarbene centre affording a 3-member intermediate ring (carbon-dimetallacyclic cyclopropane). A president for metal-carbene bonds acting as ligands to vacant coordination sites on Pt has been reported by Stone and co-workers a long time ago.[19] Elimination of a $[W(CO)_5Cl]^-$ leads to the formation of a cationic triscarbene fragment. In the absence of a directing tertiary amine in the aromatic substituent of the carbene carbon (**D1a** and **D1b**), a further activation and coordination of a sixth carbene ligand is not facilitated because of a less activated W-carbene complex. For the complexes containing

large carbene ligands (**D3a**, **D3b**, **D4a** and **D4b**), the sixth carbene ligand cannot be orientated for coordination due to steric interactions influencing the approach of a carbene ligand. The possible mechanism by which the final carbene ligand coordinates in **D2a** and **D2b** is shown in Scheme 5.3.

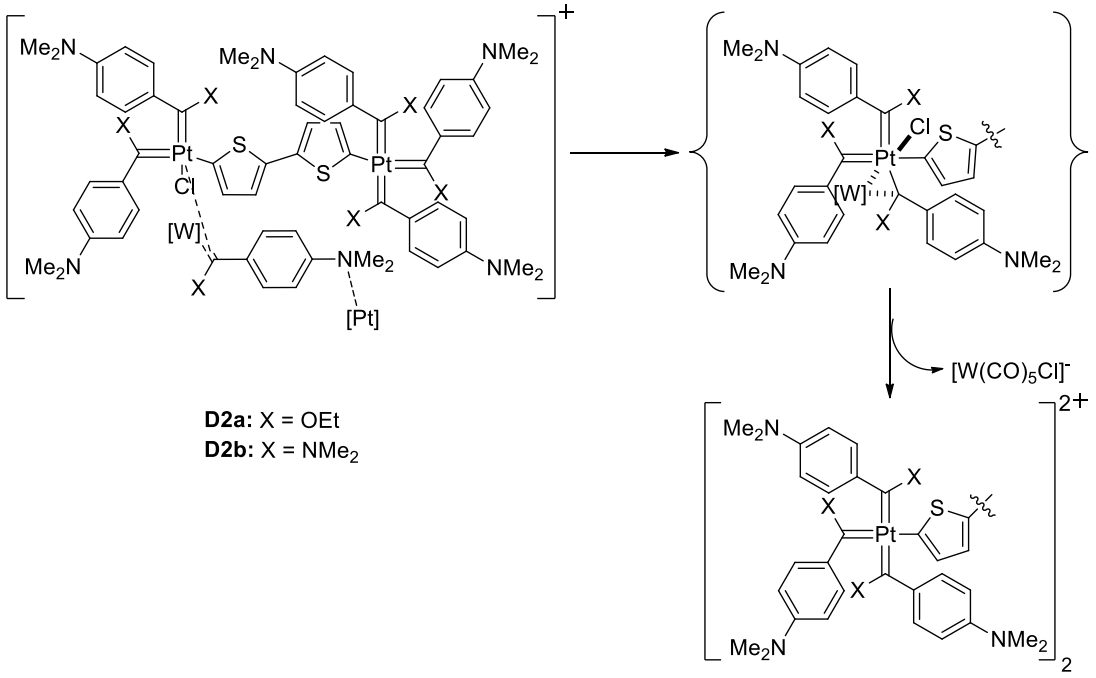

Scheme 5.3. Formation of the hexacarbene binuclear Pt(II) complexes of D2a and D2b

Taking all considerations into account there are three major aspects that control the product formation during the transmetallation reaction of a carbene ligand in binuclear Pt(II) rods. The first aspect is electronic effects. In all cases, more than 4 carbene ligands coordinate in a single complex. This would imply that the metal requires less electron density to accommodate another carbene ligand – a situation created by displacing a chloride and leaving a cationic Pt moiety. The bithienylene bridge between the two metal centres in **D1** – **D4** provides electronic contact and some electron density by distribution, when needed. It is for this reason that all the complexes formed in this series contain at least three carbene ligands on one of the metal centres (ethoxy- and aminocarbene ligands). Since metal centres are directly linked with a conjugated linker it must be assumed that they directly influence each other electronically and sterically.

The second aspect to consider is intermediate formation, and here the steric properties of the carbene ligand being coordinated is important. As the mechanism of the reactions is believed to rely largely on the approach of a tungsten carbene complex to the Pt(II) centre, steric properties will play a major role. If there is not enough space for η^2-coordination, the carbene complex which will participate in the transmetallation reaction, will not be able to coordinate. As has been previously illustrated, the approach and alignment of an uncoordinated carbene complex will determine whether the complex will be able to coordinate. The last aspect to consider is the charge effect that becomes important when a chloro-ligand is replaced by a carbene ligand, forming a cationic complex. This represents a mechanism whereby excess electron density is removed from the metal centre. Also, a positive charge on the complex will bind the carbene ligands stronger to the Pt(II) centre.

The products in general imply that a carbene ligand is favoured in a cationic environment when compared to a chloro ligand. It suggests that the COD ligands at both metal centres are readily replaced by four carbene ligands before any further substitution reactions occur. It also supports an increase in orbital overlap between all the parts of the binuclear Pt rod and implies that the coordination of a third carbene ligand on one metal centre can directly influence the second metal centre that the same substitution reaction is less likely to occur.

5.2.2 NMR Spectroscopy

The NMR spectra of **D1** – **D4** are complex due to the different sets of signals generated by the different groups of ligands coordinated to the two Pt(II) centres present in each complex. Although difficult to analyse, it is possible to determine how many ligands coordinate in each of the binuclear complexes due to the presence of the bithienylene bridge. The bithienylene bridge further reveals whether the two Pt(II) centres are symmetrical or asymmetrical, with the bridge being represented by either two or four proton signals, respectively. However, for the larger ligands pronounced signal overlap and in some cases, poor resolution within the spectra becomes a problem with peak assignment. ^{31}P and ^{19}F NMR spectra are used to confirm the presence of the

counter ions, indicating that more than two carbene ligands are coordinated at one of the two Pt centres in the rod.

^{1}H NMR Spectroscopy

From the NMR spectra of the ethoxy- and aminocarbene complexes, most of the compounds form asymmetric products. For these complexes four different signals for the 5,5'-{2,2'-dithienylene} bridge are observed as well as three different sets of chemical shift values for the different groups of carbene ligands. The chemical shift values for the bithienylene linkers in both the ethoxy- and aminocarbene complexes of **D1**, **D3** and **D4** are significantly different, that it must be concluded that the Pt(II) atoms are found in different electronic environments. A reason for the difference between the Pt(II) centres is the number of coordinated carbene ligands to each metal centre and this, in effect, will influence the charge present on the metal and its ligands. A different charge on the two metal centres within a complex would imply that significant differences in the chemical shift values in the NMR spectra between the two metal centres and the coordinated ligands are expected. For most of the compounds being investigated three carbene ligands are coordinated to one Pt(II) atom, which then has a greater positive charge. Two carbene ligands are coordinated to the other Pt atom which represents a charge closer to being neutral. The overall complex has a +1 charge. This charge will explain the significant difference between the corresponding positions within the dithienyl linker. Also, the cationic Pt(II) fragment with three carbene ligands display proton resonances for the carbene substituents which are downfield (α-H's) compared to similar resonances of the neutral Pt(II) biscarbene fragment (β-H's). To illustrate these aspects, the ^{1}H NMR spectra of **D1b** and **D2b** will be discussed in greater detail.

The NMR spectra of **D2a** and **D2b** show only a single set of signals for the bithienylene bridge indicating that the two metal centres are identical. The presence of the PF_6^- counter ion (confirmed with NMR) indicates that the compounds are charged. As it has been confirmed that three carbene ligands can coordinate to a single metal centre, it is likely that three carbene ligands have coordinated to both the metal centres, thus creating a doubly charged hexacarbene complex.

Table 5.1. ^{1}H NMR chemical shifts (ppm) of D1a, D3a and D4a in CD_2Cl_2

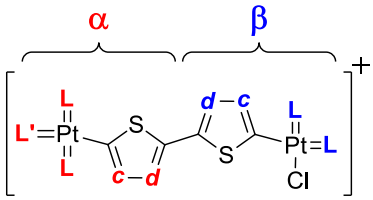

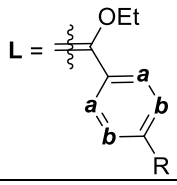

D1a: R = H
D3a: R = $N(PhBr)_2$
D4a: R = NPh_2

	L	*a*	*b*	CH_2	CH_3	*c*	*d*
D1a	α	7.87	7.54	n.o.*	1.54	n.o.	6.91
		dd, *J* = 8.4, 1.4	dd, *J* = 7.5, 7.4		s *(br)*		d, *J* = 3.7
	α'	7.83	7.55	n.o.*	1.54		
		dd, *J* = 8.4, 1.4	dd, *J* = 6.9, 7.0		s *(br)*		
	β	7.75	7.44	n.o.*	1.54	7.37	7.16
		s *(br)*	s *(br)*		s *(br)*	d, *J* = 3.7	d, *J* = 4.0
D3a	α	7.51	7.06	n.o.*	1.53	7.61	n.o.
		d, *J* = 8.8	d *(br)*, *J* = 8.6		t, *J* = 7.1	d, *J* = 4.0	
	α'	7.58	7.06	n.o.*	1.69		
		d, *J* = 8.8	d *(br)*, *J* = 8.6		t, *J* = 7.1		
	β	7.46	7.06	n.o.*	1.47	7.24	7.19
		dd, *J* = 8.8, 3.0	d *(br)*, *J* = 8.6		t, *J* = 7.0	d, *J* = 4.0	d, *J* = 4.4
D4a	α	7.42	7.20	n.o.*	1.58	7.47	6.73
		d, *J* = 7.8	d *(br)*, *J* = 7.9		s *(br)*	d, J = 4.1	d, *J* = 4.2
	α'	7.46	7.22 – 7.20	n.o.*	1.66		
		d, *J* = 7.9	m		t, *J* = 7.1		
	β	7.38	7.18 – 7.14	n.o.*	1.51	7.25	6.95
		d, *J* = 7.8	m		t, *J* = 7.1	d, *J* = 3.9	d, *J* = 4.2

* Not observed due to $^{3}J_{\{Pt\}H}$ coupling

Table 5.2. ^{1}H NMR chemical shifts (ppm) of D1b, D3b and D4b in CD_2Cl_2

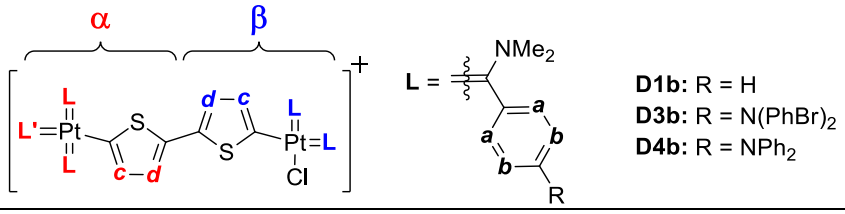

		a	*b*	NMe	NMe	*c*	*d*
D1b	α	7.50 – 7.45	7.33	4.17	3.14	7.39	6.73
		m	dd, *J* = 8.0, 7.5	s	s	d, *J* = 5.2	d, *J* = 5.0
	α'	7.50 – 7.45	7.50 – 7.45	3.92	3.35		
		m	m	s	s		
	β	7.03	7.11	3.55	3.05	7.28	7.19
		d, *J* = 7.7	s *(br)*	s	s	d, *J* = 3.7	d, *J* = 4.5
D3b	α	7.50	7.10	4.18	3.23	7.48	6.89
		d, *J* = 8.7	d, *J* = 8.7	s	s	d, *J* = 4.4	d, *J* = 5.0
	α'	7.46	7.06	3.83	3.45		
		d, *J* = 8.7	d, *J* = 8.8	s	s		
	β	7.43	7.09	3.71	3.12	7.22	7.17
		d *(br)*, *J* = 8.6	d, *J* = 6.7	s	s	d, *J* = 3.7	d, *J* = 4.6
D4b	α	7.41	6.99	4.17	3.29	7.47	6.90
		d, *J* = 8.5	d, *J* = 8.8	s	s	d, *J* = 4.4	s *(br)*
	α'	7.66	7.01	3.71	3.13		
		d, *J* = 8.8	d, *J* = 8.8	s	s		
	β	7.39	6.96	3.46	3.02	7.21	7.17
		d, *J* = 8.1	d, *J* = 8.7	s	s	d, *J* = 4.4	d, *J* = 4.7

* Not observed due to $^{3}J_{\{Pt\}H}$ coupling

The ^{1}H NMR spectra of the complexes further show differences within the coordinated ligands and can be ascribed to a *trans* effect. Four sets of signals are expected for the asymmetric complexes. At the positively charged Pt(II) atom two ligands are *trans* to each other while a third ligand is *trans* to the bithienylene bridge. At the neutral metal centre one ligand is *trans* to a chloro ligand while the other is *trans* to the bithienylene bridge. It is evident however, that only three sets of signals are observed for the asymmetric compounds: one set representing the ligands *trans* to each other at the positive metal centre (**α**–ligands), one set representing the ligand *trans* to the bithienylene bridge at the positive metal centre (**α'**–ligand), and one set representing both the ligands coordinated to the neutral Pt(II) atom (**β**–ligands). It seems that the chloro ligand and

bithienylene bridge have similar *trans* effects such that the carbene ligands coordinated to the neutral metal centre display similar or slightly broadened ^{1}H NMR chemical shifts. The same effect is observed for the symmetrical, doubly charged hexacarbene complexes (**D2a** and **D2b**), in which the ligands *trans* to each (**γ**–ligands) have different chemical shifts from the ligands *trans* to the bithienylene bridge (**ε**–ligands). This complicates individual assignments and in some instances group assignments are made or some chemical shifts are not observed (n.o.).

Table 5.1, Table 5.2 and Table 5.3 list selected ^{1}H NMR assignments of the ethoxy- and aminocarbene complexes of **D1** to **D4**. The assignments are made according to the figure shown in each table.

Table 5.3. ^{1}H NMR chemical shifts (ppm) of the ethoxy- and aminocarbene complexes of D2 in CD_2Cl_2

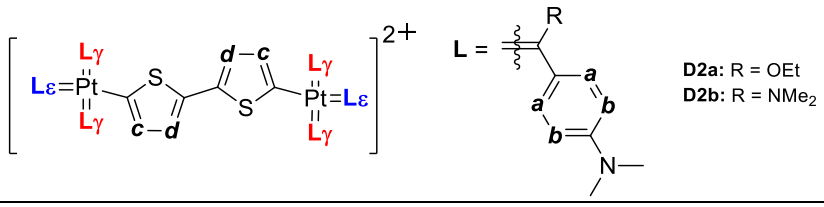

		aryl		dithienyl		R	
		a	***b***	***c***	***d***		
D2a (R = OEt)	**γ**	8.42	6.61	7.59	7.37	n.o.*	1.47
		d, *J* = 9.1	d, *J* = 9.3	d, *J* = 3.9	d, *J* = 3.9		t, *J* = 7.2
	ε	7.88	6.75				
		d, *J* = 9.0	d, *J* = 9.1				
D2b (R = NMe_2)	**Γ**	7.33	6.76	7.42	7.13	3.73	3.13
		d, *J* = 8.7	d, *J* = 9.0	d, *J* = 4.2	d, *J* = 3.7	s	s
	ε	7.32	6.73			3.47	3.02
		d, *J* = 8.8	d, *J* = 8.9			s	s

* Not observed due to $^{3}J_{\{Pt\}H}$ coupling

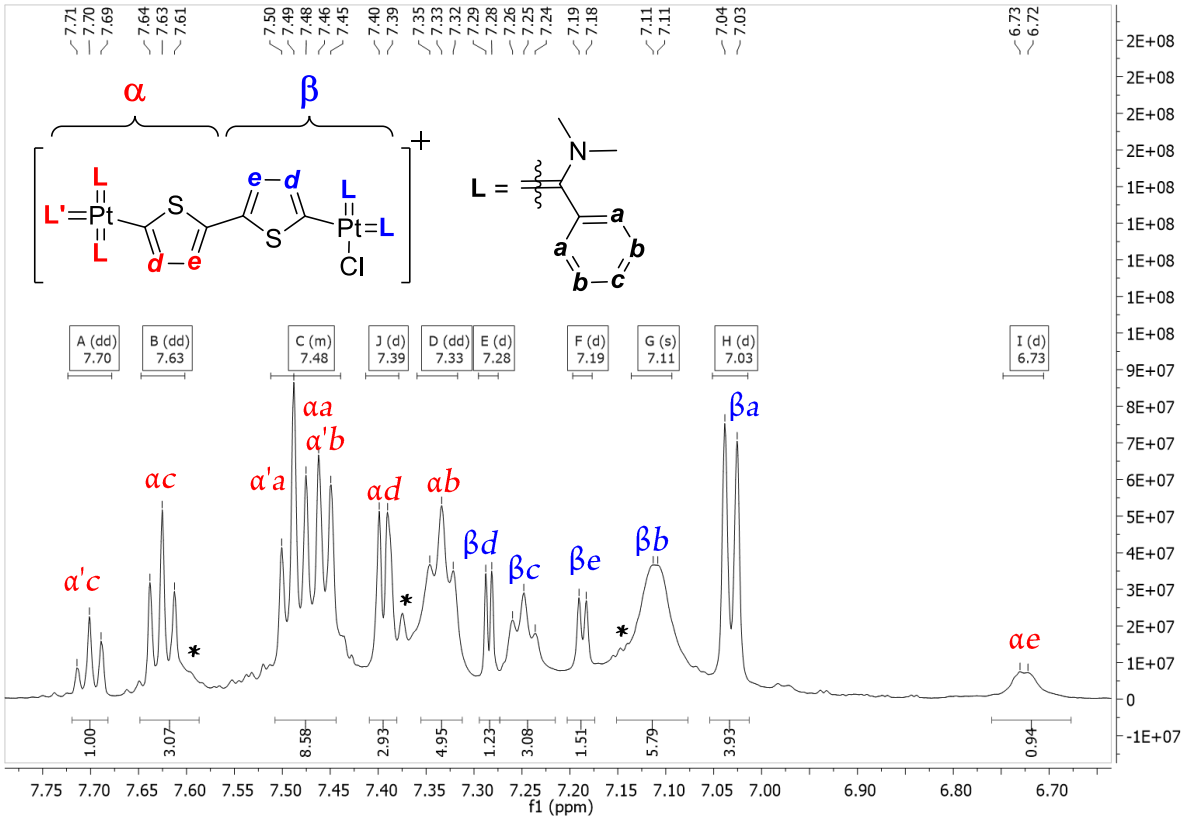

Figure 5.5. ^{1}H NMR spectrum of the aromatic region of D1b recorded in CD_2Cl_2 at room temperature

The ^{1}H NMR spectrum of **D1b** is shown in Figure 5.5. The 2D NMR spectra of the compound can be found in the Appendix. The two Pt fragments of the pentacarbene binuclear complex are asymmetrically orientated with a positive charge predominately on the triscarbene fragment. As a result, the spectrum (excluding the thiophene resonances) for the aromatic region is divided into two sections separated at around 7.30 ppm. To the right, upfield, the biscarbene benzene substituents (β-hydrogens) are found while the triscarbene fragments (α-hydrogens) are downfield from this marker. Also, observed in the spectrum are weak resonances of a decomposition product marked with a "*" symbol in Figure 5.5.

It is evident from the spectrum that there are three sets of signals in a ratio of 1:2:2. The clear difference in the sets of ligand signals is ascribed to the positive charge of one metal centre containing the three coordinated carbene ligands and the neutral Pt(II) centre containing only two ligands. The carbene ligand *trans* to the bithienylene bridge, coordinated to the positive

Pt(II) atom, is unique, while the two carbene ligands *trans* to each other are identical. The carbene ligands in the upfield region, despite having different ligands *trans* to them, have similar chemical shifts for the benzene protons as reflected by the fairly well-resolved doublet for the *o*-protons. Notable is the fact that the protons in the *p*-position of the triscarbene fragment are found furthest downfield. The protons for the bithienylene bridge are identified by their integration as well as their small *J*-coupling value which lie in the range of approximately 3 – 5 Hz. For **D1b**, four different protons signals are observed as doublets at 7.39, 7.28, 7.19 and 6.73 ppm.

The pentacarbene complexes containing the triarylamine carbene ligands are not as clear. **D3b** displays six doublets (two overlapping and one supported by other smaller doublets of lower intensity) which account for all the protons. The upfield signals are assigned to those belonging to the benzene protons in *o*-positions to the nitrogen atoms while the downfield peaks are assigned to the protons *ortho* to the carbene carbon and bromo substituents.

The bithienylene bridge can act as a distributor of electron density over the whole molecule which should affect chemical shifts.[20] This would further explain the differences in the chemical shift values of the protons within the bithienylene bridge of the asymmetric complexes. Further, the thiophene ring directly coordinated to the positively charged Pt(II) centre shows a large difference in the chemical shift values between the two proton signals in the ring. The difference in the two signals assigned for the protons of the thiophene ring bonded to the neutral Pt(II) centre is much smaller and are found between the two signals of the other thiophene ring. For the compounds containing the larger triphenylamine derivative carbene ligands, the bithienylene bridge protons are not always visible due to signal overlap with the many aromatic protons. In these cases, the presence of the bithienylene bridge can be confirmed from the ^{13}C NMR spectra, mass spectrometry (MS) and elemental analysis.

The ^{1}H NMR spectra of the ethoxycarbene complexes all lack the presence of a clear and well-resolved -CH_2 chemical shift for the ethoxy group. This is likely due to the proximity of the CH_2

group to the Pt(II) atom which is known to show significant coupling and peak broadening. In previously reported Pt(II) alkoxycarbene complexes the chemical shift peak of the OCH_2-group appear as a broad singlet.[21] The absence of the -CH_2 peaks in both the ^1H and ^{13}C NMR spectra for most of the complexes is likely due to too short data acquisition time during the experiments. However, the presence of the -CH_3 peak in the NMR spectra show that the expected ethoxy carbene products are obtained.

For the aminocarbene complexes increased electron density is provided to the carbene carbon by the nitrogen atom of the carbene's dimethylamine substituent, thus less stabilisation is required from the aromatic substituent of the carbene carbon. It is therefore expected that the aromatic protons on the carbene ligands will be found upfield compared to the ethoxycarbene complexes. This is observed when the data of Table 5.1 and Table 5.2 is compared. The significant electron delocalisation from the amine substituents to the carebene carbon is realised as two different signals are observed for the dimethylamine group. The dimethylamine substituent is locked into place by the π electron delocalisation from the nitrogen atom to the carbene carbon, thus forcing one methyl group to point towards the metal-complex while the other is pointing away. In all cases three sets of signals are observed for each of the complexes. They are assigned according to integration as well as chemical shift value as the ligands coordinated to a positive Pt(II) atom will appear downfield relative to the ligands coordinated to the neutral Pt(II) atom.

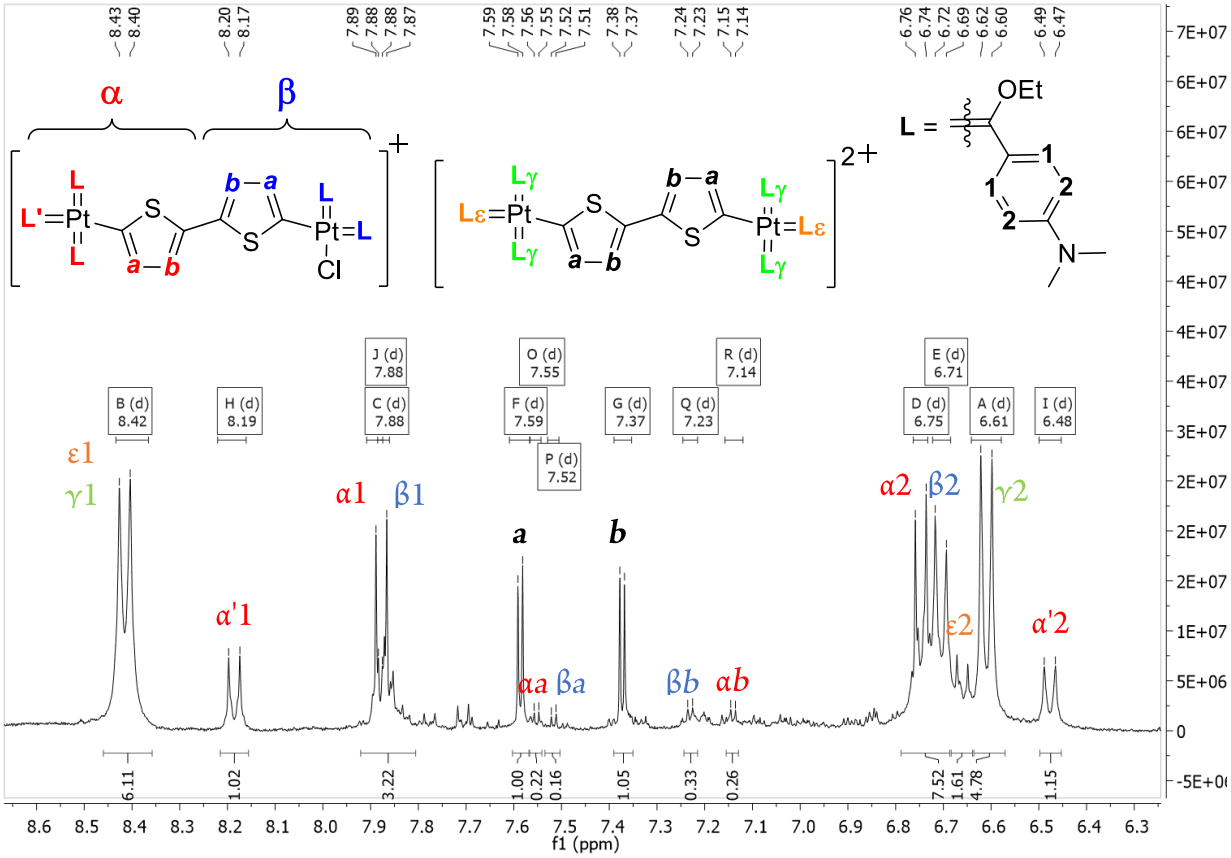

Figure 5.6. ^{1}H NMR spectrum of the aromatic region of a mixture for penta- (blue and red) and hexacarbene (green and orange) complexes of D2a in CD_2Cl_2 at ambient temperature.

The complexes containing the dimethylaniline ethoxy- and aminocarbene ligands (**D2a** and **D2b**) are the only complexes in which an additional carbene ligand coordinate to form a +2 charged symmetrically substituted compound. The complexes contain six carbene ligands and are only possible because of the smaller aniline substituent and favourable electronic properties. This class of compounds is not observed for **D1a** and **D1b**. As an example of the formation of the hexacarbene complex from the pentacarbene complex, the aromatic region of the ^{1}H NMR spectrum of **D2a**, before completion of the reaction, is shown. The aromatic signals representing each of the complexes are indicated in Figure 5.6. As for the pentacarbene complexes discussed earlier, four different doublets are observed for the bithienylene bridge at 7.55, 7.52, 7.23 and 7.14 ppm with coupling constants between 3.9 and 4.1 Hz. The sets of signals representing the three

different groups of ligands present in the pentacarbene complexes are also observed and clearly marked in Figure 5.6.

The hexacarbene complex shows a symmetrically substituted structure with three doublets representing the carbene ligands: one downfield for the protons *ortho* to the carbene carbons and two downfield signals representing the protons *ortho* to the amino substituent. There is a small difference, likely caused by H-bonding or the *trans* effect, between the *o*-protons of the ligands *trans* to each other (**Lγ** in Figure 5.6) and those *trans* to the bithienylene bridge (**Lε** in Figure 5.6). The donating properties of the nitrogen and the electron-withdrawing properties of the Fischer carbene are demonstrated by a ~2 ppm separation between the two groups of signals. Further, there is a single set of bithienylene doublets at 7.59 and 7.37 ppm (J = 3.9 Hz), indicating that the two Pt(II) centres are the same. The presence of the CH_2 signal from the ethoxy substituents is not clear and appears as a broad singlet at ~5.3 ppm. A definite peak is not observed as the solvent signal is present at this position. The broadened CH_3 peak of the ethoxy substituents is observed at 1.47 ppm.

The comparison of **D2a** and **D2b** reveals that the delocalisation of electron density from the distant NMe_2 of the aromatic substituent of the carbene, towards the carbene carbon of **D2a** is more pronounced than for **D2b**. This is evident from the increased shielding and deshielding effects of the protons in the aromatic substituents of the carbene ligands of **D2a** compared **D2b** (this topic is fully discussed in Chapter 3). The positions of the proton chemical shifts representing the bithienylene bridge reveal the overall effect of the contribution of the heteroatom as a substituent to the carbene carbon. In **D2a** the two bithienylene protons are observed at 7.59 and 7.37 ppm (J = 3.9 Hz) while those of **D2b** are observed at 7.42 and 7.13 ppm (J = 4.2 and 3.7 respectively). The clear downfield appearance of the signals in **D2a** compared to **D2b** indicates that the bridge provides more electron density to the metal centres in **D2a** than **D2b**.

^{13}C NMR Spectroscopy

Table 5.4. ^{13}C NMR chemical shift values of the ethoxy- and aminocarbene complexes of D1, D3 and D4 in CD_2Cl_2

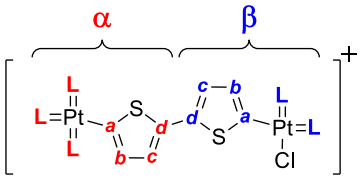

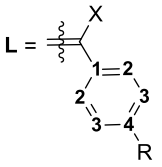

D1a: X = OEt, R = H
D3a: X = OEt, R = $N(PhBr)_2$
D4a: X = OEt, R = NPh_2
D1b: X = NMe_2, R = H
D3b: X = NMe_2, R = $N(PhBr)_2$
D4b: X = NMe_2, R = NPh_2

			Arene				Ethoxy		Bithienylene bridge			
		Carb	1	2	3	4	CH_2	CH_3	a	b	c	d
D1a	α	n.o.	151.6	136.0	129.1	132.6	n.o.*	14.5	n.o.	133.9	129.9	n.o.
	α'	n.o.	n.o.	138.0	129.5	132.6	n.o.*	14.5				
	β	207.4	150.3	132.9	126.6	129.4	n.o.*	14.8	n.o.	125.5	122.6	n.o.
D3a	α	237.0	154.3	133.1	127.5	145.9	n.o.*	15.5	144.0	136.2	131.1	135.1
	α'	292.8	151.4	133.8	127.6	146.4	n.o.*	14.9				
	β	186.0	146.0	132.7	127.4	145.9	n.o.*	14.7	141.1	126.0	124.1	133.8
D4a	α	208.7	153.1	130.0	127.6	146.9	n.o.*	15.5	147.1	133.1	131.8	133.4
	α'	285.3	152.4	130.1	128.4	147.3	n.o.*	14.7				
	β	183.4	149.5	129.9	127.5	145.0	n.o.*	14.3	140.3	124.8	124.7	133.2

			Arene				Dimethylamine		Bithienylene bridge			
		Carb	1	2	3	4	NCH_3	NCH_3	a	b	c	d
D1b	α	213.3	146.7	123.8	129.3	129.7	49.6	46.3	145.1	133.3	121.2	133.9
	α'	239.0	159.2	129.0	128.1	132.7	50.1	45.4				
	β	169.4	145.3	122.9	128.5	129.2	48.0	44.5	134.1	130.9	123.7	127.3
D3b	α	213.6	152.7	133.2	128.2	146.0	49.7	46.5	145.7	132.7	122.0	133.5
	α'	238.3	157.6	133.2	127.9	147.7	50.5	45.1				
	β	169.9	151.9	132.8	126.9	145.0	47.9	44.6	133.9	130.1	122.7	126.5
D4b	α	213.2	156.5	130.3	124.4	148.3	49.6	44.6	146.6	132.0	121.4	131.4
	α'	n.o.	156.3	133.0	125.4	148.9	51.3	46.4				
	β	171.6	153.7	130.0	124.1	145.8	47.7	46.6	133.4	130.3	123.4	126.4

* Not observed due to $^3J_{\{Pt\}C}$ coupling

Selected ^{13}C NMR signals the ethoxy- and aminocarbene complexes of **D1**, **D3** and **D4** are listed in Table 5.4 while those of the respective complexes of **D2** are listed in Table 5.5. For a full assignment of all chemical shift values please refer to the experimental section of the chapter.

Table 5.5. ^{13}C NMR chemical shift values of D2a and D2b in CD_2Cl_2

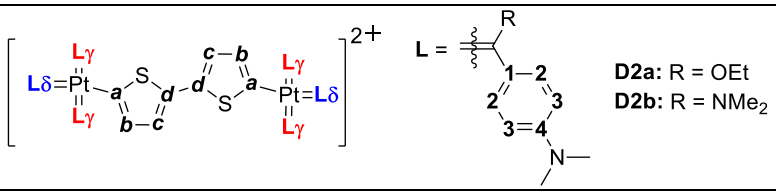

			Arene				Bithienylene bridge				OEt / NMe_2	
		Carb	1	2	3	4	*a*	*b*	*c*	*d*	X_A	X_B
D2a	γ	n.o.	156.9	132.0	110.8	125.3	155.1	137.7	130.1	130.8	77.6	14.8
	ε		157.0	134.1	111.3	125.8						
D2b	γ	213.6	151.2	134.5	111.3	126.6	150.0	143.9	123.0	129.7	40.3	40.3
	ε		151.2	134.7	111.4	126.8					46.3	44.2

An important observation for all the compounds under discussion is the absence of the Pt-C coupling constants which are expected for the complexes.[21] The reason for this is the large signal to noise ratio because of poor solubility which are always observed in the ^{13}C NMR spectra of the compounds. For this same reason, some of the *ipso*- as well as carbene carbon resonances are not observed for the complexes. This is especially prominent for the ethoxycarbene complexes.

The ^{13}C NMR spectra for the asymmetrical complexes of **D1**, **D3** and **D4** show clear duplication of signals for each carbon in the ligands as well as the eight different signals observed for the bithienylene bridge between the two metal centres. In general, the signals assigned to the ligands coordinated to the positively charge Pt(II) centre (**α**)are found downfield compared to those coordinated to the neutral Pt(II) fragment (**β**). It is further expected that the different electronic environments in which the ligands are coordinated (*trans* to a carbene ligand and *trans* to a chloro ligand while coordinated to the positive Pt(II) atom, or coordinated to the neutral Pt(II) atom) will also influence the position of signals which often lead to broadened or separate signals referring to the same position of a ligand.

From Chapter 4, it has been determined that a neutral bisethoxycarbene complex containing an aromatic substituent has a chemical shift value at approximately 240 ppm. The clear electronic influence of the bithienylene bridge is observed for the binuclear complexes as the carbene

chemical shifts for the ligands coordinated to the neutral Pt(II) atom appear at 186.0 and 183.4 ppm for **D3a** and **D4a** respectively. The clear downfield shift for the carbene signals indicate that a significant amount of electron density is contributed from the bridge – directly to the metal centre and indirectly to the carbene ligands. The two carbene ligands *trans* to each other coordinated to the positively charged Pt(II) centre have carbene chemical shift values of 237.0 and 208.7 ppm for **D3a** and **D4a**, respectively. The carbene ligand coordinated to the same metal centre, *trans* to the bithienylene bridge appear significantly downfield and have respective chemical shifts of 292.8 and 285.3 ppm for **D3a** and **D4a**. From these observations, it is evident that the position at which the ligand is coordinated and the ligand coordinated *trans* to it, greatly influence the electronic environment of each of the individual carbene ligands. It is further expected that steric interactions of the larger ligands will also influence the electronic properties of the individual ligands. The asymmetrical ethoxycarbene complexes further display prominent differences in the assignments of the bithienylene bridge carbons, thus indicating that the electron density present on the bithienylene bridge is influenced by the carbene ligands coordinated to the Pt(II) centres.

The ^{13}C NMR spectrum of the carbene and aromatic region of **D1b** is shown in Figure 5.7. The three carbene carbon signals at 238.9, 213.3 and 169.4 ppm are evident and their significant difference is evident of the difference in charge on the metal centres as well as the difference in electronic properties caused by the *trans* effect. In general, chemical shifts the **α′**-ligand, *trans* to the bithienylene bridge, are found slightly downfield compared to the **α**-ligands (*trans* to each other) while the two **β**-ligands (coordinated to the neutral Pt(II) atom) are found significantly upfield relative to the **α**-ligands. Further, three sets of methyl peaks are observed between 44.5 and 50.1 ppm, representing the peaks of the dimethylamine substituents of the carbene carbons. Eight unique signals are observed for the bithienylene bridge, again signifying the asymmetrical nature of the compound.

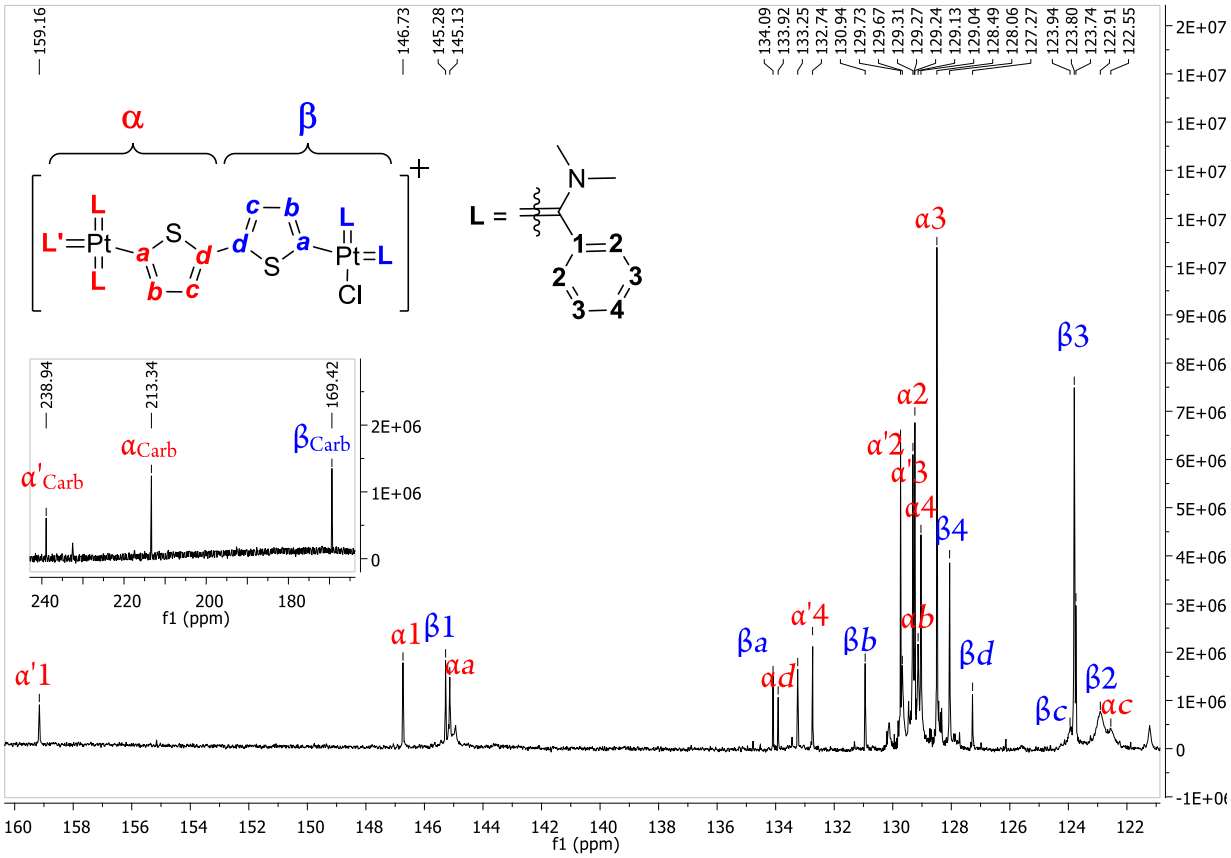

Figure 5.7. ^{13}C NMR spectrum of the carbene and aromatic region of D1b recorded in CD_2Cl_2 at room temperature

The ^{13}C NMR spectra of the aminolysed carbene complexes show that the carbene signals as well as all the signals of the bithienylene bridge are found at approximately the same values for all the asymmetrical complexes. This indicates that the complexes formed are not influenced to any extent by the aromatic group which is a substituent of the carbene carbon. All the carbene chemical shift values for the three- and two-coordinated metal centres are observed at ~213.4 and ~170.0 ppm respectively. As the eight different values assigned for the chemical shift values for the bridge also remain relatively unchanged between all the complexes, it is concluded that the two- and three-coordinated Pt(II) centres across the complexes are exposed to the same electronic environment. This further supports the initial observation that the aromatic substituent of an aminocarbene complex is not electronically affected by the carbene carbon and its bonding properties to Pt(II).

For the ethoxy- and aminocarbene complexes of **D2**, a single set of signals is observed for the bithienylene bridge. For the ethoxycarbene complex these are observed at 155.1, 137.7, 130.8 and 130.1 ppm. This is slightly downfield compared to those for the aminolysed carbene complex. Again, no carbene signal is observed for **D2a** while that of **D2b** is observed at 213.6 ppm. This value corresponds very well with those observed for the carbene signals of the aminolysed carbene ligands present on the positively charged Pt(II) centre of the asymmetrical complexes.

5.2.3 High-Resolution Mass Spectrometry

The high-resolution mass spectrometry (HRMS) of the complexes not only reveals key components present in the complexes, but also gives an indication as to the stability of the complexes and which bonds are more prone to substitution or breakage.

Upon ionisation of all complexes, the compounds were broken apart. For the ethoxy carbene complexes, fragmented ions of **D1a** and **D2a** are observed. However, there was no indication that parts of **D3a** and **D4a** had survived the ionisation process to give data fit for use in the identification of parts of the complexes. The aminolysed carbene complexes showed more stability such that molecular fragments were identified that contained several carbene ligands, a Pt(II) centre as well as the bithienylene bridge.

The fragments identified for the ethoxycarbene complexes are listed in Table 5.6. **D1a** is the only complex which has been ionised such that the two Pt(II) centres are present, separated by the bithienylene bridge, while three carbene ligands as well as a chloro ligand are coordinated between the two metal centres. In **D2a** the most prominent peak is assigned as a single metal centre containing a chloro ligand as well as three coordinated ethoxycarbene ligands. The presence of the chloro ligand comes as a surprise, at it is not expected that there should be a great amount of chloro ligand present in a pure sample of the complex. As will also be observed for the aminocarbene complexes, the ionisation environment likely contained a chlorinated component. As this is the case for all the complexes, it must be assumed that the bithienylene bridge dissociates

easily from a Pt(II) centre which then readily reacts with a chlorine atom in the surrounding environment.

Table 5.6. HRMS of the highest m/z cations obtained for D1a – D4a

	Molecular fraction	m/z Calculated	Obtained
D1a	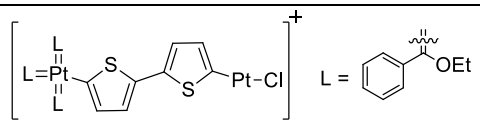 M' = $C_{35}H_{34}O_3S_2Pt_2Cl$	$[M']^+ = 987.0875$	$[M']^+ = 987.0889$
D2a	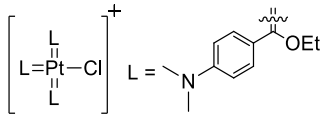 M' = $C_{74}H_{94}N_6O_6S_2Pt_2$	$[M']^+ = 762.2768$	$[M']^+ = 762.2787$
D3a*	–	–	–
D4a*	–	–	–

* No fragments identified

There are no significant fragments identified for **D3a** and **D4a** which seems to completely dissociate during the ionisation step of the measurement.

The positive fragments which have been identified for the aminocarbene complexes are all mononuclear fragments as listed in Table 5.7. A general fragmentation pattern is found from three major fragment ions observed in the spetra of **D1b** –**D4b**. It is likely that upon exposure to the harsh environment during the ionisation step of the analysis, the compounds are more prone to dissociate between the Pt(II) metal centre and the bithienylene bridge. This occurs initially at the neutral Pt(II) end of the molecule. Cleaving of the Pt–C(thiophene) bond at the biscarbene side is associated with a chlorine to replace the Pt fragment. As a result, the principal fragment ion of highest m/z value is obtained (**I** - Table 5.7). The latter loses the bithienylene part by Pt(II)–C(thiophene) bond cleavage and is replaced at the metal site by a chloro ligand (**II**). The fragmentation of a carbene ligand from **II** affords a biscarbene-chloro Pt fragment which is also a product of the first fragmentation (**I**). During the dissociation of either the metal or the bridge,

chlorine atoms present in the surroundings during the ionisation step can then easily coordinate to or react with the exposed molecular sites.

Table 5.7. HRMS of m/z fragment cations obtained for the aminocarbene complexes of D1 – D4

		I 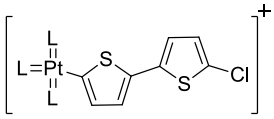		II 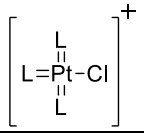		III 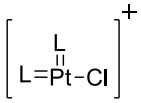	
		m/z		m/z		m/z	
		Calc	Obt	Calc	Obt	Calc	Obt
D1b	L = 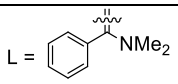	793.1765	793.1754	630.2012	630.2027	497.1069	497.1096
D2b	L = 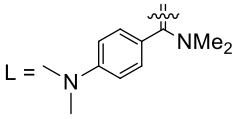	922.3031	922.3028	759.3278	759.3263	528.1943	582.1887
D3b	L = 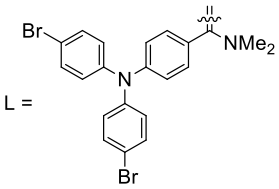	1766.8518	1766.8511	1604.8786	1604.8789	–	–
D4b	L = 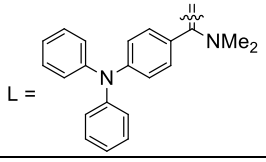	1295.3919	1295.3910	1131.4165	1131.4136	–	–

5.2.4 UV/Vis Absorption Spectroscopy

As for Chapter 4, the UV/Vis absorption spectroscopy is measured in different solvents (solvatochromism) to identify possible charge transfer processes in the complexes upon excitation. The solvents used for this study are DCM, THF and MeCN. The shift in the bands often gives an indication as to the polarity of the excited state of the complex. A ligand field (LF) transition will not necessarily cause a large shift between the spectra as charge redistribution is spatially very limited.[22] It is however expected that a charge transfer band will show a significant shift within the different solvents. Since the complexes are all positive of charge, the excited state will likely be less polar upon excitation. Thus, it is expected that neutral complexes will show

positive solvatochromism (red shift) in more polar solvents while charged complexes will probably show negative solvatochromism (blue shift) in more polar solvents.

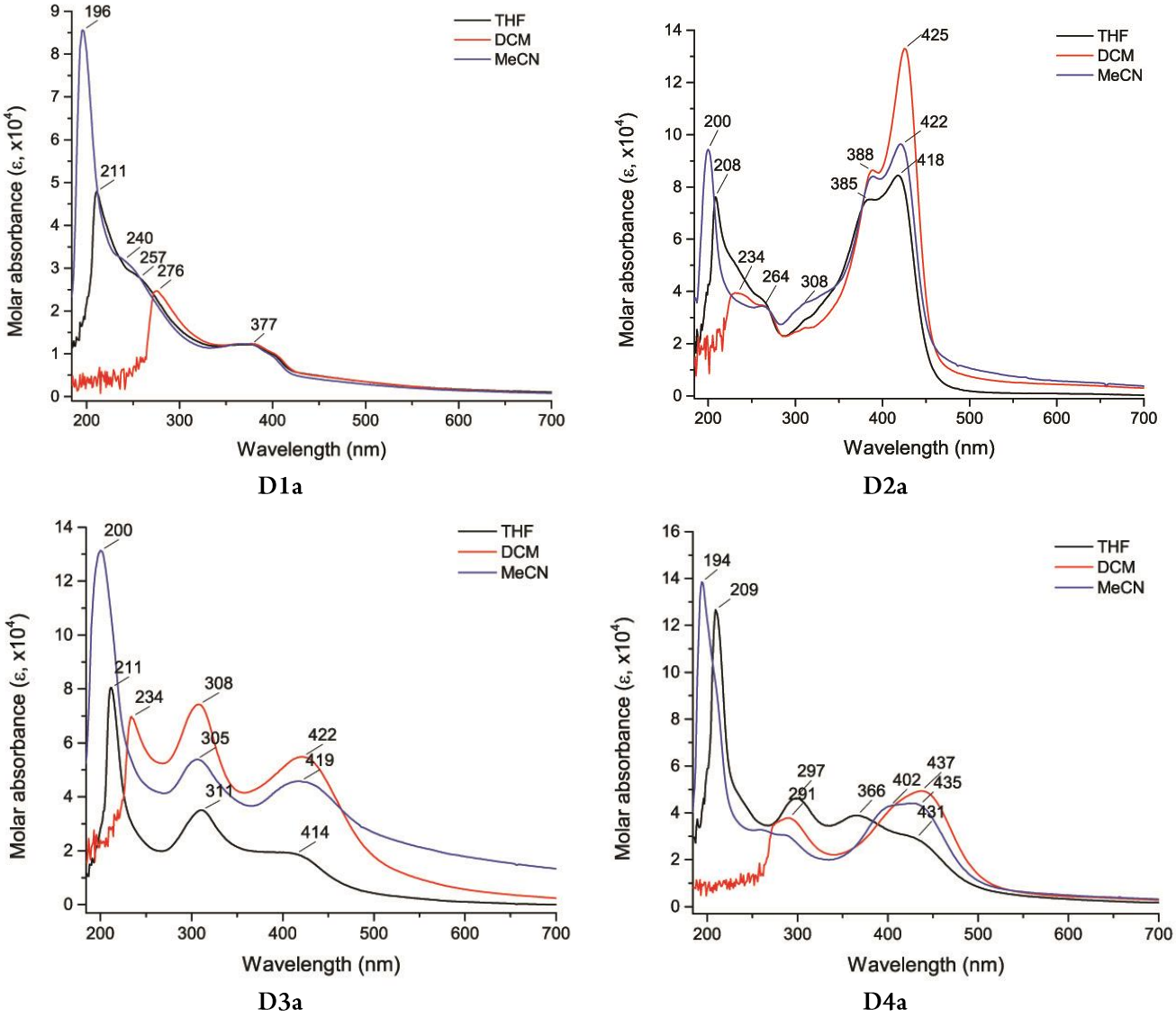

Figure 5.8. Molar absorbance spectra of D1a – D4a in THF, DCM and MeCN at room temperature

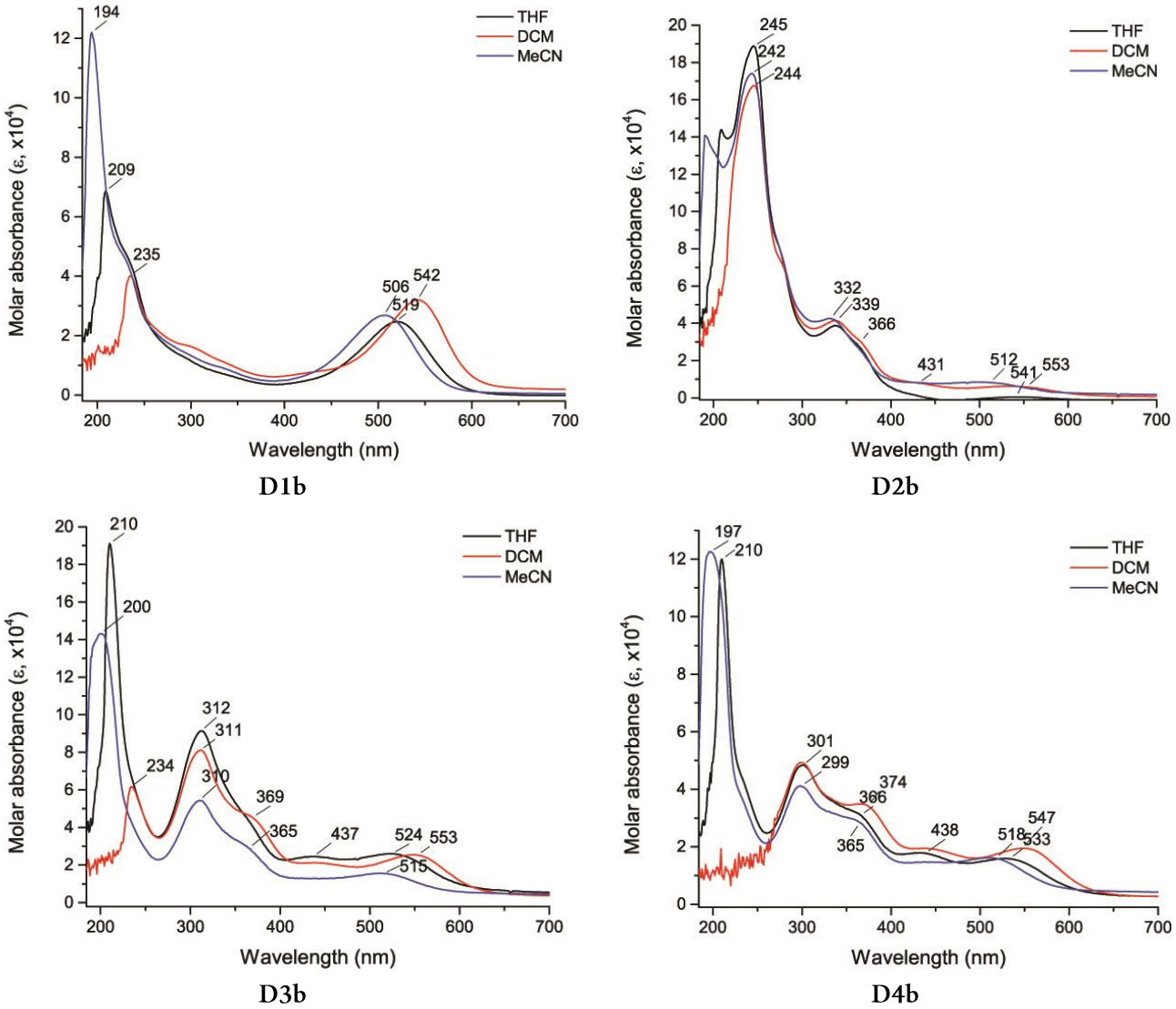

Figure 5.9. Molar absorbance spectra of D1b – D4b in THF, DCM and MeCN at room temperature

The ethoxycarbene complexes are yellow upon solvation while the aminocarbene complexes range from pink to brown. The absorbance of the ethoxy- and aminocarbene complexes in the different solvents are shown in Figure 5.8 and Figure 5.9 respectively. All the complexes show strong ligand-field (LF) transitions between 200 and 280 nm ($\varepsilon > 8x10^4\ M^{-1}.cm^{-1}$). Absorbance of lower intensity ($\varepsilon \sim 2x10^4\ M^{-1}.cm^{-1}$) is observed for the charge transfer (CT) bands at wavelengths above 340nm. At this point the CT bands cannot be assigned as it is unclear where the orbitals are found on the molecules. Multiple bands for both the LF transitions as well as the CT bands are expected for all the complexes. Each compound contains two metal centres, each with several

coordinated carbene ligands. For the ethoxy- and aminocarbene complexes of **D1**, **D3** and **D4**, the two Pt(II) centres are different in charge and the number of coordinated ligands. Further, additional bands, compared to the mononuclear carbene complexes, are expected due to the presence of the bithienylene bridge which can also contribute to charge transfer processes that occur upon photoexcitation of the complexes.

As observed in the absorbance spectra of the complexes, there are multiple CT bands visible in each spectrum ranging from one (**D1a** and **D1b**) to three bands for the large complexes (**D3a**, **D3b**, **D4a** and **D4b**). This does not only show that these complexes undergo multiple CT processes, but also that the processes occurring during excitation are quite complex.

Table 5.8. Charge transfer (CT) bands for the D Series complexes in different solvents at room temperature

Ethoxycarbene complexes				Aminocarbene complexes			
	Solvent				Solvent		
	THF	CH_2Cl_2	MeCN		THF	CH_2Cl_2	MeCN
D1a	377	377	377	**D1b**	519	542	506
D2a	308	308	308	**D2b**	339	339	332
	355	358	358		355	355	355
	418	425	422				
D3a	311	308	305	**D3b**	312	311	310
	414	422	419		–	369	365
					437	448	–
					524	553	515
D4a	366	–	402	**D4b**	366	374	365
	431	437	435		438	440	–
					533	547	518

In general, the aminocarbene complexes (**D1b**, **D2b**, **D3b** and **D4b**) show CT bands at longer wavelengths than the ethoxycarbene complexes. The CT bands are listed in Table 5.8. The bands listed are those found above 300 nm where significant shifts are observed upon solvation in different solvents and those that contribute to the emission experiments at 298 and 77 K (*vide infra*).

5.2.5 *Steady-State Emission Spectroscopy*

For some years, binuclear Pt(II) complexes have been studied in order to investigate metal-metal interactions during photoexcitation of the complexes. There are several studies that show that emissive properties of such complexes containing a flexible bridge can be manipulated or enhanced under certain conditions.[7,11,23–25] There are however, not many examples that investigate the photophysical properties of binuclear complexes where a rigid bridge connects two Pt(II) centres. For the complexes that do exist, it is evident that multicomponent emission is observed either as short-lived π-π* ligand-based transitions or longer-lived MLCT transitions which often show phosphorescence.[26,27] It is further also observed that different emissive pathways are followed at different temperatures.[7]

The complexes currently under investigation contain several strong σ-donating and π-accepting ligands. Under these circumstances, it is expected that there will be a significant interaction between the carbene ligands and the Pt(II) valence d-electrons. Further, the metal is expected to have a significant contribution to the valence shell of the ligands (some, if not all). Should this be the case, the presence of the metal will allow for excitons to reach spin-forbidden triplet states and phosphorescence is expected for the complexes as excitons return to the ground state. The two Pt(II) centres in the complexes are linked via a bithienylene bridge that is σ-bonded to each of the metals. There are several examples where it has been shown that in such cases, there is not a strong interaction between the valence d-d* orbitals of the metal and the π-cloud of the bridge and thus no heavy metal effect is observed.[28–30] With the information that is currently available for the complexes under investigation, the extent of the interaction between the bridge and the metal centres is not evident.

The statements above, make it clear that the emission for the complexes is expected to be complex as there are two metal centres to which several Fischer carbene ligands are coordinated as well as a bithienylene bridge which is also known as a good hole conductor. To simplify this study, the focus will remain on the emission spectroscopy of the complexes recorded in THF at 298 K.

Table 5.9 and Table 5.10 list the peak maxima of the absorbance, excitation and emission bands for the ethoxy- and aminocarbene complexes, respectively, at 298 and 77 K. The Stokes shift (between excitation and emission spectra) for the 298 K measurements are shown in wavenumbers. It further displays the multicomponent lifetimes (τ) of the emission (determined by fitting a time-dependent exponential decay function to the emission at a certain wavelength), and the fractional intensities of the decay components. Finally, it shows the quantum yields (Φ) for the complexes, determined by using an integration sphere at 298 K.

Blue multicomponent emission is observed for all the complexes with lifetimes between 0.6 and 8.9 ns, indicating fluorescence. Excitation and emission spectra have also been recorded at 77 K in MeTHF (which can be found in the Appendix of the thesis), but will only be used to investigate and explain the different emissive processes that are observed at room temperature. All steady-state photoluminescent spectra of the ethoxy- and aminocarbene complexes are shown in Figure 5.10 and Figure 5.11, respectively. The ethoxy- and aminocarbene complexes will be discussed separately after which a general comparison will follow.

Ethoxycarbene complexes

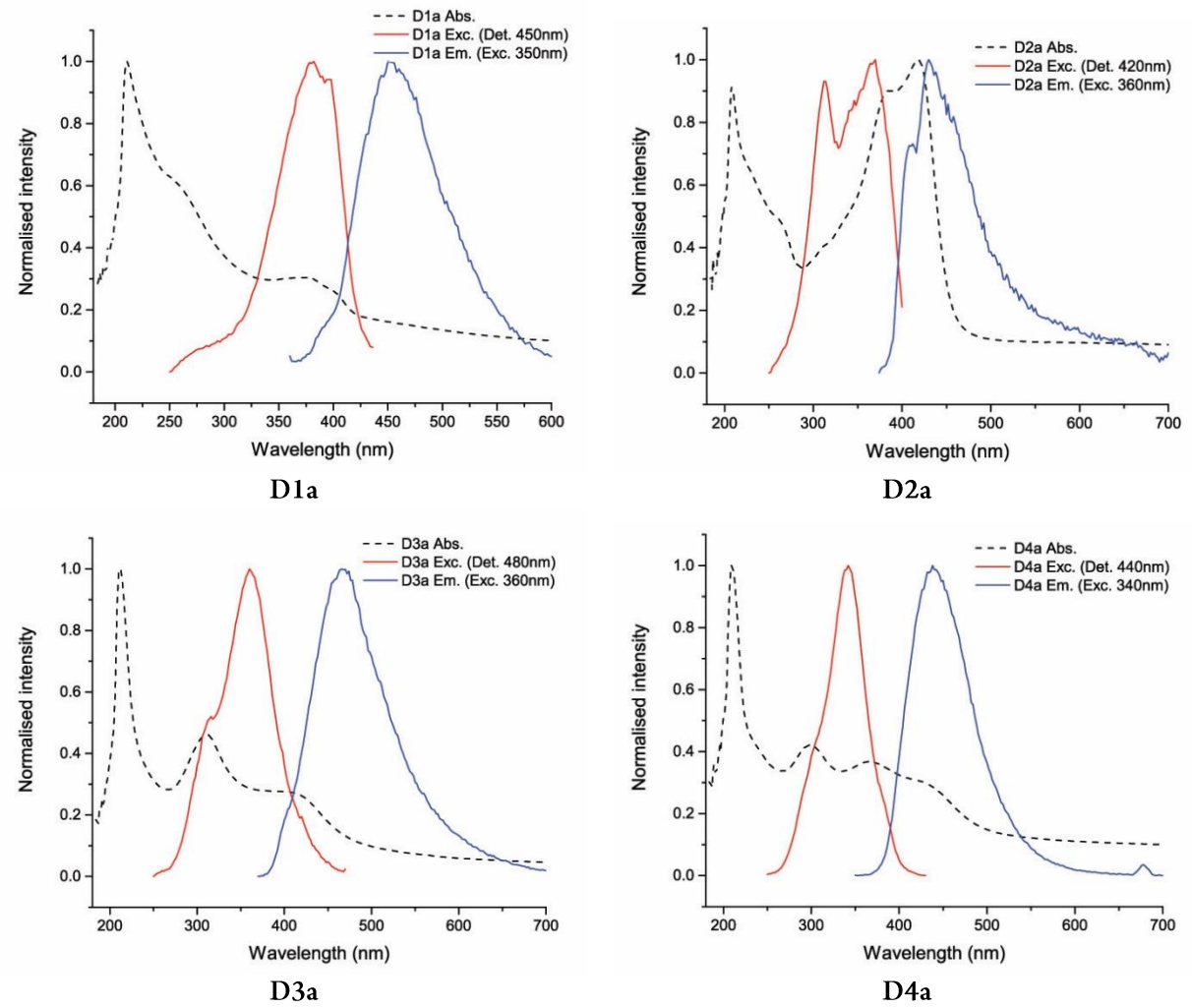

Figure 5.10. Absorbance, excitation and emission spectra of the ethoxycarbene complexes of D1 – D4 at 298K in THF

In **D1a** two-component emission is observed between 400 and 600 nm with lifetimes of 2.5 and 0.6 ns. There is a small degree of absorbance observed at these wavelengths. The excitation band leading to the emission, has a λ_{max} of 382 nm and falls directly over the shoulder band of the absorbance spectrum observed between 320 and 400 nm. The slight overlapping of the emission with the absorbance spectrum indicates that some of the fluorescence being observed originates from the first excited singlet state (S_1). The Stokes shift falls above what is expected for fluorescence with a value of 4054 cm^{-1}. A Stokes shift of between 400 and 3000 cm^{-1} usually indicates fluorescence, while a Stokes shift of above 5000 cm^{-1} indicates phosphorescence.[31–33]

However, the short lifetimes of the emission further support that it is indeed fluorescence being observed.

Table 5.9. Absorbance (THF), Excitation and Emission spectra of D1a – D4a at 298 K (THF) and 77 K (MeTHF)

	Abs.	Exc.		Em. λ_{maz}/nm				Φ
	CT λ_{maz}/nm	λ_{maz}/nm 298 K	λ_{maz}/nm 77 K	(Stokes shift/cm^{-1}) 298 K	(τ/ns [%][a])	λ_{maz}/nm 77 K	(τ/ns [%][a])	THF 298 K
D1a	380	382	390	452 (4054)	2.5 [44]	424	25.3 [66]	0.005
			412		0.6 [56]		5.0 [34]	
						452	15.2 [29]	
							2.6 [54]	
							1.1 [17]	
						478	13.9 [44]	
							2.4 [56]	
D2a	383	312	450	430 (3771)	7.6 [38]	400	9.9 [54]	0.002
	418	370	400		1.3 [62]		1.5 [46]	
						518	5.42 [32]	
							1.5 [51]	
							0.2 [17]	
D3a	412	360	340	466 (6319)	5.2 [17]	476	15.2 [26]	0.010
			382		2.1 [46]		3.5 [60]	
			428		0.7 [37]		0.7 [14]	
						550	3.4 [72]	
							0.7 [28]	
D4a	366	342	384	438 (6409)	8.3 [24]	454	23.4 [32]	0.057
	426		430		1.4 [76]		4.0 [68]	
						572	5.9 [60]	
							2.0 [40]	

[a]Fractional intensities of decay components

The Stokes shift of **D2a** is slightly smaller than that of **D1a** (4054 and 3771 cm^{-1}). The two-component emission has lifetimes of 7.6 and 1.3 ns. The absorbance and emission spectra show some overlap between 390 and 450 nm, indicating fluorescence from the first excited state is being observed. As two-component emission is observed at these wavelengths, it is likely that the emission originates from multiple singlet states that have similar potentials. It is clear that these emissive states are not only accessed by absorption from the ground state, as the excitation for the emission occurs at shorter wavelengths. It is proposed that excitation to higher energy levels takes

place which then relaxes, via internal conversion or vibrational relaxation, to lower singlet energy levels from where emission observed. **D2a** is a symmetrical compound and both metal centres and their coordinated carbene ligands are likely contributing to the emission observed. However, this will only be fully realised upon an extensive DFT study as well as additional photophysical measurements.

The emission of **D3a** and **D4a** have similar properties than **D1a** and **D2a**, as they too display multicomponent emission with λ_{max} at 466 and 438 nm, respectively, that display lifetimes between 0.7 and 8.3 ns. For these two compounds a significantly large Stokes shift is observed (~6350 cm^{-1}) between the excitation and emission spectra, indicating that the emission likely originates mostly from higher excited states that relaxes via non-emissive pathways to lower singlet states from where emission is then observed.

Aminocarbene complexes

Figure 5.11 displays the absorbance, excitation and emission spectra of **D1b** – **D4b**. As for the ethoxycarbene complexes, Table 5.10 lists the recorded spectroscopic data of the aminocarbene complexes.

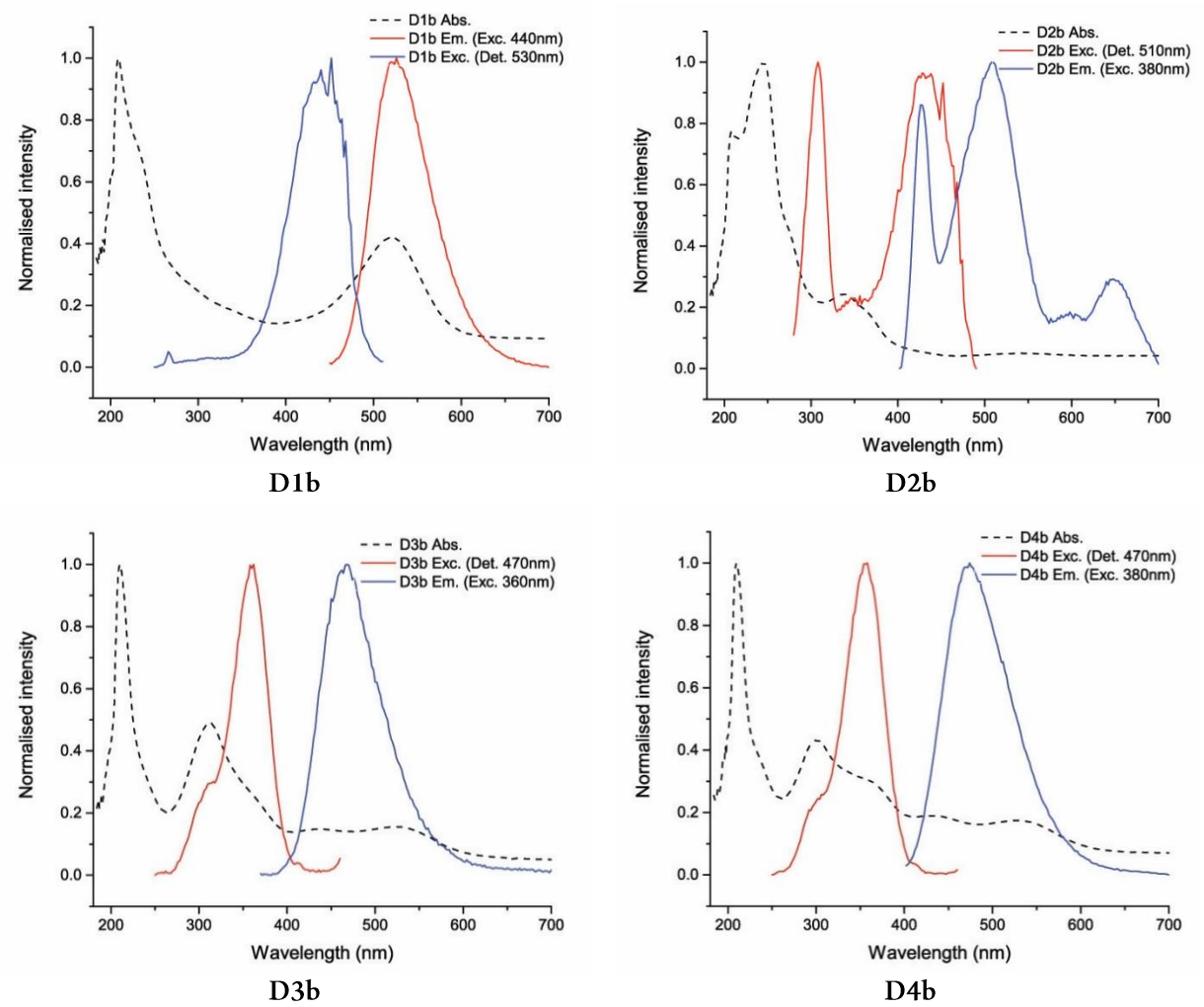

Figure 5.11. Absorbance, excitation and emission spectra of D1b and D2b at 298K in THF

D1b and **D3b** display similar photoluminescent properties as those of the ethoxycarbene complexes. These properties include multicomponent emission with large Stokes shifts (4054 and 6319 cm^{-1} for **D1b** and **D3b**, respectively) between the excitation and emission wavelengths. One of the emissive components for each complex is assigned as fluorescence from the first excited singlet state as there are some overlap between the emission and the absorbance spectrum at the shorter wavelengths while the other components originate from different singlet energy levels. It is again proposed that the emissive states are accessed through high energy excitation to high singlet energy levels. The excitons reach the emissive states through non-radiative pathways from where emission is then observed as the exciton returns to the ground state.

Table 5.10. Absorbance (THF), Excitation and Emission spectra of D1b – D4b at 298 K (THF) and 77 K (MeTHF)

	Abs.	Excitation		Emission λ_{maz}/nm				Φ
	CT λ_{maz}/nm	λ_{maz}/nm 298 K	λ_{maz}/nm 77 K	(Stokes shift/cm^{-1}) 298 K	(τ/ns [%][a])	λ_{maz}/nm 77 K	(τ/ns [%][a])	THF 298 K
D1b	517	440	422	526 (3716)	1.5 [14]	478	4.8 [11]	0.014
			500		0.5 [86]		2.3 [89]	
						554	23.8 [63]	
							4.9 [37]	
D2b	335	380	370	428 (2951)		416	11.4 [16]	0.000
		428	442	508 (6631)	3.3 [38]		1.9 [84]	
			530		0.5 [62]	500	13.1 [45]	
				648 (10884)			1.9 [55]	
						568	26.2 [62]	
							6.6 [38]	
D3b	312	310	320	468 (6410)	7.1 [16]	478	13.3 [31]	0.014
	357	360	368		3.0 [75]		2.8 [69]	
	438		450		0.7 [9]	508	17.2 [51]	
	529		544				2.7 [49]	
						582	22.2 [69]	
							4.7 [31]	
D4b	366	374	312	472 (5552)	8.9 [100]	502	16.8 [31]	0.020
	434		368				3.6 [69]	
	529		470			584	14.7 [63]	
							2.7 [37]	

[a]Fractional intensities of decay components

D2b is the only complex that show multiple excitation and emission peaks at room temperature. The emission peaks are sharp and well defined and are caused by high energy (300 nm) and lower energy excitation (390 – 490 nm). The latter's excitation band falls directly over the first sharp emission band. Another broad emission peak between 450 and 570 nm is observed which is assigned as fluorescence as the two-component emission at these wavelengths have lifetimes of 0.5 and 3.3 ns. **D2b** shows weak absorbance at 541 nm in THF: the absorbance peak is slightly more prominent in DCM and MeCN than THF (Figure 5.9). This absorbance band likely represents the HOMO–LUMO transition, as it is expected to be the lowest energy transition. Thus, the emission observed with a λ_{max} of 508 nm is assigned as fluorescence from the first excited

singlet state. The emission observed at shorter wavelengths (λ_{max} = 428 nm) is also assigned as fluorescence which originates from a singlet state of high energy (higher than the first singlet state). As the emission band and excitation wavelengths for the lower energy emission show direct overlap, it suggests that ground state excitation to this singlet state leads to the lower energy emission. The lower energy emission (observed at longer wavelengths) originates from multiple singlet states – also assigned as fluorescence as the lifetimes of the emissive components are short. It is clear that the compound has multiple singlet states at different potentials from which emission is observed.

In a similar case, emission originating from multiple emissive sites on several diamine dithiolated Pt(II) complexes has been reported by the research group of Eisenberg and observed at different temperatures.[34]

The excitation and emission spectroscopy of **D4b** at 298 K roughly matches that of **D3b** with the exception that the emission consists out of a single component with a lifetime of 8.9 ns. The lifetime of the emission observed between 400 and 590 nm (λ_{max} = 473 nm) is long for fluorescence, but as the emission observed is lying over two absorbance bands, it is likely that fluorescence is indeed being observed. The lowest energy absorbance band (likely the HOMO–LUMO transition) is slightly red-shifted relative to the emission peak with a λ_{max} of 532 nm. As for all other complexes, the emission originates upon excitation between 280 and 400 nm. The excitation falls over an absorbance band (λ_{max} = 300 nm) and its shoulder band, indicating that the compound is excited from the ground state to an S_n excited state. The excitons likely reach the emissive state via vibrational relaxation.

General Comparison

The 77 K excitation and emission spectra recorded for both ethoxy- and aminocarbene complexes in MeTHF are noted in Table 5.9 and Table 5.10 and the spectra can be found in the Appendix. Important aspects of the spectra recorded at 77 K include: additional multicomponent emissive processes are observed for all complexes which appears red-shifted in addition to the emission

observed at 298 K. Janssen published an example of a perylenediimide dimeric aggregate which displays different emission patterns at different temperatures. For the specified complexes, they found that different decay channels are being followed at different solvent temperatures.[35] Haines further emphasised temperature dependent emission by illustrating that emission occurs from a different site of a Pt(II) complex ("trap-site") when the temperature falls below 100 K.[36] These examples show that it is possible for different emission pathways to be followed at different temperatures which is proposed as to why different emissive processes are observed at different temperatures for the ethoxy- and aminocarbene complexes of **D1 – D4**.

As an example, the emission at 77 K of **D3a** is shown in Figure 5.12. The excitation band, at 77 K, for the additional emissive process lies over the emission band observed at 298 K (250 – 500 nm), thus indicating that the additional emission is observed upon excitation of any given complex from the ground state to S_1 and emissive states at similar energy levels. Given that the lifetimes observed for the additional emissive process is slightly longer at 77 K (especially for the aminocarbene complexes) than those observed for the emission at 298 K, it is possible that phosphorescence is being observed at 77 K. The lifetimes are much shorter than expected for phosphorescence of Pt(II) complexes which still casts doubt as to whether the emission originates from an excited

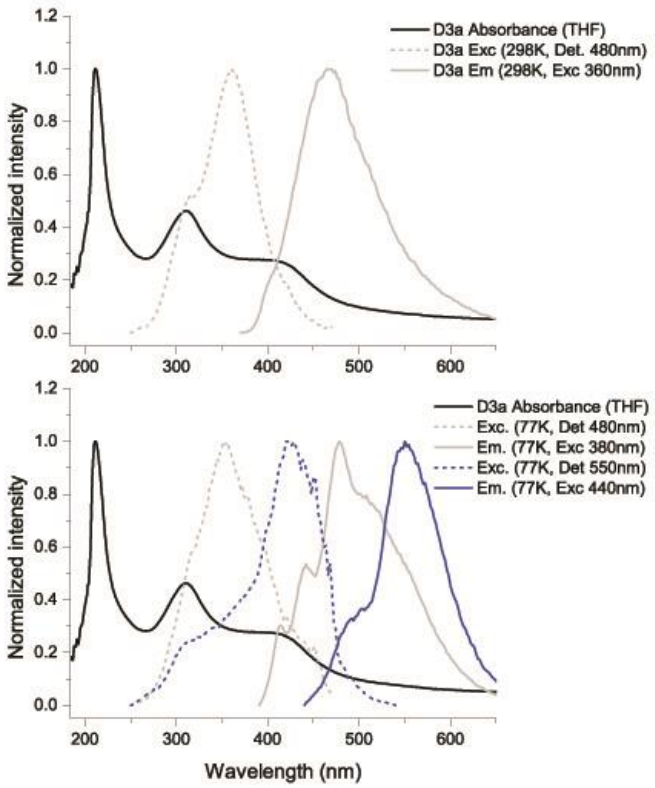

Figure 5.12. Absorbance, excitation and emission spectra for D3a at 298 K/THF (top) and at 77 K/MeTHF (bottom)

singlet or triplet state. It is necessary to add that the longest absorbance wavelength represents the smallest (lowest) allowed energy transition – the HOMO → LUMO transition. There are no spin-allowed energy levels below S_1 from where the emission can originate. Therefore, the emission originates either from spin-forbidden triplet energy levels or from excitons at higher energy singlet states that do not necessarily return to the ground state (S_0), but rather to a "trap-site" (S_n). It is clear, however, that the lifetime of the emission is short which indicates that the latter statement is more viable. The same observations are made for all the complexes at 77 K and shows that additional emissive state/s are accessed at cold temperatures.

When 298 K absorption and emission spectra the ethoxy- and aminocarbene complexes are compared, charge transfer bands in the absorption spectra for the aminocarbene complexes are observed at longer wavelengths than those of the ethoxycarbene complexes. In effect, this shows that the HOMO–LUMO gap of the aminocarbene complexes are narrower than those of the ethoxycarbene complexes. At 298 K there is no significant difference between the emission observed for the different complexes as excitation to the presumably S_1 state, does not necessarily lead to emission at room temperature. The difference in the emission spectra between the different carbene complexes is realised in the emission spectra at 77 K. Further, as solely fluorescence is observed in the emission spectroscopy, there is no indication that the metal participates in excited state processes. In Chapter 4, it was clear that the Pt(II) centre had a significant contribution to the delayed fluorescence observed at both 298 K and the phosphorescence observed at 77 K. It is evident from the emission for the binuclear complexes, that only emission from excited singlet states are observed at room temperature. For both the ethoxy- and aminocarbene complexes, the emission originates from an emissive state which can likely be assigned to the S_1 state. It is evident for all complexes, that the S_1 state is not reached upon excitation from $S_0 \rightarrow S_1$, but rather by excitation from $S_0 \rightarrow S_n$ which then reaches S_1 through vibrational relaxation. This reasoning will explain the large Stokes shift between the excitation and emission for each complex. With the data currently available, it is not possible to conclusively state

from where the emission originates, but the multicomponent nature of the emission could indicate that it is ligand based.

D2a and **D2b** are the only two symmetrical compounds analysed, each containing six coordinated carbene ligands. The differences in the emission spectra between these two complexes and the asymmetrical complexes are firstly observed in their absorbance spectra. **D2a** has a large molar absorbance in the region where the charge transfer bands for the ethoxycarbene complexes are observed (350 – 450 nm). **D2b** on the other hand has a very low molar absorption for its charge transfer bands (500 – 600 nm) compared to the asymmetrical aminocarbene complexes. **D2a** and **D2b** show excitation at short wavelengths (high energy transitions) as well as higher energy emission. The most prominent difference between the symmetrical and asymmetrical complexes are their low quantum yields of 0.002 and 0.000 respectively. **D2a** and **D2b** both have a prominent excitation band in the spectra at 298 K at 308 and 312 nm respectively. This band is assigned as the π–π^* transition of the bithienylene bridge. A similar complex which has phosphine ligands coordinated to the Pt(II) instead of carbene ligands has been published by Sonogashira in 1992.[17] The recorded absorbance spectrum of the compound in cyclohexane has $\pi \rightarrow \pi^*$ transition for the bithienylene bridge between 300 and 400 nm while the MLCT band has a considerably weaker molar absorbance at ~412 nm. Even if the $\pi \rightarrow \pi^*$ transition of the bithienylene bridge is observed, fluorescence back to the ground state from the transition is not observed, but rather emission from a much lower singlet energy level, probably reached through vibrational relaxation. As the band is only observed for **D2a** and **D2b**, it is evident that the symmetrical nature of the complexes allows for some of the emission observed.

In Table 5.11 the rate constants of the observed emission for the complexes are listed: τ_{comp} is calculated from the different lifetime decay values and their contributing intensity to the emission observed at λ_{max} ($\tau_{comp} = k_1\tau_1+k_2\tau_2+$etc., where k is the fractional intensity of the lifetime component and τ is the lifetime). The radiative rate constants for the complexes (k_r) are smaller than the non-radiative rate constants (k_{nr}), indicating that the emission is not the main process by

which excitons return to the ground state. As there is no indication of any phosphorescence observed for the compounds at 298 K, it is postulated that the alternative pathway by which the excitons return to the ground state is via a non-emissive triplet state pathway. Once the excitons pass through the ISC process to a spin-forbidden triplet state, the excitons return to the ground state through a process other than emission.

Table 5.11. Luminescence properties of the ethoxy- and aminocarbene complexes of D1 – D4 at 298 K in THF

	λ_{max}[a] (nm)	Φ[b]	τ_{comp}[c] (ns)	k_r[d] (s^{-1})	k_{nr}[e] (s^{-1})
D1a	452	0.005	1.44	$3.482x10^5$	$6.929x10^7$
D2a	430	0.002	3.70	$5.414x10^4$	$2.702x10^7$
D3a	466	0.010	2.11	$4.742x10^5$	$4.694x10^7$
D4a	438	0.057	3.06	$1.865x10^6$	$3.086x10^7$
D1b	526	0.014	0.64	$2.188x10^6$	$1.541x10^7$
D2b	508	0.000	1.56	0.000	0.000
D3b	468	0.014	3.45	$4.059x10^5$	$2.859x10^7$
D4b	472	0.020	8.90	$2.247x10^5$	$1.101x10^7$

[a] Emission maximum. [b] Quantum yield at 298 K in THF. [c] Average emission lifetimes. [d] Radiative rate constant calculated with $k_r = \Phi/\tau_{comp}$. [e] Nonradiative rate constant was calculated using $k_{nr} = k_r(1 - \Phi)/\Phi$

Comparing the different carbene ligands present in the asymmetrical complexes, there is no clear pattern observed in emission lifetimes or energy of the transitions observed. The emission spectra for the ethoxy- and aminocarbene complexes of **D1** – **D4** at 298 K originates from spin-allowed transitions alone. The low quantum yields of the emission and obvious lack of phosphorescence support the fact that the Pt(II) centres do not play a role in the emission observed. The emission at 298 K originates from singlet states that have similar potentials. These states are not directly accessed upon excitation of the ground state, but are reached through vibrational relaxation from higher energy singlet states.

Further, the emission observed is likely ligand based as multiple emissive processes are being observed.

As it is clear that emission is not the main pathway which is followed upon photoexcitation of the Series D complexes, it is necessary to investigate the ultra-fast processes that occur upon excitation of the compounds. This is partly achieved by means of femtosecond transient absorption spectroscopy.

5.2.6 Femtosecond Transient Absorption Spectroscopy (TAS)

Femtosecond pump-probe TAS studies are performed on the ethoxy- and aminocarbene complexes of **D1** – **D4** in THF at 298 K. From the emission spectroscopy, it has been established that no phosphorescence of the compounds is observed at room temperature which is expected for compounds containing a Pt(II) atom. Even at 77 K, the emission lifetimes are too short to imply that phosphorescence is observed. As the quantum yields of the emission for the compounds are low, it becomes evident that emission is not the primary pathway by which excitons return to the ground state upon photoexcitation. TAS will allow for the investigation of ultra-fast processes (events) that occur upon photoexcitation of the compounds at room temperature other than emission. This may include excited state absorption (ESA), intersystem crossing (ISC), stimulated emission (SE), product absorption (PA), charge transfer (CT) and charge separated (CS) states. The ultra-fast technique will also allow for a detailed description of the processes that can only be postulated by emission studies alone.

Please refer to the TAS section of Chapter 4 for a more detailed description of the technique. As in Chapter 4, the EADS – obtained using a sequential model in the Global Fit Analysis (using Glotaran[37]) – will be analysed. The TAS of the ethoxy- and aminocarbene complexes will be generally discussed as the respective groups of complexes display similar properties. Unique spectral data for each complex can be found in the Appendix.

Ethoxycarbene complexes

Upon photoexcitation of **D1a**, the first component is observed at τ_0 (no time delay between the pump and probe pulse) in Figure 5.13 and has a lifetime of 35.15 (±0.06) ps. At short wavelengths ΔA falls below zero indicating that either SE or a GSB is being observed. The fluorescence (spontaneous emission) of the compound occurs at the same wavelengths, however, the emission experiments have established that the shortest component for the fluorescence has a lifetime of 0.6 ns and is therefore not observed. Further, the lifetime of SE is expected in the same order of fluorescence as it originates from the same singlet energy state/s. The short lifetime of the first component will then support that a GSB is being observed at the short wavelengths. At longer wavelengths, strong absorbance between 464 and 600 nm, with a λ_{max} at 546 nm and a shoulder band at slightly shorter wavelengths, is observed. As the component is observed at τ_0, ESA is expected, however, the lifetime of the component suggests that the absorbance of a more stable intermediate or product is being observed (PA). To support this statement, the GSB is also observed, indicating that the product which is showing absorbance has ground state absorbance at ~440 nm. Another important observation for the PA, is that the peak is broad and likely represents more than one product which is similar but spatially separated, but this can only be confirmed with TD-DFT calculations.

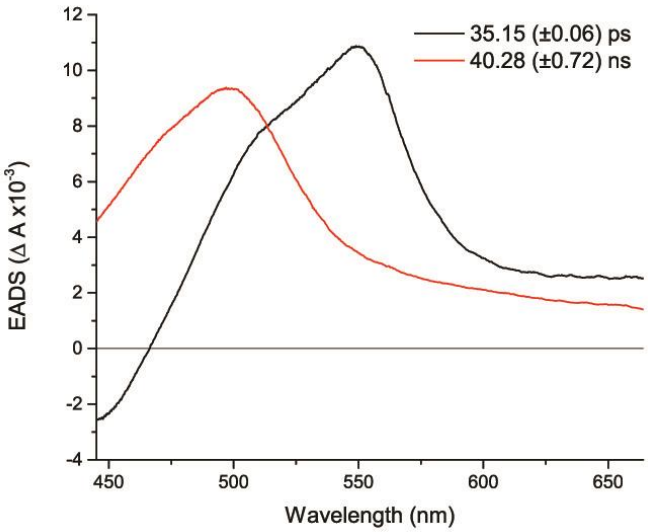

Figure 5.13. EADS for D1a in THF at 298 K

As the PA of the first component is already observed at τ_0, there is no indication of whether the stable intermediate is a singlet or triplet state product. ESA (or triplet absorption (TA)) for all the other complexes are observed (*vide infra*) with an approximate lifetime of 1.5 ps which supports

that an ISC process has taken place. For Pt(II) complexes, the lifetime of ESA for the first triplet state (T_1) falls between 0.15 and 10 ps.[38–40] On the assumption that an ISC process has occurred in **D1a**, the PA observed at τ_0 is ascribed to a stable triplet product. The component decays into an even more stable triplet state product, indicating that it is most likely a charge transfer product.

The second component in Figure 5.13 has a lifetime of 40.28 (±0.72) ns and is observed from a time delay of 35.15 ps and longer. This product shows strong absorbance with λ_{max} at 498 nm and a tail which shows absorbance at longer wavelengths. With the data currently available, the product that forms remains speculative and can be a stable triplet state, charge separated state or an isomerised state.[41]

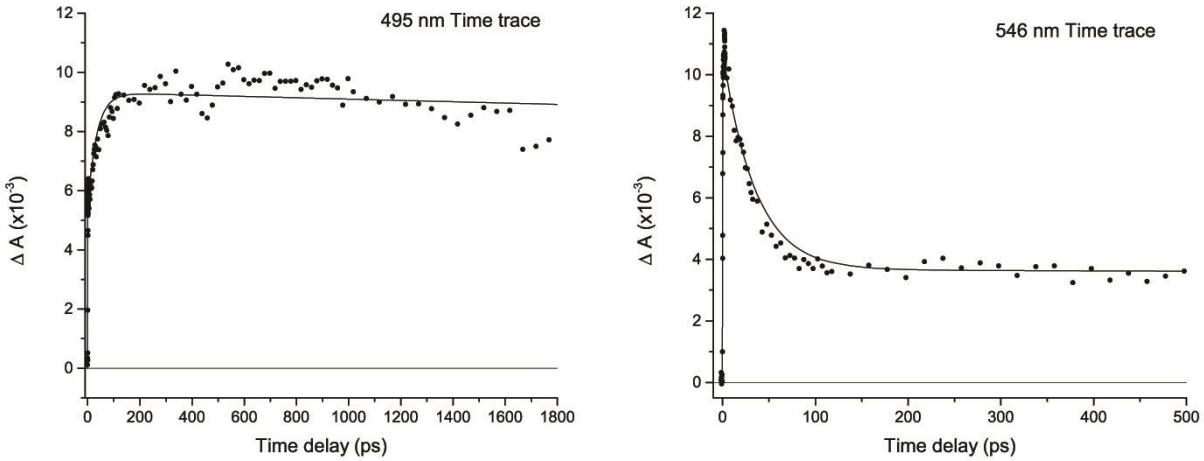

Figure 5.14. D1a TAS 495 nm (left) and 546 nm (right) time traces recorded in THF at 298 K with a 387.5 nm excitation pulse

The recorded (scatter plot) and the corresponding Global Fit Analysis (line plot) of the time traces for **D1a** at 495 nm and 546 nm are shown in Figure 5.14. The 495 nm time trace (left) represents the growth of the last long-lived product with a lifetime of 40.28 (±0.72) ns. The initial growth of the product is well represented by the model; however, its lifetime shows a large margin of error. Despite this observation, the Global Fit Analysis gives an approximate estimation for the lifetime of this product. As it is evident that the lifetime of this product falls beyond the scale of the instrumentation, nanosecond TAS will need to be performed to accurately measure its

lifetime. [The nanosecond TAS is not performed in this project as a laser that functions on a different timescale is required, i.e., different instrumentation is required.]

The time trace at 546 nm shows the formation and decay of what has been assigned the CT state. It is clear that the calculated model describes the data well at this wavelength as the excitation and decay is clearly represented. It is further evident that a long-lived product shows absorbance at long time delays (> 100 ps) and is observed beyond the timescale of the instrumentation.

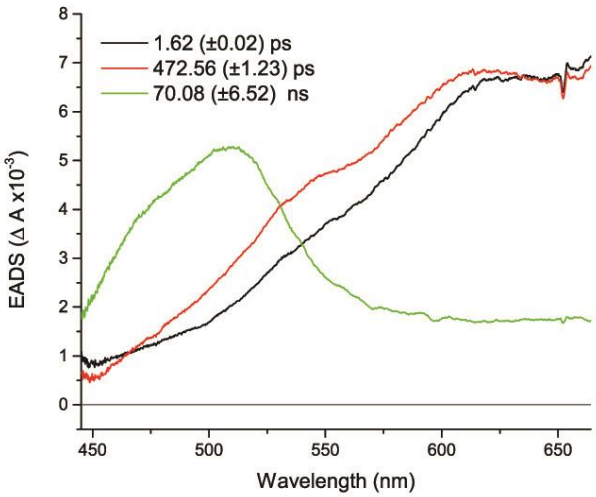

Figure 5.15. EADS for D3a in THF at 298 K

A more general example is that of **D3a** (EADS displayed in Figure 5.15), which shows the previously mentioned ESA of the proposed triplet states in its first transient (τ_0) which has a lifetime of 1.62 (±0.02) ps. The second transient displays very similar absorbance to that of the first, but has a significantly longer lifetime of 472.56 (±1.23) ps. It is postulated that this transient represents the PA which was observed in the first transient of **D1a**, which likely represents a CT state as it decays into another product. The final transient is observed from time delays of 473 ps and shows strong absorbance with a λ_{max} of 510 nm and has a lifetime of 70.08 (±6.52) ns.

The 504 nm time trace of **D3a** is shown in Figure 5.16. It represents the long-lived final product that forms upon excitation. It is evident that the product forms slowly and still illustrates growth at a time delay of 1800 ps. The lifetime calculated through the Global Fit Analysis will again only be an approximation as it is clear that the lifetime of this product is significantly long.

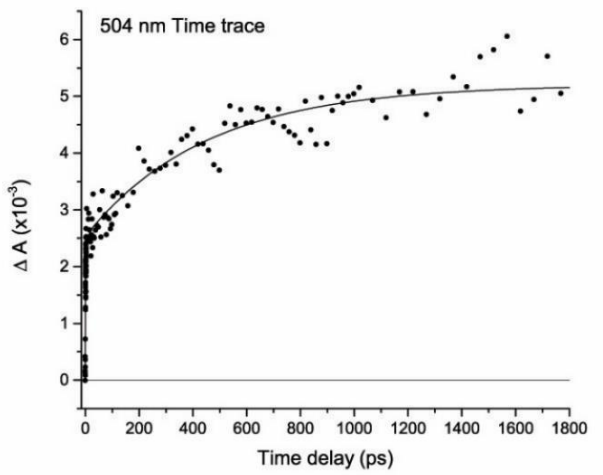

Figure 5.16. D3a TAS 504 nm time trace recorded in THF at 298 K with a 387.5 nm excitation pulse

The TAS of **D2a** and **D4a** follow a similar pattern as that of **D3a**. Their TAS spectra and corresponding time traces can be found in the Appendix.

In the EADS of **D2a** – **D4a**, ESA is observed which is ascribed to triplet state absorbance as Pt(II) facilitates a fast ISC due to its strong spin-orbit coupling.[3,42] Further, lifetimes recorded for the transients closely match those of the ESA for other recorded Pt(II) complexes (references can be found in the TAS discussion of **D1a**). The ESA of **D1a** is not observed presumably because the excited triplet state immediately decays into a more stable triplet CT state. The absorbance of the CT states is observed as a broad, featureless band for most of the complexes. A possible reason for this observation is the presence of multiple but similar products that are separated in space. This is possible, if the products that form are based on the carbene ligands. As each complex contains multiple, spatially separated, yet similar carbene ligands, the excited state products that form on each ligand are expected to be similar. In each case these triplet states will show decay as another more stable triplet state product is formed. The final product for all the ethoxycarbene complexes, shows absorbance at ~500 nm and displays a lifetime in the ns timescale.

The lifetimes, as determined from the Global Fit Analysis, for all observed transients are listed in Table 5.12. The triplet ESA, the CT state and the final stable product are denoted as T_{ESA}, T_{CT}

and T_{SP}, respectively. It is important to note that the lifetime of T_{CT} is reported in ps while that of T_{SP} is reported in ns.

Table 5.12. Lifetimes of T_{ESA}, T_{CT} and T_{SP} of D1a – D4a obtained from Global Fit Analysis using a sequential model

	Triplet state lifetime		
	T_{ESA} (τ/ps)	T_{CT} (τ/ps)	T_{SP} (τ/ns)
D1a	n.o.	35.15 (±0.06)	40.28 (±0.72)
D2a	1.50 (±0.01)	95.62 (±0.37)	28.85 (±1.51)
D3a	1.62 (±0.02)	472.56 (±1.23)	70.08 (±6.52)
D4a	1.52 (±0.03)	237.92 (±2.64)	8.41 (±0.24)

With the information currently available, it is not possible to state what the stable product is. The stable product of **D3a** shows the greatest stability as its lifetime is the longest, followed by **D1a**, **D2a** and **D4a** with respective lifetimes of 70.08 (±6.52), 40.28 (±0.72), 28.85 (±1.51) and 8.41 (±0.24) ns. The reason for the difference in the lifetimes cannot be determined until the identity of the stable product has been confirmed.

Aminocarbene complexes

The TAS spectra of the aminocarbene complexes generally follow the same trends as the ethoxycarbene complexes with one important exception: the long-lived transient presumably represents two products that show absorbance. SE is also observed for all the aminocarbene complexes at longer time delays.

For example, **D3b** displays three components. The first component has a lifetime of 2.53 (±0.02) ps which is assigned as ESA. The second component displays a lifetime of 20.25 (±0.08) ps in which two different products show absorbance. In the final component, PA for the same products is presumably still observed, however, SE is also present between 425 and 559 nm. The SE matches the 7.1 ns component of the fluorescence which was observed in the steady-state emission spectroscopy with a λ_{max} at 468 nm.

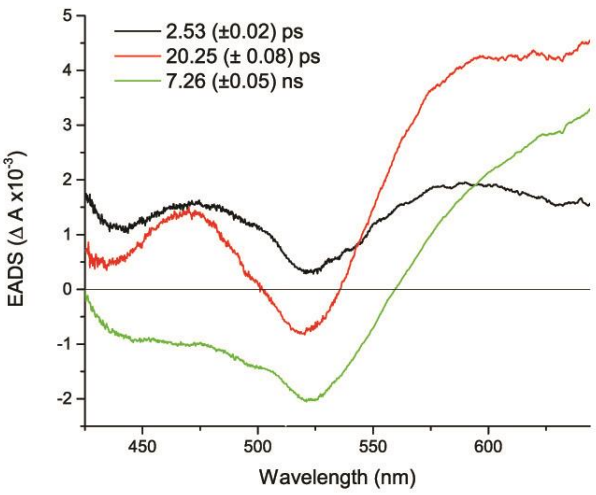

Figure 5.17. EADS for D3b in THF at 298 K

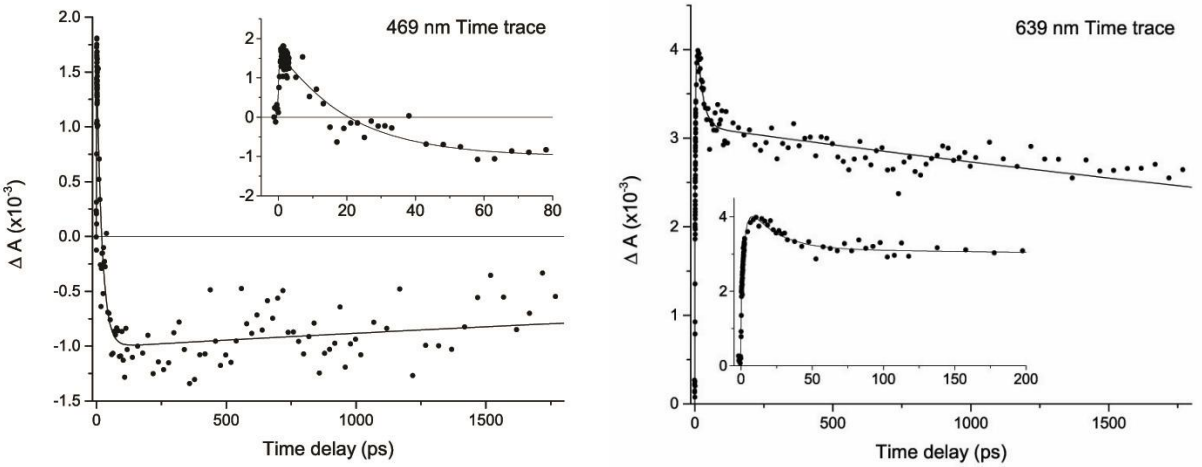

Figure 5.18. D3b TAS 469 nm (left) and 639 nm (right) time traces recorded in THF at 298 K with a 387.5 nm excitation pulse

The time traces of **D3b** at 469 and 639 nm are shown in Figure 5.18. The 469 nm time trace shows the ESA an PA ($\Delta A > 0$) at the shorter time delays as well as the SE ($\Delta A < 0$) at the long time delays. The 639 nm time trace allows for the differentiation of two separate products, which has been assigned as a single product, showing absorbance: a short-lived component and a long-lived component. It is likely that the short-lived component (lifetime = 20.25 (±0.08) ps) is a CT state that decays into the long-lived product with a lifetime of 7.26 (±0.05) ns. From this, it is evident

that the 2nd and 3rd transient display absorbance of products of different lifetimes but similar absorbance.

In a comparative analysis of the aminocarbene complexes, it is evident that ESA is observed after which two PA absorbance bands are observed. The products represented by these bands are best observed for **D3b** and not necessarily clear for all complexes as the final and persistent products display similar absorbance bands which display lifetimes in the nanosecond timescale. In most cases, there are a small shift of the PA bands at longer wavelengths between the proposed CT state and that of the final, long-lived product.

As the two persistent products display the same lifetime, it is proposed that the two products represent a charge separated (CS) state that forms upon 387.5 nm excitation of the aminocarbene complexes. Their EADS spectra can be found in the Appendix. As two distinct products show absorbance, the two polarons represented by each of the absorbance bands are likely spatially separated.

The lifetimes for the triplet ESA (T_{ESA}), triplet CT (T_{CT}) and the triplet charge separated state (T_{CS}) for all the aminocarbene complexes are shown in Table 5.13. The EADS for all the aminocarbene complexes can be found in the Appendix. The lifetimes for the T_{ESA} and T_{CT} are reported in ps while that of T_{CS} are reported in ns.

Table 5.13. Lifetimes of T_{ESA} and T_{CS} of D1b – D4b obtained from Global Fit Analysis using a sequential model

	T_{ESA} (τ/ps)	T_{CT} (τ/ps)	T_{CS} (τ/ns)
D1b	1.56 (±0.01)	n.o.	539.33 (±207.07)
D2b	2.70 (±0.02)	13.32 (±0.13)	3.64 (±0.02)
D3b	2.53 (±0.02)	20.25 (±0.08)	7.27 (±0.05)
D4b	1.12 (±0.01)	21.87 (±0.14)	19.45 (±0.79)

As the T_{CS} of **D1b** has such a large standard error, it is not possible to state that it is the lifetime of the charge separated state. As for the ethoxycarbene complexes, nanosecond TAS is required for an accurate determination of the lifetime of T_{CS} of the aminocarbene complexes.

Comparing the products that form upon excitation, it is evident that similar products are formed for all complexes. The same long-lived triplet state products show absorbance with peak maxima at approximately 484 and 630 nm. As the products are the same, it is likely that the two different polarons are present on the bithienylene bridge and the carbene carbon as these groups are the same for all the complexes. The aromatic substituents of the carbene carbons are not expected to play a role as the carbene carbon receives its stabilisation mainly from its metal and amine substituents.

General comparison: Ethoxy- and Aminocarbene complexes

It has been established that for both the ethoxy- and aminocarbene complexes, long-lived triplet excited state products form on photoexcitation and charge redistribution. PA for a single stable product is observed for the ethoxycarbene complexes, however, every complex also displays featureless absorption towards longer wavelengths. The aminocarbene complexes show absorbance for two stable products with the same lifetime. It has been further proposed that the PA representing the two products is indicative of a triplet CS state where the polarons are spatially separated.

As the ethoxy- and aminocarbene complexes are relatively similar, it is expected that the ethoxycarbene complexes will also be able to form the CS state on photoexcitation. If the stable product that forms for the ethoxycarbene complexes at long time delays, represents one polaron, it is likely that the broad, featureless PA observed towards longer wavelengths represents the second polaron. Assuming that this is indeed the case, the positions for the two polarons are on the bithienylene bridge and one of the carbene ligands.

Oligothiophenes have been shown to readily donate electrons to their surroundings upon photoexcitation and are able to carry a charge [43–46]. Several independent sources place the absorbance of an unsubstituted positive bithiophene radical at approximately 400 nm[47–50] while substituted bithiophene polarons show absorbance at ~600 nm and above, depending on the degree of conjugation between the bithiophene group and its substituents.[43,51]. Further, carbene carbons are known to accommodate negative charges.[52–55] Thus, it is proposed that the positive and negative polarons reside on the bithienylene bridge and the carbene carbon of one of the ligands coordinated to a Pt(II) centre, respectively.

The peak assignments and lifetimes (in nanoseconds) of the two polarons that make up the CS state in the ethoxy- and aminocarbene complexes of **D1** – **D4** are listed in Table 5.14.

Table 5.14. Peak positions and calculated lifetimes (Global Fit Analysis) for the CS state components for D1 – D4

Complex	Product 1 (λ_{max}/nm)	Product 2 (λ_{max}/nm)	Lifetime (τ/ns)
D1a	496.52	n.o.	40.284 (±0.717)
D2a	496.95	n.o.	28.852 (±1.513)
D3a	507.89	n.o.	70.083 (±6.521)
D4a	503.92	n.o.	8.410 (±0.241)
D1b	483.33	627.17	539.327 (±207.072)
D2b	463.19	644.29	3.643 (±0.021)
D3b	470.83	>643.22	7.265 (±0.051)
D4b	465.00	634.22	19.450 (±0.789)

From the data, it is evident that the ethoxycarbene complexes generally have longer lifetimes than those of the aminocarbene complexes. **D1b** has an exceptionally long calculated lifetime, but the standard error for this value is too large to conclusively state that it does indeed have a long lifetime. Several examples in literature of mono- and binuclear Pt(II) complexes in which triplet CS states form, show that the expected lifetimes of these states are anywhere between 0.7 and 180 ns.[45,56–58] This shows that the calculated lifetimes for all the complexes are well within the expected bounds for triplet CS states of Pt(II) complexes.

A summary of the important points that have been observed using TAS of **D1** – **D4**:

- There is little indication as to the position of the HOMO and LUMO.
- The λ_{max} for the ESA for the ethoxycarbene complexes are all different from each other. Thus, the ESA likely originates on the carbene ligands.
- The λ_{max} for the ESA for the aminocarbene complexes remain relatively constant. Thus, the ESA for the aminocarbene complexes is likely based on the carbene carbons and their stabilising amine substituents.
- The final aspect to consider is the absorbance of the proposed two polarons observed for the aminocarbene complexes remains relatively constant for all complexes. It is postulated that the negative polaron will form on the carbene carbon due to its electron withdrawing character while the positive polaron will be situated on the bithienylene bridge. As the carbene carbon, Pt(II) centres and bithienylene bridge of the amino complexes are not significantly influenced by their aromatic substituents, it is expected that the energy levels – occupied and empty – will have approximately the same potentials between all the complexes. Thus, no significant differences are expected in the absorbance bands for the polarons situated on the carbene carbon and bithienylene bridge of the aminocarbene complexes. This is indeed observed.

All data has been interpreted assuming only one Pt(II) centre per binuclear complex is excited at any one time. Most of the complexes are asymmetric with one Pt(II) centre having a positive charge and three coordinated carbene ligands while the other Pt(II) centre has two coordinated carbene ligands and one chloro ligand (neutral charge). It is expected that the positively charged Pt(II) centre and its coordinated ligands will have the greatest contribution to the valence electrons of the complex and thus will be the photoactive part of the complex. This is further supported by **D2a** and **D2b**, which are both symmetrical with three coordinated carbene ligands at both metal centres, and show no significant photophysical differences from the asymmetrical complexes.

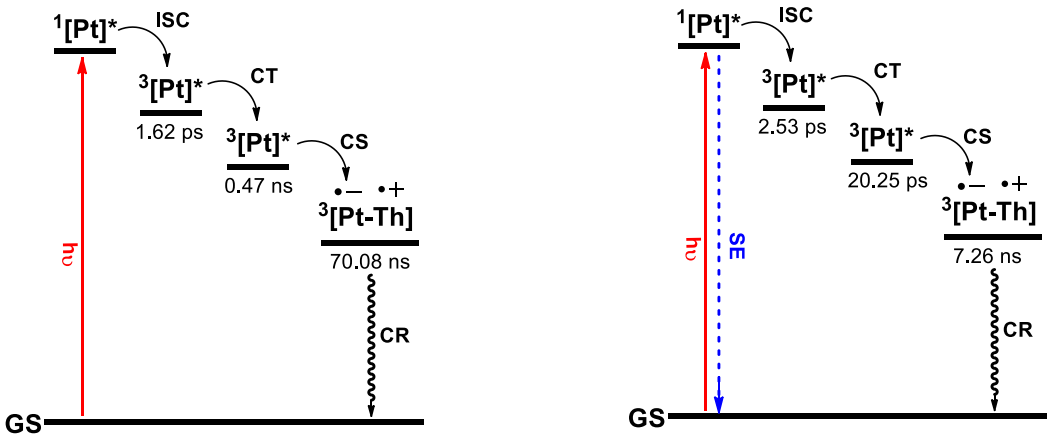

Figure 5.19. Energy level diagram that represents the processes that occur upon excitation of the C3a (left) and C3b (right). GS: ground state, SE: stimulated emission, ISC: intersystem crossing, CT: charge transfer, CS: charge separation and CR: charge recombination

As examples, the proposed excited state products and lifetimes observed during the femtosecond TAS of **C3a** and **C3b** are schematically shown in Figure 5.19. It becomes evident that it is essential to understand what kind of CT processes occur to fully understand the mechanisms of formation of the proposed CS states. In the next section of the study, mononuclear and binuclear complexes will be compared as to have a more complete understanding as to the processes that occur upon photoexcitation at 387.5 nm.

5.3 Experimental

UV/Vis absorption and Emission spectroscopy

Please see the experimental section of Chapter 4.

Transient absorption spectroscopy (TAS)

Please see the experimental section of Chapter 4.

General synthesis

Please refer to the General synthesis section of Chapter 4.

Synthesis of Pt(COD)Cl$_2$

Please refer to the synthesis of Pt(COD)Cl$_2$ in Chapter 4.

Synthesis of 2,5'-substituted dithienylene derivatives of platinum[17]

Pt(COD)Cl_2 and 2,5'-bis(trimethylstannyl)-5-(2'-thienyl)thiophene was suspended in 40 mL CH_2Cl_2 and allowed to reflux for four hours. The cream suspension immediately started to form a yellow precipitate. After four hours, the solvent was evaporated *in vacuo* and the yellow product was washed with hexane five times. The bright yellow product was allowed to dry under vacuum. Yield = 85 %.

Synthesis of W carbene (B Series) complexes ***B1a – B4a*** *and* ***B1b – B4b***

Please refer to the synthesis of the tungsten(0) pentacarbonyl carbene complexes in Chapter 3.

Synthesis of the D Series complexes: ***D1a – D4a*** *and* ***D1b – D4b***

Please refer to Table 5.15 for individual reagent variables and yields for each complex. n mmol (excess) of a specified tungsten carbene complex was dissolved in 20 ml dried dichloromethane. m mmol [Cl(COD)Pt(μ-2,5'-C_4H_2S-C_4H_2S)Pt(COD)Cl] as well as excess dried KPF_6 was suspended in the same mixture while stirring under inert conditions. The reaction was allowed to reflux for 24 hours under inert conditions after which the reaction was allowed to cool down to room temperature. The product mixture was canula-filtered and then titrated into rapidly stirring hexane (for the ethoxy carbene complexes) or diethylether (for the amino carbene complexes). The titration was repeated until no more colour was observed in solution. The yellow (ethoxy-carbene complexes) or pink (amino-carbene complexes) product was allowed to dry *in vacuo* for two hours.

Table 5.15. Series D experimental variables and yields

Complex	W carbene complex (n)	(COD)ClPt–⟨S⟩–⟨S⟩–PtCl(COD)	Product colour	Yield	% Yield
D1a	**B1a** 0.882 mmol (0.404 g)	0.110 mmol (0.0930 g)	Yellow	0.0980 g	63.4
D2a	**B2a** 0.800 mmol (0.378 g)	0.0500 mmol (0.0421 g)	Yellow	0.0561 g	58.8
D3a	**B3a** 0.400 mmol (0.313 g)	0.0500 mmol (0.0421 g)	Yellow	0.0372 g	24.5
D4a	**B4a** 0.333 mmol (0.208 g)	0.0416 mmol (0.0350 g)	Yellow	0.0238 g	25.5
D1b	**B1b** 1.09 mmol (0.493 g)	0.136 mmol (0.1145 g)	Pink	0.0480 g	25.2
D2b	**B2b** 0.800 mmol (0.378 g)	0.0500 mmol (0.0421 g)	Pink	0.0633 g	66.6
D3b	**B3b** 0.400 mmol 0.313 g	0.0500 mmol (0.0421 g)	Pink	0.0560 g	37.0
D4b	**B4b** 0.216 mmol (0.135 g)	0.270 mmol (0.0230 g)	Pink	0.0162 g	2.68

Characterisation

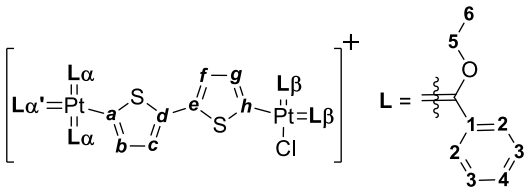

Figure 5.20. NMR assignments of D1a

D1a: $C_{53}H_{54}O_5S_2PPt_2ClF_6$. ^{1}H NMR ($CD_2Cl_2$, 400 MHz) δ 7.87 (dd, *J* = 8.4, 1.4 Hz, 4H, H**α2**), 7.83 (dd, *J* = 8.4, 1.4 Hz, 2H, H**α'2**), 7.75 (s (br), 4H, H**β2**), 7.64 (ddd, *J* = 8.4, 7.3, 1.4 Hz, 3H, H**α4** and H**α'4**), 7.55 (dd, *J* = 6.9, 7.0 Hz, 2H, H**α'3**), 7.54 (dd, *J* = 7.5, 7.4 Hz, 4H, H**α3**), 7.52 – 7.51 (m, 2H, H**β4**), 7.44 (s (br), 4H, H**β3**), 7.37 (d, *J* = 3.7 Hz, 1H, H***g***), 7.16 (d, *J* = 4.0 Hz, 1H, H***f***), 6.91 (d, *J* = 3.7 Hz, H***c***), (H***b***, n.o.), (H**α5**, H**α'5** and H**β5**, n.o.), 1.54 (s *(br)*, 15H, H**α6**, H**α'6** and H**β6**). ^{13}C NMR (CD_2Cl_2, 101 MHz) δ (Cα_{Carb}

and C***α'***$_{Carb}$, n.o.), 207.4 (C**β**$_{Carb}$), (C***α'*****1**, n.o.), 151.6 (C***α*****1**), 150.3 (C**β1**), 138.0 (C***α'*****2**), 136.0 (C***α*****2**), 133.9 (C***b***), 132.9 (C**β2**), 132.6 (C***α*****4**), 132.6 (C***α'*****4**), 129.9 (C***c***), 129.5 (C***α'*****3**), 129.4 (C**β4**), 129.1 (C***α*****3**), 126.6 (C**β3**), 125.5 (C***g***), 122.6 (C***f***), (C***a***, C***d***, C***e*** and C***h***, n.o.), (C***α*****5**, C***α'*****5** and C**β5**, n.o.), 14.8 (C**β6**), 14.5 (C***α*****6** and C***α'*****6**). ESI-MS (2.8 V, positive mode, *m/z*): calcd for [M - 2L*]$^+$ 987.0875; found 987.0889. *L = carbene ligand.

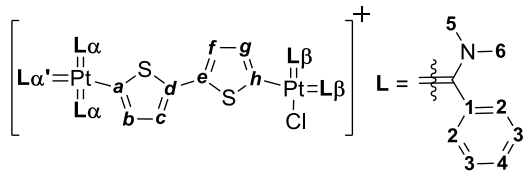

Figure 5.21. NMR assignments of D1b

D1b: $C_{53}H_{59}N_5S_2PPt_2ClF_6$. ^{1}H NMR ($CD_2Cl_2$, 600 MHz) δ 7.70 (dd, *J* = 8.2, 7.5 Hz, 1H, H***α'*****4**), 7.63 (dd, *J* = 7.7, 7.5 Hz, 2H, H***α*****4**), 7.50 – 7.45 (m, 8H, H***α'*****2**, H***α*****2**, and H***α'*****3**), 7.39 (d, *J* = 5.2 Hz, 1H, H***b***). 7.33 (dd, *J* = 8.0, 7.5 Hz, 4H, H***α*****3**), 7.28 (d, *J* = 3.7 Hz, 1H, H***g***), 7.25 (dd, *J* = 8.8, 7.2 Hz, 2H, H**β4**), 7.19 (d, *J* = 4.5 Hz, H***f***), 7.11 (s (*br*), 4H, H**β3**), 7.03 (d, *J* = 7.7 Hz, 4H, H**β2**), 6.73 (d, *J* = 5.0 Hz, 1H, H***c***), 4.17 (s, 6H, H***α*****5**), 3.92 (s, 3H, H***α'*****5**), 3.55 (s, 6H, H**β5**), 3.35 (s, 3H, H***α'*****6**), 3.14 (s, 6H, H***α*****6**), 3.05 (s, 6H, H**β6**). ^{13}C NMR (CD_2Cl_2, 151 MHz) δ 239.0 (C***α'***$_{Carb}$), 213.3 (C***α***$_{Carb}$), 169.4 (C**β**$_{Carb}$), 159.2 (C***α'*****1**), 146.7 (C***α*****1**), 145.3 (C**β1**), 145.1 (C***a***), 134.1 (C***h***), 133.9 (C***d***), 132.7 (C***α'*****4**), 130.9 (C***g***), 129.7 (C***α'*****2**), 129.3 (C***α'*****3**), 129.2 (C***α*****2**), 129.1 (C***b***), 129.0 (C***α*****4**), 128.5 (C***α*****3**), 128.1 (C**β4**), 127.3 (C***e***), 123.9 (C***f***), 123.8 (C**β2**), 122.9 (C***f***), 122.9 (C**β3**), 122.6 (C***c***), 50.1 (C***α'*****5**), 49.6 (C***α*****5**), 48.0 (C**β5**), 46.3 (C***α*****6**), 45.4 (C***α'*****6**), 44.5 (C**β6**). ESI-MS (2.8 V, positive mode, *m/z*): M = [**D1b** - (Pt+2L*+Cl)], calcd for [M + K]$^+$ 798.1776; found 798.1788. *L = carbene ligand. EA: calcd C = 45.44 %, H = 4.25 %; found C = 45.25 %, H = 4.28 %.

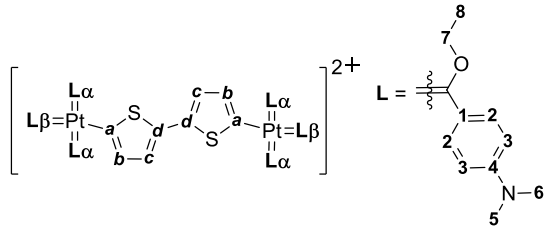

Figure 5.22. NMR assignments of D2a

D2a: $C_{74}H_{94}N_6O_6S_2P_2Pt_2F_{12}$. ^{1}H NMR ($CD_2Cl_2$, 400 MHz) δ 8.42 (d, *J* = 9.1 Hz, 12H, H***α*****2** and H**β2**), 7.59 (d, *J* = 3.9 Hz, 2H, H***b***), 7.37 (d, *J* = 3.9 Hz, 2H, H***c***), 6.66 (d, *J* = 9.1 Hz, 4H, H**β3**), 6.61 (d, *J* = 9.3 Hz, 8H, H***α*****3**), (H***α*****7** and H**β7**, n.o.), 3.19 (s, 12H, H**β5** and H**β6**), 3.12 (s, 24H, H***α*****5** and H***α*****6**), 1.57 (t, *J* = 7.1 Hz, 6H, H**β8**),

1.47 (t, *J* = 7.2 Hz, 12H, H**α8**). ^{13}C NMR (CD_2Cl_2, 101 MHz) δ (C**α**$_{Carb}$ and C**β**$_{Carb}$, n.o.), 157.0 (C**β1**), 156.9 (C**α1**), 155.1 (C***a***), 137.7 (C***b***), 134.1 (C**β2**), 132.0 (C**α2**), 130.8 (C***d***), 130.1 (C***c***), 125.8 (C**β4**), 125.3 (C**α4**), 111.3 (C**β3**), 110.8 (C**α3**), (C**β7**, n.o.), 77.6 (C**α7**), 40.6 (C**β5** and C**β6**), 40.5 (C**α5** and C**α6**), 15.2 (C**β8**), 14.8 (C**α8**). ESI-MS (2.8 V, positive mode, *m/z*): M = [Pt + 3L*], calcd for $[M + K]^+$ 763.2703; found 763.2802. *L = carbene ligand. EA: calcd C = 46.59 %, H = 4.97 %; found C = 46.52 %, H = 4.94 %.

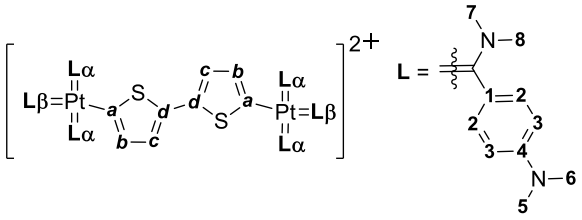

Figure 5.23. NMR assignments of D2b

D2b: $C_{74}H_{100}N_{12}S_2P_2Pt_2F_{12}$. ^{1}H NMR ($CD_2Cl_2$, 400 MHz) δ 7.42 (d, *J* = 4.2 Hz, 2H, H***b***), 7.33 (d, *J* = 8.7 Hz, 8H, H**α2**), 7.32 (d, *J* = 8.8 Hz, 4H, H**β2**), 7.13 (d, *J* = 3.7 Hz, 2H, H***c***), 6.76 (d, *J* = 9.0 Hz, 8H, H**α3**), 6.73 (d, *J* = 8.9 Hz, 4H, H**β3**), 3.73 (s, 6H, H**β7**), 3.47 (s, 6H, H**β8**), 3.13 (s, 12H, H**α7**), 3.02 (s, 12H, H**α8**), 3.00 (s, 36H, H**α5**, H**α6**, H**β5** and H**β6**). ^{13}C NMR (CD_2Cl_2, 101 MHz) δ 213.6 (C**α**$_{Carb}$), (C**β**$_{Carb}$, n.o.), 151.2 (C**β1**), 150.9 (C**α1**), 150.0 (C***a***), 143.9 (C***b***), 134.7 (C**β2**), 134.5 (C**α2**), 129.7 (C***d***), 126.8 (C**β4**), 126.6 (C**α4**), 123.0 (C***c***), 111.4 (C**β3**), 111.3 (C**α3**), 47.6 (C**β7**), 47.5 (C**α7**), 44.8 (C**β8**), 44.2 (C**α8**), 40.3 (C**α5**, C**α6**, C**β5** and C**β6**). ESI-MS (2.8 V, positive mode, *m/z*): M = [**D2b** – (Pt+2L*+Cl)], calcd for $[M + K]^+$ 925.3009; found 925.3038. *L = carbene ligand.

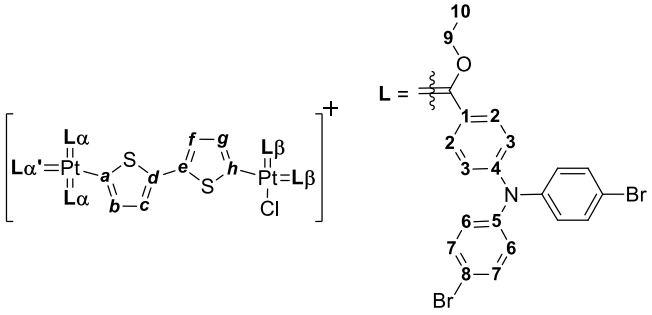

Figure 5.24. NMR assignments of D3a

D3a: $C_{113}H_{89}O_5N_5S_2PPt_2F_6ClBr_{10}$. ^{1}H NMR ($CD_2Cl_2$, 400 MHz) δ 7.61 (d, *J* = 4.0 Hz, 1H, H***b***), 7.58 (d, *J* = 8.8 Hz, 2H, H**α'2**), 7.51 (d, *J* = 8.8 Hz, 4H, H**α2**), 7.46 (dd, *J* = 8.8, 3.0 Hz, 4H, H**β2**), 7.42 – 7.29 (m, 20H, H**α7**, H**α'7** and H**β7**), 7.24 (d, *J* = 4.0 Hz, 1H, H***g***), 7.19 (d, *J* = 4.4 Hz, 1H, H***f***), 7.06 (d (br), *J* = 8.6 Hz, 10H, H**α3**, H**α'3** and H**β3**), 7.01 – 6.90 (m, 20H, H**α6**, H**α'6** and H**β6**), (H***c***, n.o.), (H**α9**, H**α'9** and H**β9**, n.o.), 1.69 (t, *J* = 7.1 Hz, 3H, H**α'10**), 1.53 (t, *J* = 7.1 Hz, 6H, H**α10**), 1.47 (t, *J* = 7.0 Hz, 6H,

H**β10**). ^{13}C NMR (CD_2Cl_2, 101 MHz) δ 292.8 (C**α'**$_{Carb}$), 237.0 (C**α**$_{Carb}$), 186.0 (C**β**$_{Carb}$), 154.3 (C**α1**), 151.4 (C**α'1**), 146.4 (C**α'4**), 146.0 (C**β1**), 145.9 (C**α4**), 145.9 (C**β4**), 145.8 (C**α'5**), 145.6 (C**α5**), 144.3 (C**β5**), 144.0 (C***a***), 141.1 (C***h***), 136.2 (C***b***), 135.1 (C***d***), 133.8 (C**α'2**), 133.8 (C***e***), 133.5 (C**α7**), 133.1 (C**β7**), 133.1 (C**α2**), 132.8 (C**α'7**), 132.7 (C**β2**), 131.1 (C***c***), 129.0 (C**α'6**), 128.6 (C**α6**), 127.6 (C**α'3**), 127.6 (C**β6**), 127.5 (C**α3**), 127.4 (C**β3**), 126.0 (C***g***), 124.1 (C***f***), 121.3 (C**α'8**), 119.8 (C**α8**), 118.1 (C**β8**), (C**α9**, C**α'9** and C**β9**, n.o.), 15.5 (C**α10**), 14.9 (C**α'10**), 14.7 (C**β10**). EA: calcd C = 44.78 %, H = 2.96 %; found C = 44.67 %, H = 2.96 %.

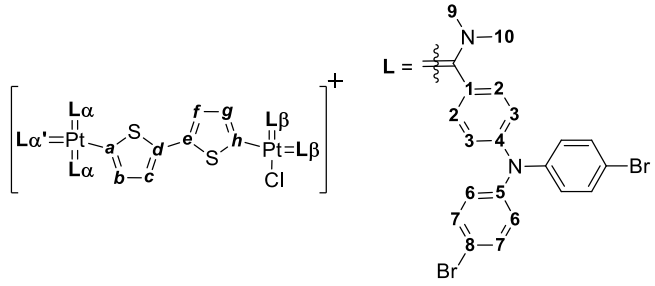

Figure 5.25. NMR assignments of D3b

D3b: $C_{113}H_{94}N_{10}S_2PPt_2F_6ClBr_{10}$. ^{1}H NMR ($CD_2Cl_2$, 400 MHz) δ 7.50 (d, *J* = 8.7 Hz, 4H, H**α2**), 7.48 (d, *J* = 4.4 Hz, 1H, H***b***), 7.46 (d, *J* = 8.7 Hz, 2H, H**α'2**), 7.43 (d (br), *J* = 8.6 Hz, 12H, H**β2** and H**α7**), 7.37 (d, *J* = 8.7 Hz, 8H, H**β7**), 7.28 (d, *J* = 8.8 Hz, 4H, H**α'7**), 7.22 (d, *J* = 3.7 Hz, 1H, H***g***), 7.17 (d, *J* = 4.6 Hz, 1H, H***f***), 7.10 (d, *J* = 8.7 Hz, 4H, H**α3**), 7.09 (d, *J* = 6.7 Hz, 4H. H**β3**), 7.06 (d, *J* = 8.8 Hz, 2H, H**α'3**), 6.99 (dd, *J* = 9.0, 2.4 Hz, 20H, H**α6**, H**α'6** and H**β6**), 6.89 (d, *J* = 5.0 Hz, 1H, H***f***), 4.18 (s, 6H, C**α9**), 3.83 (s, 3H, C**α'9**), 3.71 (s, 6H, **Hβ9**), 3.45 (s, 3H, H**α'10**), 3.23 (s, 3H, H**α10**), 3.12 (s, 6H, H**β10**). ^{13}C NMR (CD_2Cl_2, 101 MHz) δ 238.3 (C**α'**$_{Carb}$), 213.6 (C**α**$_{Carb}$), 169.9 (C**β**$_{Carb}$), 157.6 (C**α'1**), 152.7 (C**α1**), 151.9 (C**β1**), 147.7 (C**α'4**), 146.5 (C**α'5**), 146.4 (C**α5**), 146.2 (C**β5**), 146.0 (C**α4**), 145.7 (C***a***), 145.0 (C**β4**), 133.9 (C***h***), 133.5 (C***d***), 133.5 (C**α'7**), 133.2 (C**α2**), 133.2 (C**α'2**), 133.0 (C**α7**), 132.9 (C**β7**), 132.8 (C**β2**), 132.7 (C***b***), 130.1 (C***g***), 128.2 (C**α3**), 127.9 (C**α'3**), 126.9 (C**β3**), 126.8 (C**α6**), 126.7 (C**β6**), 126.6 (C**α'6**), 126.5 (C***e***), 122.7 (C***f***), 122.0 (C***c***), 117.0 (C**α8**), 116.6 (C**β8**), 166.4 (C**α'8**), 50.5 (C**α'9**), 49.7 (C**α9**), 47.9 (C**β9**), 46.5 (C**α10**), 45.1 (C**α'10**), 44.6 (C**β10**). ESI-MS (2.8 V, positive mode, *m/z*): M = [**D3b** – (Pt+2L*+Cl)], calcd for $[M + K]^+$ 1766.8508; found 1766.8511. *L = carbene ligand. EA: calcd C = 44.86 %, H = 3.13 %; found C = 45.15 %, H = 2.96 %.

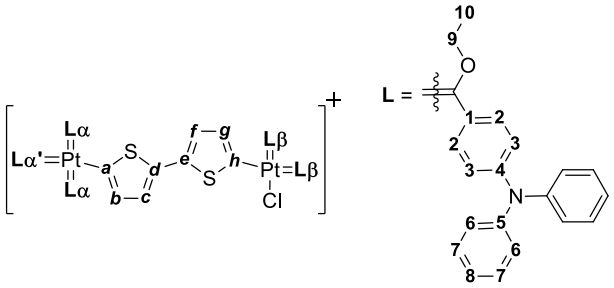

Figure 5.26. NMR assignments of D4a

D4a: $C_{113}H_{99}O_5N_5S_2PPt_2F_6Cl$. ^1H NMR (CD_2Cl_2, 400 MHz) δ 7.47 (d, J = 4.1 Hz, 1H, H***b***), 7.46 (d, *J* = 7.9 Hz, 2H, H**α'2**), 7.42 (d, *J* = 7.8 Hz, 4H, H**α2**), 7.38 (d, *J* = 7.8 Hz, 4H, H**β2**), 7.38 – 7.35 (m, 4H, H**α'7**), 7.35 – 7.30 (m, 8H, H**α7**), 7.30 – 7.27 (m, 8H, H**β7**), 7.25 (d, *J* = 3.9 Hz, 1H, H***g***), 7.22 – 7.20 (m, 4H, H**α'3** and H**α'8**), 7.20 (d (br), *J* = 7.9 Hz, 8H, H**α3** and H**α8**), 7.18 – 7.14 (m, H**β3** and H**β8**), 7.10 (d, *J* = 7.7 Hz, 4H, H**α'6**), 7.07 – 7.00 (m, 8H, H**α6**), 6.95 (d, *J* = 4.2 Hz, 1H, H***f***), 6.89 – 6.75 (m, 8H, H**β6**), 6.73 (d, *J* = 4.2 Hz, 1H, H***c***), (H**α9**, H**α'9** and H**β9**, n.o.), 1.66 (t, *J* = 7.1 Hz, 3H, H**α'10**) 1.58 (s (br), 6H, H**α10**), 1.51 (t, *J* = 7.1 Hz, 6H, H**β10**). ^{13}C NMR (CD_2Cl_2, 101 MHz) δ 285.3 (C**α'**$_{Carb}$), 208.7 (C**α**$_{Carb}$), 183.4 (C**β**$_{Carb}$), 153.1 (C**α1**), 152.4 (C**α'1**), 149.5 (C**β1**), 148.3 (C**α5**), 148.1 (C**α'5**), 147.3 (C**α'4**), 147.1 (C***a***), 146.9 (C**α4**), 145.4 (C**β5**), 145.0 (C**β4**), 140.3 (C***h***), 133.4 (C***d***), 133.2 (C***e***), 133.1 (C***b***), 131.8 (C***c***), 130.4 (C**α'7**), 130.4 (C**α7**), 130.1 (C**α'2**), 130.0 (C**α2**), 129.9 (C**β2**), 129.6 (C**β7**), 128.4 (C**α'3**), 128.0 (C**α'6**), 127.6 (C**α6**), 127.6 (C**α3**), 127.5 (C**β3**), 127.4 (C**β6**), 124.8 (C***g***), 124.7 (C***f***), 117.6 (C**α'8**), 117.0 (C**α8**), 116.9 (C**β8**), (C**α'9**, C**α9** and C**β9**, n.o.), 15.5 (C**α10**), 14.7 (C**α'10**), 14.3 (C**β10**).

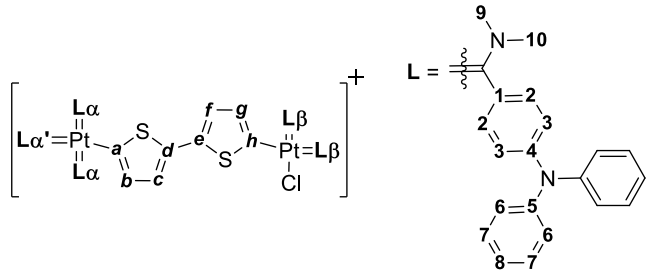

Figure 5.27. NMR assignments of D4b

D4b: $C_{113}H_{104}N_{10}S_2PPt_2F_6Cl$. ^1H NMR (CD_2Cl_2, 400 MHz) δ 7.66 (d, *J* = 8.8 Hz, 2H, H**α'2**), 7.47 (d, *J* = 4.4 Hz, 1H, H***b***), 7.41 (d, *J* = 8.5 Hz, 4H, H**α2**), 7.39 (d, *J* = 8.1 Hz, 4H, H**β2**), 7.34 (dd, *J* = 8.5, 8.0 Hz, 12H, H**α7** and H**α'7**), 7.26 (dd, *J* = 8.5, 8.4 Hz, 8H, H**β7**), 7.21 (d, *J* = 4.4 Hz, 1H, H***g***), 7.17 (d, *J* = 4.7 Hz, 1H, H***f***), 7.12 (d (br), *J* = 8.4 Hz, 20H, H**α6**, H**α'6** and H**β6**), 7.07 (dd, *J* = 7.5, 7.5 Hz, 10H, H**α8**, H**α'8** and H**β8**), 7.01 (d, *J* = 8.8 Hz, 2H, H**α'3**), 6.99 (d, *J* = 8.8 Hz, 4H, H**α3**), 6.96 (d, *J* = 8.7 Hz, 4H, H**β3**), 6.90 (s(*br*), 1H,

H***c***), 4.17 (s, 6H, H**α9**), 3.71 (s, 3H, H**α'9**), 3.46 (s, 6H, H**β9**), 3.29 (s, 6H, H**α10**), 3.13 (s, 3H, H**α'10**), 3.02 (s, H**β10**). ^{13}C NMR (CD_2Cl_2, 101 MHz) δ (C**α'**$_{Carb}$, n.o.), 213.2 (C**α**$_{Carb}$), 171.6 (C**β**$_{Carb}$), 156.5 (C**α1**), 156.3 (C**α'1**), 153.7 (C**β1**), 148.9 (C**α'4**), 148.3 (C**α4**), 147.6 (C**α'5**), 147.5 (C**α5**), 147.3 (C**β5**), 146.6 (C***a***), 145.8 (C**β4**), 133.4 (C***h***), 133.0 (C**α'2**), 132.0 (C***b***), 131.4 (C***d***), 130.3 (C**α2**), 130.3 (C***g***), 130.1 (C**α'7**), 130.0 (C**β2**), 129.9 (C**α7**), 129.8 (C**β7**), 126.4 (C***e***), 125.9 (C**α'6**), C125.6 (C**α6**), 125.5 (C**β6**), 125.4 (C**α'3**),124.4 (C**α3**), 124.1 (C**β3**), 123.4 (C***f***), 122.0 (C**α8**), 121.5 (C**α'8**), 121.4 (C***c***), 121.3 (C**β8**), 51.3 (C**α'9**), 49.6 (C**α9**), 47.7 (C**β9**), 46.4 (C**α'10**), 44.6 (C**α10**), 46.6 (C**β10**). ESI-MS (2.8 V, positive mode, *m/z*): M = [**D4b** – (Pt+2L*+Cl)], calcd for $[M + K]^+$ 1297.3898; found 1297.3887. *L = carbene ligand. EA: calcd C = 60.68 %, H = 4.69 %; found C = 60.36 %, H = 5.13 %.

5.4 References

[1] S. Archer, J. A. Weinstein, *Coord. Chem. Rev.* **2012**, *256*, 2530–2561.

[2] J. Kalinowski, V. Fattori, M. Cocchi, J. A. G. Williams, *Coord. Chem. Rev.* **2011**, *255*, 2401–2425.

[3] K. Li, G. S. Ming Tong, Q. Wan, G. Cheng, W.-Y. Tong, W.-H. Ang, W.-L. Kwong, C.-M. Che, *Chem. Sci.* **2016**, *7*, 1653–1673.

[4] R. I. Dmitriev, N. O'Donnell, D. B. Papkovsky, *Bioconjugate Chem.* **2016**, *27*, 439–445.

[5] Q. Zhao, X. Zhou, T. Cao, K. Y. Zhang, L. Yang, S. Liu, H. Liang, H. Yang, F. Li, W. Huang, *Chem. Sci.* **2015**, *6*, 1825–1831.

[6] X. Ma, J. Zhang, J. Cao, X. Yao, T. Cao, Y. Gong, C. Zhao, H. Tian, *Chem. Sci.* **2016**, *7*, 4582–4588.

[7] I. Mathew, Y. Li, Z. Li, W. Sun, *Dalton Trans.* **2010**, *39*, 11201.

[8] Z. Ji, S. Li, Y. Li, W. Sun, *Inorg. Chem.* **2010**, *49*, 1337–46.

[9] V. W.-W. Yam, K. M.-C. Wong, N. Zhu, *Angew. Chem. Int. Ed.* **2003**, *42*, 1400–1403.

[10] E. C.-H. Kwok, M.-Y. Chan, K. M.-C. Wong, V. W.-W. Yam, *Polyhedron* **2016**, *120*, 54–59.

[11] P. Xu, H. Wu, H. Jia, S. Ye, P. Du, *Organometallics* **2014**, *33*, 2738–2746.

[12] C. K. M. Chan, C.-H. Tao, K.-F. Li, K. Man-Chung Wong, N. Zhu, K.-W. Cheah, V. W.-W. Yam, *J. Organomet. Chem.* **2011**, *696*, 1163–1173.

[13] C. K. M. Chan, C.-H. Tao, K.-F. Li, K. M.-C. Wong, N. Zhu, K.-W. Cheah, V. W.-W. Yam, *Dalton Trans.* **2011**, *40*, 10670.

[14] L.-J. Chen, J. Zhang, J. He, X.-D. Xu, N.-W. Wu, D.-X. Wang, Z. Abliz, H.-B. Yang, *Organometallics* **2011**, *30*, 5590–5594.

[15] I. Stengel, C. A. Strassert, L. De Cola, P. Bäuerle, *Organometallics* **2014**, *33*, 1345–1355.

[16] F. Guo, K. Ogawa, Y.-G. Kim, E. O. Danilov, F. N. Castellano, J. R. Reynolds, K. S. Schanze, *Phys. Chem. Chem. Phys.* **2007**, *9*, 2724.

[17] S. Kotani, K. Shiina, K. Sonogashira, *J. Organomet. Chem.* **1992**, *429*, 403–413.

[18] R. C. Klet, J. A. Labinger, J. E. Bercaw, *Organometallics* **2012**, *31*, 6652–6657.

[19] T. V. Ashworth, J. A. K. Howard, F. G. A. Stone, *J. Chem. Soc., Dalton Trans.* **1980**, 1609–1614.

[20] M. Landman, J. Ramontja, M. van Staden, D. I. Bezuidenhout, P. H. van Rooyen, D. C. Liles, S. Lotz, *Inorg. Chim. Acta* **2010**, *363*, 705–717.

[21] M. Werner, T. Lis, C. Bruhn, R. Lindner, D. Steinborn, *Organometallics* **2006**, *25*, 5946–5954.

[22] S. Barlow, H. E. Bunting, C. Ringham, J. C. Green, G. U. Bublitz, S. G. Boxer, J. W. Perry, S. R. Marder, *J. Am. Chem. Soc.* **1999**, *121*, 3715–3723.

[23] Y. Kajitani, K. Tsuge, Y. Sasaki, M. Kato, *Chem. Eur. J.* **2012**, *18*, 11196–11200.

[24] K.-W. Wang, J.-L. Chen, Y.-M. Cheng, M.-W. Chung, C.-C. Hsieh, G.-H. Lee, P.-T. Chou, K. Chen, Y. Chi, *Inorg. Chem.* **2010**, *49*, 1372–1383.

[25] W. Sun, H. Zhu, P. M. Barron, *Chem. Mater.* **2006**, *18*, 2602–2610.

[26] M.-H. Nguyen, C.-Y. Wong, J. H. K. Yip, *Organometallics* **2013**, *32*, 1620–1629.

[27] W. He, M. Y. Livshits, D. A. Dickie, J. Yang, R. Quinnett, J. J. Rack, Q. Wu, Y. Qin, *Chem.*

Sci. **2016**, *7*, 5798–5804.

[28] H. Weissman, E. Shirman, T. Ben-Moshe, R. Cohen, G. Leitus, L. J. W. Shimon, B. Rybtchinski, *Inorg. Chem.* **2007**, *46*, 4790–4792.

[29] S. Lentijo, G. Aullón, J. A. Miguel, P. Espinet, *Dalton Trans.* **2013**, *42*, 6353.

[30] M. L. Muro, F. N. Castellano, *Dalton Trans.* **2007**, *33*, 4659.

[31] Y. Cao, M. O. Wolf, B. O. Patrick, *Inorg. Chem.* **2016**, *55*, 8985–8993.

[32] P. Irmler, R. F. Winter, *Dalton Trans.* **2016**, *45*, 10420–10434.

[33] F. Geist, A. Jackel, R. F. Winter, *Inorg. Chem.* **2015**, *54*, 10946–10957.

[34] J. A. Zuleta, J. M. Bevilacqua, J. M. Rehm, R. Eisenberg, *Inorg. Chem.* **1992**, *31*, 1332–1337.

[35] D. Veldman, S. M. A. Chopin, S. C. J. Meskers, M. M. Groeneveld, R. M. Williams, R. A. J. Janssen, *J. Phys. Chem. A* **2008**, *112*, 5846–5857.

[36] R. Büchner, J. S. Field, R. J. Haines, C. T. Cunningham, D. R. McMillin, *Inorg. Chem.* **1997**, *36*, 3952–3956.

[37] J. J. Snellenburg, S. P. Laptenok, R. Seger, K. M. Mullen, I. H. M. van Stokkum, *J. Stat. Softw.* **2012**, *49*, 1–22.

[38] R. M. van der Veen, A. Cannizzo, F. van Mourik, A. J. Vlček, M. Chergui, *J. Am. Chem. Soc.* **2011**, *133*, 305–315.

[39] S. E. Brown-Xu, M. S. J. Kelley, K. A. Fransted, A. Chakraborty, G. C. Schatz, F. N. Castellano, L. X. Chen, *J. Phys. Chem. A* **2016**, *120*, 543–550.

[40] F. N. Castellano, *Acc. Chem. Res.* **2015**, *48*, 828–839.

[41] R. Berera, R. van Grondelle, J. T. M. Kennis, *Photosynth. Res.* **2009**, *101*, 105–118.

[42] M. Z. Shafikov, D. N. Kozhevnikov, M. Bodensteiner, F. Brandl, R. Czerwieniec, *Inorg. Chem.* **2016**, *55*, 7457–7466.

[43] R. S. Becker, J. Seixas de Melo, A. L. Maçanita, F. Elisei, *J. Phys. Chem.* **1996**, *100*, 18683–18695.

[44] V. Wintgens, P. Valat, F. Garnier, *J. Phys. Chem.* **1994**, *98*, 228–232.

[45] P. A. Scattergood, M. Delor, I. V Sazanovich, O. V Bouganov, S. A. Tikhomirov, A. S. Stasheuski, A. W. Parker, G. M. Greetham, M. Towrie, E. S. Davies, A. J. H. M. Meijer, J. A. Weinstein, *Dalton Trans.* **2014**, *43*, 17677–93.

[46] C. Lu, M. Fujitsuka, T. Majima, *J. Phys. Chem. C* **2017**, *121*, 649–655.

[47] S. S. Emmi, M. D'Angelantonio, G. Poggi, G. Beggiato, N. Camaioni, A. Geri, A. Martelli, D. Pietropaolo, G. Zotti, *Res. Chem. Intermed.* **1998**, *24*, 1–14.

[48] A. Iagatti, R. Flamini, M. Nocchetti, L. Latterini, *J. Phys. Chem. C* **2013**, *117*, 23996–24002.

[49] T. Keszthelyi, M. M.-L. Grage, J. F. Offersgaard, R. Wilbrandt, C. Svendsen, O. S. Mortensen, J. K. Pedersen, H. J. A. Jensen, *J. Phys. Chem. A* **2000**, *104*, 2808–2823.

[50] T. Cardolaccia, A. M. Funston, M. E. Kose, J. M. Keller, J. R. Miller, K. S. Schanze, *J. Phys. Chem. B* **2007**, *111*, 10871–10880.

[51] L. G. Reuter, A. G. Bonn, A. C. Stückl, B. He, P. B. Pati, S. S. Zade, O. S. Wenger, *J. Phys. Chem. A* **2012**, *116*, 7345–7352.

[52] C. A. Merlic, D. Xu, *J. Am. Chem. Soc.* **1991**, *113*, 9855–9856.

[53] R. N. McDonald, W. Y. Gung, *J. Am. Chem. Soc.* **1987**, *109*, 7328–7334.

[54] C. C. Comanescu, M. Vyushkova, V. M. Iluc, *Chem. Sci.* **2015**, *6*, 4570–4579.

[55] P. Cui, V. M. Iluc, *Chem. Sci.* **2015**, *6*, 7343–7354.

[56] J. Best, I. V. Sazanovich, H. Adams, R. D. Bennett, E. S. Davies, A. J. H. M. Meijer, M. Towrie, S. A. Tikhomirov, O. V. Bouganov, M. D. Ward, J. A. Weinstein, *Inorg. Chem.* **2010**, *49*, 10041–10056.

[57] C. Liao, J. E. Yarnell, K. D. Glusac, K. S. Schanze, *J. Phys. Chem. B* **2010**, *114*, 14763–14771.

[58] S.-H. Lee, C. T.-L. Chan, K. M.-C. Wong, W. H. Lam, W.-M. Kwok, V. W.-W. Yam, *J. Am. Chem. Soc.* **2014**, *136*, 10041–10052.

CHAPTER 6

MONONUCLEAR VS BRIDGED BINUCLEAR Pt(II) MULTICARBENE COMPLEXES

A case study of ethoxy- and aminocarbene complexes with bis(bromophenyl-1,4)phenylene-1,4-amine substituents

6.1 Introduction

There are several examples of bridged Pt(II) complexes, of which most are designed so that metal-metal interactions can occur and influence the resulting photophysical properties.[1–3] Examples of rigid bridged Pt(II) complexes in literature are symmetrical and it is not always possible to determine the effect of a second metal centre in the complex.[4–6] As some of the binuclear complexes synthesised in this study are asymmetrical, they are expected to show differences between the two metal centres when compared to their mononuclear analogues.

The aim is to compare and investigate how the additional bithienylene bridge and extra metal centre of the binuclear complexes influence the processes that occur for these complexes upon photoexcitation. Analysis methods used in the study include cyclovoltammetry, spectro-electrochemistry, UV/VIS absorption spectroscopy, transient absorption spectroscopy and DFT calculations. A case study will be conducted on the complexes containing ethoxy- and aminocarbene ligands derived from tris(4-bromophenyl)amine. The ligand itself is known for its

electron donating character and is well-known for its photoactive properties. [7–11] The complexes that will be compared are a representative sample of all the complexes with the C complexes being fragments of the D complexes and are shown in Figure 6.1.

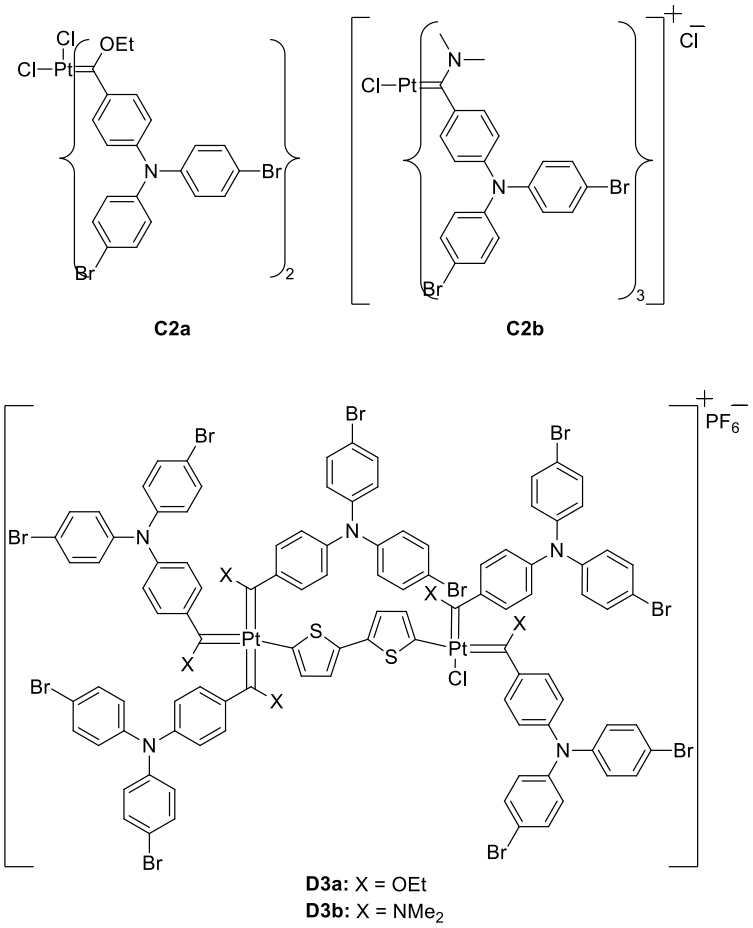

Figure 6.1. Structural representation of C2a, C2b, D3a and D3b

6.2 Results and Discussion

The synthesis and characterisation of the ethoxy-and aminocarbene mononuclear (**C2a** and **C2b**) and binuclear (**D3a** and **D3b**) complexes have been discussed in Chapter 4 and 5, respectively. For the rest of the study the focus will remain on a comparison between the photophysical and electrochemical properties of the complexes.

6.2.1 UV/Vis Spectroscopy

The UV/Vis spectra, recorded in THF, show differences between the **C** and **D** complexes (Chapters 4 and 5). Both the mononuclear and binuclear complexes show high absorbance. A direct comparison of the molar absorbance of **C2a** and **D3a** against wavelengths in THF at room temperature is shown in Figure 6.2. The figure reveals that **D3a** has a significantly higher molar absorbance between 200 and 370 nm than **C2a**. **D3a** also shows additional absorbance bands between 400 and 600 nm. As **C2a** is a mononuclear neutral biscarbene complex, the extra bands are expected to represent the additional metal centre containing three carbene ligands in the binuclear complexes as well as the bithienylene bridge. The strong absorbance band at 211 nm for both complexes is assigned as the $\pi \rightarrow \pi^*$ (LF) transition of the carbene ligands present in each complex.[12]

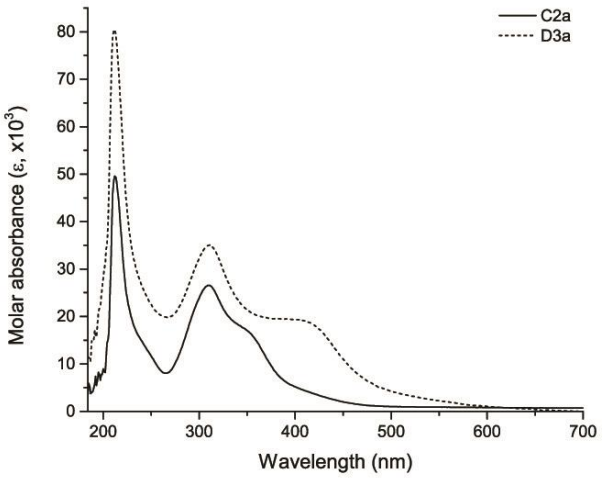

Figure 6.2. UV/Vis spectrum of C2a and D3a in THF at 298 K

The broad band and its shoulder observed at 309 nm for both complexes can likely be assigned as an intra-ligand based charge transfer (LL'CT) band at a single Pt(II) centre (the band is likely represented by both metal centres of **D3a**). Further, Sonagashira has previously assigned the $\pi \rightarrow \pi^*$ transitions of the bithienylene bridge between two Pt(II) centres between 300 and 400 nm and the MLCT as a weak absorbance band between 400 and 470 nm.[13] It is likely that the same $\pi \rightarrow \pi^*$ transition can be assigned for the absorbance observed between 300 and 400 nm in **D3a**. Although a clear peak is not observed at these wavelengths, the high molar absorbance at these wavelengths probably represents this transition. The MLCT bands between the Pt centres and their coordinated

carbene ligands are presumably being observed at approximately 400 nm as both complexes show absorbance at the specified wavelength. The increased molar absorbance of this band in **D3a** will support this assignment as the additional metal centre will lead to an increase in intensity of this transition. As per the assignment of the MLCT band between the bithienylene bridge and metal, the band is also expected between 400 and 470 nm in **D3a**. The increased intensity of the absorbance at these wavelengths of **D3a** compared to that of **C2a** supports the assignment. The lowest energy band for **D3a** (~500 nm) can then be assigned as a ligand to ligand with metal character charge transfer (LL'MCCT) band between the bithienylene bridge and a carbene ligand.

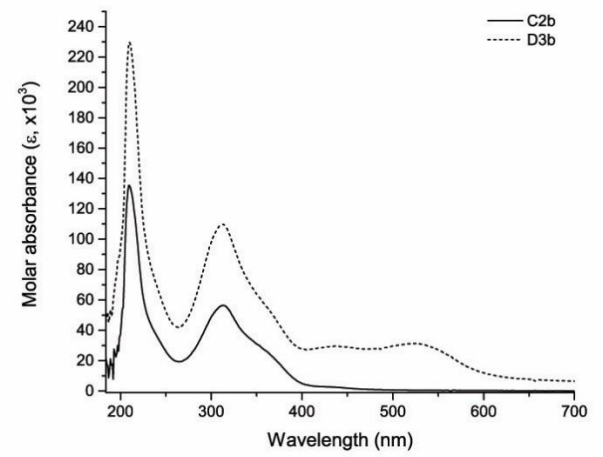

Figure 6.3. UV/Vis spectrum of C2b and D3b in THF at 298 K

A plot of the molar absorbance vs wavelengths of **C2b** and **D3b** in THF at 298 K are shown in Figure 6.3. The assignments as described for **C2a** and **D3a** are similar for the complexes: a carbene ligand based $\pi \rightarrow \pi^*$ transition at 210 nm. The broad band with a λ_{max} at ~313 nm and its shoulder representing the LL'CT band between carbene ligands coordinated to a Pt(II) centre as well as the additional $\pi \rightarrow \pi^*$ transitions of the bithienylene bridge. A broad undefined band observed at 437 nm is assigned as the MLCT for the carbene ligands as well as the bithienylene bridge. Finally, the LL'MCCT band for **D3b** is found at slightly lower energy wavelengths compared to **D3a** (513 and 500 nm respectively). This would indicate a slightly narrowed gap between the HOMO and LUMO energy levels for **D3b** compared with that of **D3a** is expected.

The UV/Vis peak assignments and molar absorptivity for all complexes recorded in THF are shown in Table 6.1.

Table 6.1. UV/Vis peak assignments of C2a, D3a, C2b and D3b recorded in THF at 298 K

	Carbene ligand based transitions λ_{max}/nm (ε x10^3/L.mol^{-1}.cm^{-1})			Bithienylene bridge based transitions[a] λ_{max}/nm (ε x10^3/L.mol^{-1}.cm^{-1})		Intra ligand charge transfer λ_{max}/nm (ε x10^3/L.mol^{-1}.cm^{-1})
	$\pi \rightarrow \pi^*$	LL'CT	MLCT	$\pi \rightarrow \pi^*$	MLCT	LL'MCCT
C2a	212 (49.6)	310 (26.6) 352, *sh* (16.7)	419 (3.7)	–	–	–
D3a	211 (80.4)	310 (35.0) 352, *sh* (21.1)	411 (19.0)	310 (35.0) 352, *sh* (21.1)	411 (19.0)	510 (3.7)
C2b	210 (135.4)	313 (56.5) 352, *sh* (29.9)	432 (2.7)	–	–	–
D3b	210 (229.7)	312 (109.8) 353, *sh* (61.5)	433 (29.5)	312 (109.8) 353, *sh* (61.5)	433 (29.5)	526 (31.2)

[a] Overlapping ligand-based transitions

6.2.2 Steady-State Emission Spectroscopy

A prominent difference between the mononuclear and binuclear Pt(II) multicarbene complexes are the processes by which the excitons return to the ground state after photoactivation. The pathways are mostly non-radiative as is observed from the poor quantum yields of the compounds' emission. The absorbance, excitation and emission data at 298 and 77 K are listed in Table 6.2 for the complexes under investigation.

Table 6.2. Absorbance, Excitation and Emission spectra of C2a, D3a, C2b and D3b at 298 K (THF) and 77 K (MeTHF)

	Abs.	Exc.	Em. (298 K)		Em. (77 K)		Φ
	CT λ_{maz}/nm	λ_{maz}/nm	λ_{maz}/nm (Stokes shift/cm^{-1})	τ_0/ns [%][a]	λ_{maz}/nm	τ_0/ns [%][a]	298 K
C2a	312 357	362	466 (6165)	7.69 [16] 2.78 [49] 0.82 [35]	480	4.43 [55] 1.61 [45]	0.001
D3a	412	360	466 (6319)	5.2 [17] 2.1 [46] 0.7 [37]	476 550	15.2 [26] 3.5 [60] 0.7 [14] 3.4 [72] 0.7 [28]	0.010
C2b	362 436	358	470 (6656)	5.83 [22] 2.55 [76] 0.19 [2]	480	3.38 [71] 0.84 [29]	0.029
D3b	312 357 438 529	360	468 (6410)	7.1 [16] 3.0 [75] 0.7 [9]	478 508 582	13.3 [31] 2.8 [69] 17.2 [51] 2.7 [49] 22.2 [69] 4.7 [31]	0.014

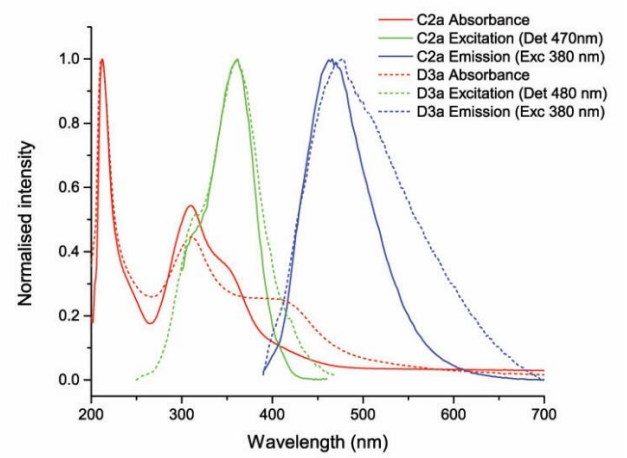

Figure 6.4. Normalised absorbance, excitation and emission spectra of C2a (solid lines) and D3a (dashed lines)

Figure 6.4 shows the normalised excitation and emission spectra of **C2a** and **D3a** in THF at 298 K. The excitation bands for the two complexes are similar and fall over the bands previously assigned as the intra-ligand charge transfer (LL'CT) bands between the different carbene ligands coordinated to the same metal centre. Although the peak maxima of the excitation spectra match exactly, the excitation peak of **D3a** is broadened compared to **C2a**. The same is observed for the emission. The peak maxima of the

emission for the two complexes fall over each other, but the emission of **D3a** extends to slightly longer wavelengths. It is postulated that the small differences between the spectra are caused by the fact that **C2a** is a neutral biscarbene complex while **D3a** contains an additional positively charged Pt(II) centre to which three carbene ligands are coordinated. As the transitions between the ligands coordinated to each centre will be similar, it is expected that there are differences in energy potentials between the two centres. The transitions in question do not represent the HOMO → LUMO transition, but rather, transitions of higher energy. As the Stokes shift is large between the excitation and emission bands, but still fall over some absorption bands, it is likely that the compound is excited from the ground state to a higher singlet state (higher than LUMO), relaxes to a lower singlet excited state via a non-radiative pathway (likely vibrational relaxation) to reach the emissive singlet state from which the emission is observed. This will explain the large Stokes shift while fluorescent lifetimes are still observed. It is clear, however, that no phosphorescence for the compounds is being observed as the lifetimes are too short for Pt(II) complexes displaying phosphorescence.

Figure 6.5 shows the absorbance, excitation and emission spectra for **C2b** and **D3b**. The emission spectra are identical. This does not only indicate that there is no emission observed that originates from the bithienylene bridge, but that the emission observed is solely ligand based and likely originates, from the carbene ligands coordinated to the positively charged Pt(II) centre. Thus, the emission observed from the complexes can be assigned as ligand-based emission that originates from the LL′CT bands.

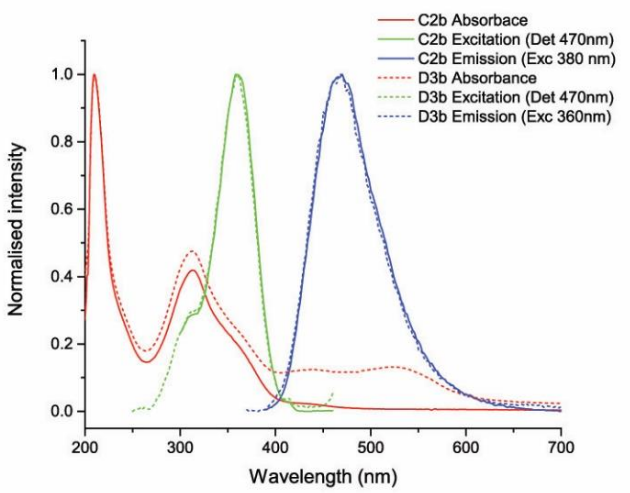

Figure 6.5. Normalised absorbance, excitation and emission spectra of C2b (solid lines) and D3b (dashed lines)

For **D3a** there is a ten-fold increase in the quantum yield of the observed emission in comparing the mononuclear with the binuclear complexes. The increase in the number of ligand-based transitions that occur for **D3a** will play a role, as well as the energy levels of the contributing orbitals. Upon addition of the second metal centre for the aminocarbene complexes (**D3b**), the quantum yield is approximately half compared to the mononuclear complex (**C2b**). **C2b** is a positively charged triscarbene complex, thus the compound displays a large amount of charge transfers that can lead emission. On addition of the bithienylene bridge and the additional metal centre (**D3b**), a non-radiative pathway is accessed upon photoexcitation of the complex, reducing its emissive quantum yield compared to that of the mononuclear analogue, **C2b**.

From these observations, the positively charged triscarbene metal centre is the major contributor to the emission observed. It is postulated that the LL′CT between the ligands cause the fluorescence being observed for all the complexes. From the clear reduction in the quantum yield for the binuclear aminocarbene complex compared to the corresponding mononuclear carbene complex, it is evident that the presence of the bithienylene bridge allows for an additional non-radiative pathway by which the excitons return to the ground state.

6.2.3 DFT Calculations

From the DFT calculations of **D3a** the graphical representations of the orbitals are determined and are shown in Figure 6.6. The HOMO is located on the bithienylene bridge while the LUMO is located on one of the carbene ligands coordinated to the positively charged Pt(II) centre. It is further evident that there is some metal contribution to the HOMO and LUMO but the two orbitals are mainly bridge and ligand based, respectively. Further, the LUMO, LUMO+1 and LUMO+2 orbitals are all found on the carbene ligands coordinated to the positively charged Pt(II) centre while the HOMO-1 and HOMO-2 orbitals are located on the carbene ligands coordinated to the neutral Pt(II) centre.

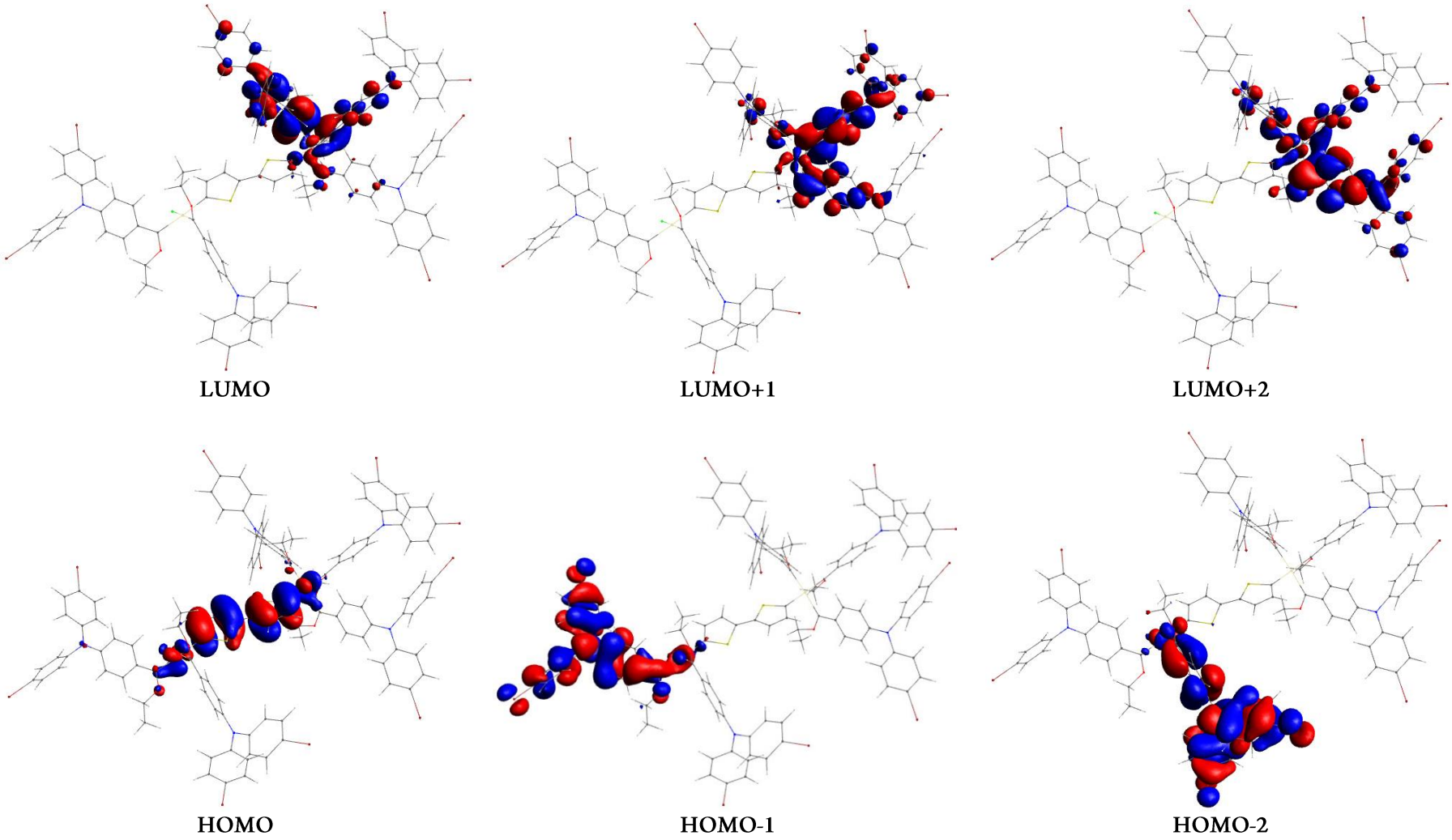

Figure 6.6. Graphical representations of the frontal molecular orbitals of D3a

Thus, the HOMO → LUMO transition for **D3a** is ligand-based and is represented by the lowest energy absorption observed in the UV/Vis spectrum for the compound. It is expected that the same HOMO → LUMO transition occurs for **D3b**. As the transition occurs at higher wavelengths, it is evident that the HOMO–LUMO gap of **D3b** is slightly smaller than that of **D3a** as the absorbance for the transitions in THF occur at ~532 and ~500 nm, respectively.

6.2.4 Cyclovoltammetry

The UV/Vis absorption and steady state emission spectroscopy as well as the DFT calculations have given insight as to the positions of the HOMO and LUMO orbitals and the subsequent transitions and charge transfer processes that occur during photoexcitation. Using cyclovoltammetry, the ease of oxidation, the stability of electrochemically generated radicals as well as the energy gap between the HOMO and LUMO orbitals of the complexes can be investigated.

Table 6.3. Oxidation and reduction half-wave potentials of complexes C2a, D3a, C2b and D3b in CH_2Cl_2/0.1 M $[NBu_4][B\{C_6H_3(CF_3)_2\text{-}3,5\}_4]$ buffer against equimolar amounts of decamethylferrocene/decamethylferrocenium standard at 100mV/s

Complex			Oxidation				Reduction			
		$DmFc^{0/+}$ i/μA	E_{pc}/V [i_{pc}/μA]	E_{pa}/V [i_{pa}/μA]	ΔE/V [i_{pc}/i_{pa}]	$E_{1/2}$/V	E_{pc}/V [i_{pc}/μA]	E_{pa}/V [i_{pa}/μA]	ΔE/V [i_{pc}/i_{pa}]	$E_{1/2}$/V
C2a		3.06	0.6232 [1.34]	0.7151 [1.82]	0.092 [0.73]	0.6692	-1.7790[b] [1.51]	–	–	–
D3a[a]	**1**	1.39	0.6345 [1.84]	0.7001 [1.95]	0.065 [0.95]	0.6673	-1.8151[b] [1.52]	–	–	–
	2		0.8041 [2.01]	0.8820 [1.95]	0.078 [0.97]	0.8431	-2.0702[b] [1.62]	–	–	–
C2b		3.61	0.8183 [2.82]	0.9414 [3.62]	0.123 [0.78]	0.8799	–[c]	–	–	–
D3b[a]	**1**	2.03	0.4073 [2.12]	0.4731 [3.33]	0.066 [0.64]	0.4402	–[c]	–	–	–
	2		0.8517 [2.68]	1.0443 [2.53]	0.193 [0.94]	0.9480	–[c]	–	–	–

[a] Multiple oxidation and/or reduction processes observed. [b] Irreversible oxidation or reduction process. [c] No reduction observed within the solvent window.

Table 6.3 contains a summary of the data that will be discussed where i_{pc} and i_{pa} represent the cathodic and anodic current, E_{pc} and E_{pa}, the cathodic and anodic potential, and $E_{1/2}$, the half-wave potential of an electrochemical oxidation or reduction process.

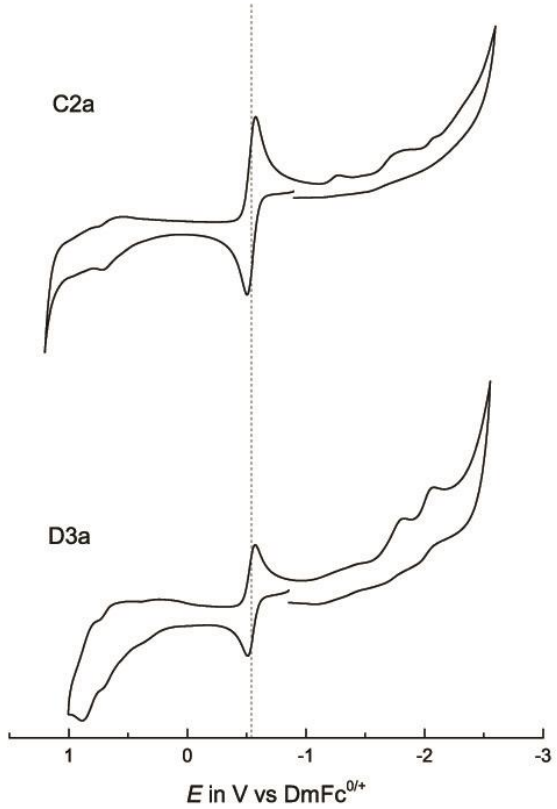

Figure 6.7. Cyclovoltammograms of C2a (top) and D3a (bottom) recorded in CH_2Cl_2/0.1 M $[NBu_4][B\{C_6H_3(CF_3)_2\text{-}3,5\}_4]$ buffer against a decamethylferrocene/decamethylferrocenium standard at 100mV/s

In Figure 6.7 the cyclovoltammograms of **C2a** (top) and **D3a** (bottom) are shown recorded in DCM against a decamethylferrocene/ decamethylferrocenium standard. Each of the cyclovoltammograms are measured against approximate equimolar amounts of decamethylferrocene. Thus, the oxidation and reduction of the reference indicates a single electron oxidation or reduction process. For **C2a**, a single one-electron oxidation is observed before the compound decomposes upon a second oxidation. The first oxidation at different rates reveal that the process is an irreversible oxidation. Further, a single one-electron irreversible reduction process is observed before reduction of the solvent takes place. The possible sites of oxidation of **C2a** include the metal centre and the tertiary amine present in each of the carbene ligands. A two-electron oxidation is expected for the metal ($Pt^{II} \rightarrow Pt^{IV}$) thus the first oxidation represents the oxidation of the nitrogen atom present in the carbene ligands as a one-electron oxidation for the compound is observed.

For **D3a**, two oxidation and reduction processes are observed which are both irreversible. The oxidation processes fall close to each other which indicates that HOMO orbital and the

subsequent filled orbitals just below it, all have similar potentials. The DFT calculations, which have been reported earlier for **D3a**, show that the LUMO and subsequent unoccupied orbitals are located on the carbene ligands coordinated to the positively charged Pt(II) centre. In accordance with the DFT calculations, the sites for the reductions can be assigned to the carbene carbons of two of the ligands. The expected radicals will be reactive and therefore irreversible reduction processes are expected. By comparing the two multi- ethoxycarbene complexes, it becomes evident that the first oxidation of both complexes is a single electron process and occurs at similar potentials (669.2 and 667.3 mV for **C2a** and **D3a** respectively). From the UV/Vis spectroscopy of both complexes it is however evident that the HOMO for the complexes are not found on similar sites of the complexes even if their first oxidation processes occur at similar potentials. The first oxidation of **D3a** is expected to occur on the bithienylene bridge, if the HOMO of **D3a** is indeed found on the bithienylene bridge as is supported by the UV/Vis spectroscopy as well as the DFT calculations. The second oxidation of **D3a** is expected to occur on the tertiary amine of one of the carbene ligands. In accordance with the DFT calculations, the particular ligand will be coordinated to the neutral Pt(II) centre. The irreversible reductions for both the ethoxycarbene complexes are expected to occur on the carbene carbons (for **D3a** – the ligands coordinated to the positively charged Pt(II) centre) and are similar (-1.779 and -1.815 V for **C2a** and **D3a**, respectively). The presence of the second reduction for **D3a** soon after the first while no second reduction is observed for **C2a** indicates that increased electron density is present for **C2a** after the first reduction. This is expected as the Pt centre of **C2a** is originally neutral before reduction while that of **D3a** is positively charged.

The cyclovoltammograms for **C2b** and **D3b** in DCM are shown in Figure 6.8. A single, presumably reversible (*vide infra*), oxidation for **C2b** is seen (Figure 6.8, top) in which small shoulders are observed for the broad half-wave potential at 0.88 V. The oxidation is assigned as that of the triphenylamine of one of the three carbene ligands. It is evident that the oxidation is ligand based, as a two-electron oxidation process would have been expected for the oxidation of

the Pt(II) atom. The broadening of the oxidation peak of **C2b** can indicate that two of the carbene ligands present in the complex have similar first oxidation potentials. It can be further reasoned that the position of the oxidation centre is one of the carbene ligands *cis* to the chloro ligand coordinated to the Pt(II) centre. The broadening of the oxidation peak shows that one of two similar ligands undergo a single electron oxidation. As it is possible that the two ligands are not the same (different electronic environments), the slight broadening of the half-wave potential is expected. No reduction potential for **C2b** is observed within the solvent window as the LUMO is likely situated on the carbene carbons of one of the three ligands which is highly stabilised by electron density provided from its nitrogen heteroatom.

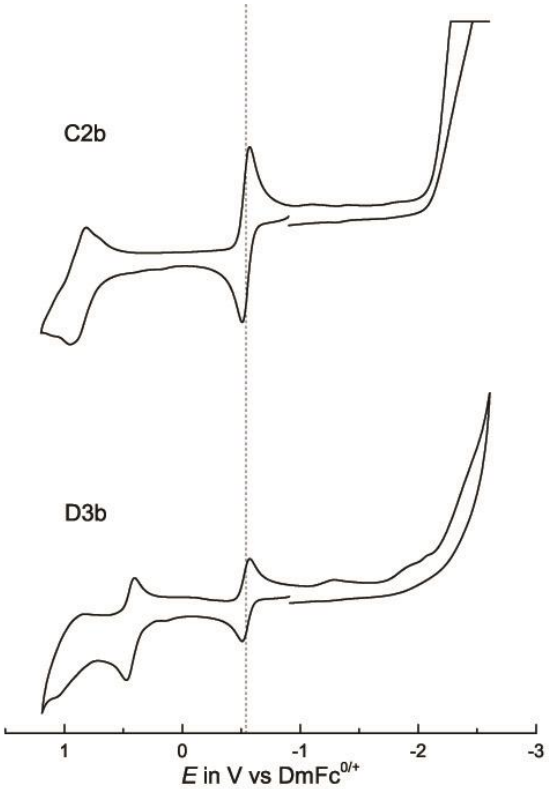

Figure 6.8. Cyclovoltammograms of C2b (top) and D3b (bottom) recorded CH_2Cl_2/0.1 M $[NBu_4][B\{C_6H_3(CF_3)_2\text{-}3,5\}_4]$ buffer against a decamethylferrocene/decamethylferrocenium standard at 100mV/s

Two oxidation processes for **D3b** are observed in Figure 6.8 (bottom) at half-wave potentials of 0.44 and 0.95 V before the complex decomposes upon further oxidation. Both oxidations are one-electron processes compared to the approximately equimolar amount of decamethylferrocene in the sample. Although the first oxidation displays some degree of reversibility it can formally be assigned as irreversible (*vide infra*). No reductions are observed for the complex within the solvent window. It is expected that the LUMO is situated on one of the carbene ligands coordinated to the positively charged Pt(II) centre. It has been mentioned above that the both the first oxidations of **C2b** and **D3b** show some degree of reversibility, but further analysis is required to fully conclude whether the oxidations are indeed

reversible or not. By analysing the cathodic and anodic peak potentials of the oxidation process at different rates, as well as the resulting half wave potential, the processes can be classified. Table 6.4 and Table 6.5 contain the peak currents and their ratios as well as the potentials at which they were recorded for **C2b** and **D3b** respectively. Figure 6.9 shows the cyclovoltammograms of the first oxidation processes for the two complexes at different rates.

Table 6.4. Peak currents and peak current ratios of C2b at different scan rates in DCM/0.1 M NBu_4PF_6 buffer against a ferrocene/ferrocenium standard

Scan rate /mV.s^{-1}	i_{pc} /µA	i_{pa} /µA	i_{pc}/i_{pa}	E_{pc} /V	E_{pa} /V	ΔE_p /V	$E_{1/2}$ /V
50	1.00	1.05	0.95	0.6430	0.7186	0.0755	0.6808
100	1.63	1.69	0.97	0.6423	0.7239	0.0816	0.6831
200	2.70	2.74	0.98	0.6340	0.7273	0.0933	0.6806
400	4.69	4.55	1.03	0.6274	0.7305	0.1031	0.6789
600	6.47	6.04	1.07	0.6174	0.7373	0.1199	0.6773
800	8.26	7.40	1.12	0.6107	0.7422	0.1314	0.6765
1000	9.92	8.69	1.14	0.5990	0.7522	0.1532	0.6756
1500	13.76	11.52	1.20	0.5792	0.7639	0.1847	0.6716
2000	17.51	14.24	1.23	0.5624	0.7805	0.2181	0.6715

Table 6.5. Peak currents and peak current ratios of D3b at different scan rates in CH_2Cl_2/0.1 M NBu_4PF_6 buffer against a ferrocene/ferrocenium standard

Scan rate /mV.s^{-1}	i_{pc} /µA	i_{pa} /µA	i_{pc}/i_{pa}	E_{pc} /V	E_{pa} /V	ΔE_p /V	$E_{1/2}$ /V
50	0.56	1.11	0.50	0.2073	0.2718	0.0645	0.2396
100	0.99	1.70	0.58	0.2043	0.2787	0.0744	0.2415
200	1.44	2.37	0.61	0.1985	0.2875	0.0890	0.2430
400	1.83	3.16	0.58	0.1945	0.2993	0.1048	0.2469
600	2.43	4.33	0.56	0.1878	0.3073	0.1195	0.2475
800	2.94	5.48	0.54	0.1805	0.3120	0.1316	0.2463
1000	3.23	6.06	0.53	0.1794	0.3179	0.1385	0.2487
1500	3.94	7.78	0.51	0.1711	0.3298	0.1586	0.2505
2000	4.66	9.41	0.50	0.1717	0.3385	0.1668	0.2551

The peak potentials and resulting current for the oxidation and rereduction of **C2b**, shown in Table 6.4, indicate that the process is not reversible, but rather quasi-reversible. This is deduced from the increasing ΔE_p value between E_{pc} and E_{pa} as the rate of the process is increased which deviates far from the expected value of 59 mV for reversible one-electron processes at all rates.[14] It is further evident that the first oxidation of **D3b** is irreversible as the i_{pc}/i_{pa} value deviates far from 1 which is the expected norm for a reversible oxidation or reduction process.[14]

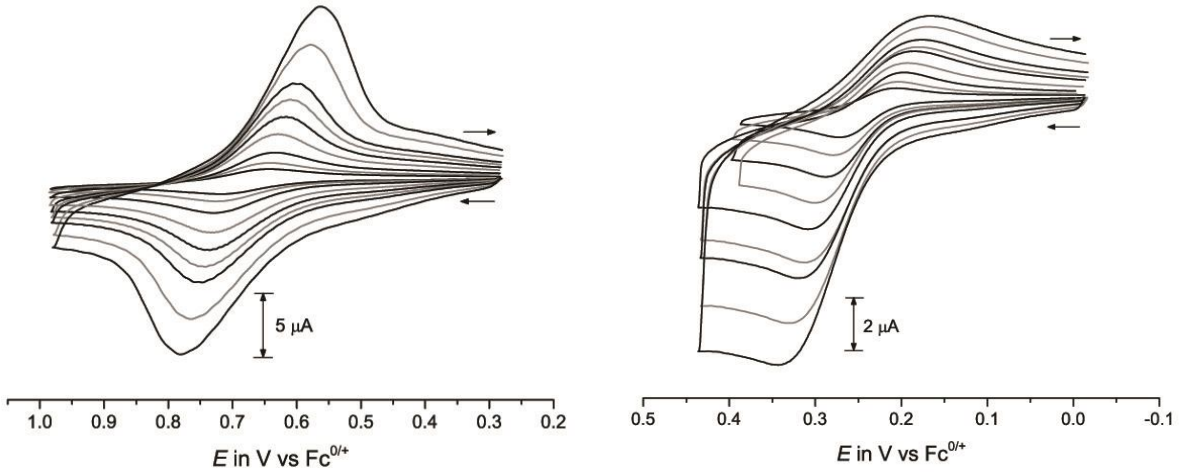

Figure 6.9. First oxidation of C2b (left) and D3b (right) in CH_2Cl_2/0.1 M NBu_4PF_6 buffer at scan rates of 50, 100, 200, 400, 600, 800, 1000, 1500 and 2000 mV/s

Referring to Figure 6.8, comparing the oxidation potentials for **C2b** and **D3b**, it is evident that the site of first oxidation for the two complexes are not the same. The second oxidation of **D3b** matches the first oxidation of **C2b** more closely at $E_{1/2}$ of 818.3 and 851.7 mV for the two respective oxidations. The site of first oxidation of **D3a** – with accompanying DFT calculations – have been postulated to occur on the bithienylene bridge. It is expected that the first oxidation site for **D3b** will be similar followed by the second oxidation which occurs on one of the triphenylamine fragments of the carbene ligands.

Comparing the oxidation potentials of the mononuclear complexes it is evident that the first oxidation of **C2a** occurs at a lower potential than that of **C2b** with respective half wave potentials

of 669.2 and 879.9 mV. As the oxidations for both complexes occur on the triphenylamine fragment present in a carbene ligand, the observation is unexpected. Throughout Chapter 4 it has been repeatedly shown that the stabilisation of the ethoxycarbene complexes occur from both the aromatic substituent as well as the ethoxy substituent of the carbene carbons while the aromatic substituents play an insignificant role in the stabilisation of the aminocarbene complexes. Thus, it is expected that the oxidation of the triphenylamine moiety present in the aromatic substituents of the aminocarbene complexes will occur before that of the ethoxycarbene complexes. The point can be argued that more electron density is available on the *p*-substituted triphenylamine of the aminocarbene complexes as little electron density from the aromatic substituent is delocalised to contribute to the stabilisation of the carbene carbon. However, it has been shown by the research group of Walter that compounds containing π-donating or withdrawing substituents lower the free energies of the triphenylamminium radical ion as the substituents stabilise the formed radicals better than an unsubstituted triphenylamminium radical ion.[15,16] It can also be argued that the Pt(II) centre for the mononuclear trisaminocarbene complex contains a positive charge which can lead to an overall increase of the free energy of the compound. The conclusive answer is obtained by investigating the second oxidation potentials of the binuclear complexes.

The first oxidation potentials of the binuclear complexes represent the oxidation of the bithienylene bridge. The first oxidation of the ethoxycarbene complex occur at a more positive potential than that of the aminocarbene complex at respective potentials of 667.3 and 440.2 mV. This shows that the bithienylene bridge in **D3a** contributes directly to the stabilisation of the positive Pt(II) centre and likely indirectly to the stabilisation of the carbene carbons present in the complex. The significantly lower oxidation potential of the bithienylene bridge in **D3b** indicates an increased electron density present on the bridge compared to that of **D3a.**

The second oxidation of both **D3a** and **D3b** is expected to occur at the neutral Pt(II) centre, to which the chloro ligand is coordinated. This oxidation occurs on the aromatic substituents of one

of the two carbene ligands. In this case, the oxidation potentials can be directly compared as both the complexes are the same except for the heteroatoms responsible for the stabilisation of the carbene carbons. The second oxidation potentials for **D3a** and **D3b** have values of 843.1 and 948.0 mV, respectively. With the data currently available, it is not possible to conclude why the second oxidation of D3b occurs at a more positive potential than that of D3a, as structural changes within the complexes are possible after the first oxidation. It is, however, likely that the oxidation occurs on the triphenylamine to form a triphenylamminium radical ion and this oxidation potential is influenced by the free energies of the product and reactant.

Thus, the cyclovoltammetry study reveals that the single electron oxidation and reduction of **C2a** is irreversible while the single electron oxidation of **C2b** is quasi-reversible. The oxidations occur on the triphenylamine substituents of the carbene ligands in both complexes. Two irreversible oxidation and reduction processes are observed in the solvent window of **D3a** while only two irreversible oxidation processes are observed for **D3b**. The first oxidations for both complexes occur on the bithienylene bridge while the second oxidations occur on the triphenylamine substituents of the carbene ligands coordinated to the neutral Pt(II) centre. For the mononuclear and binuclear Pt(II) complexes the oxidation of the triphenylamine substituents of the ethoxycarbene complexes occurred before that of the aminocarbene complexes as the stabilisation of the formed radicals is much greater for the ethoxycarbene complexes than that of the aminocarbene complexes.

6.2.5 *UV/Vis Spectroelectrochemistry*

The oxidation of **C2b** has been assigned as quasi-reversible and can be seen as fully reversible at low oxidation rates (Table 6.4). The oxidation and rereduction of the oxidation of **C2b** can thus be monitored by making use of spectroelectrochemistry. The UV/Vis spectrum of the compound is monitored during the first oxidation of the complex. The resulting overlain UV/Vis spectra recorded during the oxidation of **C2b** are shown in Figure 6.10.

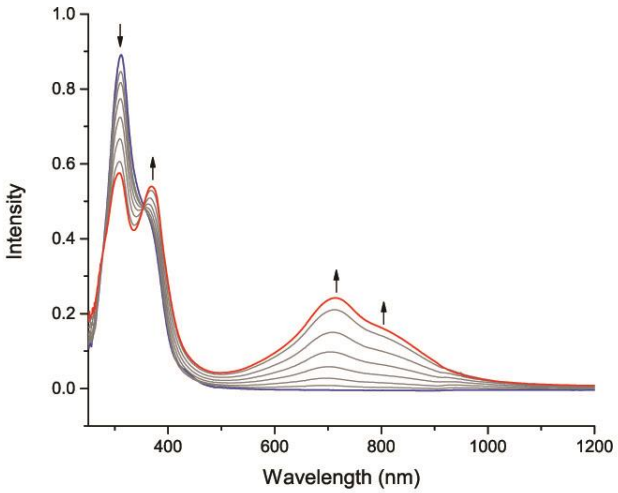

Figure 6.10. UV/Vis spectroscopic changes during the first oxidation of complex C2b in NBu_4PF_6/0.2 M 1,2-$C_2H_4Cl_2$

A clear shift to higher wavelengths are observed for the band representing the aromatic ligand-based $\pi \rightarrow \pi^*$ transitions (Shift from 312 nm to 368 nm). A broad peak forms at 714 nm upon oxidation of **C2b** which is characteristic for a *p*-substituted triphenylammonium positive radical.[17] The observation of this band shows that the HOMO is indeed located on the tertiary amine present on one of the aromatic substituents of the carbene carbons. At the slow rate of oxidation, the process is reversible and the original spectrum is obtained upon reduction of the oxidised species.

As all the other compounds only show irreversible oxidation and reduction processes, it is not possible to investigate their UV/Vis spectra during oxidation without considering that other possible products can form during the oxidation or reduction processes.

6.2.6 *Femtosecond Transient Absorption Spectroscopy (TAS)*

The mono- and binuclear complexes carrying the 4-bromo-substituted triphenylamine ethoxy- and aminocarbene ligands have similar emission spectra at room temperature. On

photoexcitation, the compounds show fluorescence at room temperature even though phosphorescence for complexes are expected due to the presence of the Pt(II) atom. The low quantum yields recorded for the complexes indicate that most of the excitons return to the ground state via a dominant non-emissive pathway. To compare the processes and pathways by which the excitons return to ground state, the femtosecond TAS of the ethoxy- and aminocarbene ligands of the mono- and binuclear complexes are compared.

In Figure 6.11 the EADS, obtained from the Global Fit Analysis of the TAS measurements of **C2a** and **D3a** are shown. For a methodical description for the EADS and TAS measurements, please refer to Chapter 4. In Chapter 4 and 5 the respective spectra for both complexes have been discussed. From the comparison of the two sets of data, it becomes evident that in both cases, the triplet manifold for the complexes are accessed through an ISC process facilitated by the Pt(II) atom (**C2a** and **D3a**).

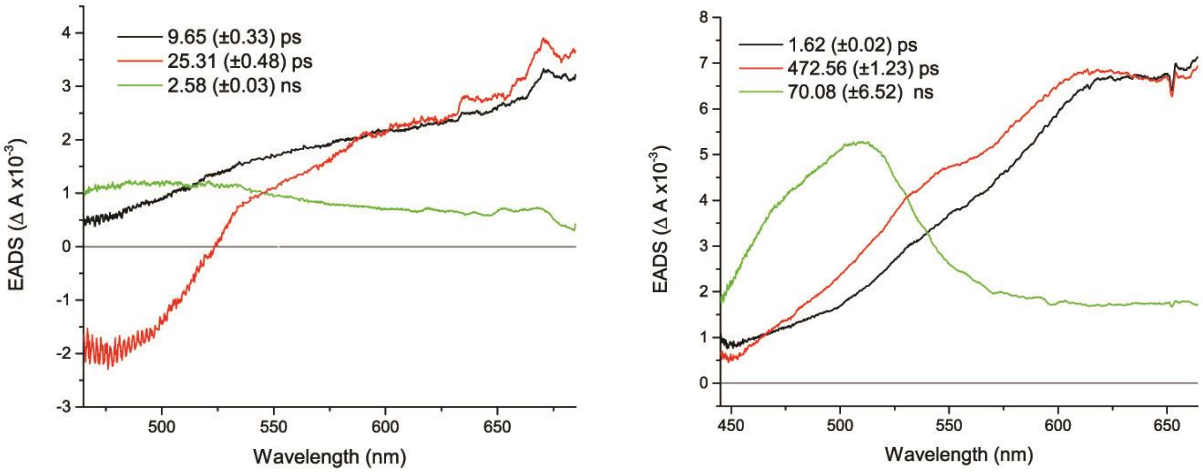

Figure 6.11. EADS of C2a (left) and D3a (right) obtained through Global Fit analysis (sequential model) of their TAS in THF at 298 K

From the cyclovoltammetry it has been established that the HOMO of **C2a** is largely located on one of the triphenylamine ligands, however, it is likely that the metal centre has a large contribution to the HOMO due to the significant π-orbital overlap between the carbene carbon, the aromatic substituent, and the metal centre. In Chapter 4 it has been proposed that the first

transient of **C2a** displays ESA of triplet states. Its second transient shows a GSB at short wavelengths while broad PA is observed at longer wavelengths. The PA has been assigned to a CT product as it decays into a more stable triplet state product which shows weak absorbance in the third transient with a peak maximum at 504 nm and a lifetime of 2.58 (±0.03) ns.

The excitation wavelength for both complexes is 387.5 nm which represents the LL′CT and MLCT bands between the carbene ligands coordinated to a single Pt(II) centre in **C2a** and **D3a**. For **D3a** the excitation wavelength also represents the $\pi \rightarrow \pi^*$ transition for the bithienylene bridge. For both **C2a** and **D3a**, a CT product forms upon excitation, from which a more stable triplet state product is observed at long time delays with a λ_{max} at 510 nm.

The final stable product observed for all the binuclear ethoxycarbene complexes, shows absorbance at a λ_{max} between 510 – 520 nm. In Chapter 5 this product has been assigned as a triplet state product carrying a formal charge – positive or negative. Bithiophene compounds are well known for their hole-conducting abilities[18,19] and carbene carbons have been known to accommodate negative charges.[20–23] Thus, the absorbing charge separated products are assigned as a positive radical on the bithienylene bridge and a negative radical on one of the carbene ligands coordinated to the positively charged Pt(II) centre. The EADS of **C2a** – with no bithienylene bridge – shows similar processes occurring as that of **D3a**, albeit with much shorter lifetimes. From this observation, it is possible to conclude that the persistent triplet state product observed for **D3a** is the negative polaron of a charge separated state that is probably located on the carbene carbon. As a similar product is also observed in **C2a**, it is likely that this product can also be assigned as a CS state, however its calculated lifetime is significantly shorter compared to that of **D3a** (2.58 (±0.03) ns for **C2a**; 70.08 (±6.52) ns for **D3a**). The much shorter lifetime of the CS state in **C2a** is likely caused by the fact that the isolated charges cannot necessarily be stabilised. For two separated charges to form within these complexes, it would mean each charge would need to be located on a different carbene ligand. As there are no indication of a second triplet state

product showing absorbance in the analysis window, it is proposed that the product observed is formed from a charge redistribution in the compound and returns to the ground state via a non-emissive pathway – likely vibrational relaxation.

Table 6.6. Peak positions and lifetimes for the charge separated state components

	$Carb^{\bullet-}$ λ_{max}/nm	$BiTh^{\bullet+}$ λ_{max}/nm	Lifetime (τ)
C2a	508.80	–[a]	25.31 (±0.48) ps
D3a	507.89	>661.98	70.08 (±6.52) ns[b]
C2b	480.81	–[a]	66.72 (±0.28) ps
D3b	470.83	>643.22	7.27 (±0.05) ns[b]

[a] Bithienylene bridge not present in **C** series complexes. [b] Determined using Global Fit Analysis

The final EADS transient of **D3a** shows absorbance at the longer wavelengths which points to absorbance of the other expected positive triplet radical, however, this peak is broad and featureless and its peak maximum is not observed. Similar absorbance is observed for all the binuclear ethoxycarbene complexes and thus likely represents the positive radical expected on the bithienylene bridge.

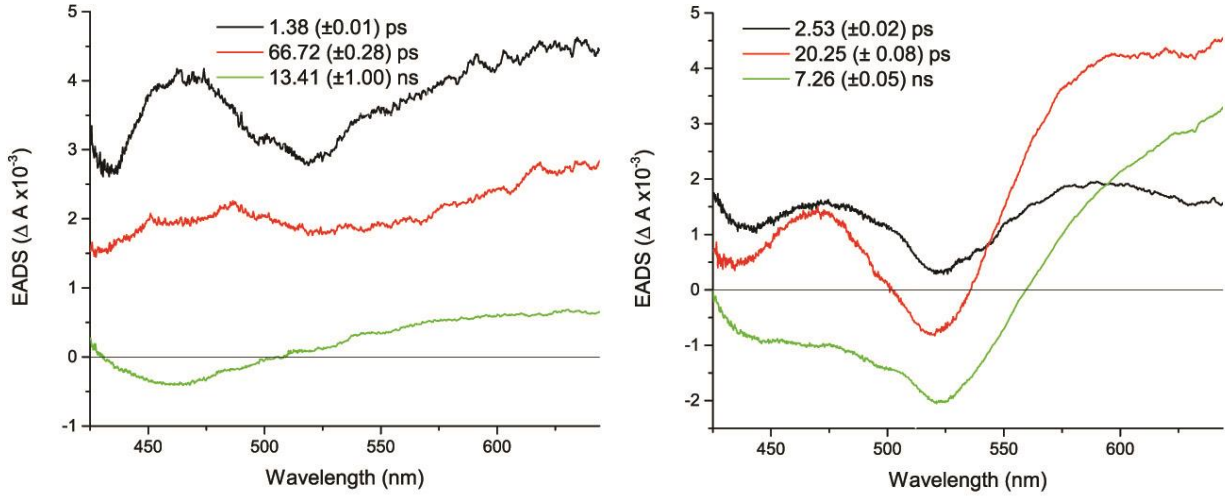

Figure 6.12. EADS of C2b (left) and D3b (right) obtained through Global Fit Analysis (sequential model) of their TAS in THF at 298 K

The EADS for **C2b** and **D3b** are shown in Figure 6.12. Both compounds display ESA in their first transients in which two peaks are evident at approximate wavelengths of 470 and 600 nm. In the second transient of **D3b**, CT products are observed which decays into the third transient, in which a stable product shows absorbance at 469 and 596 nm and SE is observed the shorter wavelengths. **C2b** shows weak PA at a λ_{max} of 480 nm of a similar nature than that of **D3b** in its second transient, and weak SE in its third transient. The most pronounced differences in the EADS of the two compounds is the intense PA in the second and third transient of **D3b**, at a λ_{max} of 596 nm, which is lacking in **C2b** and the lifetime of the two persistent products of **D3b**. Assuming that the PA at 470 nm results from a similar product within the two complexes, the lifetime of product in **D3b** is much longer than that of **C2b** (7.26 (±0.05) ns for **D3b** and 66.72 (±0.28) ps for **C2b**).

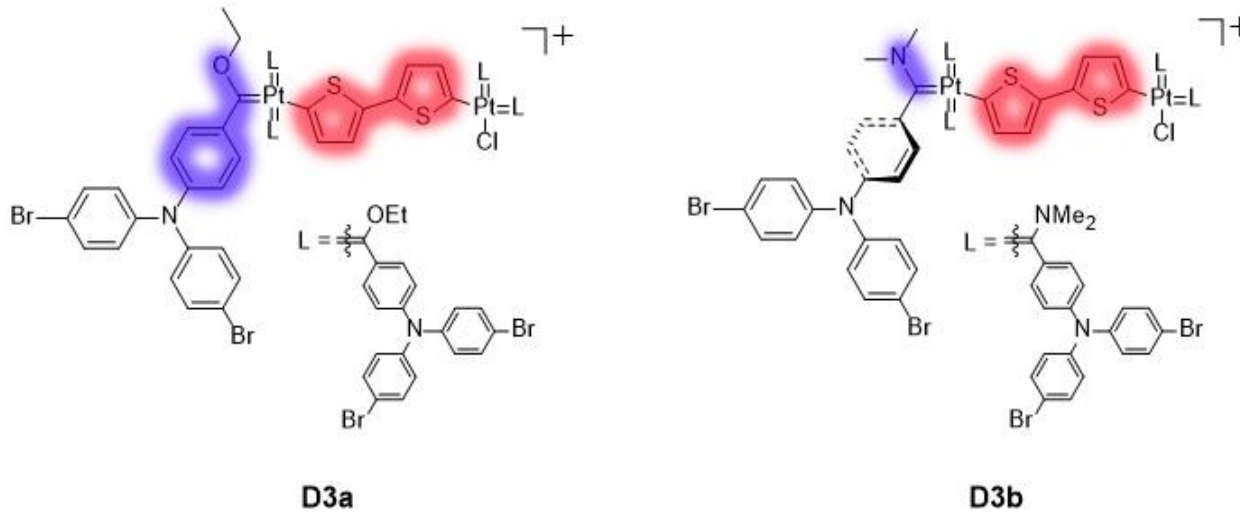

Figure 6.13. Electron accepting (blue) and electron donating (red) fragments that form a CS state in D3a and D3b on photoexcitation

For **D3a** the long-lived triplet state absorbing at shorter wavelengths has been assigned as the negative radical residing on the carbene carbon, which forms one of the components of a CS state. The absorbance of the second component is not observed. It is postulated that a CS state also forms upon excitation of **D3b** and in this case, both components show absorbance in the analysis window. From the analysis, it is further clear that the lifetime for the CS state of **D3a** is significantly longer than that of **D3b**. It is expected that the positive radical on the bithienylene bridge will have

similar characteristics in the two complexes. The likely reason for the difference in lifetime of the CS state can be attributed to the electron density present at the carbene carbon. For **D3b**, the amino substituent of the carbene carbon provides a significant amount of electron density to the carbene carbon, thus making it an electron rich environment. Thus, when a negative radical is formed on the carbene carbon, it will experience an electron-rich environment and will readily "decompose" through the charge recombination process. The same cannot be said for the ethoxy substituent of the carbene carbon in **D3a**, which does not create an electron excessive environment around the carbene carbon. When the negative radical forms on the carbene carbon of **D3a**, it is readily stabilised by the conjugated system that extends from the distant nitrogen substituent of the phenyl ring to the carbene carbon. The concept is illustrated in Figure 6.13.

6.3 Experimental

UV/Vis absorption and Emission spectroscopy

Please see the experimental section of Chapter 4.

Electrochemical and Spectroscopic Measurements

The electrochemical experiments were performed in a vacuum-tight, one-compartment cell. Pt and Ag wires were used as the counter and reference electrodes, respectively, while a platinum electrode was used as the working electrode. The working electrode was polished with 0.25 μm diamond paste (Buehler-Wirtz) before measurements. NBu_4BArF ($BArF = B\{C_6H_3(CF_3)_2\text{-}3,5\}_4^-$) (0.25 mM) was used as the supporting electrolyte. Referencing was done with addition of ferrocene or decamethylferrocene (DmFc) as an internal standard to the analyte solution after all data of interest had been acquired. Representative sets of scans were repeated with the added standard. Final referencing was done against the ferrocene/ferrocenium ($Cp_2Fe^{0/+}$) couple with $E_{½}$ ($DmFc^{0/+}$) = -540 mV vs. $Cp_2Fe^{0/+}$ using DCM/NBu_4BArF as supporting electrolyte.

Electrochemical data was acquired with a computer-controlled BAS potentiostat. A CaF_2 OTTLE cell was used where Pt-mesh acted as the working and counter electrode and a silver wire as the

pseudo-reference electrode. FT-IR spectra were recorded on a Thermo is10 instrument. UV-Vis/NIR spectra were obtained on a TIDAS fiber optic diode array spectrometer (combined MCS UV/NIR and PGS NIR instrumentation) from j&m in HELLMA quartz cuvettes with 0.1 cm 10 optical path lengths.

DFT calculations

A DFT study was conducted on the ground state of **D3a** using Gaussian 09 program packages[24] in THF as solvent. The compound was optimised using the B3LYP functional with triple-ζ valence basis set 6-31G(d,p)[25,26] on all atoms except Pt and Br on which the LANL2DZ[27–29] basis set was used.

Transient absorption spectroscopy

Please see the experimental section of Chapter 4.

Synthesis

Please see the experimental section of Chapter 4 and Chapter 5.

6.4 References

[1] W. Sun, H. Zhu, P. M. Barron, *Chem. Mater.* **2006**, *18*, 2602–2610.

[2] K.-W. Wang, J.-L. Chen, Y.-M. Cheng, M.-W. Chung, C.-C. Hsieh, G.-H. Lee, P.-T. Chou, K. Chen, Y. Chi, *Inorg. Chem.* **2010**, *49*, 1372–1383.

[3] Y. Kajitani, K. Tsuge, Y. Sasaki, M. Kato, *Chem. Eur. J.* **2012**, *18*, 11196–11200.

[4] M.-H. Nguyen, C.-Y. Wong, J. H. K. Yip, *Organometallics* **2013**, *32*, 1620–1629.

[5] W. He, M. Y. Livshits, D. A. Dickie, J. Yang, R. Quinnett, J. J. Rack, Q. Wu, Y. Qin, *Chem. Sci.* **2016**, *7*, 5798–5804.

[6] P. Xu, H. Wu, H. Jia, S. Ye, P. Du, *Organometallics* **2014**, *33*, 2738–2746.

[7] Z. Ning, H. Tian, *Chem. Commun.* **2009**, 5483–95.

[8] Y. Shirota, H. Kageyama, *Chem. Rev.* **2007**, *107*, 953–1010.

[9] W. A. Arcos, R. R. Guimarães, B. Insuasty, K. Araki, A. Ortiz, *J. Mol. Struct.* **2016**, *1111*,

157–165.

[10] W. Xu, B. Peng, J. Chen, M. Liang, F. Cai, *J. Phys. Chem. C* **2008**, *112*, 874–880.

[11] J.-H. Wu, W.-C. Chen, G.-S. Liou, *Polym. Chem.* **2016**, *7*, 1569–1576.

[12] N. Weststrate, I. Fernández, D. C. Liles, N. van Jaarsveld, S. Lotz, *Organometallics* **2015**, *34*, 696–710.

[13] S. Kotani, K. Shiina, K. Sonogashira, *J. Organomet. Chem.* **1992**, *429*, 403–413.

[14] A. J. Bard, L. R. Faulkner, *Electrochemical Methods: Fundamental and Applications, 2nd Edition*, John Wiley & Sons, Inc., New York, **2001**.

[15] L. Hagopian, G. Koehler, R. I. Walter, *J. Phys. Chem.* **1967**, *71*, 2290–2296.

[16] R. I. Walter, *J. Am. Chem. Soc.* **1966**, *88*, 1923–1930.

[17] S. Amthor, B. Noller, C. Lambert, *Chem. Phys.* **2005**, *316*, 141–152.

[18] P. A. Scattergood, M. Delor, I. V. Sazanovich, O. V. Bouganov, S. A. Tikhomirov, A. S. Stasheuski, A. W. Parker, G. M. Greetham, M. Towrie, E. S. Davies, A. J. H. M. Meijer, J. A. Weinstein, *Dalton Trans.* **2014**, *43*, 17677–17693.

[19] C. Lu, M. Fujitsuka, T. Majima, *J. Phys. Chem. C* **2017**, *121*, 649–655.

[20] C. A. Merlic, D. Xu, *J. Am. Chem. Soc.* **1991**, *113*, 9855–9856.

[21] R. N. McDonald, W. Y. Gung, *J. Am. Chem. Soc.* **1987**, *109*, 7328–7334.

[22] P. Cui, V. M. Iluc, *Chem. Sci.* **2015**, *6*, 7343–7354.

[23] C. C. Comanescu, M. Vyushkova, V. M. Iluc, *Chem. Sci.* **2015**, *6*, 4570–4579.

[24] Gaussian 09, Revision D.01, M. J. Frisch, G. W. Trucks, H. B. Schlegel, G. E. Scuseria, M. A. Robb, J. R. Cheeseman, G. Scalmani, V. Barone, B. Mennucci, G. A. Petersson, H. Nakatsuji, M. Caricato, X. Li, H. P. Hratchian, A. F. Izmaylov, J. Bloino, G. Zheng, J. L. Sonnenberg, M. Hada, M. Ehara, K. Toyota, R. Fukuda, J. Hasegawa, M. Ishida, T. Nakajima, Y. Honda, O. Kitao, H. Nakai, T. Vreven, J. A. Montgomery, Jr., J. E. Peralta, F. Ogliaro, M. Bearpark, J. J. Heyd, E. Brothers, K. N. Kudin, V. N. Staroverov, R. Kobayashi, J. Normand, K. Raghavachari, A. Rendell, J. C. Burant, S. S. Iyengar, J. Tomasi, M. Cossi,

N. Rega, J. M. Millam, M. Klene, J. E. Knox, J. B. Cross, V. Bakken, C. Adamo, J. Jaramillo, R. Gomperts, R. E. Stratmann, O. Yazyev, A. J. Austin, R. Cammi, C. Pomelli, J. W. Ochterski, R. L. Martin, K. Morokuma, V. G. Zakrzewski, G. A. Voth, P. Salvador, J. J. Dannenberg, S. Dapprich, A. D. Daniels, Ö. Farkas, J. B. Foresman, J. V. Ortiz, J. Cioslowski, and D. J. Fox, Gaussian, Inc., Wallingford CT, **2009**.

[25] G. A. Petersson, A. Bennett, T. G. Tensfeldt, M. A. Al-Laham, W. A. Shirley, J. Mantzaris, *J. Chem. Phys.* **1988**, *89*, 2193–2218.

[26] G. A. Petersson, M. A. Al-Laham, *J. Chem. Phys.* **1991**, *94*, 6081–6090.

[27] P. J. Hay, W. R. Wadt, *J. Chem. Phys.* **1985**, *82*, 270–283.

[28] W. R. Wadt, P. J. Hay, *J. Chem. Phys.* **1985**, *82*, 284–298.

[29] P. J. Hay, W. R. Wadt, *J. Chem. Phys.* **1985**, *82*, 299–310.

CHAPTER 7

CONCLUSION

During this study, the effectiveness of Fischer carbene units to act as electron acceptors in large molecules that also contain electron donor functions, was investigated. In all the examples, the donor function was linked by a conjugated spacer to the Fischer carbene moiety. Fundamental studies have been conducted with the aim that electronic properties will become more understandable and eventually controllable and have the potential to find application in modern smart materials.

7.1 Electron delocalisation in arene rings containing electron donating and competitive electron withdrawing substituents

W(0) Fischer ethoxycarbene substituents were synthesised on N,N-dimethylaniline (**A1**) and anisole (**A2**), coordinated in a η^6-fashion to a $Cr(CO)_3$ fragment. Four different carbene complexes of **A1** were obtained with carbene complexes that formed at the *o*- (**A1a**), *m*- (**A1b**) and *p*-positions (**A1c**) of the benzene ring relative to the dimethylamino substituent. In addition, a tetracarbonyl complex (**A1d**) with a bidentate nitrogen-carbene chelate ring was also isolated. The formation of the different products reveal that upon η^6-coordination of N,N-dimethylaniline, all the positions of the arene ring are activated. It was shown that the products obtained from the synthesis of the **A1** derivatives could be controlled by reaction conditions. The anisole precursor (**A2**) was shown to be solely activated on the *o*-positions relative to the methoxy substituent of

the ring. A *bis*- (**A2a**), *mono*- (**A2b**) and a chelate (**A2c**) complex were isolated from the subsequent reactions of **A2** with excess *n*BuLi, $W(CO)_6$ and alkylation agent.

From the spectroscopic data, it was evident that the amount of electron density available for the stabilisation of the carbene carbon decreased upon coordination of the aromatic ring to the $Cr(CO)_3$ group. It was further shown that the electron density donated into the aromatic ring by an electron donating ring substituent to stabilise the Fischer carbene, directly influenced the bonding of the $Cr(CO)_3$ group. In the presence of the NMe_2 group in *p*-position relative to the carbene substituent, more electron density is pulled into the ring from the NMe_2 group than for the other isomers. It was evident that upon coordination of the heteroatom (NMe_2 or OMe) to the tungsten tetracarbonyl fragment to form chelate rings, available electron density of the heteroatoms was lost.

Cyclovoltammetry measurements indicated that **A1a** – **A1d** underwent electrochemically reversible first oxidation and irreversible second oxidation processes while the derivatives of **A2** displayed two irreversible oxidation processes. IR spectroelectrochemistry measurements of the **A1** derivatives indicated that the first oxidation is based at the $Cr(CO)_3$ group for **A1a** – **A1c** and does not cause significant differences in the carbonyl vibration patterns of the $W(CO)_5$ group. The IR spectroelectrochemistry indicated that the first oxidation of **A1d** did not occur on the chromium tricarbonyl group, unlike for **A1a** – **A1c**, but on the chelate ring. The DFT calculations confirm that the positions of the HOMO orbitals of unchelated complexes are located on the $Cr(CO)_3$ fragment and LUMO orbitals are generally located on the metal-carbene fragment.

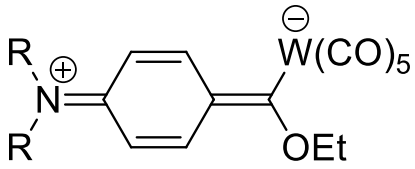

Figure 7.1. Stabilisation of an ethoxycarbene complexes through the π-delocalisation of electron density from the distant nitrogen substituent

The X-ray crystal structures indicate ring distortion for all complexes and it is evident that the carbene carbon is stabilised predominately by the tungsten carbonyl and ethoxy substituents of the carbene carbon. **A1c** experiences additional stabilisation by the distant dimethylamino substituent via the arene ring. Thus, the study shows that a tertiary amine at the *p*-position relative to the amine is an ideal substituent for the indirect and distant stabilisation of a carbene carbon on an arene ring (Figure 7.1).

7.2 Benzylic W(0) Fischer ethoxy- and aminocarbene complexes with tertiary amines *para* to the carbene substituent

Ethoxy and dimethylamino Fischer carbene complexes of W(0) were synthesised with phenylamine substituents. The dimethylaminocarbene complexes were synthesised by means of a novel method, using readily accessible chemicals. It was shown that for carbene carbon stabilisation, the ethoxycarbene compounds rely on electron density provided by the delocalisation of the distant nitrogen lone pair of electrons via the arene ring which acts as a "remote donor". For each of the different ethoxycarbene complexes, the substituents of the remote amine influenced the amount of electron density which could be used for the stabilisation of the Fischer carbene complex. In aminocarbene complexes, the carbene carbons were mainly stabilised by their metal and amino substituents and do not show a dependency on π-delocalisation from their aromatic groups. Further, it was established that the reduction of the complexes take place on the carbene carbon while the oxidation of the complexes take place on the aromatic amine rather than the tungsten carbonyl group.

7.3 Mononuclear Pt(II) Fischer carbene complexes: synthesis and photophysical properties

Pt(II) Fischer multicarbene complexes were synthesised through a transmetallation approach from tungsten pentacarbonyl. The tungsten carbonyl Fischer carbene complexes synthesised in Chapter 3 and $Pt(COD)Cl_2$ were used as starting materials in the transmetallation reaction. Two ethoxycarbene ligands coordinate to a Pt(II) atom to form a neutral biscarbene complex, while three aminocarbene ligands coordinate to form cationic triscarbene complexes. The identity of the complexes was confirmed with NMR spectroscopy, elemental analysis and mass spectrometry. Structures of the N,N-dimethylaniline carbene analogues were also confirmed by X-Ray crystallography. The differences in coordination of the ethoxy- and aminocarbene ligands were ascribed to differences in electron density available at the carbene carbon. The more electron rich aminocarbene forces a further carbene uptake facilitated by the formation of a cationic Pt(II) centre. The synthesised complexes are stable at room temperature and can be stored under inert conditions.

Upon photoexcitation, the synthesised complexes displayed weak multicomponent blue fluorescence and delayed fluorescence at room temperature. The low emission quantum yields, in conjunction with femtosecond transient absorption spectroscopy, indicated that the prominent pathway by which the excitons returned to the ground state was via a non-emissive triplet state pathway. As a result, the potential use of these complexes as emitters is not feasible.

7.4 Binuclear Pt(II) Fischer multicarbene rods: synthesis and photophysical properties

Several binuclear bithienylene bridged Pt(II) multicarbene complexes were synthesised through a carbene transmetallation approach: pentacarbene mono-cations or hexacarbene di-cations. The number of carbene ligands in the final binuclear Pt(II) rod were determined by both electronic and steric effects. A balance between the electronic properties of the Fischer carbene ligands –

affected by the aromatic and heteroatomic substituents – and the overall electronic effect (which is a function of the charge on the platinum complex), were important.

The compounds display multicomponent fluorescence in THF at 298 K which has been assigned ligand-based emission. No phosphorescence for the complexes was observed. The presence of an ISC process was established using femtosecond transient absorption spectroscopy. The technique further allowed for the identification of a persistent triplet state upon photoactivation, observed in all the binuclear multicarbene complexes with calculated lifetimes of between 3 and 70 ns.

Two different triplet state products showed persistent absorbance simultaneously for all the aminocarbene complexes, while only one persistent triplet state product was observed within the analysis window for the ethoxycarbene complexes (Figure 7.2). Thus, it has been proposed that charge separated states are formed upon photoexcitation for all the bithienylene bridged binuclear Pt(II) multicarbene complexes. As the two triplet state products observed for the aminocarbene complexes displayed absorbance at similar wavelengths, it was proposed that the likely positions of the formal positive and negative polarons are on the bithienylene bridge and the carbene carbon, respectively.

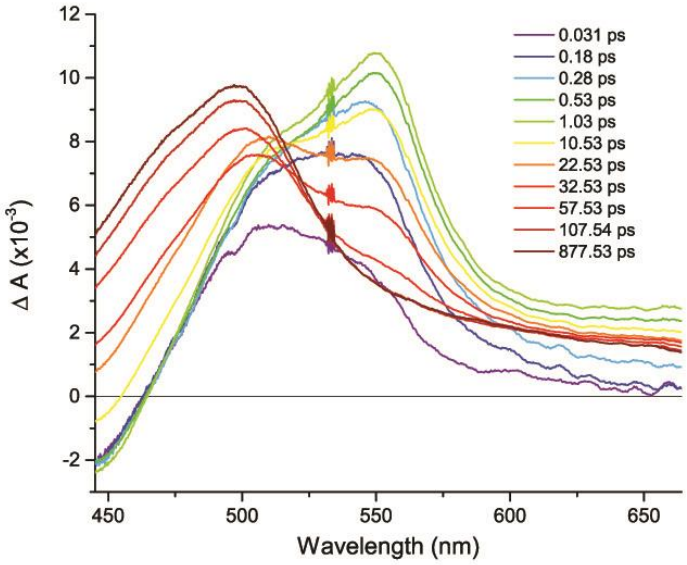

Figure 7.2. Transient absorption spectrum for D1a in THF showing the persistent absorbance of a triplet state product at long time delays

7.5 Mono- and binuclear Pt(II) multicarbene complexes compared

The comparative study between mono- and binuclear Pt(II) complexes carrying ethoxy- and aminocarbene complexes with bis(bromophenyl-1,4)phenylene-1,4-amine substituents revealed that there were significant electronic differences between the complexes due to the additional bithienylene bridge and metal centre for the binuclear compounds.

The UV/Vis absorption spectroscopy revealed that the mono- and binuclear complexes similar absorbance bands at the high energy wavelengths. Additional ligand-to-ligand charge transfers and metal-to-ligand charge transfer bands were observed for the binuclear complexes. The emission spectroscopy of the complexes showed that the fluorescence observed originates solely from the carbene ligands coordinated to the Pt(II) centres. The emission was more efficient for Pt(II) complexes to which three carbene ligands were coordinated. It was further observed that for the binuclear complexes, the bithienylene bridge allowed access to a non-emissive pathway by which excitons returned to the ground state – significantly reducing the quantum yield of the emission observed for the complexes.

Through cyclovoltammetry it was established that oxidation occurred preferentially at a tertiary amine and reduction at a carbene carbon site. This result, supported by DFT calculations, showed that the HOMO orbitals of the mononuclear complexes are located on the tertiary amine of one of a coordinated carbene ligands. The LUMO was located on the carbene carbon of one of the ligands. The HOMO orbitals of the binuclear complexes were located on the bithienylene bridge while the LUMO orbitals were located on one of the ligands' carbene carbons coordinated to the positively charged Pt(II) atom. The cyclovoltammetry further showed that the oxidation of the ethoxycarbene ligands occurred before that of the aminocarbene ligands. The formed radical in each case was better stabilised by the larger π-conjugation which extended from the remote nitrogen to the carbene carbon in the ethoxycarbene ligands compared to the aminocarbene ligands.

Finally, the comparison of the femtosecond transient absorption spectroscopy of the complexes indicated that all the products underwent an intersystem crossing (ISC) process and displayed absorption of a spin forbidden triplet state. The same triplet state product formed upon photoexcitation and charge distribution in **C2a** (short-lived) and **D3a** (persistent). It was postulated that the transient species was a triplet state product in which a formal negative polaron was situated on a carbene carbon – a product of a charge separated (CS) state (Figure 7.3). The positive triplet state polaron was not observed for **D3a**. In **C2b**, absorbance of a triplet state was discerned before stimulated emission (SE) was observed at longer time delays. **D3b**, however, displayed the absorbance of two triplet state products which resembled those formed upon photoexcitation of **D3a**. It was proposed that the second long-lived triplet state product showing absorbance at longer wavelengths belonged to that of the positive polaron present on the bithienylene bridge.

It can therefore be concluded that the second metal and its coordinated carbene ligands lead to an increase in amount of photo-activated transitions responsible for the emission – which consequently leads to an increase of the emission quantum yield. In direct competition with the photo-activated transitions that leads to the emission, is the pathway the excitons follow to form the CS state in the presence of the bithienylene bridge.

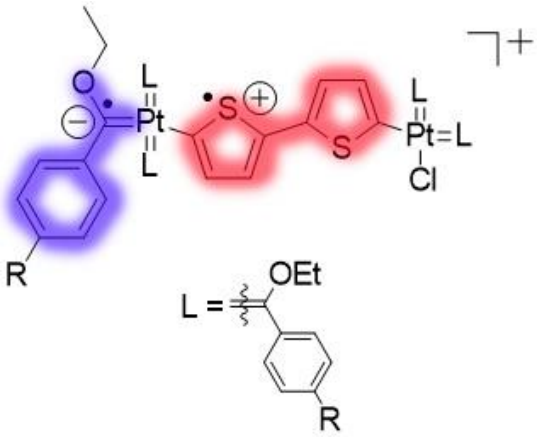

Figure 7.3. Proposed positions of the separated charges that form on the binuclear bridged ethoxycarbene complexes upon photoexcitation

It was shown that the ethoxycarbene complexes have longer CS state lifetimes than the aminocarbene complexes, which indicated that they were able to better stabilise the formed polarons before charge recombination occured.

7.6 Conclusive summary

The study conclusively showed that Fischer carbene complexes situated at the *p*-position relative to an amine substituent was remotely stabilised through electron delocalisation from the distant nitrogen. It was further illustrated that several of such stabilised carbene ligands can be transferred to Pt(II) metal nodes through a transmetallation approach without carbene selfdimerisation taking place. The formed mono- and binuclear Pt(II) carbene complexes were photoactive and displayed ligand-based fluorescence. Upon photoactivation at 380 nm of the binuclear multicarbene complexes, a charge separated state was formed. Although the position and quantum yield of this state have not been conclusively determined, this is the first study to indicate that acyclic heteroatom stabilised carbene ligands have potential in photoactive materials.

7.7 Future research

The study illustrated that Fischer carbene complexes can be incorporated into macromolecular assemblies using a metal exchange or carbene transfer reaction. Even though the reactions were successful, the number of carbene ligands that were transferred and the charges of the complexes could not necessarily be controlled. The reaction conditions and properties of the carbene ligands themselves need to be better understood as to properly apply and control the reactions in the synthesis of Fischer carbene containing materials of Pt(II) and other transition metals.

The compounds that have been investigated are complex and there are numerous characteristics of the complexes that are unclear. As it has been established that Fischer carbene complexes can be used to separate charges in the excited state, this aspect must be further investigated. Compounds that are easier to synthesise and less complex will enable a study of Fischer carbene complexes' fundamental photophysical properties and how these can be controlled and manipulated.

This study has laid some ground work for the incorporation of Fischer carbene complexes in macromolecules and materials and revealed that these ligands have potential applications in

electronic devices. It now remains to investigate whether Fischer carbene ligands can indeed be used in electronic devices.

APPENDIX

Throughout the thesis several references have been made to the Appendix. The Appendix can be found on the disc included with this thesis. The Table of Contents for the data that appears in the Appendix are given below.